Ground state properties of antiferromagnetic spin-1/2 Heisenberg systems in external fields[1]

Andreas Fledderjohann
Physics Department, University of Wuppertal, D-42097 Wuppertal, Germany

Abstract:
The present work investigates the influence of external perturbations on the ground states of spin-1/2 antiferromagnetic Heisenberg chains and two-dimensional spin lattices. The lifting of the well-known zero-energy excitations (soft modes) of the unperturbed Heisenberg chain due to suitably chosen periodicities of applied perturbations is presented. The evolution of excitation energies and transition matrix elements is described by a complete set of differential equations and scaling solutions for small perturbations are discussed. A variety of topic quasi-one-dimensional spin systems (spin-Peierls chain, spin ladders in different geometries) are then embedded in the descriptive scheme of periodically perturbed Heisenberg chains. In particular, the energy gaps and, most noticeable, the formation of magnetization plateaus occurring in these systems are discussed in a single prediction scheme related to the soft mode positions of the previously unperturbed chain. Plateaus due to various kinds of perturbations are furthermore shown to be observable in static correlation functions of the perturbed chain. Particular emphasis is laid on the consideration of processes of spontaneous breaking of symmetry. The latter aspect is discussed for translationally invariant perturbations that do not provide an explicit change of the periodicity of the spin system. The presented investigations finally turn to two-dimensional spin systems first addressing the formation of a non-zero staggered magnetization (long range order) for increased two-dimensionality in terms of a translationally invariant perturbed (helical) spin system. Finally, first stages of a present study on the formation of magnetization plateaus in square spin lattices with frustrating diagonal couplings are given.

[1]Habilitationsschrift im Sinne von 3 Abs. 2 der Habilitationsordnung des Fachbereichs Naturwissenschaften I der Bergischen Universitaet- Gesamthochschule Wuppertal.

Contents

Chapter 1

Introduction

The physics of quantum spins is not even a century old and is deeply connected with the origin of quantum mechanics itself. It began in the early 1920s with the investigation and classification of the origins of the Zeeman effect and the spectral multiplicity of atomic spectra by *Sommerfeld, Pauli and Landé.*

A lot of work was necessary to achieve a consistent classification scheme of atomic spectra and moreover to develop a concise understanding of the "self-rotating electron". In 1925-26, important ideas like the exclusion principle, the electron spin and Thomas' theory appeared and *Heisenberg* and *Schrödinger* developed matrix and wave mechanics, respectively.

The attempt of incorporating spin into quantum mechanics was first done by *Pauli* [171] (1927) introducing the Pauli matrices, however, a complete and relativistic theory was first achieved and established by *Dirac* [64] one year later in 1928.

We will now narrow down the broad field of further developments of quantum spin, e.g. proton spin, spinors, isospin, elementary particles, .., and concentrate on the coupling of spins and in particular its appearing in the condensed matter theory of magnetism. First, however, *Tomonaga's The Theory of Spin* only lately given in English translation shall be recommended for an exhaustive treatment of the topic. The phenomenon of magnetism is inextricably linked with quantum mechanics since a truely classical system cannot have a magnetic moment in the thermodynamical limit (TDL) – even if a magnetic field is applied. We will further narrow down the broad field of magnetism in condensed matter (see e.g. [12, 153]) to systems that form spontaneous magnetic moments that even exist prior to the application of an external magnetic field. The latter requires magnetic moments and electron spins to arrange in a regular pattern. The simplest of these patterns is the ferromagnet showing a complete alignment of spins. Then, antiferro- and ferrimagnetic types –with different degrees of freedom like tilted or spirally ordered spins– do follow. Here, the simple antiferromagnet (parallel spins with alternating orientation) is the only regular spin pattern that has no finite spontaneous magnetic moment (saturation moment).

The study of ferromagnetism has a long history (cf. e.g. *Gilbert's De Magnete* [93]). Ferromagnetism is much easier and directly to observe than other forms of magnetic order as e.g. ferri- or antiferromagnetism. The latter phenomena –in particular the simple antiferromagnet– require considerably more advanced experimental techniques for their study (see e.g. [12] and in particular [146, 152] for qualitative and more detailed descriptions of the theory and the use of X-ray and neutron scattering investigations in condensed matter physics). For that reason it is understandable that the study of magnetism first concentrated on the phenomenon of ferromagnetism.

A current explanation of ferromagnetism e.g. of Fe at the described time was *Weiss'* assumption of strongly interacting molecular magnets that could explain a variety of experimental results. An interpretation and explanation of these strong interactions, however, was first given by *Heisenberg.* Heisenberg gave a new interpretation of spectral terms of alkaline earths [107] and

subsequently applied his results on symmetry properties and their connection to the statistic of particles to the problem of a ferromagnetic crystal [108] where he introduced an exchange interaction between adjacent atoms. The exchange integrals had to be chosen positive in order to explain ferromagnetic order as well as Weiss' assumption of an interatomic field (the latter is proportional to the exchange integral). The tendency towards a formation of such a regular spin pattern is opposed by increasing thermal fluctuations for increasing temperatures – at a particular temperature (Curie temperature T_C for a ferromagnet, Neél temperature T_N for a simple antiferromagnet) a transition from a magnetically ordered to a disordered phase occurs. The advent and success of quantum mechanics [1] and Heisenberg's interpretation of exchange interactions set the beginning of a continuous study of "Heisenberg spin systems" for the investigation of magnetic properties of crystalline systems with localized spins. In condensed matter localized spins are usually given by ions with incompletely filled (inner) orbitals resulting in a net magnetic moment according to *Hund's rules*. The main contribution to the coupling of quantum spins in a magnetic crystal is caused by the overlap of orbitals located at adjacent sites. Therefore, a basic *Heisenberg Hamiltonian* of coupled quantum spins first of all has to take into account these nearest-neighbour pairs of spins. The quantum nature of spin results in definite signatures and deviations from a classical description of spin systems appearing the more plain the smaller the considered quantum spin and dimensionality of the considered spin system (see below). –For antiferromagnetic chains the temperature where quantum effects dominate is expected to be exponentially small $O(e^{-\pi S}$ for large S [2].
The basic form of a Heisenberg spin-S Hamiltonian with nearest-neighbour ($< i, j >$) exchange coupling J is given by

$$H \quad = \quad -J \cdot \sum_{<i,j>} \mathbf{S}_i \mathbf{S}_j \tag{1.1}$$

with i, j denoting the sites of the considered quantum spins $\mathbf{S}_i$. The scalar products $\mathbf{S}_i \mathbf{S}_i$ of the spin operators fulfill the relation $\mathbf{S}_i \mathbf{S}_i = S(S+1)$ for integer and half-odd-integer quantum spins $S = n \cdot 1/2, \quad n = 1, 2, \ldots$. The coupling J has to be chosen positively to obtain a ferromagnetic, or parallel, alignment of spins. Antiferromagnetic nearest neighbour spin couplings in a one-dimensional system (chain) will be described subsequently by retaining the positiveness of J, however, removing the sign of Hamiltonian 1.1. It should be noted that under more general conditions (higher dimension, longer ranges of couplings, non-bipartite lattices,..) a global change of the sign of the couplings will not necessarily result in an antiferromagnetic order as e.g. the sign reversal for a ferromagnet on a triangular lattice leads to a frustrated irregular spin ordering.
The influence of the type and orientation of the contributing orbitals on the resulting nature of magnetic couplings has been analyzed and partially formulated in the *Goodenough, Kanamori, Anderson rule* (e.g. resulting in a ferromagnetic exchange for the 90^0-exchange between two half-filled orbitals.
As mentioned above, the study of one-dimensional spin $S = 1/2$ Heisenberg chains addresses magnets that most enunciately show the influence of quantum fluctuations. Rather early, *Bethe* [22] (1931) and later *Hulthén* [120] (1938) gave exact results for eigenvalues and eigenstates of the chain using the *Bethe ansatz* to diagonalize the Hamiltonian. The complicate structure and rather minor exploitability of the obtained eigenstates for the interesting evaluation of correlation functions in the succession led to various further approaches as e.g. the spin wave approximation (*Anderson* (1952) [10], *Kubo* (1952) [138]) and later to the bosonization approach of the low-energy excitations (free mass-less compactified bosons, see e.g. *Tsvelik* [201]) of the

[1] Even earlier *Lenz* [142] proposed a similar classical model of coupled (classical) spins. *Ising's* solution [124] of the one-dimensional Lenz-Ising model and in particular the non-existence of a finite spontaneous magnetization was mistakenly assumed to hold for arbitrary dimensions and led to a decrease of interest in this model over a number of years (see e.g. [33]).

antiferromagnetic Heisenberg chain (*Luther and Peschel* [147] (1975)). A further important development, the numerical study of spin-1/2 Heisenberg chains, is linked to the detailed study of ferro- and antiferromagnetic chains given by *Bonner and Fisher* [32] (1964). The finite-size behaviour of small chains ($N = 2, 3, .., 11$) was discussed in much detail and shown to allow extrapolations for certain static quantities. Further applications and the wide range of numerical investigations will be addressed and partly used in later chapters.
A particular point of interest in low dimensional spin systems is the form and existence of phase transitions. In 1966, *Mermin and Wagner* [155] proved the "*Absence of ferromagnetism or antiferromagnetism in one- or two-dimensional isotropic Heisenberg models*" for temperatures $T > 0$. A phase transition at $T = 0$ could not be ruled out and indeed does occur for the spin-1/2 Heisenberg chain. As will be discussed in Chapter 2, at the *critical point* ($T = 0$) correlation functions of the chain decay as a power law as expected for a critical system. Here, it should be noted that the criticality of arbitrary-S antiferromagnetic Heisenberg chains is restricted to the sub-class of half-odd-integer spin S. According to *Haldane's conjecture* [101] the ground states of integer spin antiferromagnetic chains are massive, i.e. a finite energy gap to the lowest excitations exists. It should be remarked, however, that the latter property does not unrestrictedly hold for all integer spin chains. A generalized –bilinear-biquadratic– spin-1 model

$$H(\Theta) \quad = \quad \cos\Theta \sum_i \mathbf{S}_i\mathbf{S}_{i+1} + \sin\Theta \sum_i [\mathbf{S}_i\mathbf{S}_{i+1}]^2 \,, \tag{1.2}$$

containing the Haldane-gapped spin-1 Heisenberg model with $\Theta = 0$, e.g. contains the gap-less (critical) SU(3) symmetric *Lai-Sutherland* model for $\Theta = \pi/4$ (which is solvable in the sense of Yang-Baxter equations; see [159, 180]). The investigation of the response of a critical spin chain with integer spin to external perturbations therefore is possible, however, requiring an adequately chosen spin Hamiltonians.

Looking now at experimental realizations of low-dimensional or even quasi-one-dimensional spin systems, one has to take into account that such systems usually are 3-dimensional objects (see further discussion below). This means that at very low temperatures the formerly neglected out-of-chain or out-of-plane spin couplings will finally lead to the corresponding 3-dimensional low-T behaviour.
Quasi-one-dimensional spin systems are known and experimentally accessible in an increasing number during the last decades. Best-known and thoroughly investigated quasi-one-dimensional spin-1/2 antiferromagnets are $KCuF_3$ and $CuCl_2 \cdot 2N(C_5D_5)$ (CPC). Compounds that are displaying one-dimensional magnetic properties in most cases are classified by the presence of large non-magnetic ions separating the magnetic chains (in the cases given above formed by copper ions). In $KCuF_3$, however, the one dimensionality is attributed by Jahn-Teller distortions of the octahedral environment of the Cu^{2+} ions [114, 177]. Neutron scattering studies led to important insight into energetic and dynamical properties, supported by X-ray studies of the respective crystal structures. Valuable comparisons between the theoretical picture of spin-1/2 chains and their assumed experimental realizations could be performed. One important point is given by the dispersion relation $\omega(q)$ for the lowest excited states of the spin-1/2 antiferromagnetic chain. It first has been determined by *des Cloizeaux and Pearson* [48] (*dCP*) to be

$$\omega(q) \quad = \quad \pi J |\sin q| \tag{1.3}$$

(given for a lattice constant/nearest-neighbour separation $a \equiv 1$). Interestingly, a linear spin wave theory for classical spins –i.e. expected to give reliable descriptions in the large-S limit– gives the same q-dependence for $\omega(q)$, however a changed pre-factor (2 instead of π). The latter difference between the two extreme limits (extreme quantum limit $S = 1/2$ and classical limit $S \to \infty$ has been found reasonably well realized in experiments on the spin-1/2 material

$CuCl_2 \cdot 2N(C_5D_5)$ [67] –striking confirmation of *dCP*– and in contrast the spin-5/2 material $(CD_3)_4NMnCl_3$ (TMMC) [23]. The quasi-one-dimensionality of the magnetic spin-1/2 system was confirmed experimentally by the highly anisotropic spin wave spectrum below the Neél temperature. Investigations of the latter spin wave spectra led to the ratio of the interchain to intrachain magnetic couplings $J_a/J_c = -0.01 \pm 0.001$ of the investigated single crystal (tetragonal magnetic unit cell $(a, a, 2c)$) of $KCuF_3$ [177] showing the exceptional anisotropy of the material. In the following, neutron scattering studies (inelastic scattering, magnetic susceptibility measurements and further investigations) showed the approximate correspondence of systems like $KCuF_3$ [161, 189] and $Cu(C_6D_5COO)_2 \cdot 3D_2O$ (Copper-benzoate) [62] to the dynamical behaviour of spin-1/2 chains (see further discussion in Chapter 2) as well as incommensurate ordering phenomena along the chain direction for Cs_2CuCl_4 [50].

Investigations as well turned to the interesting case of perturbed spin systems and spin ladder systems. In the first case, the discovery of $CuGeO_3$ as the first known inorganic (quasi-one-dimensional) spin-Peierls system [105] led to an important renaissance (cf. e.g. [126]) and increase of scientific interest in this field. Shortly thereafter, NaV_2O_5 [123] joined as a second inorganic spin-Peierls material. It is interesting to note that a neutron scattering study of quasi-one-dimensional (orthorhombic) $CuGeO_3$ [164] resulted in a not so pronounced one-dimensionality (chain coupling J_c, $J_a \approx -0.01 J_c$, $J_b \approx 0.1 J_c$) as compared to the earlier discussed $KCuF_3$. The above-mentioned copper-benzoate has as well been discussed in the context of perturbation effects and the observed opening of a gap in homogeneous magnetic fields (see further discussion in Sec. 3.2.4).

Spin ladders on the other hand revealed "*Surprises on the way from one to two dimensional quantum magnets: the ladder materials*" [58] meaning the alternation from critical to massive behaviour depending on the odd or even number of legs of the considered ladder (see e.g. [59] for a current overview of ladder materials).

Both, the alternating strength of nearest-neighbour spin couplings J_1 ($J_1 = J_0\left(1 + (-1)^i \cdot \delta\right)$, dimerization δ magneto-elastically given by a periodic lattice distortion present for temperatures below the spin-Peierls temperature ($T < T_{SP}$) for spin-Peierls chains and the existence of more than one spin chain coupled to a n_l-leg ladder structure, i.e. $n_l > 1$, leads to the observation of plateaus at well defined places in the magnetization curve of the respective system. The fitting of a spin-1/2 chain Hamiltonian to experimental data of $CuGeO_3$ (e.g. susceptibilities) led to the interesting necessity of an additional –non-alternating– next-to-nearest neighbour spin coupling J_2 with a finally determined ratio $J_2/J_0 = 0.342$ [74] presenting an example for the simultaneous presence of a periodic ($(-1)^i\delta \cdot J_0$) and a translationally invariant perturbation (J_2) of the underlying spin-1/2 antiferromagnetic chain ($J_0 \sum_i \mathbf{S}_i\mathbf{S}_{i+1}$). The reaction of the latter spin chain with respect to external perturbations has been discussed taking into account the criticality, i.e. the existence of zero-energy excitations (soft modes) at field (magnetization) dependent momenta, of the Heisenberg chain. *Oshikawa, Yamanaka, Affleck* [168] presented a quantization rule giving magnetization values of possible plateaus for a considered perturbation. The formation of a magnetization plateau is accompanied by the opening of an energy gap in the excitation spectrum of the perturbed chain and certain degenaracies or changes of symmetry. For the case of translationally invariant perturbations, an occurring plateau unambiguously marks a spontaneously broken symmetry.

The situation and rigorousity of the description of (perturbed) spin systems significantly changes when turning to two-dimensional spin lattices. Exact solutions are scarce and the numerical treatment of finite spin systems is restricted to rather small systems. At present, a most comprehensive theory of the low-temperature static and dynamic behaviour of 2d square lattice quantum Heisenberg antiferromagnets is considered to be given in terms of the quantum nonlinear sigma model [45, 46, 202]. Neutron scattering studies of the square-lattice antiferromagnet $Sr_2CuO_2Cl_2$ [95] e.g. led to a qualitative agreement of Monte Carlo results and predictions of the latter model for spin-spin correlation lengths in a wide range of temperatures. A satisfying

description and in particular explanation of observed magnetization plateaus in two-dimensional systems does not exist yet. The existence of long range order (LRO) in two dimensions –a non-zero staggered magnetization– and in particular its formation when changing from one to two dimensions will be addressed later in Sec. 5.4.2.

The present work is a study of zero temperature properties of mainly antiferromagnetic spin-1/2 Heisenberg spin systems (of one and partly two dimensions) that are exposed to the influence of an additional external field or other perturbations. The discussion will first treat the case of periodic perturbations and later as well turn to translationally invariant perturbations. A point of major importance in both cases will be the loss of criticality of the in most cases underlying antiferromagnetic Heisenberg chain due to the applied perturbation. The change from a gap-less to a massive spectrum due to the applied perturbation is most suitably observed in the course of the magnetization curve of the spin system. In particular ground state level crossings and changes of symmetries in the process of the opening of an energy gap for relevant excitations of the perturbed spin chain/system are distinctively visualized in the formation of plateaus within the respective magnetization curves. The latter process will be studied by extrapolating finite-system calculations of magnetization curves ("staircases"). Moreover, the occurrence of magnetization plateaus will be accompanied by their classification with respect to the quantization rule of *Oshikawa, Yamanaka, Affleck* [168] and another soft mode approach [86]. Both prediction schemes are furthermore supplemented by an analysis of classes of static structure factors that turn out to offer methods of plateau forecasts beyond purely predictive ones.

The introductory Chapter 2 gives a rather thorough discussion of the isotropic antiferromagnetic spin-1/2 Heisenberg chain with or without the additional presence of a uniform magnetic field. Static and dynamical structure factors, the criticality of the spin chain and in particular the connections and consequences resulting from the existence of the zero-energy excitations (soft modes) as well as the proof of the latter given by *Lieb, Schultz, Mattis* (LSM) [143] will be outlined and discussed. Special attention is paid to the quality of the presented numerical results for the description of the considered Heisenberg chains. Numerical evaluations and the presentation of numerical support or evidence for certain theoretical pictures will play a dominant part in the following chapters.

Sec. 2.3 gives a brief discussion of the application of *Conformal Field Theory* results to the finite-size behaviour of certain critical quantities. Tests for the latter relations are exemplarily discussed. Finally, a short discussion of frequency-moments of the dynamical structure factor and their importance for certain problems and questions in this context [158, 80, 132] is presented.

Chapter 3 first gives a general discussion of periodically perturbed Heisenberg chains. A complete set of differential equations [84] –so called evolution equations– is given, describing the changes of excitation energies and transition matrix elements under the influence of the perturbation under consideration. The existence of a particular scaling solution for the case of a longitudinally staggered field is treated and the behaviour of weakly perturbed Heisenberg chains is studied for a variety of perturbations.

The investigation then broadens to the topical fields of ladder and spin-Peierls systems. Their discussion in terms of periodically perturbed Heisenberg chains in particular leads to certain ambiguities and the consideration of strongly perturbed chains in case of ladder Hamiltonians. Chain Hamiltonians with the respective periodic perturbations –in preparation of their discussion in Chapter 4– are presented. In addition to the cases of regular n_l-leg ladders, a number of more complex *zig-zag-* and *Kagomé*-type ladders also expressed as periodically perturbed Heisenberg chains are included.

Chapter 4 gives a thorough discussion of magnetization properties (plateaus) of the periodically perturbed spin chains introduced in Chapter 3 and extrapolations and classifications (quantization condition [168], soft mode approach [86]) of the obtained magnetization plateaus. A critical comparison of both prediction schemes is given.
The interplay of different periodic perturbations and the combination of periodic and translationally invariant perturbations is addressed as well. The discussion of regular spin ladders is used to explain the earlier assumption/observation of gapped ground states for even-leg ladders (*Dagotto, Rice* [58]), i.e. magnetization plateaus at magnetization $m = 0$.
Finally a discussion of static structure factors of perturbed systems is presented and a different way to reach at non-probabilistic predictions for the formation of magnetization plateaus is suggested.

Chapter 5 addresses the class of translationally invariant perturbations which were only briefly mentioned in the preceding chapter treated as an additional next-to-nearest neighbour spin coupling. In this chapter, some well-known translationally invariant chain Hamiltonians will be introduced. Then, a translationally invariant analogue of a 2-leg ladder –formerly described as a periodically perturbed chain– will be discussed and the freedom of the chosen mapping of the considered spin ladder on a single chain Hamiltonian will lead to the interesting phenomenon of spontaneous symmetry breaking.
Finally, the discussion turns to translationally invariant representations of two-dimensional (square) spin lattices and the possible existence of magnetization plateaus. First results of an at present ongoing investigation will be presented. Before, results of an investigation ([83]) concerning the onset of long range (magnetic) order (LRO), i.e. the occurrence of a non-zero staggered magnetization, for the transition from one- to two-dimensional spin systems will be reviewed and discussed.

Chapter 6 will finally summarize the obtained results and give a perspective of future applications of the presented investigations of perturbed antiferromagnetic spin-1/2 Heisenberg systems.
The Appendices $A - C$ are devoted to some discussion and explanations of certain methods and calculations used or refered to in the sequel of the chapters: (A) Recursion method [79, 81, 83]; (B) Calculation of magnetic saturation fields; (C) *Bulirsch-Stoer* (BST) extrapolation method [36, 110].

Chapter 2

The isotropic translation invariant antiferromagnetic Heisenberg chain

The present chapter will summarize basic properties of the spin-1/2 antiferromagnetic Heisenberg chain which will be the starting point of all further discussions.
The Hamiltonian for a N-site spin chain with periodic boundary conditions (i.e. $\mathbf{S}_{j+N} = \mathbf{S}_j$, $\mathbf{S}_j \equiv \vec{S}_j$) is given by

$$\begin{aligned} H_0 &= 2\sum_{j=0}^{N-1} \mathbf{S}_j \mathbf{S}_{j+1} && (2.1)\\ &= \sum_j \left[S_j^+ S_{j+1}^- + S_j^- S_{j+1}^+ + 2S_j^z S_{j+1}^z \right] && (2.2)\\ &= \sum_j \left[P(j,j+1) - \frac{1}{2}\mathbb{1} \right] && (2.3) \end{aligned}$$

where j denotes the sites of the chain; S^+, S^-, S^z are the $S = 1/2$ spin operators and $P(j, j+1)$ is the permutation operator. The S_j^m $(m = x, y, z)$ are related to the *Pauli* spin matrices via $S_j^m = \frac{1}{2}\sigma_j^m$ and fulfill the well-known (anti-)commutation relations:

$$\begin{gathered} \left[S_j^z, S_{j'}^\pm\right] = \pm\delta_{jj'} \cdot S_j^\pm \quad , \quad [S_j^a, S_{j'}^b] = \delta_{jj'} \cdot \epsilon_{abc} S_j^c \quad , \quad a, b, c \in \{x, y, z\} \\ \{S_j^+, S_j^-\} = \mathbb{1} \quad , \quad \left[S_j^+, S_{j'}^-\right] = 0 \quad \text{for} \quad j \neq j' \,. \end{gathered} \tag{2.4}$$

The prefactor of 2 in Eq. 2.1 is of course not really essential for the model (giving however the "clearest" appearance of the underlying $SU(2)$-symmetry) and will be skipped occasionally in the course of this chapter (not without mentioning). In any case –here and later– additional interaction terms to the Hamiltonian, external magnetic fields, etc. will be normalized to a prefactor of 1 paying tribute to the general formulation of the model.

The Hamiltonian as given above (2.1-2.3) has experienced a variety of treatments. The widely known analytical method, the Bethe ansatz (BA) (*Bethe* (1931) [22]), very early led to the determination of the infinite-system ground state energy (*Hulthen* (1938) [120]) and in the course of time (see e.g. *Mattis* (1993) [154], *Karbach* (1994) [129] and further references therein) to the determination of various other quantities. However, the BA technique is comparatively complicated and mainly useful for static or thermodynamic quantities. Moreover, its applicability

fades when modifications of the Hamiltonian (e.g. second-nearest neighbor interactions, periodic perturbations, ...) are considered.
Second to mention are ansätze and approximations for the infinite-N model, e.g. spin-wave approximations (Anderson (1952) [10]), many-particle treatments based on the fermionic representation of H_0 (see e.g. *Lieb, Schultz, Mattis* (1961) [143]), renormalization group studies (*Hallberg, Horsch, Martinez* (1995) [104] or the exp(S)-method (*Bishop* (1991/92) [24, 25, 26, 27]. Moreover, important insight in the low-energy excitation physics has been achieved by bosonization of the fermionized spin-Hamiltonian (*Luther and Peschel* (1975) [147], *Haldane* (1983) [101]).
The last techniques to mention are the group of finite-system methods as complete diagonalization (*Bonner and Fisher* (1964) [32], *Fabricius et al.* (1991, ...) [69, 72, 73]), *Lancos*-techniques [139, 145], quantum Monte Carlo (QMC) methods (e.g. *Ceperly* (1995) [44] and density matrix renormalization group (DMRG) calculations (*White* (1992/93) [212, 214], the latter method offering both treatments of finite and infinite systems.

2.1 Symmetries of the Heisenberg chain

The model (2.1-2.3) possesses a wide class of symmetries – accompanied by the related conserved quantities.
For the chosen periodic boundary conditions, H_0 is invariant under translations, rotations and reflections on the spin lattice. Furthermore, the total spin $\mathbf{S}$ and one of its components, S^z, are conserved:

$$\mathbf{S} = \sum_j \mathbf{S}_j, \quad S^z = \sum_j S_j^z \quad , \quad [H_0, \mathbf{S}] = [H_0, S^z] = 0\,. \tag{2.5}$$

Since they are translationally invariant the eigenstates of H_0 can be classified by an eigenvalue of momentum p (here and in the following the term momentum is allways used in the meaning of crystal momentum). The translation operator T, defined as

$$T \;\; = \;\; P(0,N-1)P(0,N-2)\ldots P(0,1) \tag{2.6}$$

for an N-site chain, obeys $[H_0, T] = 0$ and its application on a momentum eigenstate $|p>$ yields

$$T|p> \;\; = \;\; e^{-ip}|p> \;. \tag{2.7}$$

For a periodic chain of even length ($N = 2n$, $n \in \mathbb{N}$) the reflection operator R is given by

$$R\mathbf{S}_{N-1-j}R \;\; = \;\; \mathbf{S}_j \quad , \quad j = 0, 1, \ldots N-1 \tag{2.8}$$

and commutes with H_0, $\mathbf{S}^2$ and S^z, however it anticommutes with the momentum operator P. Since R transforms states with momentum p to $-p$, this means that exclusively in the subspace of $p = 0$ and $p = \pi$ states the reflection operator can be diagonalized in addition.
Finally, an infinite set of additional conservation laws, so called hidden symmetries shall be mentioned in short. The existence of such a set of commuting transfer matrices $T(\lambda)$ (each of them commuting with H_0) proves the integrability of the considered Heisenberg system [18, 19]. For details, references and particular applications of some of those nontrivial conservation laws for efficient numerical computation (complete and exact diagonalization of antiferromagnetic Heisenberg rings) see e.g. [68], [69].

An important quantity connected with the translational symmetry of spin chains with periodic boundary conditions (PBC) is the ground state momentum $p_0(N, S_z)$ ($S_z = \sum_x S_z(x)$) of the chain in the respective magnetization sectors $m \equiv S_z/N$ – note $[H_0, S_z] = 0$.

Spin chains can formally be subdivided in the 2 classes of systems with an even or odd number of sites. Systems of the first class, namely the usually discussed chains with an even number of sites ($N = 2n$, $n \in \mathbb{N}$), have non-degenerate ground states, i.e. ground state momenta 0 or π, that alternate for increasing/decreasing S_z-values according to

$$p_0(N = 2n, S_z) \quad = \quad \pi \cdot \left(S_z + \frac{N}{2} \right) \mod 2\pi \,. \tag{2.9}$$

The non-degenaracy of the ground state of H_0 for even N (i.e. the total spin being $S = 0$) has been proven by *Lieb, Schultz, Mattis* (1961) [143] strengthening an earlier result of *Marshall* (1955) [151] who proved the singlet character of the ground state without being able to exclude its possible degenaracy.
A second important theorem –given in the same work of Lieb, Schultz, Mattis– that concerns zero-energy excitations of the Heisenberg chain will be explained in a separate part (Sec. 2.6.2) together with some generalizations.
Turning back to the ground state momenta, it should be noted that the even-N class can be further subdivided in two subclasses ($N = 4n$, $N = 4n + 2$) that have $S_z = 0$-ground state momenta $q_0(4n, 0) = 0$ and $q_0(4n + 2, 0) = \pi$. Both classes, however, yield a fully spin-polarized ($S_z = \pm N/2$) ground state with $q_0(2n, \pm N/2) = 0$.
Spin chains of odd length ($N = 2n + 1$), forming the second class, have been shown [130] to have 2-fold degenerate ground states with ground state momenta that can be summarized as

$$q_0(N = 2n + 1, S_z) \quad = \quad \pi \cdot \left(S_z + \exp\left(i\pi(N + 1)/2\right) \cdot \left[\frac{1}{2} \pm \left(\frac{S_z}{N} - \frac{1}{2} \right) \right] \right) \mod 2\pi \tag{2.10}$$

i.e. the degeneracy disappears for $S_z/N = \pm 1/2$ again resulting in a fully polarized state with $q_0(2n + 1, \pm N/2) = 0$. As before, two different subclasses ($N = 4n - 1$, $N = 4n + 1$ with $\exp(i\pi(N + 1)/2) = \pm 1$) appear.
Due to a different finite-size behaviour (see e.g. [32]) and a lacking paramagnetic ground state ($S_z = m = 0$) – at least for finite N – spin chains of odd length are rarely treated and will as well be left out in this work.

The discussion of another powerful symmetry related to conformal invariance, will be the subject of an independent paragraph (Sec. 2.3) and the reader may as well be revised to *Faddeev and Takhtadzhan* [75] for further and more detailed discussion.

2.2 Finite-size scaling

The occurrence of singularities in certain physical quantities at so-called critical points is exclusively restricted to the thermodynamic limit (TDL), i.e. particle or spin number $N \to \infty$. Since evaluations for finite system sizes are very common and often forced by the complexity of the considered system, inevitably the connection between the behaviour of finite systems and the TDL has to be established.
This task had first been accomplished by *Fisher* (1972) [77] and *Fisher and Barber* (1972) [78], who showed that in the vicinity of a critical point (e.g. expressed by the smallness of a reduced temperature $t = (T - T_c)/T_c$ near a phase transition) and for sufficiently large N a single-variable scaling function f should exist that relates observables of a finite ($\Gamma(t, N)$) and infinite ($\Gamma(t)$) system by

$$\Gamma(t, N) \quad = \quad \Gamma(t) \cdot f(z) \,. \tag{2.11}$$

Here, $\Gamma(t)$ is supposed to behave as $\Gamma(t) \sim t^{-\phi}$ close to the critical point and the scaling variable z only depends on a combination of N and t, namely

$$z \quad = \quad \frac{N}{\xi(t)} \sim N t^{\nu} \tag{2.12}$$

with a genuine behaviour $\xi(t) \sim t^{-\nu}$ for the correlation length of an infinite system for $t \to 0$. Considering now a fixed and finite N, i.e. $\Gamma(t, N)$ must not have a singularity, the previous relations lead to

$$\Gamma(t, N) \quad = \quad f(z) \cdot \Gamma(t) \sim (Nt^{\nu})^{x} \cdot t^{-\phi} \tag{2.13}$$

and require x to be $x = \phi/\nu$ in order to prevent the occurrence of a singularity for finite N, therefore resulting in the N-dependece

$$\Gamma(t, N) \quad \sim \quad N^{\phi/\nu} \tag{2.14}$$

for $t \to 0$.
Since the Heisenberg quantum-spin model is known not to show phase transitions with ordering at finite temperatures in one and two dimensions (*Mermin, Wagner* (1966) [155]) finite-size scaling applications for Heisenberg chains usually address singularities that show a sharp signature in momentum space like the later discussed static and dynamical structure factors (SSF, DSF, see Secs. 2.5,2.49). Typical ansätze for these cases would read

$$\Gamma(q, N) \quad = \quad \Gamma(q) \cdot f(z) \quad , \quad z = N \cdot q \tag{2.15}$$

with finite chain momenta $q = (2\pi/N) \cdot n$ and n integer. These cases have been widely studied and reviewed (see e.g. [73, 128, 131, 179, 13]) In particular the applicability of relations of the given kind to data obtained from rather small system sizes has been checked – note that finite-size scaling theory gives no minimal N-value for the validity of relation 2.11.

2.3 Critical exponents, Conformal field theory

In 1970 *Polyakov* [172] realized that physical systems in the critical regime not only are scale invariant, but also a local scale invariance –the conformal invariance– had to be assumed. The link of conformal invariance to statistical mechanics has been put forward in 1984, when *Belavin, Polyakov and Zamolodchikov* (BPZ) [21] presented a wealth of applications and developments in statistical mechanics (for further references see e.g. [125, 88]).
Here, we are not going to give an introduction to conformal invariance. The reader may be advised to [110] where conformal invariance and its importance in the framework of critical phenomena is discussed. In this section we shortly want to address the determination of critical exponents in conformal field theory [29, 41].
The spin-1/2 Heisenberg chain considered in this chapter is known to be conformally invariant in case that no external magnetic field is applied. Switching on such a field results in a breaking of rotational invariance. The system, however, remains gapless and as discussed in [81] the low-energy physics of the Heisenberg model may still be assumed as being governed by conformal field theory (see also *Tsvelik* [201]). Discussing dynamical structure factors (DSFs) $S_{aa}(q, \omega)$ (cf. Sec. 2.6, $a = 3, +, -$) as the Fourier transforms of the zero-temperature dynamical correlation functions [81], the DSF $S_{aa}(q, \omega)$ was shown to have the following behaviour (q_0 denoting the ground state momentum of the Heisenberg chain for fixed magnetization m)

$$S_{aa}(q, \omega) \quad \sim \quad [\omega \pm v(m)(q - q_a(m))]^{-2\alpha_a(m)} \tag{2.16}$$

$$v(m) \quad = \quad \frac{d}{dq} E(q, m, N)\Big|_{q=q_0} = \lim_{N\to\infty} \frac{E(q_0 + 2\pi/N, m, N) - E(q_0, m, N)}{2\pi/N} \tag{2.17}$$

in the vicinity of the *soft modes* (zero energy excitations) at $q_a(m)$, i.e. $S_{aa}(q_a, \omega) \sim \omega^{-2\alpha(m)}$. Here, the critical exponents α_a and η_a of the dynamical and static structure factors (cf. Secs. 2.5, 2.6) are related via

$$\alpha_a(m) \quad = \quad 1 - \Theta_a(m) \tag{2.18}$$

$$\eta_a(m) \quad = \quad 2\Theta_a(m)\,. \tag{2.19}$$

The still unspecified quantities – scaled energy differences $\Theta_a(m)$– are very convenient for finite-size evaluations and will be addressed in more detail in Sec. 2.6.3.
In summary, assuming that conformal invariance describes the low-energy physics of gapless Heisenberg chains, critical exponents for the infrared singularities of static and dynamic structure factors may be determined via the evaluation of the spin wave velocity $v(m)$ and the scaled energy differences $\Theta_a(m)$. It should be mentioned that in the discussion sketched above the dynamical correlation function is proportional to a matrix element $A_a(m)$ which is assumed to be non-vanishing. Otherwise, the correlation function under consideration would not represent the dominant contribution to the considered DSF.
Moreover, it ought to be mentioned that we only assumed the low-energy physics being governed by conformal invariance in situations with broken rotational invariance. We will return to this assumption when reviewing in Sec. 2.6.3 numerical investigations [81] of the obtained relations discussed in this section.
Furthermore, a second investigation on the validity of the above-mentioned assumption concerning conformal invariance, being performed on Heisenberg chains in a magnetic field that are additionally exposed to a next-nearest neighbour coupling ($J_2/J_1 = \alpha$), shall be mentioned here [91]. Good agreement with the predictions of conformal invariance has been found for ($\eta_1(m,\alpha)$: $-1/2 < \alpha < 1/4$), ($\eta_3(m,\alpha) : 0 < \alpha < 1/4$). Deviations from the predictions of conformal invariance and the behaviour of related excitation spectra will be addressed in Chap. 5.
As a final remark we want to mention a work of *Affleck and Haldane* [2] on quantum spin chains and CFT. These authors used a generalized Hubbard model ([118, 16]) representation to show significant differences in the behaviour (existence of energy gaps) for half-odd-integer and integer spin antiferromagnets. We will encouter a similar form of this difference –earlier given as *Haldane's conjecture* [101]– in later discussions of spin-1/2 ladders with an odd/even number of legs.

2.4 Homogeneous external fields – Magnetization curves

The partition function Z of an isotropic nearest-neighbor chain (H_0) in a homogeneous external magnetic field ($\vec{B} = B \cdot \vec{e}_z$), i.e. H_0 commuting with $S_z^{tot} = \sum_x S_z(x)$, is given by

$$Z = e^{-\beta F} = \mathrm{Tr}\, e^{-\beta(H_0 - 2B\cdot M)} \quad ; \quad \beta = \frac{1}{k_B T} \tag{2.20}$$

$$= \mathrm{Tr}\, e^{-\beta 2N(e(m)/2 - Bm)}\,. \tag{2.21}$$

The factor of 2 in eq.2.20 has been chosen to compensate the additional factor 2 in the definition of H_0. At zero temperature the partition function is determined by the minimum of the exponent

$$\min_m\{e(m)/2 - Bm\} = \min_m\{e_0(m)/2 - Bm\} \quad ; \quad e(m) = E(m)/N$$

which yields (in case of differentiability)

$$B(m, T=0) = B(m) = \frac{\partial e(m)/2}{\partial m}\,. \tag{2.22}$$

Furthermore, the theory of thermodynamic equilibrium requires the fulfilment of the stability condition

$$\frac{\partial^2 e(m)}{\partial m^2} \geq 0\,. \tag{2.23}$$

In 1964 the magnetization curve of isotropic Heisenberg chains has as well been calculated for finite chains (*Bonner and Fisher* [32]) and analyzed by means of the Bethe ansatz (*Griffiths*

[96]). A part of these results, namely the smooth behaviour of magnetization curves of a system with a continuous (gapless) spectrum, is sketched in Fig. 2.1. They will later be compared with the corresponding curves of systems that are gapped and show magnetization plateaus.
The isotropic chain, however, has smooth derivatives of $e(m)$, a saturation field $B_{Sat} = 2$ (see also App. B) and the magnetization behaves asymptotically as

$$m(B) \quad \stackrel{B \to B_{Sat}}{\longrightarrow} \quad \frac{1}{2} - \frac{\sqrt{2}}{\pi}(B_{Sat} - B)^{1/2} + O(B_{Sat} - B) \tag{2.24}$$

closely below the saturation field B_{Sat}. This result has been obtained by Bethe ansatz calculations (*Yang and Yang*[220]) and as well been confirmed by finite-size studies [178] where the B-dependence near saturation has been compared with the case of frustrated chains (see Sec. 5.1.2).
Furthermore, the small-B behaviour of $m(B)$ at zero temperature calculated by means of the Bethe ansatz is known to be

$$m(B) \;=\; \frac{B}{\pi^2}\left(\underbrace{1}_{a} + \underbrace{\frac{-1}{2}}_{b}\frac{1}{\ln B} + \underbrace{\frac{-1}{4}}_{c}\frac{\ln|\ln B|}{\ln^2 B} + const. \cdot \frac{1}{\ln^2 B} + \ldots \right) . \tag{2.25}$$

The coefficients a, b, c are given by *Griffiths*[96], *Babujian*[15] and *Lee and Schlottmann*[140], respectively.
Using the above-mentioned results the zero-temperature susceptibility

$$\chi(B) \;=\; \frac{d}{d\,B} m(B) \tag{2.26}$$

for the 2 cases is given in leading order

$$\chi(B \ll 1) \;=\; \frac{1}{\pi^2} \cdot \left(1 - \frac{1}{2\ln B} - \frac{1}{4}\frac{\ln|\ln B|}{\ln^2 B} + \ldots \right) \tag{2.27}$$

$$\chi(B \to B_{Sat}) \;=\; \frac{1}{\sqrt{2}\pi} \cdot \frac{1}{\sqrt{B_{sat} - B}} + \ldots . \tag{2.28}$$

The result $\chi(B = 0) = 1/\pi^2$ will be refered to in Sec. 2.6.8 as one of the sum rules for frequency-moments of the dynamical spin-spin structure factor (see below).
The thermodynamic limit of $e_0(m = 0, N)/2$ is known to be [120]

$$\lim_{N\to\infty} e_0(m = 0, N) \;=\; -\ln 2 + \frac{1}{4} = -0.443147\ldots$$

and will be used in App. C as an illustration for the method of finite-size analysis of *Bulirsch, Stoer* (BST)[36] used throughout this work.
Fig. 2.1 shows the derivatives $\frac{d^n}{dm^n}\frac{e_0(m,N)}{2} = e^{(n)}(m, N))/2$, $n = 0, 1, 2$ and the magnetization curve of the isotropic chain calculated for the finite system lengths $N = 20, 22, \ldots, 28$. Here,

$$e_0^{(1)}(m, N) \;=\; \left(E_0(m_+, N) - E_0(m_-, N)\right)/2 \tag{2.29}$$

$$e_0^{(2)}(m, N) \;=\; N \cdot \left(E_0(m_+, N)\right) - 2E_0(m, N) + E_0(m_-, N)) \tag{2.30}$$

with $m_\pm = m \pm 1/N$ have been used. The magnetization curve (Fig. 2.1d) has been calculated using the Bonner-Fisher (B.-F.) technique [32]. The latter curve coincides with Fig. 2.1c reflected at the bisector of the given area.

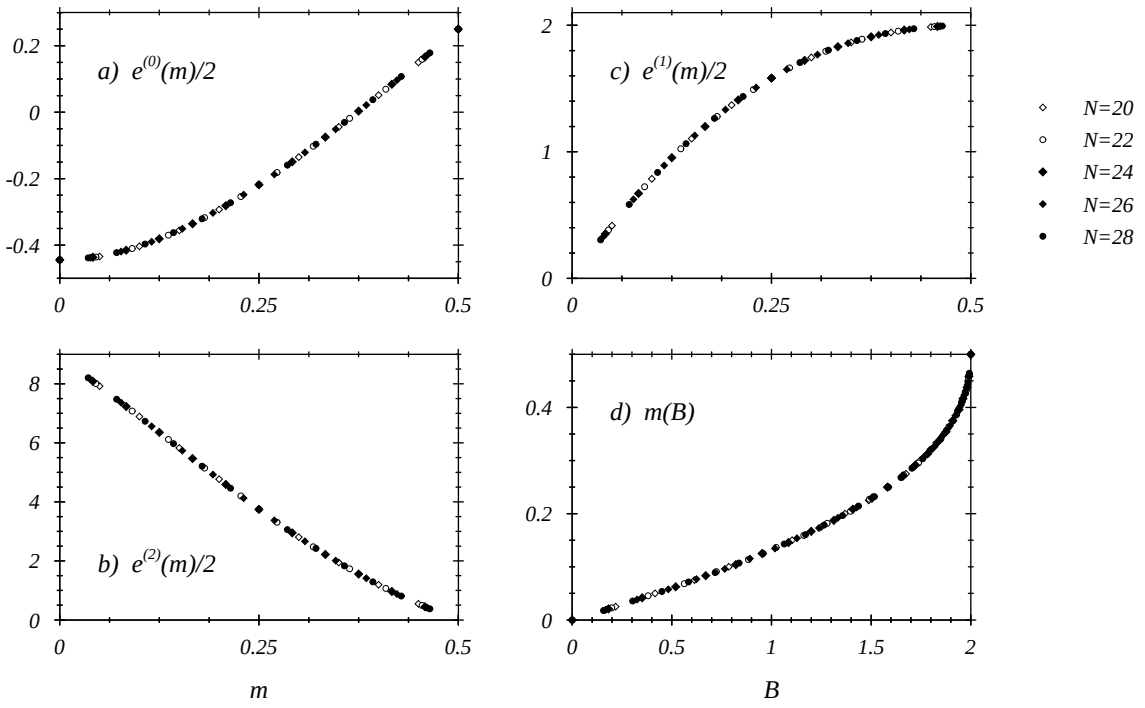

Figure 2.1: Derivatives of $e_0(m, N)/2$, Magnetization $m(B)$

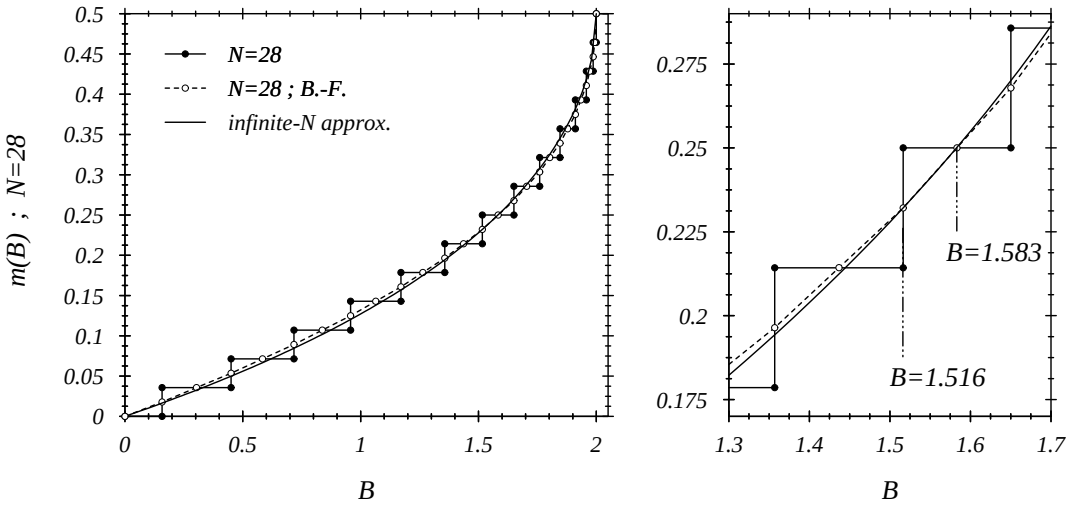

Figure 2.2: Magnetization curve for a 28-site ring and 2 infinite-N approximations (see text)

Magnetization curves calculated by means of the Bonner-Fisher (B.-F.) technique, i.e. connecting the midpoints (open circles in Fig. 2.2 of the finite-N magnetization staircase, agree rather well with another infinite-N approximation given by Müller et al. [157]

$$m(B) \quad = \quad \frac{1}{\pi} \arcsin\left(1 - \frac{\pi}{2} + \frac{\pi}{B}\right)^{-1} \tag{2.31}$$

and in particular well for magnetization $m = 0.25$ as magnified in the figure for the example of a 28-site ring. The given field values will be refered to and used later in this chapter. Without reaching Griffith's rigorousity [96] it is apparent that the range of applicability of the B.-F. technique reaches far beyond.
We finally want to analyze the m-dependence of $e_0(m) = E_0(m)/N$. Due to the behaviour $m(-B) = -m(B)$ of the magnetization a power series

$$e_0(m) \quad = \quad e_0(m = 1/2) + \sum_n A_n \left(\frac{1}{2} - m\right)^n \tag{2.32}$$

consists of odd powers of n exclusively. This is illustrated for $H = 2\sum_n (\mathbf{S}_n \mathbf{S}_{n+1} - BS_3(n))$ and system sizes $N = 20, 22, .., 28$ in Fig. 2.3

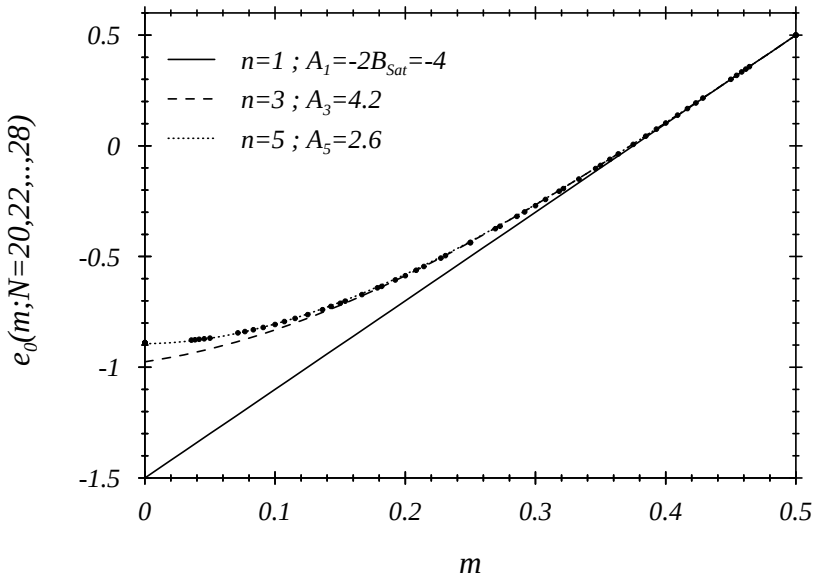

Figure 2.3: Ground state energy per site $e_0(m)$ vs. m

where subsequently the first 3 odd powers of $(1/2 - m)$ have been taken into account. In particular, the coefficient A_1 –together with the pre-factor 2 in H (Eq. 2.1)– is given by

$$A_1 \quad = \quad -\frac{d\, e_0(m)}{dm}\bigg|_{m=1/2} = -2B_{Sat} = -4 \tag{2.33}$$

($B_{Sat} = 2$ cf. App. B). A situation of particular interest –the almost linear behaviour of $e_0(m)$ close to $m = 1/2$– will again show up in the discussion of ladder systems (see Sec. 4.1.3).

2.5 Static correlations and structure factors (SSFs)

The investigation of ordering and spatial correlations in the ground state of quantum spin Heisenberg chains is nearly as old as the formulation of the model. Independent of the smallness of the quantum spin ($S = 1/2$, i.e. the extreme quantum limit), the classical Heisenberg antiferromagnet with its perfectly *Néel*-ordered ground state quite often served as a reference point in the discussion of the quantum chain/system.
At this place, only a few remarks on static quantities that will later appear to be closely related to zero-energy excitations (**soft modes**) of the Heisenberg chain will be presented.
In order to discuss translational invariant systems and in particular their spatial correlations the consideration of Fourier-transformed (with respect to chrystal momentum q) quantities often

proves to be very efficient. In the following we consider static structure factors (SSFs)

$$S_{aa}(q,m,N) \equiv <0|S_a^+(q)S_a(q)|0> \quad , \quad a=z,+,- \tag{2.34}$$

with

$$S_a(q) = \frac{1}{\sqrt{N}}\sum_{x=0}^{N-1} e^{iqx}S_a(x) \tag{2.35}$$

$$S_a(x) = \frac{1}{\sqrt{N}}\sum_{q=0}^{2\pi-2\pi/N} e^{-iqx}S_a(q) \tag{2.36}$$

$$\sum_q e^{iq(x-x')} = N\cdot\delta_{x,x'} \tag{2.37}$$

and $|0>$ being the ground state of an N-site chain with magnetization m. The SSF is given as

$$S_{aa}(q,m,N) = \frac{1}{N}\sum_{x,x'} e^{iq(x-x')} <0|S_a^+(x')S_a(x)|0> \tag{2.38}$$

$$= \sum_x e^{iqx} <0|S_a^+(0)S_a(x)|0> \tag{2.39}$$

where translational invariance has been used in the second part. Furthermore, S_{++} and S_{--} are related by the operator identity

$$S_{++}(q,m,N) = S_{--}(q,m,N) - 2m\,. \tag{2.40}$$

The transverse spin-spin SSF is given by

$$S_{xx}(q,m,N) = \frac{1}{4}(S_{++}(q,m,N)+S_{--}(q,m,N))$$

and will be discussed later. Finally it should be mentioned that in case of

$$S_a(q=0)|0> = \alpha_a(0)|0>$$

with $\alpha_a(0)\neq 0$ usually the connected part of the SSF

$$S_{aa,conn.}(q,m,N) = <0|S_a^+(q)S_a(q)|0> - |<0|S_a(q)|0>|^2$$

is considered in order to avoid peaks at $q=0$ (e.g. $\alpha_z(0)=\sqrt{N}\cdot m$).

2.5.1 Numerical results, scaling and critical exponents of the spin-spin SSF

In this paragraph investigations of singularities of SSFs –based on evaluations of rings of up to 28/(36) sites– are briefly presented and summarized –for more detailed studies and further references see e.g. [128, 131, 179].
Fig. 2.4 sketches important aspects of the behaviour of SSFs of rings in zero and non-zero magnetic field, the latter exemplified for the case of magnetization $m=1/4$ which is realized for all chain lengths $N=4n$. In this particular case, the 2 field-dependent positions

$$q_x(m)\equiv q_1(m) = 2\pi m \tag{2.41}$$

$$q_z(m)\equiv q_3(m) = \pi(1-2m) \tag{2.42}$$

of singularities in the longitudinal and transverse SSFs coincide at $q=\pi/2$.

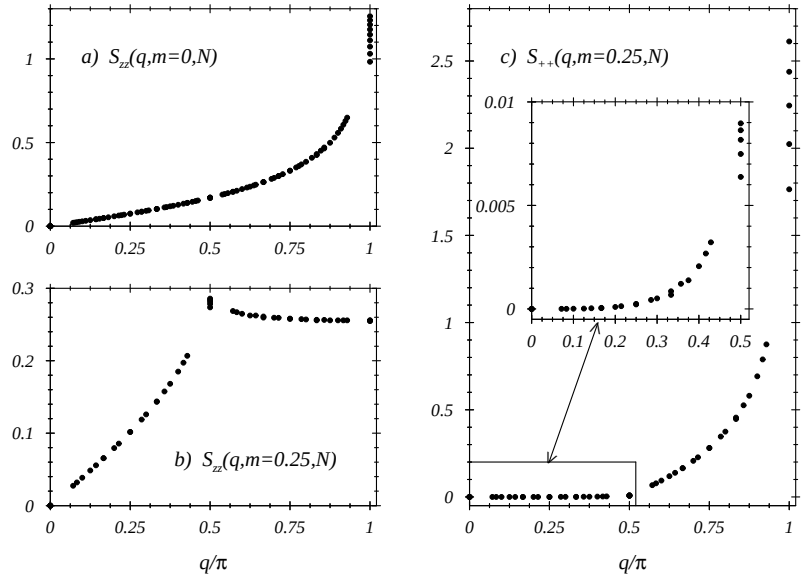

Figure 2.4: Static structure factors (SSFs) for $m = 0,\ 1/4$

The main point of attention in this section is the classification of the singular behaviour of the SSFs in the vicinity of the critical q-values $q = \pi$ and $q_{1,3}(m)$ here in particular considered for $m = 0$ and $m = 1/4$.
This will be quantified by the η-exponents η_1, η_3. The transverse SSF at momentum π behaves as

$$S_{xx}(q = \pi, m, N) \quad \stackrel{N\to\infty}{\longrightarrow} \quad const. \cdot N^{1-\eta_1(m)} \tag{2.43}$$

and the same exponent is found to describe the approach to the singularity

$$S_{xx}(q, m, \infty) \quad \stackrel{q\to\pi}{\longrightarrow} \quad const.' \cdot \left(1 - \frac{q}{\pi}\right)^{-(1-\eta_1(m))} \tag{2.44}$$

The case $m = 0$, where no further singularities between 0 and π are present, is well known. *Luther and Peschel* (1975) [147] showed for the large distance behaviour of the spin-spin correlators $< 0|\mathbf{S}(0)\mathbf{S}(x)|0 >$ of the isotropic Heisenberg chain

$$< 0|\mathbf{S}(0)\mathbf{S}(x)|0 > \quad \sim \quad \frac{(-1)^x}{x}\,, \tag{2.45}$$

i.e. logarithmic behaviour of the SSF-components (ses Sec. 2.5). Fig. 2.5 gives the almost linear behaviour in the accordingly chosen logarithmic variables expressing $\eta_1(m = 0) = \eta_3(0) = 1$. (A discernible signature of a later determined additional factor of order $(\ln N)^{1/2}$ (*Affleck et al.* (1988) [3]) to expression 2.45 lies beyond the scope of the present treatment.)
Turning now to the case $m = 1/4$, the field-dependent singularities deserve a separate discussion. Two different types of behaviour have been esstablished [81]. First, the transverse SSF shows a different exponent $(\eta_1^{\pm}(m))$ when approaching $q_1(m)$ from below $(\eta_1^{-}(m))$ or above $(\eta_1^{+}(m))$:

$$S_{xx}(q \to q_1(m) \pm 0, m, \infty) \quad \sim \quad \left|1 - \frac{q}{q_1(m)}\right|^{-(1-\eta_1(m))} \tag{2.46}$$

with exponents (cf. Fig. 2.6) $\eta_1^{-}(1/4) = 0.8 \ldots 1.2$ and $\eta_1^{+}(1/4) = 2.17$. A determination of $\eta_1(m = 1/4)$ had to be omitted since it would have required considerably longer chains. Looking

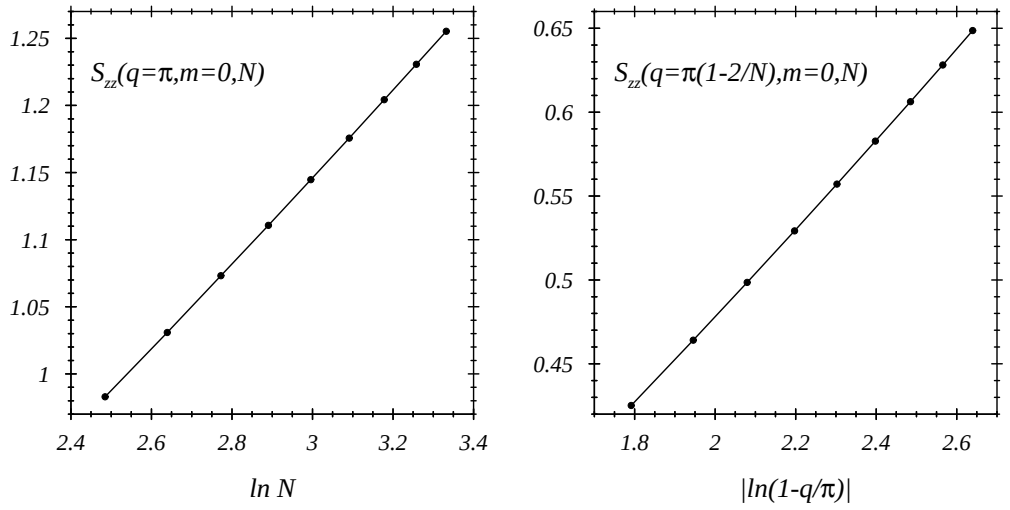

Figure 2.5: Scaling of the longitudinal SSF $S_{zz}(q, m = 0, N)$

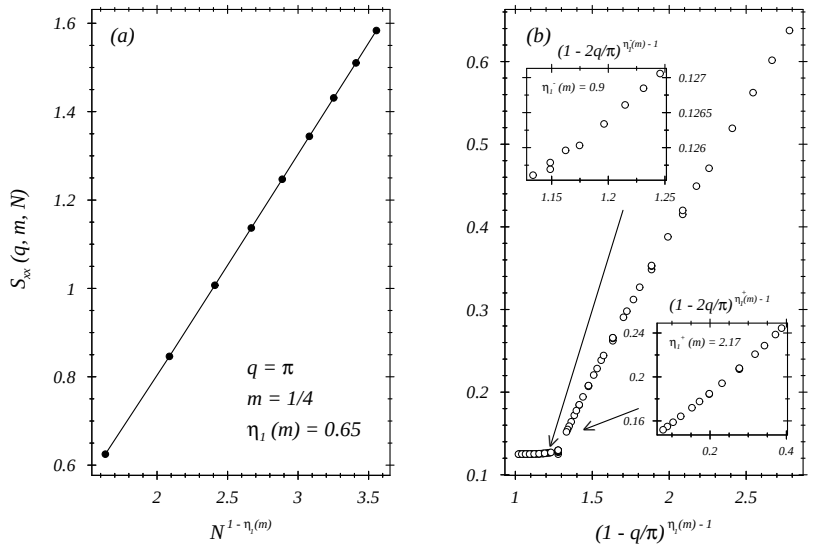

Figure 2.6: Scaling of the transverse SSF $S_{xx}(q, m = 1/4, N)$

at the given range of numerical values to assign an $\eta_1^-(1/4)$-exponent (based on the given chain lengths) a similar comment seems to be deserved.
The exponent $\eta_1(m = 1/4)$, given in 2.43, could be determined to be $\eta_1(m = 1/4) = 0.65$ (see left panel of Fig. 2.6).
Results for the longitudinal SSF are summarized in Fig. 2.7. Here, the assignment of an η-exponent for the approach of $q_3(m = 1/4)$ from the right (starting from greater q-values) turned out to be problematic on the basis of the calculated data. On the other hand, the two remaining cases (from the left; at the singularity) led to a reliable and equal-valued exponent $\eta_3(m = 1/4) = 1.51$. The approach of the singularity from the right –assuming coincidence of the η-exponent– is shown in the inset on the r.h.s. of Fig. 2.7.

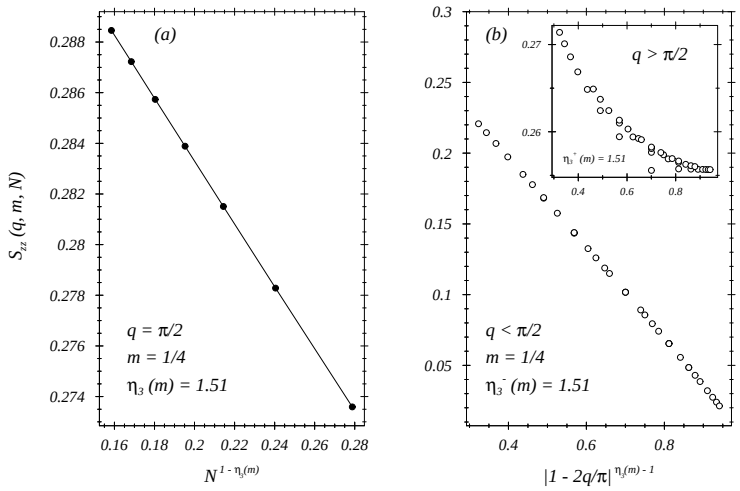

Figure 2.7: Scaling of the longitudinal SSF $S_{zz}(q, m = 1/4, N)$

At the end of this section we shall return to relation 2.39. It provides a link between the large distance behaviour of spin-spin correlators and a Fourier transform of the singularities of the SSFs in particular. Taking into account all the singularities of the spin-spin SSFs an obvious generalization of 2.45 reads:

$$< 0|S_1(0)S_1(x)|0 > \quad \stackrel{x\to\infty}{\longrightarrow} \quad \cos(\pi x)\frac{A_1(m)}{x^{\eta_1(m)}} + \cos(q_1(m)x)\left(\frac{A_1^+(m)}{x^{\eta_1^+(m)}} + \frac{A_1^-(m)}{x^{\eta_1^-(m)}}\right) \quad (2.47)$$

$$< 0|S_3(0)S_3(x)|0 >_{disc.} \quad \stackrel{x\to\infty}{\longrightarrow} \quad \cos(q_3(m)x)\frac{A_3(m)}{x^{\eta_3(m)}}\,. \quad (2.48)$$

In the sequel of the next section the relation between these critical $\eta(m)$-exponents (eqns. 2.47,2.48) and scaled energy gaps of the spin chain, as predicted by conformal field theory (CFT) (see Sec. 2.3), will be considered.

2.6 Dynamical structure factors (DSFs)

A quite general definition of zero-temperature DSFs for systems with a unique ground state reads:

$$X_{aa}(q,\omega,N,T=0) \quad = \quad \sum_n |< n|X_a(q)|0 > |^2 \cdot \delta(\omega - (E_n - E_0)) \quad (2.49)$$

$$\left(= \frac{1}{2\pi}\frac{1}{N}\sum_{x,x'} e^{iqx}\int_{-\infty}^{\infty} dt\, e^{i\omega t} < 0|X_a^+(x',t)X_a(x+x',0)|0 > \right) \quad (2.50)$$

with $|0>$ being the ground state and $|n>$ the whole set of eigenstates of the considered dynamical system (in our case given by the Hamiltonian H_0). Moreover, $X_a(x,t) = e^{-iHt}X_a(x,0)e^{iHt}$ and the familiar transformations

$$X_a(q) \quad = \quad \frac{1}{\sqrt{N}}\sum_{x=0}^{N-1} e^{iqx}X_a(x) \quad (2.51)$$

$$X_a(x) = \frac{1}{\sqrt{N}} \sum_{q=0}^{2\pi-2\pi/N} e^{-iqx} X_a(q) \tag{2.52}$$

$$\sum_q e^{iq(x-x')} = N \cdot \delta_{x,x'} \tag{2.53}$$

are used with discrete q-values $q = n \cdot (2\pi/N)$, $n = 0, 1, \ldots, N-1$.
The particular choice of X_a now determines which subsets of eigenstates contribute to the sum of excitations in 2.49. In case of the isotropic Heisenberg chain the spin-spin DSF, i.e. $X_a(q) = S_z(q), S_+(q), S_-(q)$, i.e. $a = z, +, -$, contains the most important information about the spectrum as will be discussed below. Strong restrictions on the occurrence of non-vanishing contibutions to 2.49 are given by the selection rules

$$< S_z|S_z(q)|S'_z > = 0 \quad \text{if } S_z \neq S'_z \tag{2.54}$$

$$< S_z|S_\pm(q)|S'_z > = 0 \quad \text{if not } S'_z = S_z \pm 1 \tag{2.55}$$

$$< k|S_a(q)|k' > \sim \delta_{k,k'+q \bmod 2\pi} \tag{2.56}$$

$$< S|S_a(q)|S' > = 0 \quad \text{if} \begin{cases} |S - S'| \neq 0, 1 \\ S = S' = 0 \end{cases} . \tag{2.57}$$

For example, the given rules state that finite non-diagonal components $(S_{+-}, S_{z+}, \ldots)$ do not exist.
Moreover, the static structure factors (SSFs) $X_{aa}(q, T = 0)$ already discussed are given by

$$X_{aa}(q) = \int d\omega \, X_{aa}(q, \omega) = \sum_n | < n|X_a(q)|0 > |^2 \tag{2.58}$$

which shows that all non-vanishing excitations add up to the SSF where the dominant contributions arise from the dominant elements of the DSF which will be explained below. In doing so, a particular importance will be atributed to the form of singularities of the DSF that will be deduced from the finite-size data obtained from numerical calculations based on spin chains of up to 28 sites.
Finally, some interesting examples of operators $X_a(q)$ with a different selection of non-zero transition matrix elements $< n|X_a(q)|0 >$ shall be given. The following operators do neither change total spin S nor total S_z, the latter not even changes the momentum of the state it is acting upon:

$$D_j(q) = \frac{1}{\sqrt{N}} \sum_x e^{iqx} \mathbf{S}(x) \cdot \mathbf{S}(x+j) \quad j = 1, 2, \ldots \tag{2.59}$$

$$O(q) = \mathbf{S}(-q) \cdot \mathbf{S}(q) . \tag{2.60}$$

These operators will be used in part in later chapters of this work.

2.6.1 Excitation spectra, Soft modes

As a starting point for the discussion Fig. 2.8 shows a classification of the excitation energies $\omega_n(q, m) = E_n(q, m) - E_0(m)$ $(m = S_z/N)$ for a 12-site chain $(H_0 = 2\sum_i \mathbf{S}_i\mathbf{S}_{i+1})$ and magnetization values $m = 0, 1/4$. The complete range of the excitation spectra has been truncated roughly to half of its extent, however, within the shown part all excitations and a classification of their respective total spins S are given. In addition, the left-hand part of the figure (case $m = 0$) shows the *des Cloizeaux-Pearson* [48] lower bound of excitations for the $N \to \infty$ isotropic $(m = 0)$ Heisenberg ring.

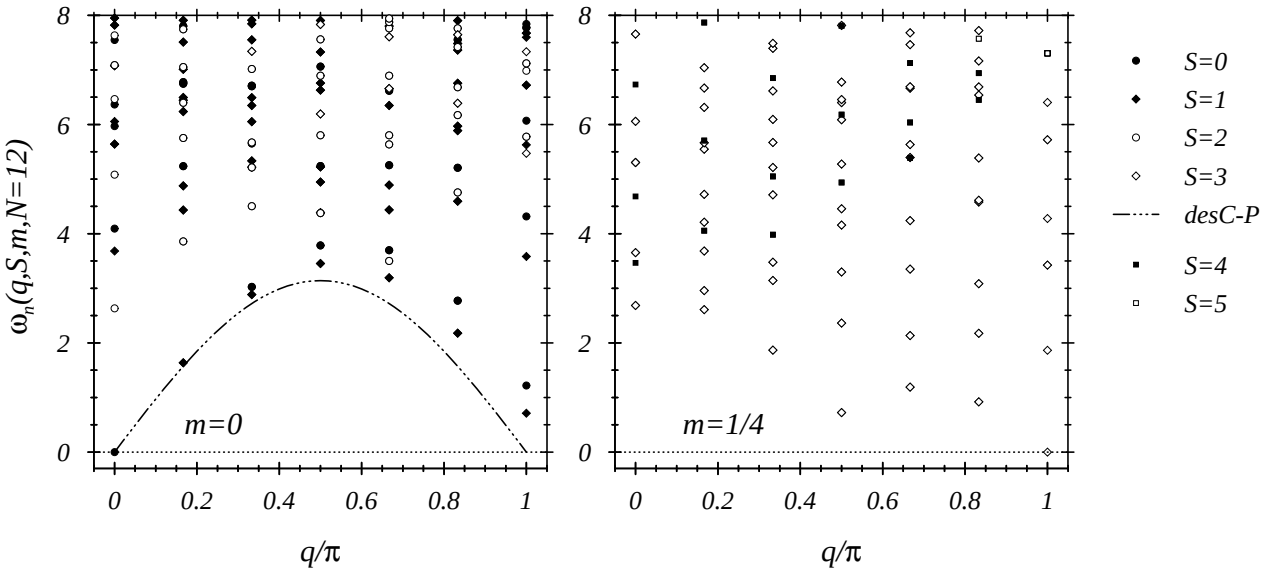

Figure 2.8: Complete diagonalization results for low excitations $\omega_n(q, S, m)$ of a 12-site chain

First of all, the 2 plots show that the ground states ($\omega_n = 0$) have total spins $S = N \cdot m = S_z$ and momenta $p_0(m)$ according to relation 2.9. Moreover, the lowest lying excitations in both cases are those that can contribute to the spin-spin DSF according to selection rule 2.57 as far as the total spin is concerned.
Second, the lowest excitations in the $m = 0$- case already show a reasonable approximation ($q > 0$) to the $N \to \infty$ limiting curve of des Cloizeaux-Pearson which becomes more clearly for longer chains (see $N = 28$ in Sec. 2.6.3).
Anticipating further features, the figure already shows traces of the zero-frequency excitations (**soft modes**) of the infinite system ($q = 0, \pi$ for $m = 0$; $q = q_z(m) = \pi(1 - 2m) = \pi/2 = q_x(m) = 2\pi m$, π for $m = 1/4$). The relation of these soft modes to symmetries of the underlying Heisenberg Hamiltonian and further important conclusions will be given in the next paragraph.

2.6.2 The *Lieb, Schultz, Mattis* construction

In 1961 Lieb, Schultz, Mattis (LSM) [143] showed that an antiferromagnetic spin-1/2 Heisenberg chain with an even number of sites has a non-degenerate ground state (i.e. total spin $S = 0$, momentum $q_0 = 0$ or π). Then, they addressed the important question of the existence of an energy gap above the ground state energy that will later be discussed for the more general case of magnetization $m > 0$. They introduced an operator (their notation is partly changed in the following)

$$U_k = e^{ik\sum_n nS_z(n)} \quad , \quad \left[S_z(n), S_z(n')\right] = \delta_{n,n'} \cdot \frac{1}{4} \cdot \mathbb{1} \tag{2.61}$$

$$= \prod_n e^{iknS_z(n)} \tag{2.62}$$

$$= \prod_n \left((\cos\frac{kn}{2}) \cdot \mathbb{1}_n + i(\sin\frac{kn}{2}) \cdot \sigma_z(n) \right) \tag{2.63}$$

with

$$U_k^{-1} S_x(n) U_k = \cos(kn) S_x(n) + \sin(kn) S_y(n) \tag{2.64}$$

$$U_k^{-1} S_y(n) U_k = -\sin(kn) S_x(n) + \cos(kn) S_y(n) \quad (2.65)$$
$$U_k^{-1} S_z(n) U_k = S_z(n)\,. \quad (2.66)$$

The states

$$|\Psi_k> \equiv U_k|\Psi_0> \quad , \quad (|k>= U_k|0>) \quad (2.67)$$

with $|0>$ being the non-degenerate ground state of $H_0 = \sum_n \mathbf{S}(n)\mathbf{S}(n+1)$ with $S_z = S = 0$. $|\Psi_k>$ has been shown to be orthogonal to the ground state ($<0|k>=0$) for momenta $k = 2\pi j/N$ with odd integer j. Restricting to the smallest permitted k-value ($k = 2\pi/N$) and making explicit use of $[H_0, S_z] = 0$, Lieb, Schultz, Mattis showed the following inequality for the energy difference $\Delta E =< 0|U_k^{-1} H_0 U_k|0> - <0|H_0|0>$ to hold:

$$\Delta E = (\cos(k) - 1) \sum_n <0|S_x(n)S_x(n+1) + S_y(n)S_y(n+1)|0> \leq \frac{2\pi^2}{N}\,. \quad (2.68)$$

Therefore, for infinite N no finite energy gap remains. The authors as well discussed generalizations to more than one dimension.

As was already mentioned in Sec. 2.1, the spin-1/2 chain retains the non-degenaracy of its ground states under the influence of a uniform magnetic field for magnetizations $m > 0$. The application of the LSM scheme, and in particular the determination of the momentum of the state $|k>$ has been given explicitely by *Oshikawa et al.* (1997) [169] and results directly from applying the generalized LSM-relation

$$T U_k T^{-1} = e^{i\pi j} e^{ikNm} \cdot U_k \quad , \quad k = 2\pi j/N \quad (2.69)$$

(here T is the translation operator defined in Sec. 2.1) to

$$T U_k|0> = T U_k T^{-1} T|0> = e^{-ip_0} T U_k T^{-1}|0> \quad (2.70)$$
$$= e^{-ip_0} e^{i\pi j} e^{ikNm} U_k|0> \quad (2.71)$$
$$= e^{-i(p_0 + j\cdot\pi(1-2m))} U_k|0> \quad (2.72)$$
$$= e^{-ip_j} U_k|0>\,. \quad (2.73)$$

The resulting momenta p_j are the momenta of the longitudinal soft modes that will be further discussed in the sequel of this chapter as well as demonstrated for finite-N evaluations in the next subsection. At present, however, we are not able to specify the precise nature of the state approaching the ground state energy and forming the soft mode, i.e. classifying what type of gap does not exist. The method so far only gives information about the existence of an additional state $U_k|0>$ – the soft mode.
Below, we apply the LSM scheme to obtain further information on the total spin of the soft mode. Before addressing this point we briefly want to add that for general m the required orthogonality condition for $<\Psi_0|\Psi_k>=0$ reads

$$e^{i\pi j(1-2m)} \neq 1\,, \quad (2.74)$$

including the choice of odd integers j for $m = 0$.

A final point that may be elucidated with the help of LSM in this context concerns the total spin of the additionally generated soft mode states $|k>= U_k|0>$ [86]. One calculates

$$<0|U_k^{-1}\mathbf{S}^2 U_k - \mathbf{S}^2|0> = 2\sum_{n<n'} \big(\cos(kn)\cos(kn') - 1\big) \cdot <0|S_x(n)S_x(n') + S_y(n)S_y(n')|0>\,. \quad (2.75)$$

Introducing

$$|f^c_{k,x}> = \frac{1}{\sqrt{N}}\sum_n \cos(kn) S_x(n)|0> \tag{2.76}$$

$$S^c_{xx}(k) \equiv < f^c_{k,x}|f^c_{k,x}> = \frac{1}{N}\sum_{n,n'} \cos(kn)\cos(kn') < 0|S_x(n)S_x(n')|0> \tag{2.77}$$

$$= \sum_n \cos(kn) < 0|S_x(n)S_x(0)|0>, \tag{2.78}$$

the difference of total spin expectation values for the states $|0>$ and $|k>$ can be expressed as

$$< 0|U_k^{-1}\mathbf{S}^2 U_k - \mathbf{S}^2|0> = N\left(S^c_{xx}(k) - S^c_{xx}(0) + S^c_{yy}(k) - S^c_{yy}(0)\right) \tag{2.79}$$

$$= 2N\left(S^c_{xx}(k) - S^c_{xx}(0)\right) \tag{2.80}$$

with

$$S^c_{xx}(k) = \frac{1}{2}\left(S_{xx}(k) + S_{xx}(-k)\right) \tag{2.81}$$

$$S_{xx}(k) = \sum_n e^{ikn} < 0|S_x(n)S_x(0)|0> . \tag{2.82}$$

While this itself does not give a definite answer, the consideration of the static structure factors (e.g. as discussed in Sec. 2.5) allows for the discussion of a small-k behaviour of

$$2N\left(S_{xx}(k = 2\pi/N, m) - S_{xx}(0, m)\right) \overset{N\to\infty}{\longrightarrow} A(m)\left(\frac{2\pi}{N}\right)^{\beta_k(m)} . \tag{2.83}$$

E.g. at $m = 0$ the right-hand side of Eq. 2.79 is non-vanishing, demanding that the soft mode state $|k>$ has total spin components greater than 0, i.e. excluding the existence of a singlet-triplet gap. The occurrence of $\beta_k(m > 0) > 0$ (see e.g. [131]) indicates that in this case the soft mode state $|k>$ has the same total spin as the ground state $|0>$.

The LSM construction and its generalizations introduced here for the (unperturbed) Heisenberg chain will be frequently refered to and applied to the more general cases evolving in the sequel of this work. In particular, we will later (see Sec. 5.3) discuss the application of the presented scheme to the case of translation invariant spin systems with long range couplings. We will show connections to plateau formations and the related spontaneous symmetry breaking in these systems.

2.6.3 Numerical results, scaling and critical exponents of the spin-spin DSF

In this section first there will be presented some numerical results for the spin-spin DSF in both zero and non-zero external magnetic field (the latter for a resulting magnetization of $m = 1/4$). Then, results of finite-size scaling applications on the determination of different types of critical quantities (see below) will be summarized.
Figs. 2.9,2.10 show excitation energies $\omega_{aa,n}(q, m, N)$ and a binning of relative weigths

$$\mathrm{w}_{aa,n}(q, m, N) = \frac{\mathrm{w}^{tot}_{aa,n}(q, m, N)}{S_{aa}(q, m, N)} = \frac{|< n|S_a(q)|0>|^2}{< 0|S^+_a(q)S_a(q)|0>} \quad , \quad a = z, +, - \tag{2.84}$$

where $|0>$ is the ground state for magnetization m and chain length N. Here, the maximum value $N = 28$ for the presented calculations has been chosen. The legend given on the left-hand side of Fig. 2.9 applies for all 4 plots. The use of relative weigths, i.e. the indepent normalization

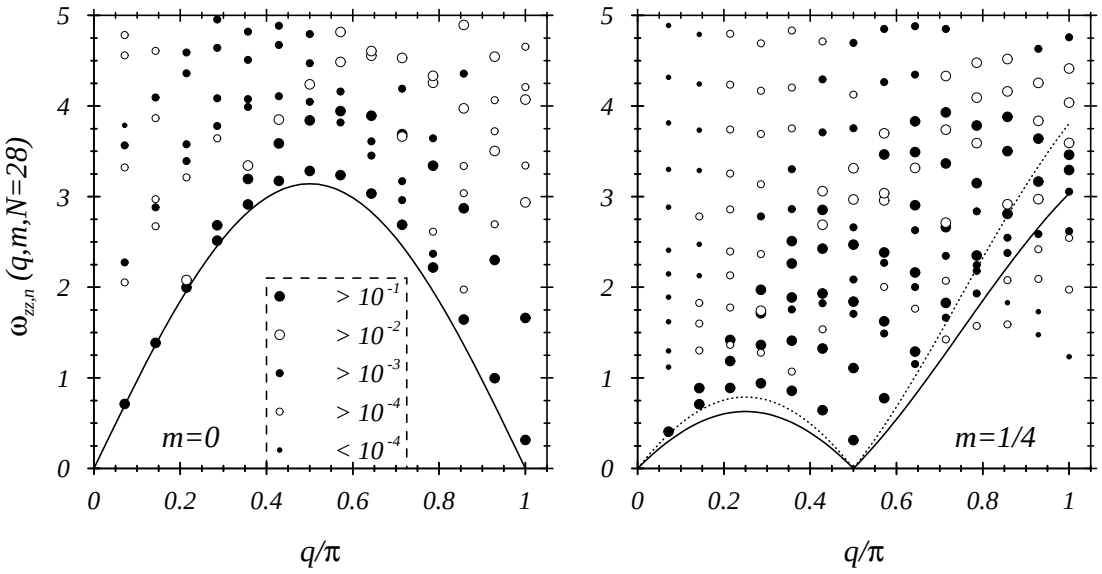

Figure 2.9: Excitations $\omega_{zz,n}(q, m = 0, 1/4, N = 28)$

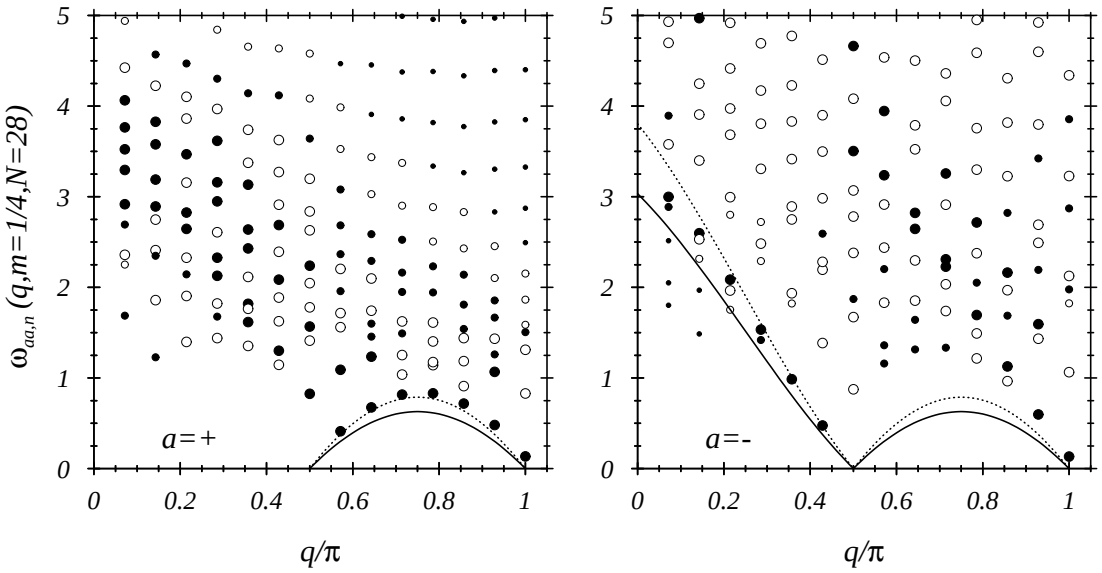

Figure 2.10: Excitations $\omega_{aa,n}(q, m = 1/4, N = 28)$ with $a = +, -$

of matrix elements $< n|S_a(q)|0 >|^2$ for each q-value, requires the additional consideration of the static structure factors (SSFs) given in Sec. 2.5 to get a general impression on the proportions of the DSFs.
The numerical evaluations of $\omega_{aa,n}$, $w_{aa,n}$ have been done using a recursion algorithm that is presented in Appendix A. The ground states needed for the application of the algorithm were calculated with *Lanczos*-techniques [139, 53] using a *Lin*-coding [145].

The excitation spectrum for zero magnetic field again shows the $N \to \infty$ lower boundary of the

energy spectrum [48] and the degree of its approximation may be contrasted with the spectrum of the 12-site chain given above. The symbols underline the dominance of weight carried by the lowest excitations.
For non-zero magnetic fields no boundaries as rigorous as des Cloizeaux-Pearsons do exist. The lines given in the concerning parts of the figures go back to Müller et al. (1981) [157] where lower boundaries of spin-wave continua have been given. These need the relation $B(m)$ and the 2 types of lines in the figures refer to the 2 cases shown in Fig. 2.2 (solid line: B=1.516; dashed line: B=1.583). Bounds for $\omega_{++}(q < \pi/2, m = 1/4, N)$ have not been given since in that region the absolute weights $\mathrm{w}_{++,n}(q, m, N) \cdot S_{++}(q, m, N)$ are almost zero (see SSF in Fig. 2.4). The most striking omission of the given boundaries may be seen in their disregard of low excitations $\omega_{zz,n}(q, m, N)$ below $q = \pi$. The existence of a soft mode at $q = \pi$ was derived by the Lieb, Schultz, Mattis argument [143] (cf. Sec. [143]), however, with no specification of the related weight. (In the numerical part of the work of Müller et al. these excitations do not appear due to limitations of managable system sizes ($N \leq 10$).)

In order to clearify and define expressions for the remaining part of this paragraph we use

$$q_1^{\pm}(m) = q_1(m) \pm \Delta_p \quad , \quad \Delta_q = \frac{2\pi}{N} \quad , \quad m^{\pm} = m \pm \frac{1}{N} = \frac{S_z}{N} \pm \frac{1}{N} \tag{2.85}$$

$$\begin{aligned} \omega_{zz}(q_3(m), m, N) &= E(q_0 + q_3(m), m, N) - E(q_0, m, N) && (2.86)\\ \omega_{xx}(\pi, m, N) &= E(q_0 + \pi, m^+, N) - E(q_0, m, N) && (2.87)\\ \omega_{\pm\pm}(q_1^{\pm}(m), m, N) &= E(q_0 + q_1^{\pm}(m), m^{\pm}, N) - E(q_0, m, N) && (2.88) \end{aligned}$$

where q_0, the ground state momentum for magnetization m, is $q_0 = 0, \pi$ according to the rules given in Sec. 2.9 and the ω_{aa} therefore belong to the lowest excitations which are going to become soft for infinite N. Extrapolating $N\omega_{aa}$ to the thermodynamic limit (TDL), namely

$$\begin{aligned} \Omega_3(m) &\equiv \lim_{N\to\infty} N\omega_{zz}(q_3(m), m, N) && (2.89)\\ \Omega_1(m) &\equiv \lim_{N\to\infty} N\omega_{xx}(\pi, m, N) && (2.90)\\ \Omega_1^{\pm}(m) &\equiv \lim_{N\to\infty} N\omega_{\pm\pm}(q_1^{\pm}(m), m, N) && (2.91) \end{aligned}$$

leads to the relation

$$\Omega_1^{\pm}(m) = \Omega_1(m) + \Omega_3(m) \tag{2.92}$$

and, using the spin-wave velocity $v(m)$

$$v(m) = \frac{d}{dq} E(q, m, N)\Big|_{q=q_0} = \lim_{N\to\infty} \frac{E(q_0 + \Delta_q, m, N) - E(q_0, m, N)}{\Delta_q}\,, \tag{2.93}$$

finally leads to the definition of the *scaled energy gaps*

$$\begin{aligned} 2\Theta_a(m) &\equiv \frac{\Omega_a(m)}{\pi v(m)} \quad , \quad a = 1, 3 && (2.94)\\ 2\Theta_1^{\pm}(m) &\equiv \frac{\Omega_1^{\pm}(m)}{\pi v(m)} = 2\left(\Theta_3(m) \pm \Theta_1(m)\right)\,. && (2.95) \end{aligned}$$

Fig. 2.11 gives results for the m-dependence of $2\Theta_{1,3}(m)$ based on a Bethe ansatz (BA) evaluation of a spin chain of 2048 spins [81] which is in accord with and supplemented by analytical

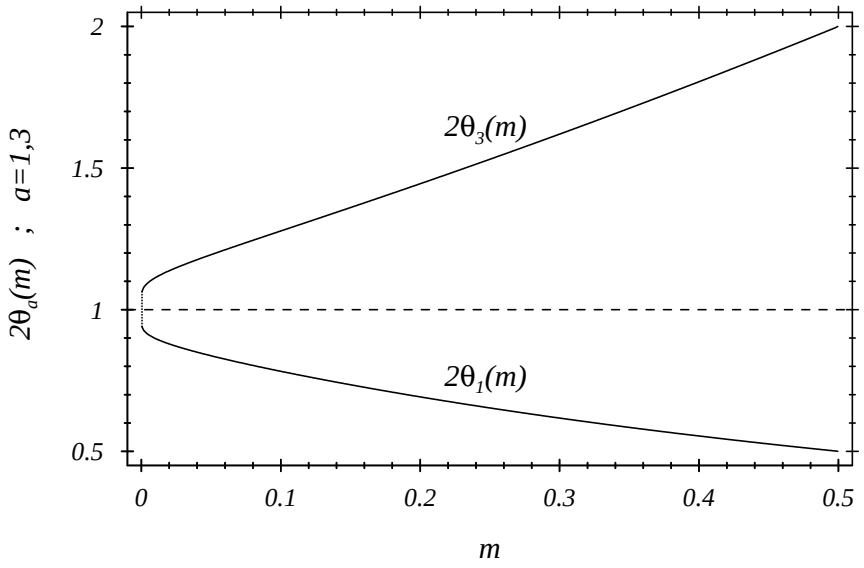

Figure 2.11: Scaled energy gaps $2\Theta_1(m)$, $2\Theta_3(m)$

results of *Bogoliubov, Izergin, and Korepin* (1986, 1987) [29, 30], namely

$$2\Theta_1(m) \quad = \quad \frac{1}{2\Theta_3(m)} \tag{2.96}$$

$$2\Theta_3(m) \quad \stackrel{m\to 0}{\longrightarrow} \quad 1 + \left(\ln \frac{1}{m^2}\right)^{-1} \tag{2.97}$$

$$2\Theta_3(m) \quad \stackrel{m\to 1/2}{\longrightarrow} \quad 1 + 2m\,. \tag{2.98}$$

In particular, the $2\Theta_a(m)$ values for the 2048-spin chain evaluated with BA methods for magnetization $m = 1/4$ read

$$2\Theta_1(m = 1/4) = 0.65308\ldots \quad , \quad 2\Theta_3(m = 1/4) = 1.58584\ldots$$
$$2\Theta_1^+(m = 1/4) = 2.23892\ldots \quad , \quad 2\Theta_1^-(m = 1/4) = 0.93276\ldots$$

which might serve for comparison.
Using the critical quantities $2\Theta(m)$, $\eta(m)$ and in addition α the exponent of the infrared singularity of the DSF that had been treated in the finite-size scaling ansatz [81]

$$S_{aa}(\omega, q, m, N) \quad = \quad \omega^{-2\alpha_a(q,m)} g_a \left(\frac{\omega}{\omega_a(q, m, N)}, n_a(q, m, N)\right) \quad , \quad a = 3, +, - \tag{2.99}$$

$$n_a(q, m, N) \quad = \quad (q - q_a(m))/\Delta_q \tag{2.100}$$

the prediction

$$2\Theta(m) \quad = \quad \eta(m) = 2(1 - \alpha(q, m)) \tag{2.101}$$

of CFT has been tested for the case of magnetization $m = 1/4$ [81].
The results, listed in Table 2.1, show a good agreement of the listed critical quantities for the first two cases with deviations lying within numerical uncertainty. The finite-size dependence of the weight of the lowest excitation dominantly influencing the value of α is seemingly in

q	a	$2\Theta_a^{(\pm)}(m)$	$\eta_a^{(\pm)}(m)$	$2(1-\alpha_s(q,m))$	s
$q_3(m)$	3	1.5312	1.51	1.54	3
π	1	0.6531	0.65	0.62 | 0.68	+|−
$q_1^+(m)$	1	2.1843	2.17	2.40	+
$q_1^-(m)$	1	0.8781	0.8-1.2	2.1	−

Table 2.1: Critical quantities $2\Theta(m)$, $\eta(m)$ and $2(1-\alpha(m))$ at soft-mode positions for $m = 1/4$

accordance with the prediction of CFT. In the 3rd case the exponent $2(1-\alpha_+(q_1^+(m),m))$ is about 15% greater than the remaining two ones that agree rather well.
Only in the last case, where the former dominance of the lowest excitations in carrying the major part of spectral weight is no longer manifest, numerical data cannot establish identity 2.101.

Now, we will intermediately leave the subject of spin chains exposed to a uniform magnetic field and turn to an important topic of the field-free model, analytical ansätze for the dynamical structure factor (DSF), that so far still long for an extension to finite magnetic fields.

2.6.4 The *Müller* ansatz (MA) for the spin-spin DSF

On the basis of finite-size calculations (DSF for small rings), matching of infrared exponents and sum rule considerations *Müller et al.* [156] proposed in 1981 the following ansatz for the DSF of the 1-dimensional Heisenberg antiferromagnet in zero magnetic field:

$$(2\pi)\cdot S^{MA}(q,\omega) \;=\; A\cdot\frac{\Theta(\omega-\omega_l(q))\Theta(\omega_u(q)-\omega)}{\sqrt{\omega^2-\omega_l^2(q)}} \tag{2.102}$$

where "MA" symbolizes the later well-known name "Müller ansatz" and A is a constant $O(1)$. The factor (2π) in Eq. 2.102 has been added to Müller's original formulation in order to use the standard notation (for frequency-moments, sum rules, etc.) in the following.
The important observation leading to the ansatz was that the dominant contribution of excitations forming the DSF have been recognized to be a particular class of Bethe ansatz [22] solutions – the so-called 2-spinon solutions. For infinite systems these excitations are confined to the 2-spinon continuum that is bounded by the lower (l) and upper (u) boundaries

$$\omega_l(q) \;=\; \frac{\pi}{2}\sin q \tag{2.103}$$

$$\omega_u(q) \;=\; \pi\sin\frac{q}{2} \tag{2.104}$$

where the Hamiltonian $H_0 = \sum_i \mathbf{S}_i\mathbf{S}_{i+1}$ underlies (the continuum is sketched on the left-hand side of Fig. 2.12.) The lower boundary had been first calculated by *des Cloiyeaux, Pearson* [48]. Moreover, using the methods of *des Cloizeaux, Pearson* [48] and *des Cloizeaux, Gaudin* [49] Müller et al. [156, 157] determined the whole variety of 2-spinon excitations for $0 \le q \le \pi$ and $0 \le q_m \le q$ to be

$$\omega_m(q) \;=\; \pi\sin\frac{q}{2}\cos\left(\frac{q}{2}-\frac{q_m}{2}\right) \tag{2.105}$$

with m denoting the different branches of solutions ($\omega_l(q) = \omega(q_m = 0)$, $\omega_u(q) = \omega(q_m = \pi)$).
In 1975 *Luther and Peschel* [147] determined the threshold exponent α of $S(q=\pi,\omega)|_{\omega\to 0} \sim \omega^{-\alpha}$, i.e. the infrared singularity of $S(q=\pi,\omega)$, to be $\alpha = 1/2$ which is fulfilled by the ansatz 2.102.

Guided by the well-known exact result of the XX-model (see 5.1.1), namely the factorization of $S^{XX}(q,\omega) = D^{XX}(q,\omega) \cdot M^{XX}(q,\omega)$ in the smooth transition-rate function M and the density of states (DOS) D, Müller et al. [156] found evidence (no proof) that the exact 2-spinon DSF should be of the form

$$(2\pi) \cdot S^{2-sp}(q,\omega) \quad = \quad M^{2-sp}(q,\omega) \cdot D^{2-sp}(q,\omega) \tag{2.106}$$

with the 2-spinon DOS

$$D^{2-sp}(q,\omega) \quad = \quad \frac{\Theta(\omega - \omega_l(q))(\Theta(\omega_u(q) - \omega)}{\sqrt{\omega_u^2(q) - \omega^2}}\,, \tag{2.107}$$

On one hand Müller knew that 2.102 could not fulfill a sequence of checked sum rules for a unique choice of the parameter A (see e.g.[157]), on the other hand he proved that 2.102 shows the correct q-dependence for all odd frequency-moments

$$K_{zz}^{(n)}(q) \quad = \quad \int d\omega\, \omega^n S(q,\omega)\,. \tag{2.108}$$

In addition, the sum rules considered could be satisfied by using values of A from a quite small interval ($1 \leq A \leq 1.5$).
Since its first formulation $S^{MA}(q,\omega)$ underwent several tests and in particular experienced experimental confirmations based on inelastic neutron scattering (INS) experiments on quasi 1-dimensional systems [189, 62]. In summary, many pieces of evidence have been collected to show that the *Müller ansatz* covers in general the detailed dynamical picture of the Heisenberg chain to a large extent.
In the next section further developments, namely the exact determination of $M^{2-sp}(q,\omega)$ achieved in 1996 will be given. After this and a brief look at an attempted modification of the Müller ansatz, the different ansätze will be discussed in the framework of frequency-moments of the respective ansätze/solutions and compared with the frequency-moments of the total DSF of the Heisemberg chain.

2.6.5 Complete solution for the 2-spinon part of the spin-spin-DSF

In 1996 *Bougourzi et al.*[31] were able to derive the exact contribution of the 2-spinon part for $M(q,\omega)$ in a work that has been based on the context of quantum groups. Shortly thereafter, *Bougourzi, Karbach and Müller*[132] presented analytical expressions for the 2-spinon contribution $M^{2-sp}(q,\omega)$ and, based on the earlier conjecure [156] for the 2-spinon DOS 2.107 expressions for the 2-spinon DSF $S^{2-sp}(q,\omega) = D^{2-sp}(q,\omega)M^{2-sp}(q,\omega)$. In particular, a proper separation of a singular part in the result of [31] led to

$$M^{2-sp}(q,\omega) \quad = \quad \frac{1}{2}\exp\left[\frac{1}{2}\left(I_0 + \ln\left(t\sinh^2\frac{\pi t}{4}\right) + h(t)\right)\right] \tag{2.109}$$

with

$$\begin{aligned} I_0 &= 0.3677103\ldots \\ t &= \frac{4}{\pi}\ln(z+\sqrt{z^2-1}) \quad , \quad z = \sqrt{\frac{\omega_u^2(q)-\omega_l^2(q)}{\omega^2-\omega_l^2(q)}} \\ h(t) &= Ci(t) + \int_1^\infty \frac{dx}{x}\frac{\cos(xt)}{\cosh^2 x} - \int_0^1 \frac{dx}{x}\frac{\cos(xt)}{\coth^2 x}\,. \end{aligned}$$

The right-hand side of Fig. 2.12 shows for the case of $q = \pi/2$ a direct comparison of the earlier Müller ansatz $S^{MA}(q,\omega)$ and the 2-spinon solution $S^{2-sp}(q,\omega)$ given above. The figure already

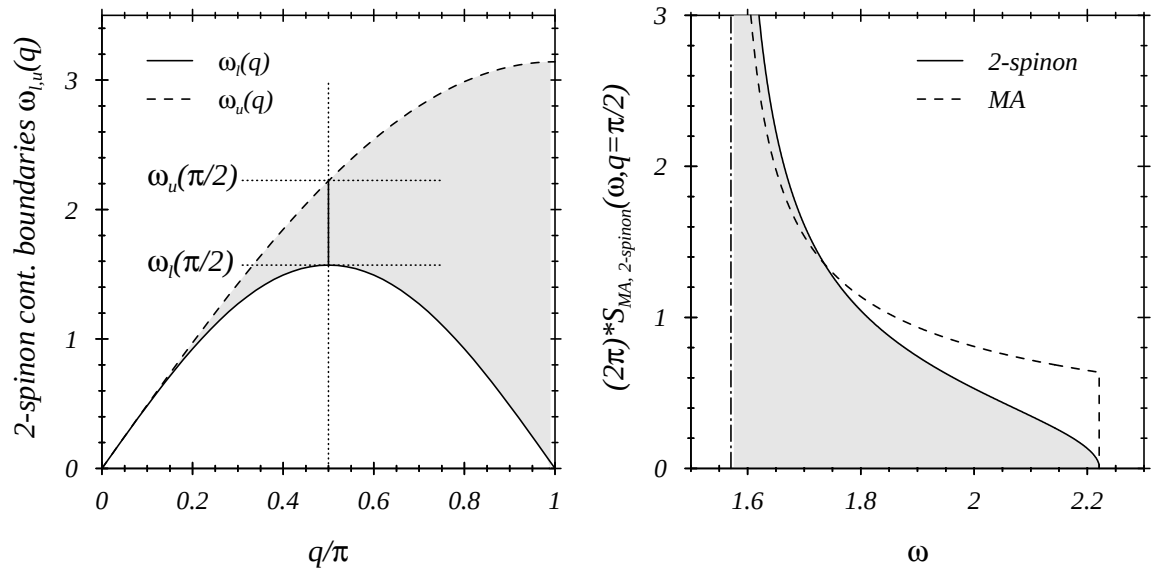

Figure 2.12: 2-spinon continuum and DSFs (MA, 2-spinon) at $q = \pi/2$

contains the key essentials that hold for all q-values: While the step-like behaviour of $S^{MA}(q,\omega)$ at $\omega = \omega_u$ overexpresses the spectral weight at higher frequencies it diverges less pronounced at the lower boundary $\omega_l(q)$ (analytical expressions see below).
For the numerical calculation the alternative formula [133]

$$\begin{aligned} S^{2-sp}(q,\omega) &= S^{MA}(q,\omega)\cdot\left(C'\cdot t\cdot e^{-f(t)}\right) \\ f(t) &= \int_0^\infty \frac{dx}{x}\left(\frac{\sin\frac{xt}{2}}{\cosh x}\right)^2 \\ C' &= 0.814272459\ldots \end{aligned} \tag{2.110}$$

has been used. The fast decay of the integrand of $f(t)$ allows the controlled limitation of the numerical integration to a finite interval and the advantageous use of finite-interval routines (e.g. NAG-routine D01AJF). A more detailed study of the behaviour of $S^{2-sp}(q,\omega)$ close to the spectral boundaries resulted in [132]:

$$(2\pi)\cdot S^{2-sp}(q,\omega) \overset{\omega\to\omega_l}{\longrightarrow} \frac{\sqrt{C/2}}{\pi}\left(\frac{\omega_u^2(q)-\omega_l^2(q)}{\omega_l(q)(\omega_u^2(q)-\omega^2)}\right)^{1/2}\cdot\sqrt{\frac{-\ln(\omega-\omega_l(q))}{\omega-\omega_l(q)}} \tag{2.111}$$

$$(2\pi)\cdot S^{2-sp}(q,\omega) \overset{\omega\to\omega_u}{\longrightarrow} \frac{4\sqrt{2}C}{\pi}\frac{\sqrt{\omega_u(q)}}{\omega_u^2(q)-\omega_l^2(q)}\cdot\sqrt{\omega_u(q)-\omega} \tag{2.112}$$

$$C = \frac{1}{2}e^{I_0} = 0.72221\ldots, \tag{2.113}$$

where minor mistakes in [132] have been corrected and again for reasons of standardization a factor (2π) has been added. In particular this means that the singularity of the 2-spinon DSF for $\omega\to\omega_l(\pi)$ behaves at the soft mode momentum $q=\pi$ as

$$(2\pi)\cdot S^{2-sp}(q=\pi,\omega) \overset{\omega\to 0}{\sim} \frac{1}{\omega}\sqrt{\ln\frac{1}{\omega}}, \tag{2.114}$$

i.e. compared with the Müller ansatz it contains a logarithmically enhanced infrared singularity. Again, besides the soft mode the divergence of the DSF at the lower boundary of the 2-spinon continuum is less pronounced (see formulas).
As a final comparison it should be added that the degree of fulfillment of the simple sum rule

$$I_T = \int_0^{2\pi} \frac{dq}{2\pi} \int_0^{\infty} d\omega S_{zz}(q,\omega) \quad = \quad |<0|S_z(x=0)|0>|^2 = \frac{1}{4} \tag{2.115}$$

has been checked for the MA ($A = 1$) and the 2-spinon solution [157, 132] with the result

$$I_T^{MA} = 0.7424.. \cdot I_T \quad , \quad I_T^{2-sp.} = 0.7289.. \cdot I_T \, . \tag{2.116}$$

In the following two sections the concept of frequency-moments will be discussed which supplies further insight into the comparison of the discussed ansätze and above that into the question of place value of the whole 2-spinon part within the dynamics of the isotropic Heisenberg model.

2.6.6 Frequency-moments for the spin-spin DSF

As mentioned earlier frequency-moments for Heisenberg chains have so far been considered for the case of zero magnetization [158, 80] in order to check ansätze for the dynamical structure factor $S_{xx}(q,\omega) = S_{zz}(q,\omega)$. As pointed out by *Müller* [158] odd frequency moments are given in the form

$$K_{zz}^{(l)}(q,N) \quad = \quad \sum_{n=0}^{l} T_{zz,n}^{(l)}(N) \cdot (1-\cos q)^l \quad , \quad T_{zz,0}^{(l)}(N) = 0 \tag{2.117}$$

the $T_{zz,n}^{(l)}$ containing spin correlations which at most exceed $n+1$- sites on the ring of spins. The latter property does not hold for even moments.
Before dicussing the importance of sum rules on the basis of frequency-moments the extension to the case of a spin chain in a uniform magnetic field will be treated. Zero-temperature frequency-moments are defined as

$$\begin{aligned} K_{aa}^{(l)}(q,T=0) \quad &= \quad \int d\omega \, \omega^l \, S_{aa}(q,\omega) \quad , \quad a = x,z \\ &= \quad \sum_n \int d\omega \, \omega^l \, \delta(\omega - (E_{m,n} - E_{m,0}))| < n|S_a(q)|m > |^2 \\ &= \quad \sum_n (E_{m,n} - E_{m,0})^l | < n|S_a(q)|m > |^2 \\ &= \quad < m|S_a^+(q)(H - E_{m,0})^l S_a(q)|m > \, . \end{aligned} \tag{2.118}$$

Here, $|m>$ is the ground state in the sector with $S_z/N = m$ and $|n>$ are excited states. The Hamiltonian H reads

$$H \quad = \quad H_0 - B \sum_x S_z(x) \equiv H_0 - B\hat{S}_z \tag{2.119}$$

$$E_{m,0} \quad = \quad E_0 - BS_z \quad = E_0 - NBm \tag{2.120}$$

with E_0 refering to the ground state energy of H_0 in the S_z- sector $S_z = Nm$. For this discussion the prefactor 2 in H_0 will be omitted – it results in factors 2^l in $K^{(l)}$ in case of a properly scaled

B. Moreover, the magnetic field B causing the non-zero magnetization $m(B)$ considered in the following will be used as the approximated $N \to \infty$- value (cf. [157])

$$B(m) \;=\; \pi\left(\frac{\pi}{2} - 1 + \frac{1}{\sin(\pi m)}\right)^{-1} . \tag{2.121}$$

The reduced symmetry in spin space requires the additional evaluation of the transverse x, y-components of

$$\begin{aligned} & < m|S_a^+(q)(H - E_{m,0})^l S_a(q)|m > \\ = \quad & < m|S_a^+(q)\left[H_0 - B\hat{S}_z - (E_0 - NBm)\right]^l S_a(q)|m > , \end{aligned}$$

leading to the terms

$$\begin{aligned} \underline{a = z} \quad & < m|S_z(H_0 - E_0)^l S_z|m > \\ \underline{a = +} \quad & < m|S_-(H_0 - (E_0 + B))^l S_+|m > \\ \underline{a = -} \quad & < m|S_+(H_0 - (E_0 - B))^l S_-|m > \end{aligned}$$

where S_x, S_y have been expressed by the raising and lowering operators S_+, S_-. For the analytical calculation of odd moments it is convenient to use the commutator form (see e.g.[158]):

$$K_{aa}^{(n)}(q) \;=\; \frac{1}{2} < m|[\ldots[S_a^+(q), H], H], \ldots, H], S_a(q)]|m > \tag{2.122}$$

including $(n+1)$- commutators. As an example consider

$$K_{xx}^{(1)}(q) \;=\; \frac{1}{2}\cdot\frac{1}{4} < m|[[S_+(-q) + S_-(-q), H_0 - B\hat{S}_z], S_+(q) + S_-(q)]|m > \tag{2.123}$$

$$\;=\; (\text{part B=0}) - \frac{B}{8} < m|[[S_+(-q) + S_-(-q), \hat{S}_z], S_+(q) + S_-(q)]|m > \tag{2.124}$$

$$\;=\; (\text{part B=0}) + \frac{1}{2}Bm \tag{2.125}$$

where

$$\begin{aligned} [S_-(-q), \hat{S}_z] \;&=\; S_-(-q) \\ [S_+(-q), \hat{S}_z] \;&=\; -S_+(-q) \\ [S_-(-q), S_+(q)] \;&=\; -\frac{2}{N}\hat{S}_z \end{aligned}$$

has been used and (part $B = 0$) yields

$$K_{xx}^{(1)}(q)\Big|_{m,\,B=0} \;=\; -\Big(< m|S_1(x)S_1(x+1) + S_z(x)S_z(x+1)|m > \Big)(1 - \cos q) \tag{2.126}$$

$$\;=\; -\Big(< m|\frac{1}{2}S_+(x)S_-(x+1) + S_z(x)S_z(x+1)|m > \Big)(1 - \cos q) \tag{2.127}$$

This result is to be compared with the longitudinal component

$$K_{zz}^{(1)}(q) \;=\; -2 < m|S_z(x)S_z(x+1)|m > (1 - \cos q) \tag{2.128}$$

and it shows the identity of logitudinal and transverse components in the isotropic zero-field case ($m = 0$) with $T^{(1)}_{xx,1} = T^{(1)}_{zz,1} = -\frac{2}{3}E_0/N$. This $m = 0$-result has been given in 1975 as one of a small number of sum rules for the DSF by *Hohenberg and Brinkman* [116]:

$$K^{(1)}(q, m = 0) \quad = \quad -\frac{2}{3}\frac{E_0}{N}(1 - \cos q)\,. \tag{2.129}$$

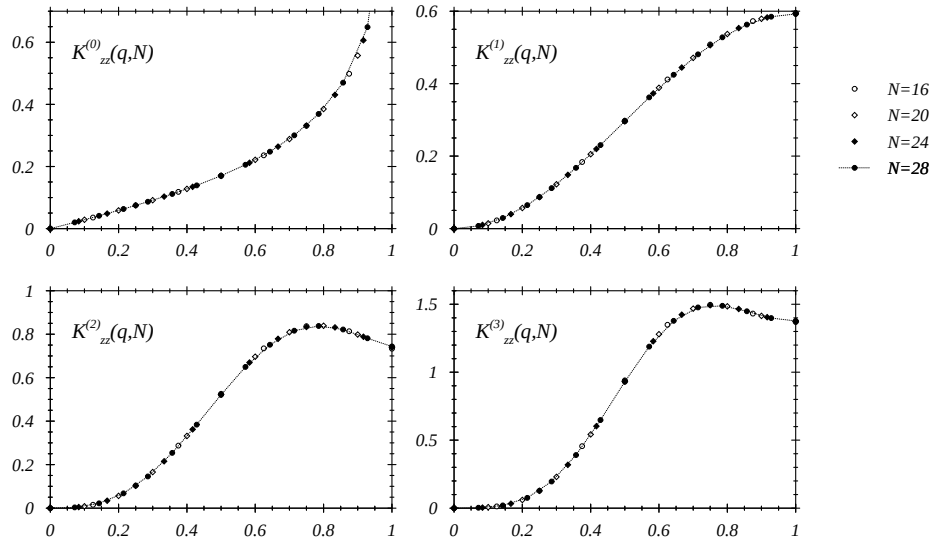

Figure 2.13: Frequency moments $K^{(l)}_{zz}(q, N)$ vs. q/π, $l = 0, 1, 2, 3$ for magnetization $m = 0$

Figs. (2.13,2.14) show frequency-moments $K^{(l)}_{xx}(q, N), K^{(l)}_{zz}(q, N)$ for $l = 0, 1, 2, 3$ versus q/π for magnetizations $m = 0$ and $m = 1/4$. In the latter case the K_{zz} curves allways start at $K^{(l)}_{zz}(q = 0, N) = 0$. Calculations of $T^{(l=odd)}_{aa,n}$ for $n, l > 1$ are rather costly and results shall not be presented here. Only as a remark it should be added that $T^{(1)}_{xx,0} = Bm/2, \quad T^{(3)}_{xx,0} = B^3m/2, \ldots$. Moreover, the figures indicate that finite-size corrections for the shown frequency-moments are rather weak and controllable [79, 80]. The used system sizes already supply a very good tool in order to compare analytical ansatzes for the DSF or its 2-spinon part with the complete Heisenberg chain where no analytical results for the DSF exist. This will be considered in the next section.

2.6.7 Frequency-moments and sum rules for the spin-spin DSF

In this paragraph numerical evaluations of the frequency-moments $n = 1, \ldots 5$ of the Heisenberg chain will be used to compare different DSF ansätze with evaluations of the DSF on the basis of the complete chain Hamiltonian and its frequency-moments. The latter are finite-N data, however with a finite-size behaviour that is negligible for the presented survey.
In the following we will consider the Frequency-moment ratios

$$\frac{K^{(n)}_i(q)}{K^{(1)}_i(q)} \quad ; \; n = 2, 3, 4, 5 \quad ; \quad i = H_0\,(a),\, , MA\,(b),\, 2 - spinon\,(c),\, \text{mod. } MA\,(d)\,,$$

whereby the DSF ansatz (d) represents a modified version of the Müller ansatz (MA) that will be briefly sketched below. All shown DSFs (Fig. 2.15) have in common that they share the

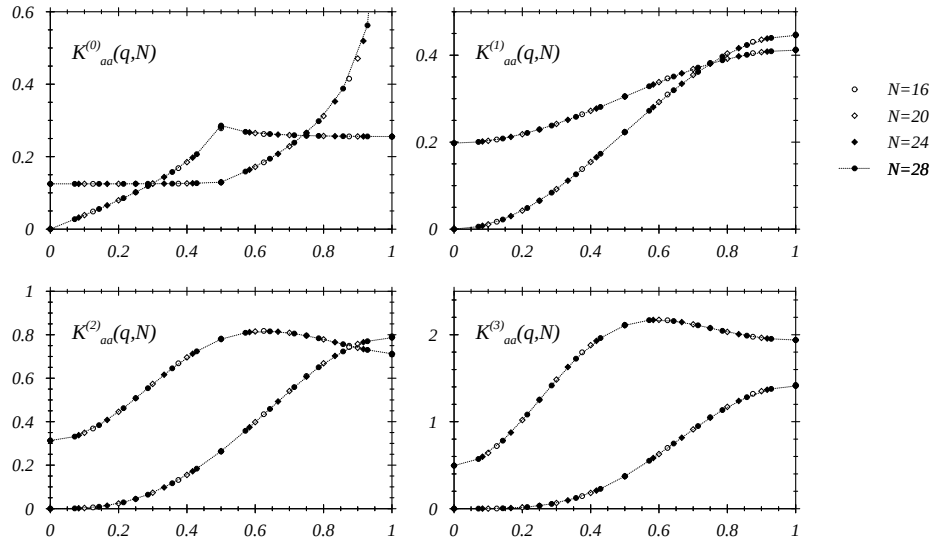

Figure 2.14: Frequency moments $K^{(l)}_{aa}(q,N)$ vs. q/π, $l = 0,1,2,3$, $a = x,z$ for magnetization $m = 1/4$

correct q-dependence of sum rule 2.129, however with prefactor ratios

$$\frac{K^{1)}_{2-sp}(q)}{K^{(1)}(q)} = 0.7130.. \quad , \quad \frac{K^{1)}_{MA}(q)}{K^{(1)}(q)} = 0.8462.. \quad , \quad \frac{K^{1)}_{mod.MA}(q)}{K^{(1)}(q)} = 1.0\,,$$

where case (a) has been used for $K^{(1)}(q)$. That both of the two ratios are lower than 1 above, shows the incompleteness of spectral weight restricted to the 2-spinon part of excitations. however, the ratio of 1 for case (d) must not interpreted as completeness. Here, the prefactor A and $\omega_u(q)$ of the Müller ansatz have been given further degrees of freedom ($A \to A(q)$, $\omega_u(q) \to u(q)\omega_u(q)$, the lower boundary $\omega_l(q)$ remained unchanged) with $A(q)$, $u(q)$ fixed by the requirement of fulfillment of the frequency-moments $K^{(-1)}(q)$ (see Sec. 2.6.8) and $K^{(0)}(q)$, $K^{(1)}(q)$. It turned out that no further conditions (sum rules) could be additionally fulfilled within this approach (cf. [79, 80]), instead, it helped to get some more insight into the 2-spinon part of the DSF prior to its rigorous determination and will be addressed in Fig. 2.15. As already might have turned out in the above discussion a reason for the consideration of frequency-moment ratios may be seen in the fact that these ratios circumvent any ambiguity in the choice of a constant prefactor (e.g. A in 2.102 which would have to be chosen $A = 1.1817$ [157] to give the correct prefactor in 2.129).
The comparison of frequency-moment ratios in Fig. 2.15 shows the following interesting points:

1. The ratios $R^{(n)}(q) = K^{(n)}(q)/K^{(1)}(q)$ approach a non-zero value for $q \to 0$ – a behaviour not present in any of the 2-spinon based ansatzes/solutions which all go to zero. This may be understood as a hint that in the long wavelength regime $R^{(n\geq 2)}_{(a)}(q)$ is dominantly given by non-2-spinon contributions (see also finite-N spectrum given below).

2. The frequency-moment ratios $R^{(n)}_{(c)}(q)$ of the exact 2-spinon solution is correctly located under the curves $R^{(n)}_{(a)}(q)$ in the whole q-interval (other than the 2-spinon excitations are not taken into account) and the coincidence of both sets of curves demonstrates the earlier observation of Müller et al. [156] that the 2-spinon excitations dominate the DSF.

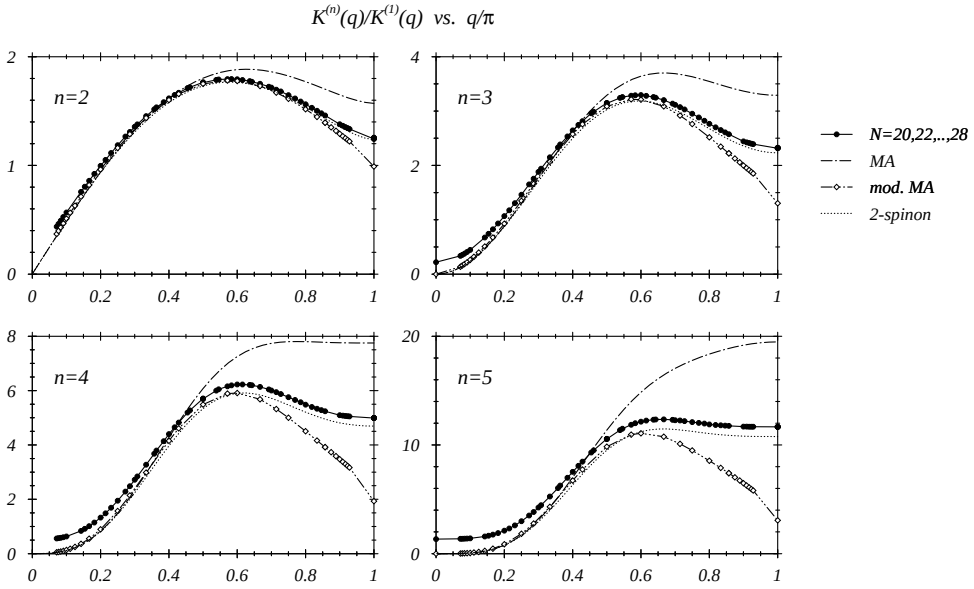

Figure 2.15: Frequency moment ratios $K^{(n)}_{zz}(q)/K^{(1)}_{zz}(q)$ vs. q/π, $n = 2, 3, 4, 5$ for magnetization $m = 0$

3. The higher the power of n of the considered frequency-moments the larger is the influence of non-2-spinon excitations – especially those at higher energies above the 2-spinon continuum (see discussion below). Therefore, $R^{(n)}_{(b,c,d)}(q)$ show stronger deviations from $R^{(n)}_{(a)}(q)$ for increasing n.

4. The ratios $R^{(n)}_{(b)}(q)$ of the Müller ansatz (MA) cross and exceed $R^{(n)}_{(a)}(q)$ at about $q \simeq \pi/3$. In retrospective of Sec. 2.6.5 this behaviour reflects the earlier argued [80] fact that $S_{MA}(q,\omega)$ underestimates the spectral weight close to the lower continuum boundary $\omega_l(q)$ and overestimates it (due to the finite-heigth step at ω_u) close to $\omega_u(q)$.

5. The above-mentioned unphysical excess of $R^{(n)}_{(a)}(q)$ could be overcome by the modified MA, however, the requirement of correct fulfillment of the mentioned moment conditions shows a strong and likewise artificial influence on the width of the contributing part of the spectrum and is sketched in the discussion given below of the complete low-energy excitation spectrum of a finite chain ($N = 28$).

Fig. 2.16 supplies information about the positions $\omega_n(q)$ and relative weights $\mathrm{w}_n(q)$ of excitations contributing to the spin-spin DSF

$$\frac{S_{zz}(q,\omega)}{S_{zz}(q)} = \sum_n \frac{|<n|S_z(q)|0>|^2}{<0|S_z(-q)S_z(q)|0>} \cdot \delta(\omega - (E_n - E_0)) \tag{2.130}$$

$$\equiv \sum_n \mathrm{w}_n(q) \cdot \delta(\omega - (E_n - E_0)) \tag{2.131}$$

for a 28-site chain. To achieve this, excitations and weights have been calculated by means of the recursion method (Appendix A) and H_0 has been chosen as $H_0 = 2 \cdot \sum_i \mathbf{S}_i\mathbf{S}_{i+1}$. The relative weights $\mathrm{w}_n(q)$ are subdivided in the given 4 ranges of values and any 2-spinon excitation is marked by a "+" in the belonging open circle (the latter classification is not being given by the recursion method but from the application of the Bethe ansatz method [22, 133]). It should

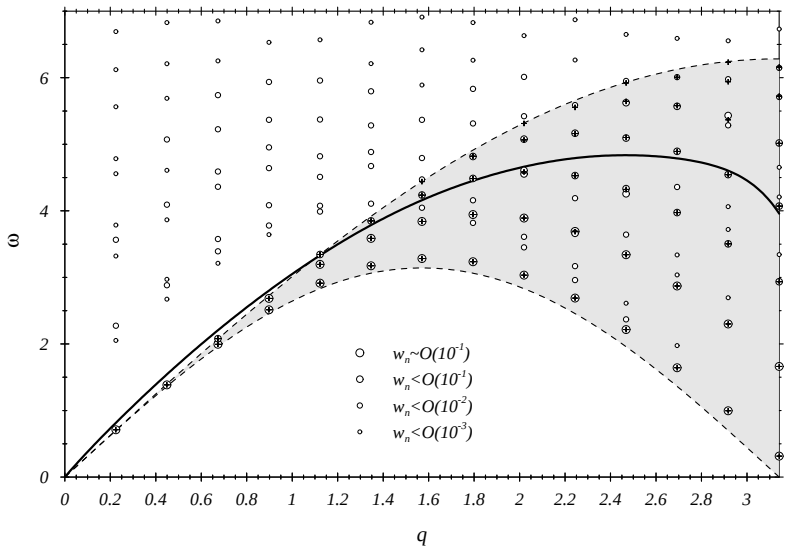

Figure 2.16: Excitation energies $\omega_n(q)$ and relative weights $\mathrm{w}_n(q)$ for a 28-site chain

be pointed out that this way of representation does not allow for an immediate comparison of spectral weights for different q-values which requires the additional knowledge of the SSF $S_{zz}(q, N)$ given in Sec. 2.5.
It shows first of all that about 2 thirds of the excitations within the 2-spinon continuum are of 2-spinon type and that these are carrying predominant weights. However, it shows as well that in particular for $q \leq \pi/3$ there is nonvanishing weight above $\omega_u(q)$, i.e. the upper boundary of the shaded 2-spinon continuum. As mentioned above these contributions, though having rather small weights, will be of increasing importance the higher the considered frequency-moments which are a rather subtle measure for the high-frequency part of the underlying spectrum.
Finally, the thick solid line in Fig. 2.16 shows the upper continuum boundary $\hat{\omega}_u(q) = u(q)\omega_u(q)$ that was enforced by the momentum requirements within the modified MA. On one hand it shows that $\omega_u(q)$ had to be exceeded for $q \leq \pi/3$ (especially to meet the conditions given by $K^{(-1,0,1)}(q \to 0)$), on the other hand it shows the growing decrease of $\hat{\omega}_u(q)$ for larger q-values. Besides a lacking attractivity and friendliness of application a gradual merit of the modified MA may be seen in the fact that its frequency-moments are well bounded by $K(n)_{(a)}(q)$, however we are not going to follow this concept any further.

At the end of this section it remains to be remarked that to the author's knowledge so far no attempt has been made to redo the explanation of INS experiments (e.g. [189, 62]) on the basis of the complete 2-spinon solution that have been successfully described with the MA-DSF before. It remains questionable how far the quite subtle differences between the two solutions should appear in an experimental situation without being overlaid by non-2-spinon excitations of the Heisenberg chain, or even beyond by deviations of the measured specimen from the idealized 1-D Heisenberg case.
Another open problem is given in the still outstanding formulation of an DSF ansatz for the presence of a (homogeneous) external magnetic field. In 1997 *Dender et al.* [63] observed for the first time an incommensurate shift of the soft mode in copper benzoate, a 1D spin-1/2 antiferromagnet. The future situation of having experimental systems at disposal only stresses the importance of such an ansatz.

2.6.8 Susceptibilities

In this final part of the chapter some remarks shall be given on static susceptibilities of Heisenberg chains.
The static susceptibility $\chi_{aa}(q)$ and its relation to the DSF is given by

$$\chi_{aa}(q) \;=\; 2 \cdot \int_0^\infty d\omega\, \omega^{-1} S_{aa}(q,\omega) = 2K_{zz}^{(-1)}(q)\,. \tag{2.132}$$

Fig. 2.17 shows three different results for $\chi_{zz}(q, m = 0)$ (for the Hamiltonian $H_0 = \sum_n \mathbf{S}(n)\mathbf{S}(n+1)$):

- Finite-size data $\chi_{zz}(q, N, m = 0)$ for $N = 16, 18, \ldots, 28$ obtained from $\omega_{zz,n}(q, N)$, $\mathrm{w}_{zz,n}(q, N)$ given by the recursion method (cf. Appendix A) and the SSF $S_{zz}(q, N)$:

$$\chi_{zz}(q, N) \;=\; 2 \cdot \sum_n \frac{1}{\omega_{zz,n}(q, N)} \cdot \mathrm{w}_{zz,n}(q, N) S_{zz}(q, N) \tag{2.133}$$

  with $\mathrm{w}_{zz,n}(q, N)S_{zz}(q, N)$ forming the total weight $| < n|S_z(q, N)|0 > |^2$.

- Evaluations of $\chi_{zz}(q)$ for the Müller ansatz (MA) and the exact 2-spinon contribution to the DSF both being introduced in this chapter.

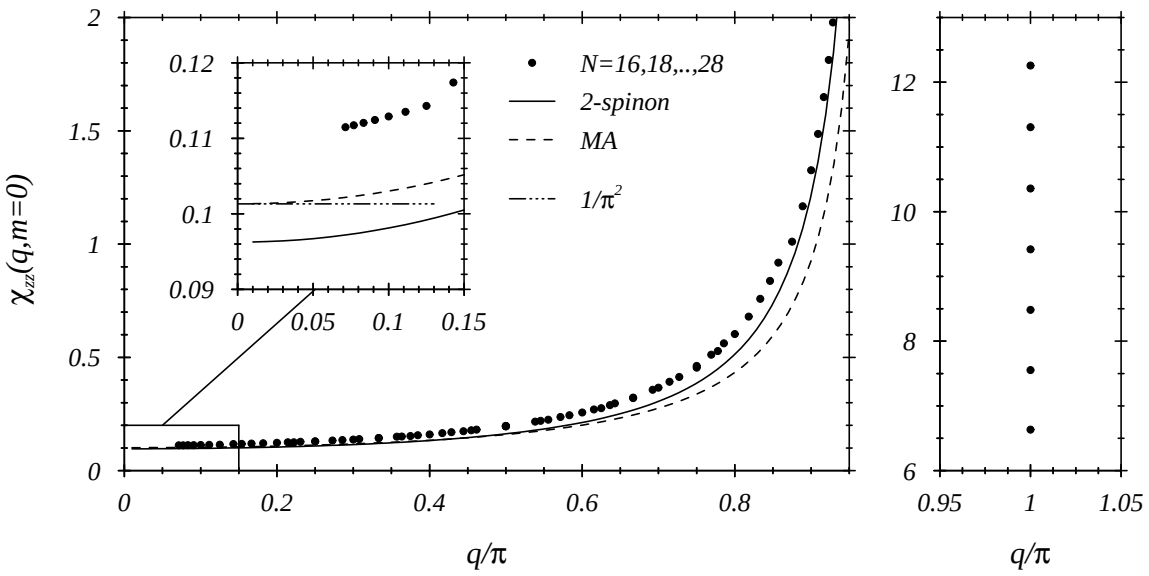

Figure 2.17: Susceptibility $\chi_{zz}(q)$ for magnetization $m = 0$

The 2 main drafts of the figure show the behaviour for $q < \pi$ (left) and $q = \pi$ (right) and the inset on the left-hand side resolves the small-q behaviour. The only well-known point in the figure [96, 220] is given by

$$\chi_{zz}(q = 0) \;=\; \frac{1}{\pi^2} \tag{2.134}$$

(see also Sec. 2.4) which is precisely fulfilled by the MA (see inset) for the choice $A = 1$ of the free constant in the ansatz (Eq. 2.102) – the choice being used for the MA in Fig. 2.17.

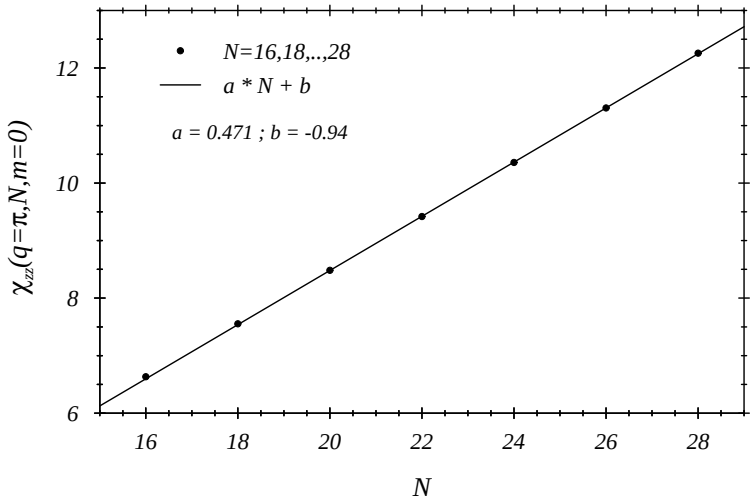

Figure 2.18: N-dependence of $\chi_{zz}(q=\pi, N)$ for magnetization $m=0$

Again, for increasing q the finite-N data are better approximated by $\chi_{zz}^{2-sp.}(q)$ for which the following relations have been shown [132]

$$\chi_{zz}^{2-sp.}(q) \quad \stackrel{q\to\pi}{\longrightarrow} \quad \sim \frac{1}{\pi - q}\left(-\ln(\pi - q)\right)^{1/2} \tag{2.135}$$

$$\chi_{zz}^{2-sp.}(\pi, N) \quad \stackrel{N\to\infty}{\longrightarrow} \quad 2\pi^{-5/2}\sqrt{2C}\cdot N\sqrt{\ln N} \tag{2.136}$$

with C being given in Sec. 2.6.5. The N-dependence of the latter relation is to be contrasted with the N-behaviour shown in the right-hand plot in Fig. 2.17; the given points show a very clear linear N-dependence presented in Fig. 2.18 together with a linear fit to the data. As mentioned before, the presented finite-chain evaluations are restricted to system sizes that are too small to resolve logarithmic corrections to algebraic behaviour (presumably not only present in the 2-spinon solution) with exponents unequal to zero (the latter is e.g. clearly resolvable in the case of the SSF at $q=\pi$, see Fig. 2.5).
The linear N-dependence of $\chi_{zz}(q=\pi, N)$ (up to some logarithmic corrections) is in accordance with $\omega_l(q=\pi, N) \sim N^{-1}$, $S_{zz}(\omega, q=\pi, N) \sim \omega^{-1}$,$S_{zz}(q=\pi, N) \sim N^0$ ($\sim \ln N$) appearing earlier in this chapter.

Finally, it should be mentioned that the left-hand side of Fig. 2.17 (main plot as well as inset) very distinctively shows some of the groups of points belonging to the same $z_i(q)$-value (cf. Sec. 2.2, Eq. 2.15) describing the approach of $q_1 = 0$ and $q_2 = \pi$:

$$z_1 \;=\; N\cdot\frac{q}{\pi} \tag{2.137}$$

$$z_2 \;=\; N\cdot\left(1-\frac{q}{\pi}\right)\,. \tag{2.138}$$

The inset clearly shows the group $z_1 = 2$, whereas the 7 members ($N = 16, 18, \ldots, 28$) of $z_2 = 2$ at the far right of the main figure are immediately ascertainable. We shall meet again this type of classification and a particular finite-size scaling application in Sec. 5.4.2.
At this place, however, finite-size scaling of the static susceptibility shall not be pursued further.

Chapter 3

Periodically perturbed spin chains

In this part we will turn to the case of a spin chain described by the Hamiltonian H_0 that is perturbed by a periodic perturbation of strength $h_a$described by $H_a(q)$:

$$H(h_a) = H_0 + h_a \cdot H_a(q) \tag{3.1}$$

$$H_0 = 2\sum_n \mathbf{S}(n)\mathbf{S}(n+1) \tag{3.2}$$

$$H_a(q) = 2\sqrt{N}X_a(q) = 2\sum_n e^{iqn}X_a(n)\,. \tag{3.3}$$

In certain cases it may be more convenient to study the perturbation modeled by

$$H_a^c(q) \equiv \frac{1}{2}\left(H_a(q) + H_a(-q)\right) = 2\sum_n \cos(qn)X_a(n)\,. \tag{3.4}$$

In this introductory chapter the wave number q of the perturbation will be restricted to the interval $q \in]0, 2\pi[$, i.e. $q \neq 0, 2\pi$. As will become clear soon, the case $q = 2\pi \cdot n$ is tied to a different initial condition when a perturbation of the Heisenberg chain with a respective momentum is applied. The latter case will be discussed separately in Chap. 5.

The outline of what follows will be 2-fold:

First, the behaviour of the Heisenberg chain under the inclusion of small periodic perturbations (i.e. opening of gaps, changes of energies, transition amplitudes, critical exponents, etc.) will be addressed and described by means of a closed set of differential equations (DEs). Here, results of the preceding chapter will serve as initial conditions of the unperturbed chain. As well, it will be shown that scaling solutions do exist, that fulfil the set of DEs order by order (neglecting the omnipresent logarithmic corrections). The latter part will be presented for one of the periodic perturbations ($2\sqrt{N}S_3(\pi)$) being introduced in the following section.

Second, we will turn away from the smallness requirement for the periodic perturbations in order to address a wide variety of interesting physical systems (spin ladders, spin-Peierls materials, ...) that make it necessary to increase the strengths of the perturbations. Here, the applicability of predictions originating from small perturbation analysis will be discussed. In particular, the discussion of dimer-like periodic perturbations will be required.

The very unambiguous fingerprint of the opening of a gap due to an applied periodic perturbation (conserving the spin component forming the magnetization), the appearance of magnetization plateaus, will be discussed later in Chap.4.

3.1 General types of periodic perturbations

The choice of types of periodic perturbations is related to their degree of interest in the contemporary discussion of quantum spin systems as well as to their generalizability to later applications. The first cases to consider are periodic perturbations of homogeneous external transverse or longitudinal fields:

$$\text{transverse:} \quad X(n) = S_x(n) \tag{3.5}$$

$$\text{longitudinal:} \quad X(n) = S_z(n)\,. \tag{3.6}$$

The second group of perturbations is the group of dimer-like spin-spin interactions $D_j(n)$ between j-th nearest neighbors that will be needed in particular be needed when tayloring new spin-geometries starting from the isotropic Heisenberg chain e.g. when describing spin ladders as linear spin systems; see Sec. 3.4:

$$\text{dimer:} \quad X(n) = D_j(n) \tag{3.7}$$

with

$$D_j(n) \equiv \mathbf{S}(n)\mathbf{S}(n+j) \quad , \quad j = 0, 1, 2, \ldots\,. \tag{3.8}$$

The discussion will be restricted to these cases including the occurrence of a simultaneous presence of some of the given types.

3.2 Theory – general description of periodic perturbations

The following review of a theoretical description and development of a scaling ansatz [84, 85] for a periodically perturbed system is based on the key elements of a system described by the Hamiltonian $H(h)$ (see below):

- Eigenvalues $E_n(N,h)$, eigenfunctions $|\Psi_n(N,h)>$:

$$H(N,h)|\Psi_n(N,h)> = E_n(N,h)|\Psi_n(N,h)> \tag{3.9}$$

- Excitation energies $\omega_{mn}(N,h)$:

$$\omega_{mn}(N,h) = E_m(N,h) - E_n(N,h) \tag{3.10}$$

- Transition amplitudes $T_{mn}(N,h)$:

$$T_{mn}(N,h) = < \Psi_m(N,h)|2\sqrt{N}X(q)|\Psi_n(N,h) > \,. \tag{3.11}$$

  Restricted to the cases $q = 0, \pi$ or using $X^c(q)$ otherwise results in a symmetric matrix T, i.e. $T_{mn} = T_{nm}$.

First, the discussion will focus on the case of a single periodic perturbation of the isotropic Heisenberg chain. Furthermore, the specification of the system size N in the following formulas will be omitted wherever misunderstanding seems avoidable.

3.2.1 Behaviour of excitation energies and transition matrix elements

A first important property evolves when looking at the changes in translational symmetry caused by $H(q)$ for a non-zero coupling strength h. It turns out that

$$T^m H(h) T^{-m} \quad = \quad H(-h) \quad , \quad \text{for} \quad m = \frac{\pi}{q} \tag{3.12}$$

holds, where T is the translation operator (intoduced in Sec. 2.1, Eqns. 2.6, 2.7). Using the momentum values of a N-site chain, i.e. $q = (2\pi/N) \cdot j$, $j = 0, 1, \ldots, N-1$ this results in

$$m \quad = \quad \frac{N}{2j} \, , \tag{3.13}$$

e.g. $m = 2$ for $q = \pi/2$ etc.. Here, a first signature of the exceptional case of $q = 2\pi n$ appears, which is not able to show the above symmetry.
At this point it should be remarked that the classification of momenta will usually be that of the unperturbed Heisenberg chain and no reductions of the 1st Brillouin zone will occur.
Making use of Eq. 3.12 the Schrödinger equation 3.9 yields

$$T^{-m} \underbrace{T^m H(h) T^{-m}}_{=H(-h)} \underbrace{T^m |\Psi_n(h)>}_{=|\Psi_n(-h)>} \quad = \quad E_n(h) T^{-m} \underbrace{T^m |\Psi_n(h)>}_{=|\Psi_n(-h)>} \tag{3.14}$$

$$\rightarrow \quad E_n(h) \quad = \quad E_n(-h) \, . \tag{3.15}$$

An immediate consequence of this relation is that for differentiable $E_n(h)$ and $q \neq 0$

$$\left. \frac{d}{dh} E_n(h) \right|_{h=0} \quad = \quad 0 \quad \forall N \text{ (even)} \tag{3.16}$$

holds. Turning again to the Schrödinger equation 3.9 it is a simple task to obtain

$$\frac{d}{dh} E_n(N,h) \quad = \quad < \Psi_n(h) | 2\sqrt{N} X(q) | \Psi_n(h) > = \, T_{nn}(N,h) \tag{3.17}$$

$$\frac{d}{dh} |\Psi_n(h)> \quad = \quad - \sum_{m \neq n} \frac{T_{mn}(N,h)}{\omega_{mn}(N,h)} |\Psi_m(h)> \tag{3.18}$$

with $T_{mn} = T_{nm}$ for real symmetric $X^c(q)$.

3.2.2 A complete set of differential equations (DEs): evolution equations

Proceeding further in evaluating 2nd derivatives of the eigenvalue equation one obtains a closed system of DEs that governs the h-dependence of the $E_n(N,h)$ and $T_{mn}(N,h)$:

$$\frac{d^2}{dh^2} E_n \quad = \quad -2 \sum_{l \neq n} \frac{|T_{ln}|^2}{\omega_{ln}} \tag{3.19}$$

$$\frac{d}{dh} T_{mn} \quad = \quad - \sum_{l \neq m,n} \left(\frac{T_{ml} T_{ln}}{\omega_{lm}} + \frac{T_{ml} T_{ln}}{\omega_{ln}} \right) - \frac{T_{mn}}{\omega_{nm}} \frac{d\omega_{nm}}{dh} \tag{3.20}$$

Turning now to the different types of periodic perturbations the initial conditions (i.e. $h = 0$) will differ for the respective cases. Eq. 3.17, however, tells that in all considered cases for $q \neq 0$

$$\left. \frac{d}{dh} E_n(h) \right|_{h=0} \quad = \quad 0$$

has to hold.
In the following, we will first apply the initial conditions and scaling properties of solutions of the evolution equations for the case of a longitudinal staggered field ($q = \pi$, $m = 0$) [84] before turning to the influence of a transverse staggered field ($q = \pi$) on a Heisenberg chain in a uniform longitudinal magnetic field as well as to the influence of a staggered longitudinal field on such a chain [85].
As an important feature the connection between the soft mode positions of the Heisenberg chain (given by LSM; see Sec.2.6.2) and the magnetization values $m_{pl.}$ of plateaus being formed under the influence of a periodic perturbation respectively several periodic perturbations will emerge.

3.2.3 Scaling solutions for a longitudinal staggered field ($q = \pi$, $m = 0$)

In the course of this section a scaling solution and its expansion for small scaling variables (see below) will be discussed completely neglecting any logarithmic correction in the initial conditions as well as in the set of evolution equations. This neglect will a posteriori be commented and to some extent justified.
The staggered longitudinal field with momentum $q = \pi$ is given as

$$H_z(q=\pi) = 2\sqrt{N}S_z(\pi) \quad = \quad 2\sum_{x=0}^{N-1} e^{i\pi x} S_z(x)\,, \tag{3.21}$$

i.e.

$$TH(h)T^{-1} = H(-h) \quad ; \quad |\Psi(-h)> = T|\Psi(h)> \tag{3.22}$$

(see Eq. 3.12). Bearing in mind to look at the soft mode position of the unperturbed infinite chain ($q_3(m=0) = \pi$) again, $1, 2, 3$ is used synonymously for x, y, z, the following classification of the unperturbed eigenstates $|\Psi_n(0)>$ with momenta $q_n = 0, \pi$ appears to be appropriate: While in case of $h \neq 0$ those 2 momenta are degenerate, for $h = 0$ we define for the 2 groups of eigenstates with momenta $q = q_0(N)$ (1), $q = q_0(N) + \pi$ (2) the following order:

$$q = q_0: \quad n = 0, 2, 4, \ldots \quad , \quad |\Psi_0(h=0)> \equiv \text{ ground state} \tag{3.23}$$

$$q = q_0 + \pi: \quad n = 1, 3, 5, \ldots \tag{3.24}$$

$$E_{2n}(N,0) < E_{2n+2}(N,0) \quad ; \quad E_{2n+1}(N,0) < E_{2n+3}(N,0)\,. \tag{3.25}$$

i.e. the 2 sequences are independently ordered and $q_0(N)$ has been given in Sec.2.1. For the energy differences ω_{m0} and transition amplitudes T_{m0} –connecting ground state and excited state m– and under the mentioned neglects we expect the following initial conditions to hold:

$$\omega_{m0}(N,0) \quad \stackrel{N\to\infty}{\longrightarrow} \quad a_{m0} \cdot N^{-1} \tag{3.26}$$

$$T_{m0}(N,0) \quad \stackrel{N\to\infty}{\longrightarrow} \quad b_{m0} \cdot N^{\kappa}\,. \tag{3.27}$$

The exponent κ ($\kappa \simeq 1/2$) will be discussed and compared with CFT results later in the following section. We Define

$$i_{mn} \quad \equiv \quad e^{i\pi(m-n)} \; = \; (-1)^{m-n}\,, \tag{3.28}$$

and coefficients $b_{m0} = 0$ for $i_{m0} = 1$. The latter relation is to be considered since the momentum change $\Delta q = \pi$ caused by the operator $S_3(\pi)$ leads to

$$T_{mn}(N,0) = 0 \quad \text{for} \quad i_{mn} = 1\,.$$

Moreover, the transition amplitudes $T_{2n-1,0}(N,0)$ are related to the matrix elements $\mathrm{w}^{tot}_{zz,n}(\pi,N)$ (cf. e.g. Sec. 2.6.3) by

$$w_{zz,n}(\pi,N,h=0) \;=\; \frac{1}{N}\cdot|T_{2n-1,0}(N,0)|^2 \quad ; \quad n=1,2,\ldots\,.$$

Turning now to a scaling ansatz, i.e. combining the 2 limits $N\to\infty$, $h\to 0$ in a fixed scaling variable

$$x \;\equiv\; N\cdot h^{\epsilon} \tag{3.29}$$

–for reasons of convenience a modification from standard finite-size scaling theory (using $y = x^{1/\epsilon}$) [173, 174] has been made–, we start assuming the following scaling behaviour for the elements of the evolution equations

$$\omega_{mn}(N,h) \;=\; h^{\epsilon}\Omega_{mn}(x) \tag{3.30}$$
$$T_{mn}(N,h) \;=\; Nh^{\sigma}\Theta_{mn}(x) \tag{3.31}$$

to hold for all $\{m,n\}$. Second, the generalized initial conditions

$$\omega_{mn}(N,0) \;\stackrel{N\to\infty}{\longrightarrow}\; a_{mn}\cdot N^{-1} \tag{3.32}$$
$$T_{mn}(N,0) \;\stackrel{N\to\infty}{\longrightarrow}\; b_{mn}\cdot N^{\kappa} \quad ; \quad b_{mn}=0 \quad \text{for} \quad i_{mn}=+1\,. \tag{3.33}$$

should result in

$$\Omega_{mn}(x) \;\stackrel{x\to 0}{\longrightarrow}\; a_{mn}x^{-1}\left(1+e_{mn}(x)\right) \tag{3.34}$$
$$\Theta_{mn}(x) \;\stackrel{x\to 0}{\longrightarrow}\; \begin{cases} a_{mn}x^{-2}f_{mn}(x) & i_{mn}=+1 \\ b_{mn}x^{-\sigma/\epsilon}\left(1+f_{mn}(x)\right) & i_{mn}=-1 \end{cases}\,. \tag{3.35}$$

As a first relation between the 3 different exponents one obtains

$$\kappa \;=\; 1-\frac{\sigma}{\epsilon}\,. \tag{3.36}$$

Discussing then conveniently chosen expressions containing $\omega_{mn}(N,h)$ and/or $T_{mn}(N,h)$, the application of the evolution equations as well as the scaling relations lead to a matching scaling behaviour when choosing [84]

$$\sigma \;=\; 2\epsilon-1\,, \tag{3.37}$$

i.e.

$$\sigma=(1-\kappa)(1+\kappa)^{-1} \quad ; \quad \epsilon=(1+\kappa)^{-1}\,, \tag{3.38}$$

so both exponents are fixed by the finite-size dependence of the initial conditions.
Finally, the consideration of the small-x behaviour, i.e. assuming an expansion of the scaling functions

$$e_{mn}(x) \;=\; e^{(0)}_{mn}x^{\phi_0}+e^{(1)}_{mn}x^{\phi_1}+\ldots \tag{3.39}$$
$$f_{mn}(x) \;=\; f^{(0)}_{mn}x^{\phi_0}+f^{(1)}_{mn}x^{\phi_1}+\ldots \tag{3.40}$$

–at the beginning allowing for different ϕ_e, ϕ_f– lead in the 2 lowest orders to $\phi_e=\phi_f$ with

$$\phi_0=2/\epsilon \quad , \quad \phi_1=2\phi_0=4/\epsilon\,. \tag{3.41}$$

Furthermore, the coefficients of the lowest order in x of the scaling functions are given by the initial values a_{mn}, b_{mn}:

$$e^{(0)}_{mn} = 2\delta^-_{mn}\frac{b^2_{mn}}{a^2_{mn}} - \frac{1}{a_{mn}}\sum_{l\neq m,n}\left[\delta^-_{lm}\frac{b^2_{lm}}{a_{lm}} - \delta^-_{ln}\frac{b^2_{ln}}{a_{ln}}\right] \tag{3.42}$$

$$i_{mn} = +1: \quad f^{(0)}_{mn} = -\sum_{l\neq m,n}\delta^-_{lm}\delta^-_{ln}\frac{b_{ml}b_{ln}}{a_{mn}}\left(\frac{1}{a_{lm}} + \frac{1}{a_{ln}}\right) \tag{3.43}$$

$$i_{mn} = -1: \ 2(e^{(0)}_{mn} + f^{(0)}_{mn}) = \sum_{l\neq m,n}\left(\delta^+_{lm}f_{ml}\frac{b_{ln}a_{ml}}{b_{mn}} + \delta^+_{ln}f_{ln}\frac{b_{ml}a_{ln}}{b_{mn}}\right)\left(\frac{1}{a_{ml}} + \frac{1}{a_{ln}}\right) \tag{3.44}$$

$$\text{with} \quad \delta^\pm_{ij} \equiv \frac{1}{2}(1 \pm (-1)^{i-j}). \tag{3.45}$$

Here, the first relation is exact while for the remaining two (cases $i_{mn} = \pm 1$) the asymptotic behaviour of the underlying relation has been used.
Then coefficients of the next order $(e, f^{(1)}_{mn})$ are determined by $\{a_{ij}, b_{ij}\}$ together with the lowest order coefficients $\{e_{ij}, f_{ij}\}$.

3.2.4 Numerical check of the finite-size scaling ansatz (staggered field, $m = 0$)

A numerical check of the scaling arguments and assumptions presented above starts with the consideration and test of the assumptions being made for the initial conditions ($h = 0$) in the last section.

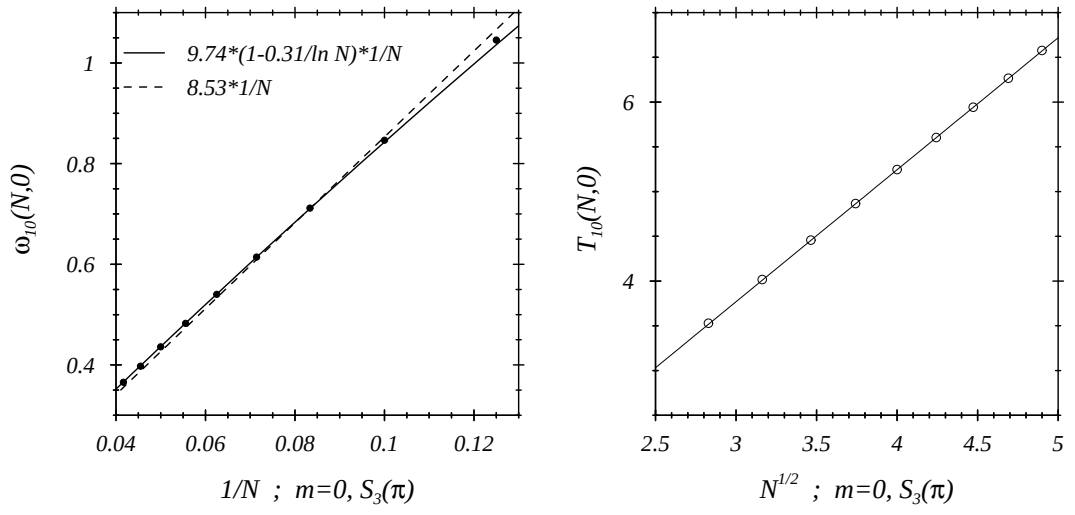

Figure 3.1: $\omega_{10}(N, 0)$, $T_{10}(N, 0)$ for $N = 8, 10, \ldots, 24$ and fits to the asymptotic behaviour

Fig. 3.1 shows the N-dependence of the lowest non-zero excitation energy $\omega_{10}(N, 0)$ and transition amplitude $T_{10}(N, 0)$ which both show an approximately linear behaviour in N^{-1} and $N^{1/2}$, respectively. The excitation energy, however, shows stronger deviations from a purely algbraic behaviour. Therefore, besides a N^{-1}-fit a fit containing as well a first logarithmic correction $N^{-1}(1 + c \cdot \frac{1}{\ln N})$ has been done (Fig. 3.1 (a)). The coefficient a_{10} in

$$\omega_{m0}(N, 0) \quad \stackrel{N\to\infty}{\longrightarrow} \quad a_{m0} \cdot N^{-1}$$

changes from $a_{10} = 8.53$ (no logarithmic corrections) to $a_{10} = 9.74$ (including the logarithmic corrections) while the exact value is $a_{10} = \pi^2 = 9.86\ldots$ [9].

Using the definition given above

$$T_{m0}(N,0) \quad \stackrel{N\to\infty}{\longrightarrow} \quad b_{m0}\cdot N^{\kappa} \quad , \quad i_{m0}=-1\,,$$

Fig. 3.1 (b) results in $\kappa \simeq 1/2$. Both, the leading algebraic behaviour of $\omega_{10}(N,0)$, $T_{10}(N,0)$ are in agreement with CFT ($\kappa = a_{10}/2\pi^2 = 1/2$; for references see e.g. [84]). In the framework of finite-system evaluations we conclude that the restriction to purely algebraic N-dependences of the initial conditions as well as for the following scaling analysis seems to be consistent within the margin of numerical accuracy.
We turn to the scaling behaviour of the perturbed quantities $\omega_{m0}(N,h)$, $T_{m0}(N,h)$. First of all, relations 3.38 determine $\epsilon = 2/3 = 2\sigma$ using $\kappa = 1/2$. Then, Eqns. 3.30, 3.34 predict scaling behaviour

$$\frac{\omega_{m0}(N,h)}{\omega_{m0}(N,0)} \quad = \quad 1+e_{m0}(x) = 1+e^{(0)}_{m0}\cdot x^{2/\epsilon}+\ldots \tag{3.46}$$

and Eqns. 3.31, 3.35 result in

$$\frac{T_{m0}(N,h)}{T_{m0}(N,0)} \quad = \quad 1+f_{m0}(x) = 1+f^{(0)}_{m0}\cdot x^{2/\epsilon}+\ldots \quad , \quad \text{for} \quad i_{m0}=-1\,, \tag{3.47}$$

i.e. the latter scaling relation restricted to $T_{m0}(N,0)\neq 0$. Eqns. 3.46, 3.47 in particular give a (in leading order) quadratic behaviour ($x^{2/\epsilon}\sim h^2$) of $X_{m0}(N,h)/X_{m0}(N,0)-1$ ($X=\omega$, T). In general only even powers of h occur which is a consequence of the initial conditions for periodic perturbations. Later (in Sec. 5.2.3) we will comment on an example of a translation invariant perturbation ($q_{pert.}=2\pi\cdot n$, $\quad n$ integer).

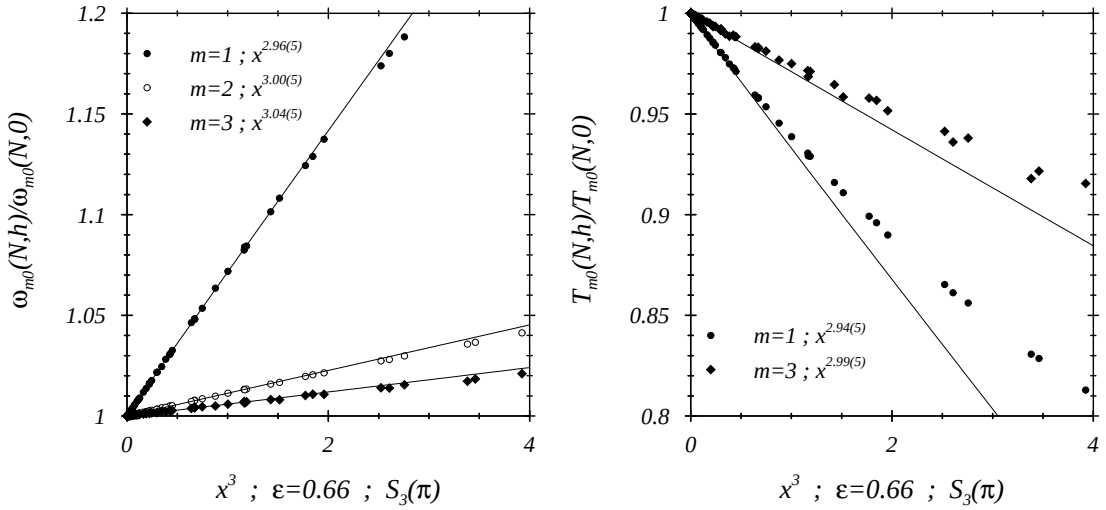

Figure 3.2: Scaling of the ratios 3.46, 3.47 for small x and $N = 8, 10, \ldots, 24$

Numerical data for the predicted type of scaling for low excitations ($m = 1, 2, 3$) and system sizes $N = 8, 10, \ldots, 24$ are shown in Fig. 3.2. Optimal scaling has been achieved for $\epsilon = 0.66$ and the region of small x agrees quite well with the $x^{2/\epsilon} = x^3$-behaviour as derived in the discussion of the scaling limit.
It should be mentioned that the numerical results shown in this section are related to the Hamiltonian $H = 2\sum_n (\mathbf{S}_n\mathbf{S}_{n+1} + \exp(i\pi n)S_3(n])$, i.e. the factor of 2 has been kept as an overall factor of the Hamiltonian. The exponents of the small-x behaviour, given in [84], remain unchanged of course.

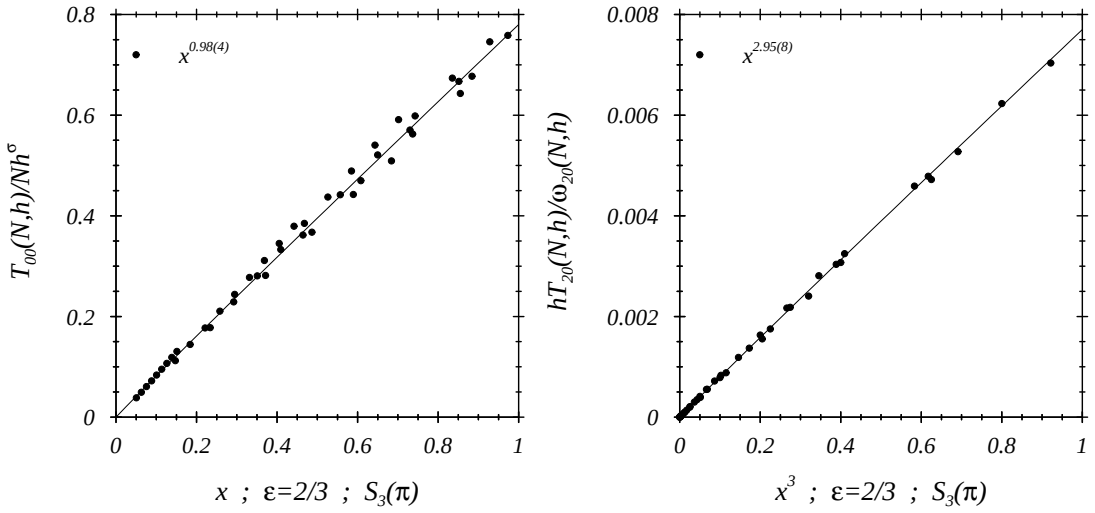

Figure 3.3: Scaling behaviour of $T_{00}(N,h)$ and $T_{20}(N,h)$ for small x

The scaling of the quantities $T_{2m,0}(N,h)$ has to be dealt with in a different way. Using e.g. Eq. 3.35 for $T_{00}(N,h)$ a scaling of type

$$T_{00}(N,h) \quad = \quad Nh^{\sigma}x^{-2}f_{00}(x)\,, \tag{3.48}$$

i.e.

$$\frac{T_{00}(N,h)}{Nh^{\sigma}} \quad = \quad f_{00}^{(0)}x + f_{00}^{(1)}x^4 + \ldots \tag{3.49}$$

($\epsilon = 2/3$) is predicted. Assuming moreover, that $T_{2m,0}(N,h)$ and $\omega_{2m,0}(N,h)/h$ scale in the same manner (see the evolution equations), we expect for instance

$$\frac{T_{20}(N,h)}{\omega_{20}(N,h)/h} \quad = \quad f_{20}(x) \tag{3.50}$$

(e.g. $\sim x^3$ for $x \ll 1$, $\epsilon = 2/3$). Both cases are shown in Fig. 3.3 and the scaling hypotheses appear to be fulfilled quite well.
A final point in this section will be a comment on the limit $x \to \infty$ which for small (non-zero!) fields h contains information on the existence of a finite gap in the TDL ($N \to \infty$). Such a gap is then predicted to open $\sim h^{\epsilon}$. As a matter of fact, a scaling analysis on the basis of finite-system evaluations appears to be easier tractable than trying to obtain a complete solution of the evolution equations for arbitrary x. For the given investigation, a BST-analysis (see also App. C) of the finite-system data led to

$$\lim_{x\to\infty} \Omega_{10}(x) = \Omega_{10}^{\infty} \quad \simeq \quad 4\,, \tag{3.51}$$

i.e. in the TDL a gap opens proportional to h^{ϵ}. Interestingly, such opening of a gap has been predicted by different theoretical approaches, it moreover has been observed experimentally (INS measurements) for copper benzoate (*Dender et al.* (1997)) [63]. Copper benzoate –so far being considered a spin-1/2 1d-Heisenberg antiferromagnet candidate– not only for the first time made the shift of the field-dependent soft mode observable, it in addition showed the opening of a gap due to the applied external magnetic field B with $E_{Gap} \sim B^{\epsilon}$, $\epsilon \simeq 2/3$. Since such a gap does not occur in a Heisenberg chain, these authors –and later more detailed *Oshikawa and Affleck*[169]–

discussed the existence of a local g-tensor for the Cu ions resulting in an additional staggered type field.
The coexistence of a staggered field (transverse or longitudinal) together with an uniform magnetic field and in particular the opening of gaps at the field-dependent and -independent soft modes will be the topic of the next section.

3.3 Coexistence of uniform and periodic perturbations

We will now switch to the discussion of a Heisenberg chain in a uniform magnetic field $\mathbf{B} = B \cdot \vec{e}_3$ that is perturbed by either a transverse or a longitudinal periodic field, i.e.

$$\begin{aligned} H &= H_0 - 2B\sqrt{N}S_3(q=0) + 2h_a\sqrt{N}S_a^c(q) \\ &\equiv H_0(B) + 2h_a\sqrt{N}S_a^c(q) \\ &= 2\sum_n \Big[\mathbf{S}(n)\mathbf{S}(n+1) - B \cdot S_3(n) + h_a \cdot \cos(qn)S_a(n)\Big] \quad ; \quad a = 1,3\,. \end{aligned} \tag{3.52}$$

The physics of the unperturbed chain –$H_0(B)$– has been outlined in Chap. 2. The quantum numbers of the ground state (Sec. 2.1: $q_0 = 0, \pi$, $S_0 = S_{z,0} = Nm$), the gapless spectrum and the monotonic slope of the magnetization curve have been discussed. In the limit of infinite N the lowest excitations of the chain reached by $S_3(q)$ and $S_\pm(q)$ acting on the ground state $|q_0, S>$

$$\omega_3(q,B,N) = E(q_0+q,S,N) - E(q_0,S,N) \tag{3.53}$$

$$\omega_\pm(q,B,N) = E(q_0+q,S\pm1,N) - E(q_0,S,N) \pm B \tag{3.54}$$

vanish for certain $q_k(m)$. The corresponding soft modes

$$q_k(m) = q_0 + k\cdot\pi(1-2m) \mod 2\pi \quad , \quad k = 0,1,2,\ldots \tag{3.55}$$

have been predicted in particular by the LSM-theorem (see Sec. 2.6.2). In the following discussion, based on finite-chain evaluations, we will again focus on the case $m = 1/4$ and on those soft mode momenta that appeared most clearly and stable in the scaling procedure presented in Sec. 2.6.3, namely

$$q_a(m) = \begin{cases} \pi & , \quad a = 1\,(,2) \\ \pi(1-2m) & , \quad a = 3 \end{cases} \,. \tag{3.56}$$

In Sec. 2.3 it has been reviewed that CFT describes the critical behaviour at the soft modes. In particular (cf. Sec. 2.6.3) the η-exponents, expressing the finite-size behaviour of the SSFs at the soft mode momenta q_a,

$$S_{aa}(q_a,N) \overset{N\to\infty}{\longrightarrow} const.\cdot N^{1-\eta_a(m)}\,, \tag{3.57}$$

are given by

$$\eta_a(m) = \frac{1}{\pi v(m)} \cdot \lim_{N\to\infty}\left(N\omega_a(q_a(m),B)\right) \tag{3.58}$$

$$v(m) = \lim_{N\to\infty}\left(E(q_0+dq,S) - E(q_0,S)\right)/dq \quad , \quad dq = \frac{2\pi}{N}\,. \tag{3.59}$$

Finally, it shall be pointed out that the finite-size behaviour of the transition amplitudes

$$2N^{1/2} < S\pm1, q_s + q_1(m), N|S_\pm(q_1(m),N)|S,q_0,N> \overset{N\to\infty}{\longrightarrow} \sim N^{\kappa_1(B)} \tag{3.60}$$

$$2N^{1/2} < S, q_s + q_3(m), N|S_3(q_3(m),N)|S,q_0,N> \overset{N\to\infty}{\longrightarrow} \sim N^{\kappa_3(B)} \tag{3.61}$$

and the behaviour of the SSFs at the soft mode momenta $q_a(m)$ (Eq. 3.57) result in the relation

$$\kappa_a(B) \;=\; 1 - \frac{\eta_a(m(B))}{2}\,, \tag{3.62}$$

leading to

$$\epsilon_a(B) \;=\; (1+\kappa_a(B))^{-1} = \frac{2}{4-\eta_a(m(B))}\,. \tag{3.63}$$

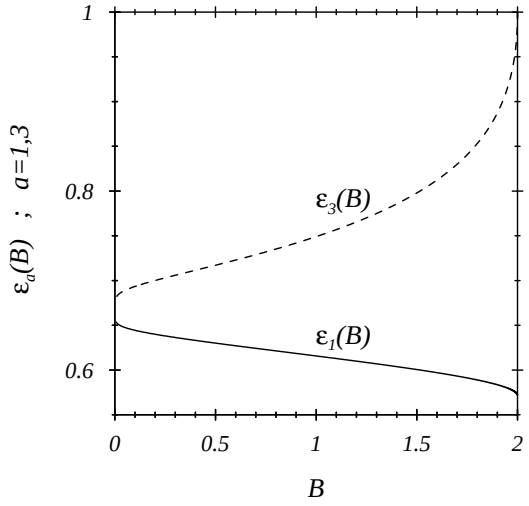

Figure 3.4: Critical exponents $\epsilon_{1,3}(B)$ determined from BA solutions for a 2048-site chain

3.3.1 Transverse staggered field in a uniform longitudinal magnetic field

Now, the evolution equations given above will be applied to the investigation of the opening of a gap under the influence of a staggered transverse field [85]. For zero uniform magnetic field Oshikawa and Affleck [169] showed that the gap rises $\sim h_1^{2/3}$. For general B the relations 3.38, 3.62 can be used to determine the exponents $\epsilon_a(B)$ from the η-exponents $\eta_a(m)$ that are accessible by Bethe ansatz (BA) calculations [84] as well as via the solution of non-linear integral equations derived from BA (quantum transfer method QTM in particular) [135]. Fig. 3.4 shows results for $\epsilon_a(B)$ resulting from BA solutions for a 2048-site chain (note, $B_{Sat}(h_1=0)=2$; see e.g. App. B). $B=0$ yields the above-mentioned exponent 2/3 related to $\kappa(B=0)=1/2$. Addressing first the soft mode at $q=\pi$, the first excited states accessable by $S_1(\pi)$ are

$$|n=\pm 1> \;=\; |q_0+\pi, S_3 = S\pm 1> \tag{3.64}$$

with

$$\omega_{\pm 1,0}(\pi,B,h_1=0) \;=\; E(q_0+\pi,S\pm 1) - E(q_0,S) \pm B \quad \stackrel{\mathbb{N}\to\infty}{\longrightarrow} \quad \sim N^{-1} \tag{3.65}$$

$$T_{\pm 1,0}(B,h_1=0) \;=\; 2N^{1/2} < \pm 1|S_\pm(\pi)|0> \quad \stackrel{\mathbb{N}\to\infty}{\longrightarrow} \quad \sim N^{\kappa_1(B)}\,. \tag{3.66}$$

A useful scaling analysis of the type

$$\frac{\omega_{10}(\pi,B,h_1)}{\omega_{10}(\pi,B,0)} \;=\; 1 + e_{10}(x,B) = 1 + \frac{1}{a_{10}} x\Omega_{10}(x) \tag{3.67}$$

with $x = Nh_1^{\epsilon_1(B)}$ requires a careful choice of B on a given finite-N magnetization plateau (see e.g. Fig. 2.2) – precisely at the 2 boundaries of such a plateau the energy differences to be scaled vanish. The midpoint $B_{\rm mid}(m, N)$ of this mentioned plateau i.e. the value of a Bonner-Fisher construction [32] coincides with the 2 gaps $\omega_{\pm 1,0}(\pi, B_{\rm mid}, 0)$ which are of equal and nonzero size. Since $< \pm 1|S_1(\pi)| \pm 1 >= 0$, this degeneracy is not lifted within 1st order perturbation theory and in the following, $B_{\rm mid}(m = 1/4, N)$ –as given in Table 3.1– will be used for the discussion of the scaling behaviour of the gap.

N	$B_{\rm mid}(m = 1/4, N)$
8	1.5642
12	1.5758
16	1.5798
20	1.5816

Table 3.1: Midpoint magnetic fields $B_{\rm mid}(N, m = 1/4)$ for the considered chain lengths

The smallness of the largest N-value used in the calculations presented below (compared with $N = 24, 28$) results from the lost conservation of S_3 for non-zero h_1 requiring to account for all different S_3-classes in the calculations. Moreover, numerical evaluations had to be restricted to the determination of the ground state energy ($q_0 = 0, \pi$) as well as the energy of the first excited state ($q = \pi, 0$), which make a direct scaling investigation at soft mode momentum $q_3(m)$ impossible.

Fig. 3.5 shows an intermediate stage of the determination of an optimal exponent describing the scaling of the excitation energy ratios (Eq. 3.67) and Fig. 3.6 gives a comparison of the scaling with the optimal scaling exponent $\epsilon_1(m = 1/4) = 0.595$ and the $m = 0$-exponent $\epsilon_1(m = 0) = 0.666$. The latter showing distinct scaling violations for $m = 1/4$.

Moreover, the plot of the energy ratios versus $x^{2/\epsilon_1(m)}$ makes use of the small-x analysis of Sec. 3.2.3 ($\phi^{(0)} = 2/\epsilon$) and the expected linear behaviour in $x^{2/\epsilon}$ is sufficiently well established for the left-hand plot in Fig. 3.6. In addition, the determined optimal value $\epsilon_1(m = 1/4) = 0.595(5)$ compares very well with $\epsilon_1(B(m = 1/4)) = 0.5975..$ as obtained from Fig. 3.4.

Now, we will turn to a different starting point, namely the discussion of the scaling of ground state energies at the soft mode positions when the field h_1 is applied (calling the lowest energy $E_0(B, 0)$ at $q = \pi/2$ ground state energy as well despite of the non-degeneracy of $E_0(B, 0; q_0 = 0, \pi)$ (see Sec. 2.1)). For that purpose, the 2nd derivative of the ground state energy (Eq. 3.19) will be 2-fold integrated and scaling results for the small-x behaviour of $\Omega_{10}(x)$, $\Theta_{10}(x)$ will be used. It is important to note that due to the momentum changes $\Delta q = \pi$ caused by $S_1(\pi)$ the 2 sets of momenta $0, \pi$ and $\pm\pi/2$ are independently described by the evolution equations. For both classes of soft mode momenta a scaling ansatz

$$\omega_{mn}(q_a, B, h_1) = h_1^{\epsilon(B)} \Omega_{mn}(x) \tag{3.68}$$

$$T_{mn}(B, h_1) = N h^{\sigma(B)} \Theta_{mn}(x) \tag{3.69}$$

is appropriate ($x = Nh_1^{\epsilon(B)}$). We will now evaluate the changes in ground state energies $\Delta E_0(B, h_1)$:

$$\Delta E_0(B, h_1) = E_0(B, h_1) - E_0(B, 0) \tag{3.70}$$

$$= \int_0^{h_1} dh_1' \int_0^{h_1'} dh_1'' \frac{d^2}{dh_1''^2} E_0(B, h_1'') \tag{3.71}$$

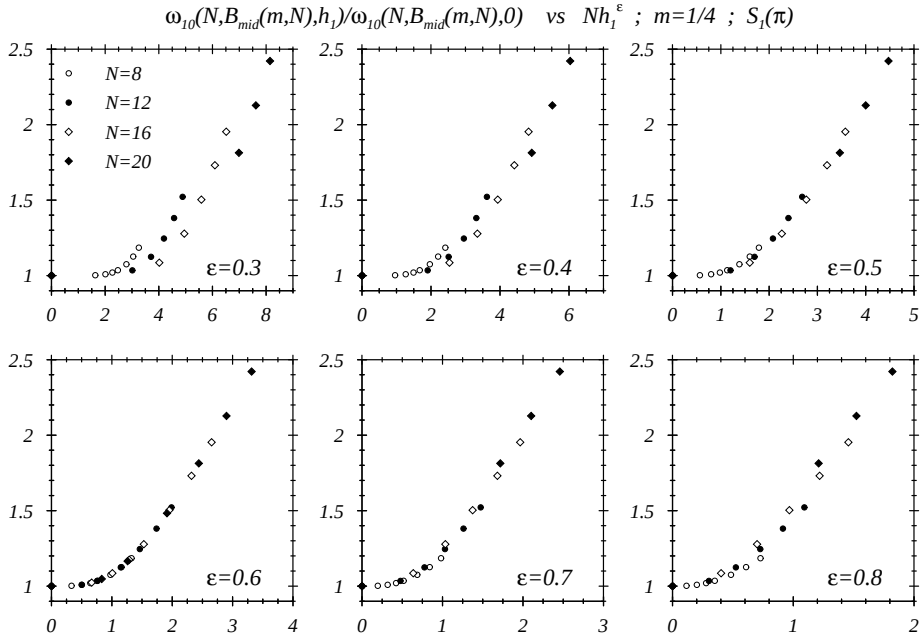

Figure 3.5: Course of the determination of the optimal scaling exponent $\epsilon_1(m = 1/4)$

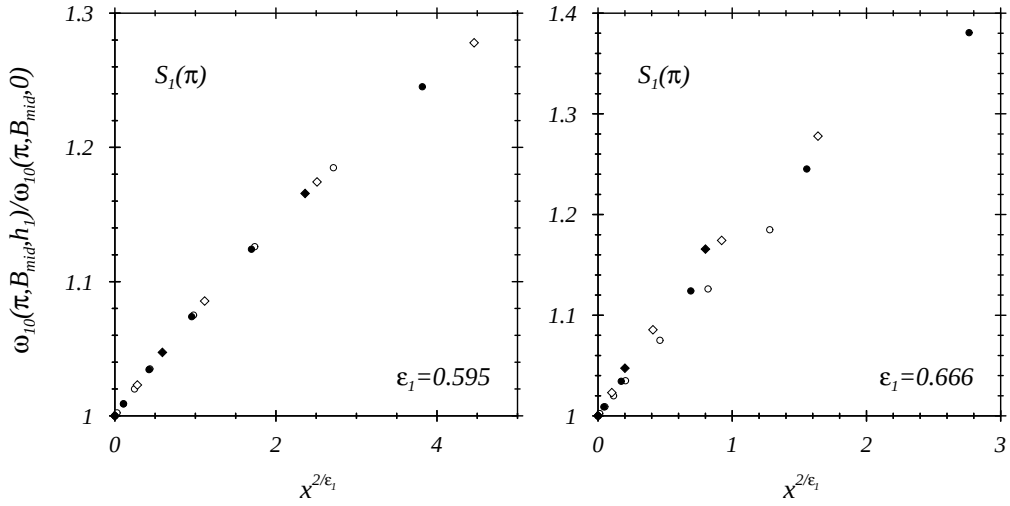

Figure 3.6: Comparison of optimal scaling $\epsilon_1(1/4) = 0.595$ and scaling with $m = 0$-exponent

and keep N fixed. The upper relation is valid due to the vanishing of the 1st derivative

$$\frac{d}{dh_1} E_0(B, h_1)\Big|_{h_1=0} \quad = \quad 2N^{1/2} < 0|S_1(\pi)|0 > \Big|_{h_1=0} = 0\,, \tag{3.72}$$

an important feature of periodic perturbations with $q \neq 0$ as has been emphasized in the first

part of this chapter. The 2nd derivative of the ground state energy (see Eq. 3.19)) reads

$$\frac{d^2}{dh_1^2}E_0 = -2\sum_{l\neq 0}\frac{|T_{l0}|^2}{\omega_{l0}} = -2(Nh_1^{\sigma(B)})^2 h_1^{-\epsilon(B)}\sum_{l\neq 0}\frac{|\Theta_{l0}|^2(x)}{\Omega_{l0}(x)} \tag{3.73}$$

$$= -2N^{1+2\kappa(B)}x^{1-2\kappa(B)}\sum_{l\neq 0}\frac{|\Theta_{l0}^2(x)|}{\Omega_{l0}(x)}\,. \tag{3.74}$$

Defining now

$$f(x) \equiv x^{1-2\kappa(B)}\sum_{l\neq 0}\frac{|\Theta_{l0}^2(x)|}{\Omega_{l0}(x)} \tag{3.75}$$

$$y \equiv x^{1/\epsilon(B)} = h_1 N^{1+\kappa(B)} \tag{3.76}$$

$\Delta E_0(B,h_1)$ is given by

$$\Delta E_0(B,h_1) = -2\left(\frac{h_1}{y}\right)^{\epsilon(B)}\int_0^y dy'\int_0^{y'} dy'' f(y'')\,. \tag{3.77}$$

The insertion of the leading orders in the small-x behaviour of $\Omega_{10}(x)$ and $\Theta_{10}(x)$ (see e.g. Eqns. 3.34, 3.35), i.e. $\Omega_{10}(x)\sim x^{-1}$, $\Theta_{10}(x)\sim x^{\kappa_1(B)-1} = x^{-2+1/\epsilon_1(B)}$, results in $f(y)\sim y^0$ and therefore

$$\Delta E_0(B,h_1) \sim -h_1^{\epsilon(B)}\cdot y^{2-\epsilon(B)} = -h_1^{\epsilon(B)}\cdot x^{2/\epsilon(B)-1}\,. \tag{3.78}$$

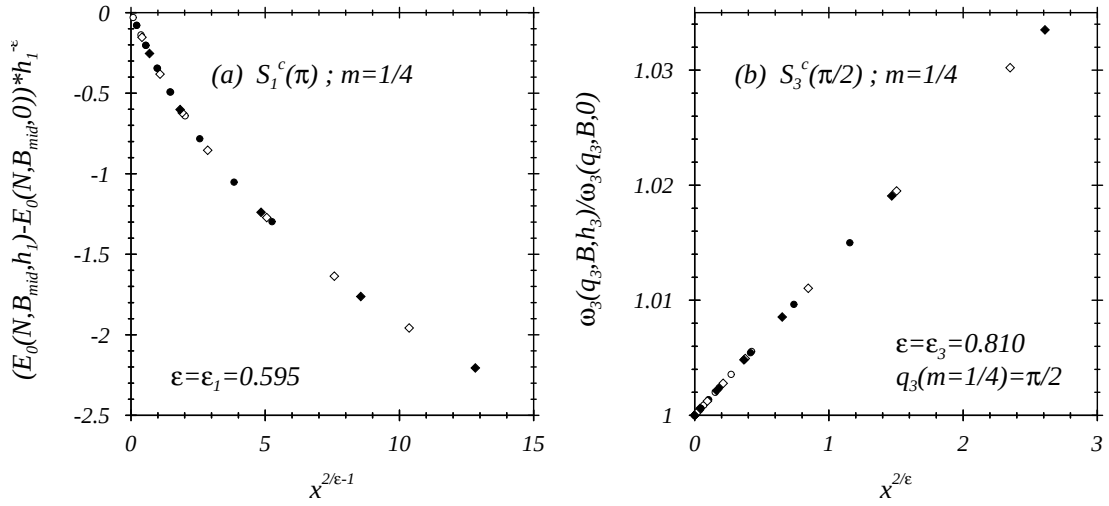

Figure 3.7: Scaling of (a) $\Delta E_0(B,h_1)$ (Eq. 3.70) and (b) gap ratio (Eq. 3.87)

A check of this type of scaling for the numerically accessible class of momenta $(0,\pi)$ is given in the left-hand side of Fig. 3.7. The figure shows a plot of $\Delta E_0(B,h_1)/h_1^{\epsilon_1(B)}$ vs. $x^{2/\epsilon-1}$ with an optimal $\epsilon=\epsilon_1=0.595$, i.e. showing the same $h_1^{\epsilon_1}$-dependence as found before for the excitation energies $\omega_{m0}(\pi,B,h_1)$ (ω_{10} to be precise).

The lowering of the ground state energy for the field dependent momenta $q=q_3(m)$, $q_3(m)+\pi$, i.e. here $q=\pm\pi/2$, requires a consideration of the respective initial conditions, namely the

knowledge of $\kappa_\pm = 1 - \eta_\pm/2$ describing the finite-size behaviour of the transition amplitudes

$$\begin{aligned} < \pm 1|2N^{1/2}S_1(\pi)|0 > &= 2N^{1/2} < q_0 + \pi + q_3(m)|S_1(\pi)|q_0 + q_3(m) \quad (3.79) \\ &= b_{\pm 1,0}(B)N^{\kappa_\pm(B)}\,. \quad (3.80) \end{aligned}$$

In [85] CFT relations between η-exponents and scaled energy differences (cf. Sec. 2.6.3) have been used to obtain

$$\eta_\pm(m) = \eta_1(m) + \frac{v_\pm(m)}{v(m)} = \eta_1(m) + 1\,. \quad (3.81)$$

Here, the slopes of the 2 dispersion curves ($v_\pm(m)$) approaching $q_3(m) \pm 2\pi/N$ and the respective slope at q_0 have been determined to be of identical size (compare e.g. Fig. 2.10; here $q_0 = \pi$). It is important to note that the above given exponents $\eta_\pm(m)$ differ from those discussed in Sec. 2.6.3 since different processes are considered. Here, we consider excitations of the lowest energy state at the soft mode $q_1(m)$ caused by the operator $S_1(\pi)$ (i.e. momentum changes $\Delta q = \pi$) while in Sec. 2.6.3 the field dependent soft mode $q_1(m)$ ($= q_3(m)$ only for $m = 1/4$) has been reached by a ground state excitation with momentum $q_1(m)$ (i.e. $\Delta q = q_1(M)$):

$$\begin{aligned} \eta_\pm(m)|_{Sec.2.6.3} &= \lim_{N\to\infty} \frac{N}{\pi v(m)} \left[E(q_0 + q_1(m) \pm 2\pi/N, m^\pm, N) - E(q_0, m, N)\right] \\ \eta_\pm(m)|_{Eq.3.81} &= \lim_{N\to\infty} \frac{N}{\pi v(m)} \left[E(q_0 + \pi + q_3(m), m^\pm, N) - E(q_0 + q_3(m), m, N)\right] \end{aligned}$$

with $m^\pm = m \pm 1/N$. For convenience, same symbols for the critical exponents have been used. Applying the results given by Eq. 3.81 one obtains

$$\epsilon_+ = \epsilon_- = \frac{2}{3 - \eta_1} > \epsilon_1 \quad (3.82)$$

leading to

$$\underbrace{(E(q_1 = q_3(m), h) - E(q_3(m), 0))}_{\sim h_1^{\epsilon_+}} \ll \underbrace{(E(q_1 = \pi, h) - E(\pi, 0))}_{\sim h_1^{\epsilon_1}} \quad \text{for} \quad h_1 \ll 1\,. \quad (3.83)$$

This means that for small perturbations h_1 the opening of a gap at the field dependent soft mode will be dominated by the much larger decrease of the true ground state energy ($q_0 = 0, \pi$). The field dependence of this opening of a gap is described by the same exponent $\epsilon_1(B)$ as in case of the field independent soft mode, i.e.

$$E(q_0 + q_3(m), S) - E(q_0, S) \sim h_1^{\epsilon_1(B)}\,. \quad (3.84)$$

3.3.2 Longitudinal staggered field in a uniform longitudinal magnetic field

We will now briefly sketch the situation of a staggered longitudinal field $\sim \sqrt{N}S_3(q)$:

$$H(B, h_3) = H_0(B) + 2h_3\sqrt{N}S_3^c(q)\,. \quad (3.85)$$

In this case, the 3-component of the total spin vector is conserved and $S_3^c(q)$ causes changes of momentum of $\pm q$ when acting on a momentum eigenstate. This means that the evolution equations couple momentum states

$$q_k = q_0 + kq \quad , \quad k = 0, 1, 2, \ldots\,. \quad (3.86)$$

Neglecting the uniform case $q = 2\pi n$, transition amplitudes $T_3(B, h_3 = 0) = 2N^{1/2} < q_0 \pm q, S|S_3(\pm q)|q_0, S >$ only show singular behaviour if q coincides with a soft mode momentum, e.g. $q = q_3(m)$:

$$\omega_3(q, B, h_3 = 0) \stackrel{N\to\infty}{\longrightarrow} a_3(B) \cdot N^{-1} \tag{3.87}$$

$$T_3(B, 0) \stackrel{N\to\infty}{\longrightarrow} b_3(B) \cdot N^{\kappa_3(B)} . \tag{3.88}$$

Following the same lines we expect a scaling behaviour of the gap

$$\frac{\omega_3(q_3, B, h_3)}{\omega_3(q_3, B, 0)} = 1 + e_3(x, B) \tag{3.89}$$

$$e_x(x, B) \sim x^{2/\epsilon_3(B)} . \tag{3.90}$$

The right-hand side of Fig. 3.7 shows an optimized finite-size scaling of ratio 3.87 on the basis of system sizes $N = 8, 12, 16, 20$ and for magnetization $m = 1/4$. The resulting exponent $\epsilon_3(m = 1/4) = 0.81..$ agrees very well with the value $\epsilon_3(m = 1/4) = 0.81011..$ derived from the data of Fig. 3.4. In the small-x regime the numerical data (rhs. Fig. 3.7) again and even better shows the linear behaviour in the predicted power of the scaling variable.
In the next chapter we will return to this briefly presented system and discuss the magnetization plateau formation under the influence of a correctly chosen periodic perturbation $h_3(q)$.

3.3.3 Periodic dimer perturbation $D_1(\pi)$, $m = 0$

At the end of the part concerned with the discussion of small periodic perturbations and their scaling properties some nearest neighbour dimer perturbations shall be considered. We start again at zero magnetization ([84]) and use

$$H = H_0 + 2h \cdot H_{D_1}(\pi) = H_0 + 2h \cdot \sqrt{N} D_1(\pi) \tag{3.91}$$

$$= 2 \sum_n \left(1 + h \cdot e^{i\pi n}\right) \mathbf{S}_n \mathbf{S}_{n+1} . \tag{3.92}$$

Hamiltonians of this kind extended by an additional (non-periodic) next-to-nearest neighbour coupling have been discussed for *spin-Peierls* systems (see e.g. [175, 35, 105]) which will be taken up again in Sec. 3.5. Here, we proceed in a way that meanwhile should appear quite habitually: first determining the exponent κ given by the initial conditions (i.e. $h = 0$), then considering the finite-size scaling predictions of type

$$\frac{\omega_{10}(N, h)}{\omega_{10}(N, 0)} = 1 + e_{10}(x) \tag{3.93}$$

$$\frac{T_{10}(N, h)}{T_{10}(N, 0)} = 1 + f_{10}(x) . \tag{3.94}$$

The first step is summarized in Fig. 3.8, where chains of $N = 8, 10, \ldots, 24$ have been evaluated. Again, $\omega_{10}(N, 0)$ shows distinct deviations from a clean $1/N$-behaviour and a fit of additional logarithmic corrections has as well been included in the respective part of the figure. However, an even stronger deviation is shown for $T_{10}(N, 0)$ – here, CFT predicts $\kappa = 1/2$ [163, 9] (as found for longitudinal staggered fields (Sec. 3.2.4). The value of $\kappa \simeq 0.37$ is influenced quite certainly by finite-size effects and $\kappa = 0.5$ is expected to be the TDL value.
Fig. 3.9, however, shows that the deviating κ-value is in agreement with the scaling of the energy- and transition amplitude ratios (Eq. 3.93, 3.94): $\kappa \simeq 0.37$, $\epsilon = (1 + \kappa)^{-1} \simeq 0.73$ and $\phi = 2/\epsilon \simeq 2.74$ are very well fulfilled by the shown quantities (note, that some of the fit values in Figs. 3.8, 3.9 show slight differences to the values given in [84] – an independent reexamination has been performed). The surprising existence of a finite-size pair of (κ, ϵ)-exponents almost

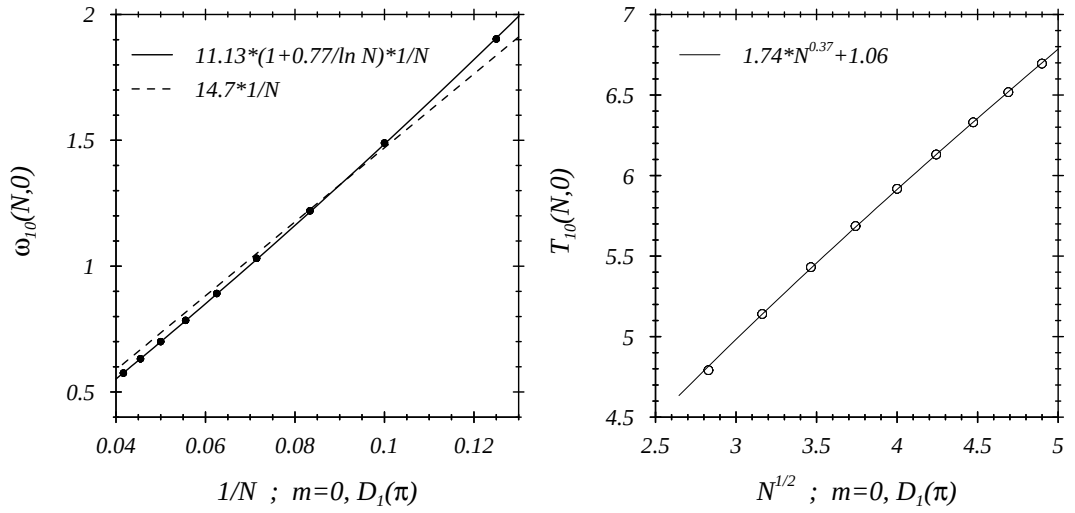

Figure 3.8: Finite-size dependence of $\omega_{10}(N,0)$ and $T_{10}(N,0)$; $N = 8, 10, \ldots, 24$

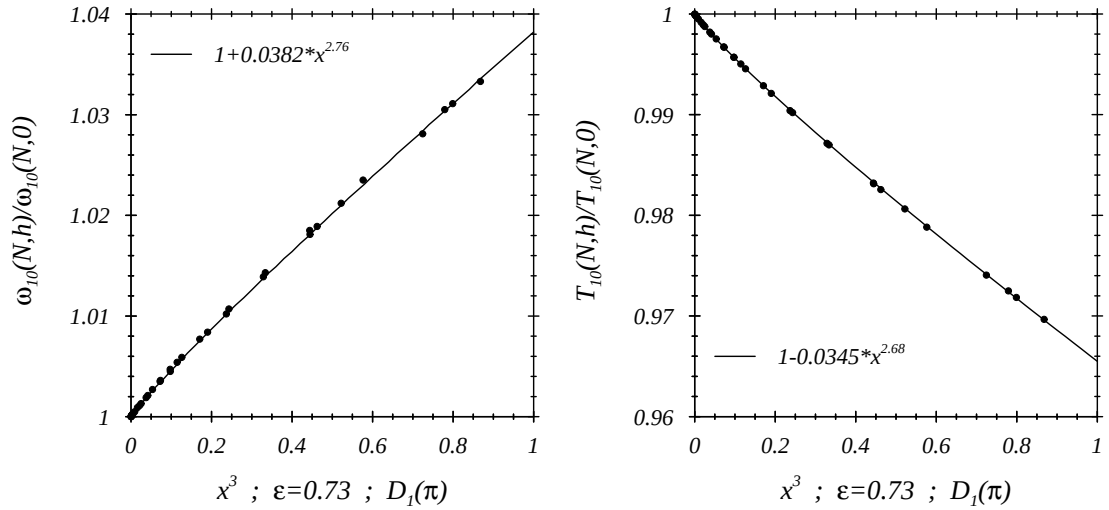

Figure 3.9: Scaling of the ratios given in Eqns. 3.93, 3.94

without contradiction to the scaling properties may be complemented with effective scaling dimensions by *Affleck and Bonner* [6]. These authors took the implications of logarithmic corrections into consideration, determining an exponent $\epsilon = 0.78$ for a 20-site chain.

Finally, 2 features shall briefly be mentioned. First, the coefficients e_{10} and f_{10} fulfill the relation

$$e_{10} + f_{10} \quad \simeq \quad 0$$

approximately. The relation that follows from Eqns. 3.42, 3.44 when neglecting contributions of all higher excitations.
Second, an analysis of the large-x behaviour analogously to the discussion given at the end of Sec. 3.2.4 results to

$$\Omega_{10}^{\infty} \quad = \quad 6.0(1)\,. \tag{3.95}$$

3.3.4 Periodic dimer perturbation $D_1^c(q)$, $m > 0$

We will now conclude the consideration of finite-size scaling behaviour of Heisenberg chains exposed to weak periodic perturbations. This will be done discussing periodic nearest neighbour dimer perturbations $N^{1/2}D_1^c(q)$ in the presence of a uniform magnetic field $\mathbf{B} = B\vec{e}_z$. A further degree of freedom is given in the additional presence of a constant second nearest neighbour coupling J_2

$$H(\alpha, B, h_q) \equiv H(B, \alpha) + 2h_q N^{1/2} D_1^c(q) \tag{3.96}$$

$$H(\alpha, B) = 2\sum_n \Big(\mathbf{S}(n)\mathbf{S}(n+1) + \alpha \cdot \mathbf{S}(n)\mathbf{S}(n+2) - B \cdot S_3(n)\Big)\,, \tag{3.97}$$

i.e. the ratio of second to nearest neighbour coupling reads $J_2/J_1 = \alpha$ with α usually designated as *frustration*. Note that J_1 is normally chosen to $J_1 \equiv 1$.
Right here it is not the point to discuss frustrated spin chains – this will be done in some more detail in Chap. 5. Here it is sufficient to note that for the 2 cases $\alpha = 0, 0.25$ considered below, the Heisenberg chain for finite N and $h_q = 0$ still is in the so-called *spin-liquid phase*, i.e. has a gapless spectrum. This behaviour ends at $\alpha = \alpha_c \simeq 0.25$, a gap is discussed to open like ($E_{gap} \sim e^{c/(\alpha-\alpha_c)}$, $\alpha > \alpha_c$) [99, 47] (however, no rigorous proof is known) and quantum numbers of the ground state change (for more details see Chap. 5).
At present we want to confine ourselves to a first consideration of the scaling of gap ratios at the location of the 1st LSM-soft mode ($k = 1$)

$$q^{(k)}(m) = k \cdot \pi(1 - 2m)\,, \tag{3.98}$$

i.e. if the momentum q of the perturbation $D_1^c q$ coincides with a soft mode momentum $q^{(k)}(m)$, the opening of a gap between the ground state $|0; \alpha, B, h_q>$ and the lowest lying state accessible via the perturbation (operator) $D_1^c(q)$ is predicted:

$$\omega^{(k)}(\alpha, B, h_q)\Big|_{q=q^{(k)}(m)} = \Big(h_{q^{(k)}(m)}\Big)^{\epsilon^{(k)}(m,\alpha)} \Omega^{(k)}(x; m, \alpha) \quad , \quad m = m(\alpha, B)\,. \tag{3.99}$$

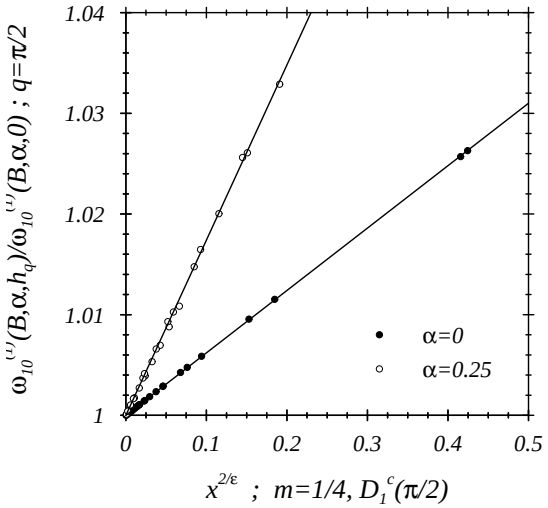

Figure 3.10: Scaling of the gap ratio (Eq. 3.100) for systems $N = 8, 12, 16$ and magnetization $m = 1/4$

The results of a check for the above-mentioned predictions are given in Fig. 3.10. There, the scaling of

$$\frac{\omega_{10}^{(1)}(\alpha, B, h_q)}{\omega_{10}^{(1)}(\alpha, B, 0)} \quad = \quad 1 + e_{10}^{(1)}(x; \alpha, B) \quad , \quad m = 1/4, \; q = \pi/2 \tag{3.100}$$

for magnetization $m = 1/4$, $q = q^{(k=1)}(m)$ (i.e. $q = \pi/2$) and the 2 frustrations $\alpha = 0$, 0.25 have been considered for system sizes $N = 8, 12, 16, 20$.
The data points (as well as the given linear fits) of the figure clearly show the scaling of the considered ratios as well as the different ϵ-exponents for the 2 frustrations that have determined to be

$$\epsilon^{(1)}(m = 1/4, \alpha) \quad = \quad \left\{ \begin{array}{lll} 0.81(1) & , & \alpha = 0 \\ 0.64(3) & , & \alpha = 0.25 \end{array} \right. . \tag{3.101}$$

Again, the gap ratio is found to scale $\sim x^{2/\epsilon}$ – note the occurrence of a misprint in [86] concerning this dependence.

We will now end the consideration of scaling behaviour of the Secs. 3.2, 3.3. It should be stressed here, that so far only small perturbations have been considered. All presented scalings have been based on h_a-perturbation strengths $h_a \in [10^{-3}, 5 \cdot 10^{-2}]$ for the given units (i.e. nearest neighbour coupling J_1 in H_0 equal to 1 – note that the prefactor 2 has always been treated as an overall prefactor of the respective Hamiltonians). This smallness will vanish when now turning to ladder geometries of spin systems. Retaining the picture of the 1-dimensional Heisenberg chain, its relationship between soft mode locations of the unperturbed chain and predictability of gap openings of periodically disturbed ones will make it affordable to turn to stronger perturbations. This procedure and moreover the limits of the above-mentioned predictability will be treated in the subsequent part of the chapter.
In addition, the next chapter will be devoted to a finite-size analysis of magnetization curves which is a very helpful technique: the formation of magnetization plateaus under the influence of periodic perturbations will be a main aspect.

3.4 Special classes I – ladder systems

In 1996 *Dagotto and Rice* [58] published the work "*Surprises on the Way from One- to Two-Dimensional Quantum Magnets: The Ladder Materials*" – a paper that has strongly influenced and amplified earlier discussion (e.g. [56] of spins on ladder systems. One of the most striking points is the different behaviour of spin-1/2 ladders with an even or odd number of legs. Fig. 3.11 shows a regular 2-leg ladder with indicated periodic boundary conditions (PBCs) along the legs (PBCs for the rungs only result in a modified rung coupling for the 2-leg ladder – see below). Ladders with an even number of legs have a finite energy gap to the lowest $S = 1$ excitation (in the TDL), an exponential decay of spin-spin correlations and ground states with purely short-range spin correlations.
In contrast to this, ladders with odd numbers of legs still show properties of a single chain: gapless behaviour with power-law fall-off of spin-spin correlations. Those fundamental differences have found experimental confirmation, e.g. for the 2-leg spin-1/2 ladders $(VO)_2P_2O_7$, $SrCu_2O_3$, organic $Cu_2(C_5H_{12}N_2)_2Cl_4$ or 3-leg ladder $Sr_2Cu_3O_5$. However, it is important to note that the description of $(VO)_2P_2O_7$ (one element out of a much wider group of ladder materials than listed here) changed [90]. Inelastic neutron scattering (INS) measurements showed that $(VO)_2P_2O_7$ has to be considered as an alternating spin chain orthogonal to the formerly assumed ladder direction.

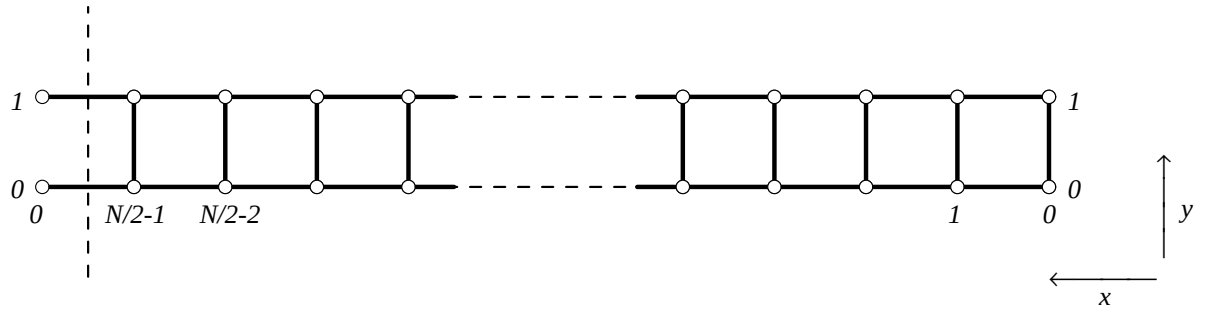

Figure 3.11: Geometry of a regular 2-leg ladder

The difference between ladders with odd and even numbers of legs finds a rather simple explanation when considering the case of rungs that are only weakly coupled in leg direction. Here, the ground states of the rungs have a total spin that is integer (even) or half-integer (odd) and the occurrence of a gap for even-leg ladders can be understood in terms of Haldane's conjecture [100, 101] for chains with integer spin. Here, the whole ladder can be considered as a single chain of integer spins formed by each rung.
It should be obvious that the discussion of more general cases (arbitrary strengths and signs of rung and leg couplings, different ladder geometries, etc.) requires different techniques. The following section contains some general considerations about the mapping of ladder structures on 1d-Heisenberg Hamiltonians, i.e. the description of ladder systems as periodically disturbed Heisenberg chains. The next chapter, however, will deal with a number of cases discussing their magnetization curves and showing the links between the magnetization values of emerging plateaus and the periodicity of the underlying periodicities of perturbations of the Heisenberg chain.

3.4.1 The liberties in mapping a ladder system on a 1-dimensional chain

In the following some of the ways of forming a one-to-one correspondence between a 1-dimensional chain and a ladder system with n_l legs will be addressed. Only focussing on regular coverings of a given ladder, one has to correct the chain Hamiltonian by adding or subtracting couplings $\mathbf{S}_j\mathbf{S}_{j+x}$ at every j-th point within a unit length n_u of the chain (e.g. subtracting the diagonal couplings in Fig. 3.12 (b),(c)). This is accomplished by adding/subtracting the periodic "perturbation(s)"

$$\sum_n f_n(n_u, j) \cdot 2\mathbf{S}_n\mathbf{S}_{n+x} \tag{3.102}$$

with

$$f_n(n_u, j) \;=\; \frac{1}{n_u}\sum_{m=0}^{n_u-1} e^{i\frac{2\pi}{n_u}(n-j)m} \;=\; \sum_{p=0}^{N/n_u-1} \delta_{n,j+p\cdot n_u} \tag{3.103}$$

to/from the chain Hamiltonian $H_0 = 2\sum_n \mathbf{S}_n\mathbf{S}_{n+1}$ expressed by the thick lines in Figs. 3.12, 3.13. Here, and in what follows $\sum_n$ always means $\sum_{n=0}^{N-1}$. Some examples for the explicit form of the $f_n(n_u, j)$ are

$$\begin{aligned} f_n(2,j) &= \frac{1}{2}\left(1+\cos\pi(n-j)\right) \\ f_n(3,j) &= \frac{1}{3}\left(1+2\cos\frac{2\pi}{3}(n-j)\right) \end{aligned} \tag{3.104}$$

$$f_n(4,j) \;=\; \frac{1}{4}\left(1+2\cos\frac{\pi}{2}(n-j)+\cos\pi(n-j)\right)\,,$$

i.e. all multiples $(2\pi/n_u)\cdot p,\ \ p=0,1,\ldots$, with $(2\pi/n_u)\cdot p \le \pi$ are contributing (note, that $f_n(1,0)=f_n(1,1)=1$):

$$f_n(n_u,j) \;=\; \frac{1}{n_u}\sum_{k'=-[n_u/2]^{+}+1}^{[n_u/2]^{-}} \cos\left(\frac{2\pi}{n_u}(k'-j)\right) \tag{3.105}$$

with $[n_u/2]^{\pm}=n_u/2$ for even n_u and $[n_u/2]^{\pm}=(n_u\pm 1)/2$ for odd n_u.

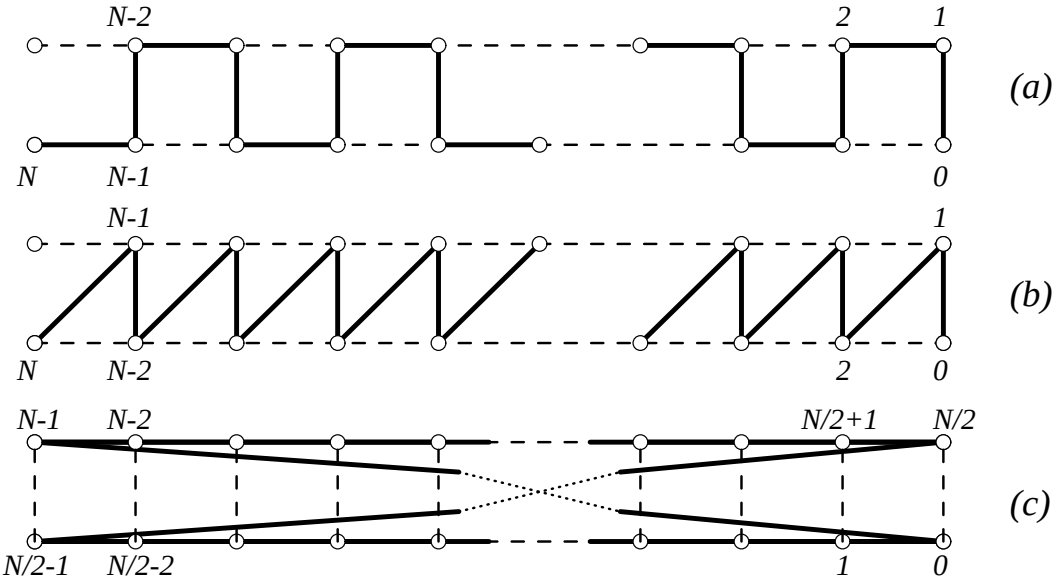

Figure 3.12: Description of (2-leg) ladders on the basis of a 1-dim. Heisenberg chain

The relations given above will now be used to express the 3 different parts $H_{\parallel}$, $H_{\perp}$, $H_{\perp}^{pbc}$ of the ladder Hamiltonian. Here, PBCs in leg direction will be assumed; their influence, however, is much weaker –disappearing for $N\to\infty$– than those for the rungs that have a sustainable impact on the (anti-)ferromagnetic spin orientation and/or frustration along the rungs of the ladder. The resulting components for the cases (a), (b), (c) in Fig. 3.12 –generalized to n_l-legged ladders– read ($\sum_n$ always meaning $\sum_{n=0}^{N-1}$):

(a)

$$H_{\perp} \;=\; H_0 - 2\sum_n f_n(n_l,n_l-1)\mathbf{S}_n\mathbf{S}_{n+1} \tag{3.106}$$

$$H_{\perp}^{pbc} \;=\; 2\sum_n f_n(n_l,0)\mathbf{S}_n\mathbf{S}_{n+n_l-1} \tag{3.107}$$

$$H_{\parallel} \;=\; 2\sum_n\sum_{j=0}^{n_l-1} f_n(n_l,j)\mathbf{S}_n\mathbf{S}_{n+2(n_l-j)-1} \tag{3.108}$$

(b)

$$H_\perp = H_0 - 2\sum_n f_n(n_l, n_l - 1)\mathbf{S}_n\mathbf{S}_{n+1} \tag{3.109}$$

$$H_\perp^{pbc} = 2\sum_n f_n(n_l, 0)\mathbf{S}_n\mathbf{S}_{n+n_l-1} \tag{3.110}$$

$$H_\parallel = 2\sum_n \mathbf{S}_n\mathbf{S}_{n+n_l} \tag{3.111}$$

(c)

$$H_\perp + H_\perp^{pbc} = 2\sum_n \mathbf{S}_n\mathbf{S}_{n+N/n_l} \tag{3.112}$$

$$H_\parallel = H_0 - 2\underbrace{\sum_n f_n(N/n_l, N/n_l - 1)\mathbf{S}_n\mathbf{S}_{n+1}}_{(*)} \tag{3.113}$$

Considering the 3 descriptions from the point of view of moderately, periodically perturbed Heisenberg chains one is led to the following observations:

1. Every single perturbation is not moderate (couplings of equal strength appear or disappear not meaning a small perturbation as discussed in Secs.3.2, 3.2.1, pp.). Instead, "moderate" can only be limited and classified by the total number of perturbations (e.g. $O(n_l)$ in term $(*)$, Eq. 3.113), or –looking from the unperturbed Heisenberg chain– by the manyfold, the periodicity and range of the additionally appearing couplings.

2. The 2-leg ladder takes a special place in the ladder scheme: First, PBCs along the rungs are simply incorporated doubling the contribution of $H_\perp$; Second, only in this case the contribution of H_0 in case (a) (Fig. 3.12) can as well be attributed to $H_\parallel$ with the same number of bonds to be corrected.

3. Scheme (b) appears to be more preferable at least considered from the point of finite-size calculations than (a) since it only contains couplings up to n_l-th nearest neighbours instead of $2n_l - 1$ in case (a). It should be noted, however, that the momenta of the contributing periodic perturbations do not differ.

4. Schemes (a) and (b) have contributions of H_0 in both the rung- and leg-part of the ladder, i.e. they do not offer a useful starting point to study weakly coupled legs or rungs in a ladder. Such investigations are usually done applying perturbation theory/bosonization techniques/renormalization group methods to the situation of weakly coupled chains/legs (see e.g. [38, 134]).

5. In the TDL term $(*)$ appearing in case (c) is negligible and the Hamiltonian $H_\perp + H_\perp^{PBC} + H_\parallel$ turns out to be completely translational invariant only containing $q = 2\pi n$-perturbations. Here, legs and rungs are decoupled, offering –in principle– weak coupling treatments. The case of translationally invariant perturbations will be postponed to Sec.5.

6. Discussion of type (c) without PBC along the rungs and $n_l > 2$ is accompanied by the occurrence of $O(N)$-periodic perturbations (see below) extending the usefulness of the concept of periodic perturbations.

Fig. 3.13 shows a more general case that in the 2 limits $n_h = 1$, $n_h = N/n_l$ contains the schemes (b) and (c) of Fig. 3.12 and might help to gain some further insight. The above discussed components of the ladder Hamiltonian read for the case of Fig. 3.13 (generalized to arbitrary n_l, n_h)

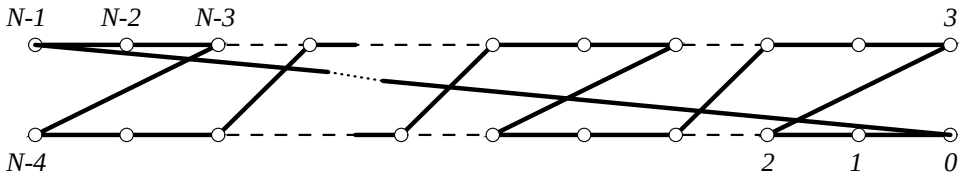

(d)

Figure 3.13: Generalized formulation for ladders of type (b) and (c); here $n_l = 2$, $n_h = 3$

(d)

$$H_\perp = 2\sum_n \sum_{j=0}^{(n_l-1)\cdot n_h-1} f_n(n_l \cdot n_h, j)\mathbf{S}_n\mathbf{S}_{n+n_h} \tag{3.114}$$

$$H_\perp^{pbc} = 2\sum_n \sum_{j=0}^{n_h-1} f_n(n_l \cdot n_h, j)\mathbf{S}_n\mathbf{S}_{n+(n_l-1)\cdot n_h} \tag{3.115}$$

$$H_\parallel = H_0 + 2\sum_n f_n(n_h, n_h-1)\left(\mathbf{S}_n\mathbf{S}_{n+(n_l-1)\cdot n_h+1} - \mathbf{S}_n\mathbf{S}_{n+1}\right) \tag{3.116}$$

containing couplings of up to $(n_l-1)\cdot n_h$ $(+1)$-nearest neighbours. For the choice $n_h = N/n_l$ the sum of the contributions $H_\perp$ and $H_\perp^{PBC}$ result in the term given above in scheme (c) – each term of its own containing $O(N)$-momentum contributions $((2\pi/N)\cdot l)$ that only in case of PBCs for the rungs disappear.
In summary, scheme (a) as well as scheme (d) (the latter in particular for $1 \ll n_h \ll N/n_l$) do not turn out to be useful as a ladder description acceptably well suited to the concept of periodically perturbed Heisenberg chains presented so far. Therefore, scheme (b) will be used in the following, scheme (c) -as repeatedly mentioned- will be postponed to Chap.5.
The ladder Hamiltonian $H_\perp$ for type (b) can be written in the form

$$H_\perp = H_0 - 2\sum_n f_n(n_l.n_l - 1)\mathbf{S}_n\mathbf{S}_{n+1} \tag{3.117}$$

$$= H_0 - 2\sum_n \frac{1}{n_l}\left\{\sum_{k'=-[n_l/2]^+ +1}^{[n_l/2]^-} \cos\left(\frac{2\pi}{n_l}k'(n-n_l+1)\right)\right\}\mathbf{S}_n\mathbf{S}_{n+1} \tag{3.118}$$

$$= H_0 - \frac{2}{n_l}\sqrt{N}\sum_{n,k'}\left(\cos(q_{k'}(n_l-1))D_1^c(q_{k'}) + \sin(q_{k'}(n_l-1))D_1^s(q_{k'})\right) \tag{3.119}$$

$$= H_0 - \frac{2}{n_l}\sqrt{N}\sum_{n,k'}\cos(q_{k'}(n_l-1))D_1^c(q_{k'}) \tag{3.120}$$

with $q_{k'} = 2\pi k/n_l$ and

$$D_j^{s,c}(q) = \frac{1}{\sqrt{N}}\sum_n \begin{matrix}\sin(qn)\\ \cos(qn)\end{matrix} \cdot \mathbf{S}_n\mathbf{S}_{n+j}\,. \tag{3.121}$$

The latter form of $H_\perp$ immediately gives the number and type of periodic perturbations appearing when this particular description of the ladder is used. The inclusion of PBCs for the rungs,

i.e. $H_\perp^{pbc}$, requires additional periodic dimer perturbations

$$H_\perp^{pbc} = \frac{2}{n_l}\sqrt{N}\sum_{k'} D^c_{n_l-1}(q_{k'})\,. \tag{3.122}$$

We will return to these representations when discussing the locations of possible magnetization plateaus for n_l-leg ladder systems in the next chapter.

We will finally discuss ladder Hamiltonians sketched in Fig. 3.11 i.e. using components x and y for the leg and rung directions, for the example of 2-leg ladders:

$$\begin{aligned} H(J_\parallel, J_\perp; B) &= 2\left(J_\parallel \sum_{y=0}^{n_l-1}\sum_{x=0}^{n_r-1} \mathbf{S}(x,y)\mathbf{S}(x+1,y) \right. \\ &\left. + J_\perp \sum_{x=0}^{n_r-1}\sum_{y=0}^{n_l-1} \mathbf{S}(x,y)\mathbf{S}(x,y+1) - B\sum_{x,y} S_3(x,y) \right) \end{aligned} \tag{3.123}$$

with $n_r = N/n_l$. Here, the situation is different and no periodic perturbations with $q \neq 2\pi n$ appear. We will encounter such situations again, when discussing more generally $q = 2\pi n$-perturbations in Chap. 5.
The following Figs. 3.14-3.17 refer to some properties of a 2-leg ladder described by Hamiltonian 3.123 and parameters $J_\parallel = 1$, $J_\perp = h = 0.5,\ -1.0$ and $B = m = 0$. These 2-leg ladders with $N = 4n,\ n \in \mathbb{N}$ have ground state momentum $\vec{q}_0 = (q_{x,0}, q_{y,0}) = (0,0)$ [215] and their lowest excitatuions ($S = 1$) can be accessed via the excitations of the DSF $S_{33}(\omega, q_x, q_y, h, N)$.

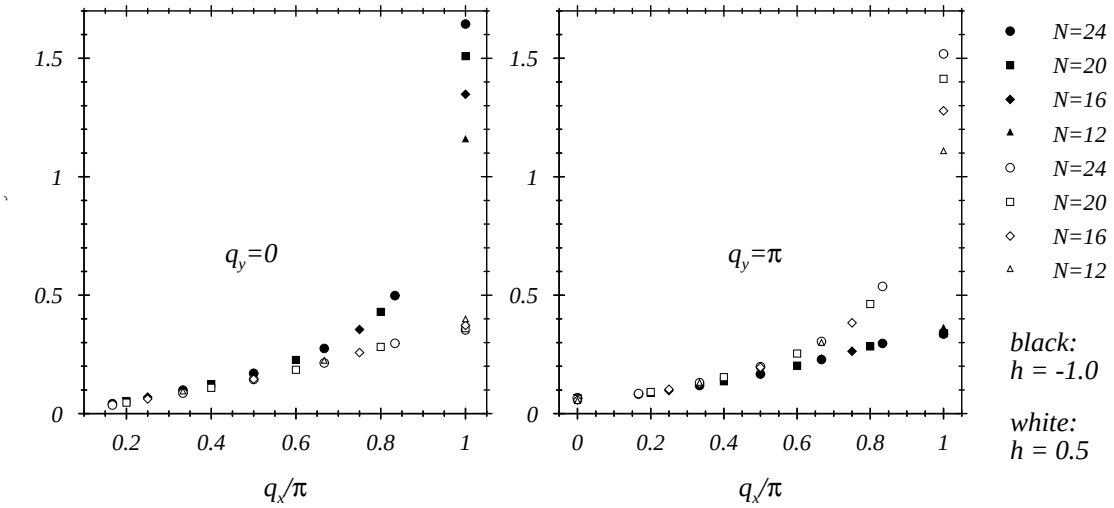

Figure 3.14: SSFs $S_{33}(\vec{q}, h, N)$ for rung couplings $h = -1.0,\ 0.5$ and $N = 12, 16, 20, 24$

Figs. 3.14-3.17 refer to situations where the inter-leg (rung) coupling h is already of substantial importance. An increasing ferromagnetic rung coupling ($h < 0$) more and more drives the ladder system to an effective spin-1 chain (the 2 spin-1/2s on a rung forming an effective spin-1) and the energy gap of the spin-1/2 ladder approaches the *Haldane* gap [100, 101] for the spin-1 chain saturating at a finite gap value $E_{gap,\,S=1} = 0.41049(2)$ [94]. – *Schollwöck and Jolicœur* [181, 182] further studied quantum spin chains with integer spin ($S = 1,\ 2$). DMRG calculations led to a significantly smaller TDL of the $S = 2$ gap ($\Delta = 0.085(5)\,J$) that would have to be discussed in the framework of the energy gap of a corresponding 4-leg spin-1/2 ladder.

For antiferromagnetic rung couplings ($h > 0$) on the other hand, the gap shows an almost linear increase in h. We will again encounter the h-dependence of the energy gap of a ladder in Chap. 5 and will not discuss this case here. Moreover, [215] contains a broad discussion of this and most of the following aspects of spin-1/2 2-leg ladders. Fig. 3.14 shows SSFs $S_{33}(q_x, q_y, h, N)$ for the mentioned h-values for both $q_y = 0, \pi$. The figure clearly shows the sign dependence of the dominant part of the SSF on h (approaching $q_x = \pi$, where the gap is located for both signs of h).

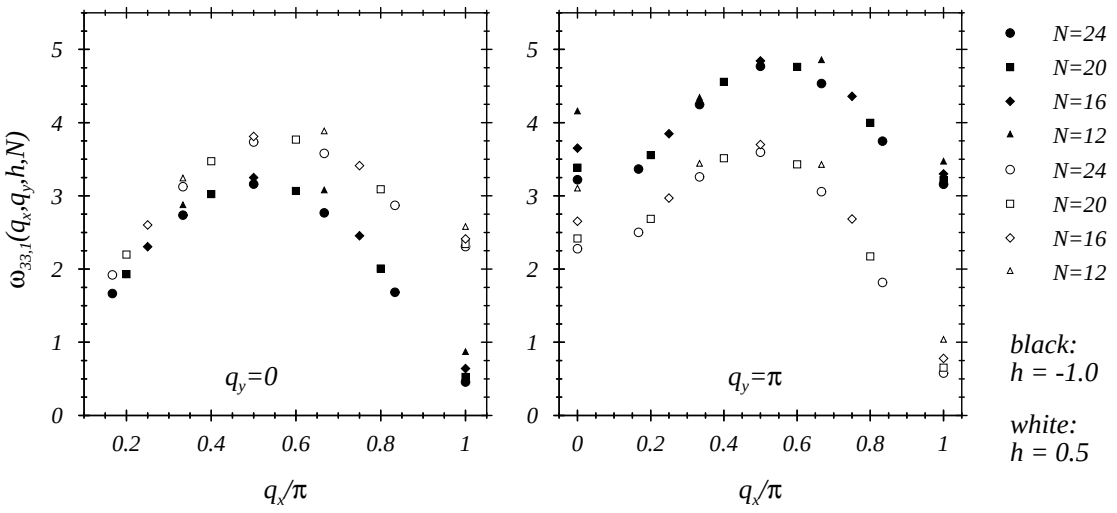

Figure 3.15: N-dependence of lowest excitations for $h = -1.0,\ 0.5$ and $N = 12, 16, 20, 24$

This is in particular demonstrated in Fig. 3.15 that shows the location of the gap at $q_x = \pi$. The dominant parts of the SSFs close to $q_x = \pi$ are clearly related to the lowest excitations of the respective ladder. The N-dependence of the increase of the dominant SSF-parts ($q_y = 0$ for $h < 0$ and $q_y = \pi$ for $h > 0$) however shows the limitations of the present range of numerical evaluations: The already mentioned approach of the ladder to a spin-1 chain with inreasingly negative rung coupling –the latter having a finite correlation length of $\xi \simeq 6.2$ [94]– and on the other hand the fitted behaviour of $S_{33}(\pi, 0, h \leq -1, N \leq 24) \sim \ln N$ manifests that the manageable system lengths are too small for a consistent determination of the large-N behaviour of $S_{33}(\pi, 0, h \leq -1, N)$ which is expected to be finite. The situation moderately changes for $h > 0$. Here, only in a small window around $h = 0.5$ $S_{33}(\pi, \pi, h > 0, N \leq 24)$ appears to behave $\sim \ln N$, however, definite answers about the infinite-N limit are out of range [215]. An extension of manageable system sizes by roughly one order of magnitude applying DMRG-techniques [214] should allow the treatment of systems that are sufficiently large to include a multiple of the above-mentioned correlation lengths.

The gaps $E_{gap}(h)$ indicated in the plots of the lowest excitation energies in Fig. 3.15 ($q_y = 0$ for $h < 0$; $q_y = \pi$ for $h > 0$) have been analyzed in [215] using a particular $N^{-1}\exp(-N/N_0)$-fit [17]. The shown cases yield $E_{gap}(-1.0) = 0.3321(2)$, $E_{gap}(0.5) = 0.4533(2)$. Moreover, for all rung couplings outside the vicinity of $h = 0$ a finite gap was observed. The explanation of the opening of the gap for small perturbations, however, remains to be accomplished. This will be postponed to Chap. 5.

Figs. 3.16, 3.17 show the low-energy part of the whole excitation spectra (parts accessible by means of the recursion method; App. A) for $S_{33}(q_x, q_y = 0, \pi, h, N)$. Especially for those q_y belonging to the excitations that form the gap at $q_x = \pi$ the branch of lowest excitations carries almost the complete spectral weight for each q_x (relative weight 0.9...1.0, see figures).

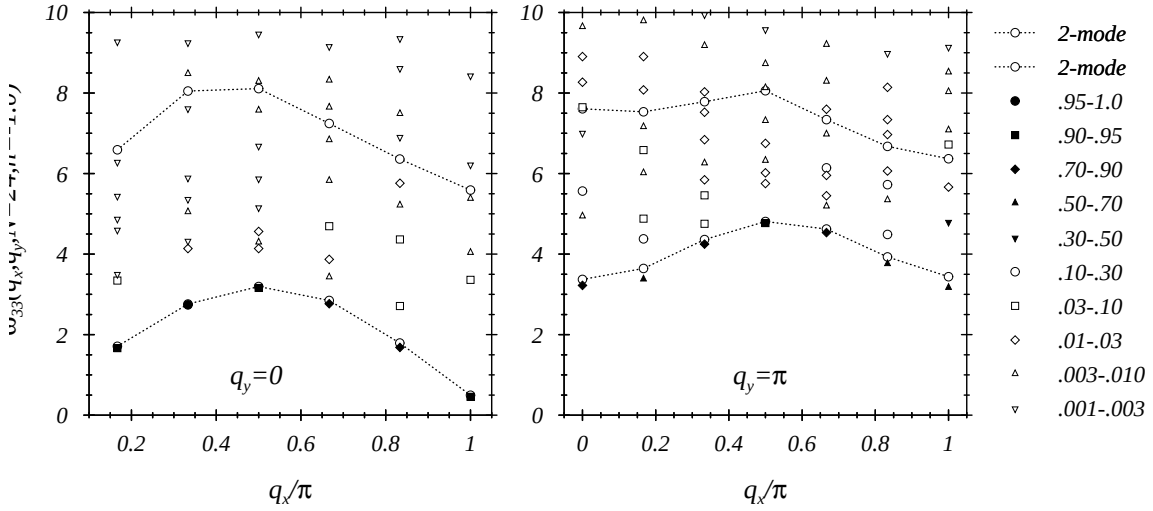

Figure 3.16: Excitation spectra ($q_y = 0, \pi$) for rung coupling $h = -1.0$ and $N = 24$

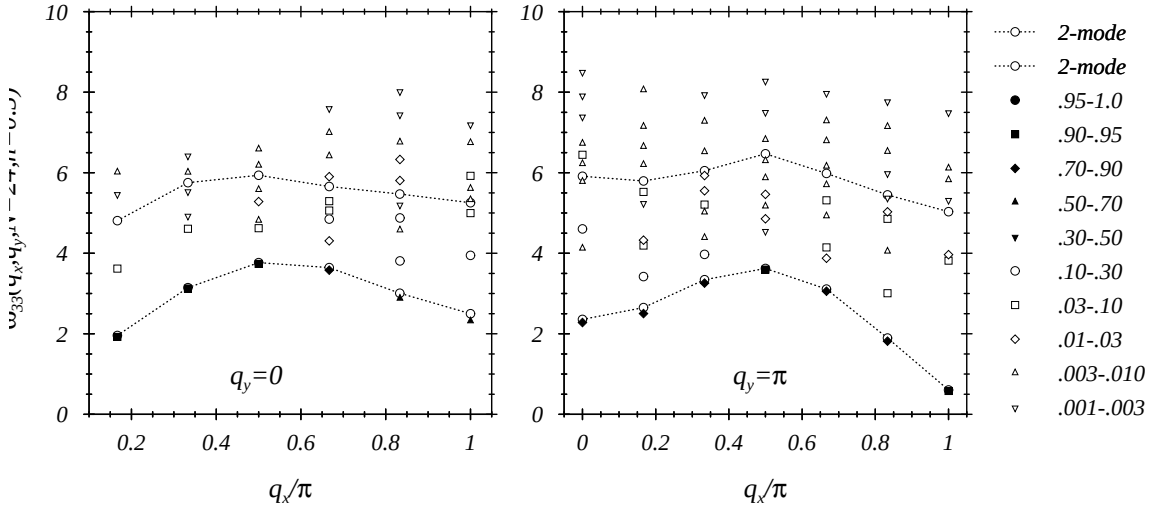

Figure 3.17: Excitation spectra ($q_y = 0, \pi$) for rung coupling $h = 0.5$ and $N = 24$

For such a situation, Figs. 3.16, 3.17 as well show the results of an approximation (here: 2-mode approximation) that does not make use of the recursion method but on frequency moments. Assuming

$$S_{33}^{2-mode}(\vec{q},\omega) \;=\; \mathrm{w}_1\delta(\omega-\omega_1)+\mathrm{w}_2\delta(\omega-\omega_2)\,, \tag{3.124}$$

the 2 weights w_j and frequencies ω_j are unequivocally determined by

$$\begin{aligned}
\mathrm{w}_2 &= K^{(0)}-\mathrm{w}_1 \\
\mathrm{w}_1 &= \left(K^{(1)}-\omega_2 K^{(0)}\right)/\left(\omega_1-\omega_2\right) \\
\omega_1 &= \left(K^{(2)}-\omega_2 K^{(1)}\right)/\left(K^{(1)}-\omega_2 K^{(0)}\right)
\end{aligned} \tag{3.125}$$

$$
\begin{aligned}
0 &= \left(K^{(2)} - 2\omega_2 K^{(1)} + \omega_2^2 K^{(0)}\right)\left(K^{(3)} - \omega_2^3 K^{(0)}\right)\left(K^{(1)} - \omega_2 K^{(0)}\right) \\
&\quad - \left(K^{(2)} - \omega_2 K^{(1)}\right)^3 + \omega_2^3 \left(K^{(1)} - \omega_2 K^{(0)}\right)^3
\end{aligned}
$$

using the frequency-moments $K^{(0)}(\vec{q}, h, N), \ldots, K^{(3)}(\vec{q}, h, N)$ (see as well Sec. 2.6.6). The figures show the good reproduction of the low-energy dispersion and the average-like consideration of the remaining spectrum (not all evaluated excitations are shown in the figures). However, it ought to be noted that this simpler form of determining lowest excitations requires the a priori knowledge of their high contribution to the total weight at the respective q-value.
Finally, Figs. 3.18, 3.19 show the 4 frequency-moments being used for the 2-mode approximation. Again, odd frequency-moments of the ladder can be expressed as

$$
K_{33}^{(2l+1)}(\vec{q}, h, N) = \sum_{n=0}^{2l+1} T_{33,n}^{(2l+1)}(h, q_y, N) \cdot (1 - \cos q_x)^l \tag{3.126}
$$

$$
T_{zz,0}^{(2l+1)}(h, N) = 0 \qquad \text{for} \quad q_y = 0 \tag{3.127}
$$

(cf. Sec. 2.6.6). The lines given for $K^{(1)}$ and $K^{(3)}$ in Figs. 3.18, 3.19 result from fitting 3.126 to the $N = 28$ data. Table 3.2 gives the results for $T_{33,l}^{(n,j)}$ for the moments $n = 1, 3$, $q_y = j \cdot \pi$ and system sizes $N = 20, 24, 28$ (Note, that the number of spins in a leg is $N/n_l = N/2$). Similar to the case of the unperturbed Heisenberg chain the frequency-moments of the spin-spin DSF only have very small finite-size contributions.

N	n	j	h	$T_{33,0}^{(n,j)}$	$T_{33,1}^{(n,j)}$	$T_{33,2}^{(n,j)}$	$T_{33,3}^{(n,j)}$	h	$T_{33,0}^{(n,j)}$	$T_{33,1}^{(n,j)}$	$T_{33,2}^{(n,j)}$	$T_{33,3}^{(n,j)}$
20	1	0	-1.0	0.0	0.562			0.5	0.0	0.561		
24	1	0	-1.0	0.0	0.560			0.5	0.0	0.557		
28	1	0	-1.0	0.0	0.559			0.5	0.0	0.556		
20	1	1	-1.0	0.270	0.562			0.5	0.179	0.561		
24	1	1	-1.0	0.271	0.560			0.5	0.182	0.557		
28	1	1	-1.0	0.272	0.559			0.5	0.184	0.556		
20	3	0	-1.0	0.0	1.827	9.268	-3.765	0.5	0.0	1.853	10.713	-3.771
24	3	0	-1.0	0.0	1.848	9.129	-3.687	0.5	0.0	1.901	10.503	-3.672
28	3	0	-1.0	0.0	1.861	9.051	-3.644	0.5	0.0	1.932	10.385	-3.617
20	3	1	-1.0	6.903	10.726	8.230	-3.765	0.5	2.510	5.546	6.954	-3.771
24	3	1	-1.0	6.846	10.739	8.103	-3.687	0.5	2.516	5.579	6.751	-3.672
28	3	1	-1.0	6.811	10.747	8.036	-3.644	0.5	2.522	5.595	6.637	-3.617

Table 3.2: Coefficients $T_{33,n}^{(2l+1)}(h, q_y, N)$ with $q_y = j \cdot \pi$ and $N = 20, 24, 28$

Note, that this time the frequency-moments $K^{(n)}$ are carrying a prefactor 2^n due to the actually used Hamiltonian 3.123.
Now we will turn to some other types of ladders that will as well be considered in the next chapter concerning the opening of gaps and formation of magnetization plateaus. These types are the so-called zig-zag and, in addition, Kagomé-like ladders.

3.4.2 Different types of ladder geometries

In this section a number of different ladder types will be introduced that have been discussed by several authors for different reasons [39, 208]. Here, the ladder systems shall be introduced

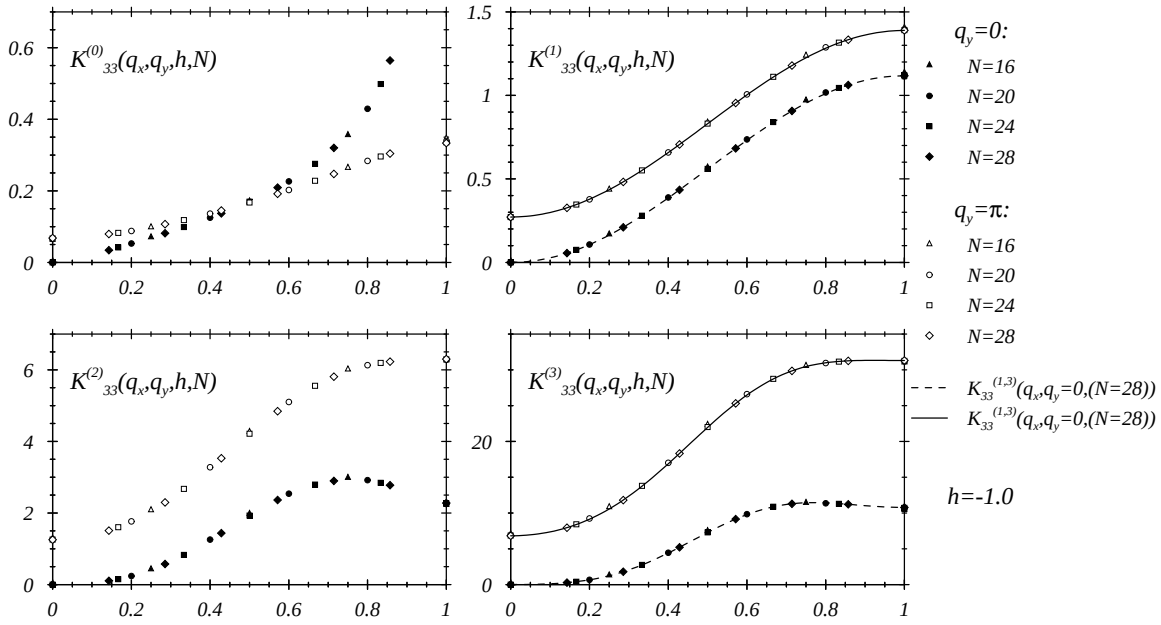

Figure 3.18: Frequency-moments $K^{(n)}(\vec{q}, h, N)$ for $h = -1.0$ an $N = 16, 20, 24, 28$

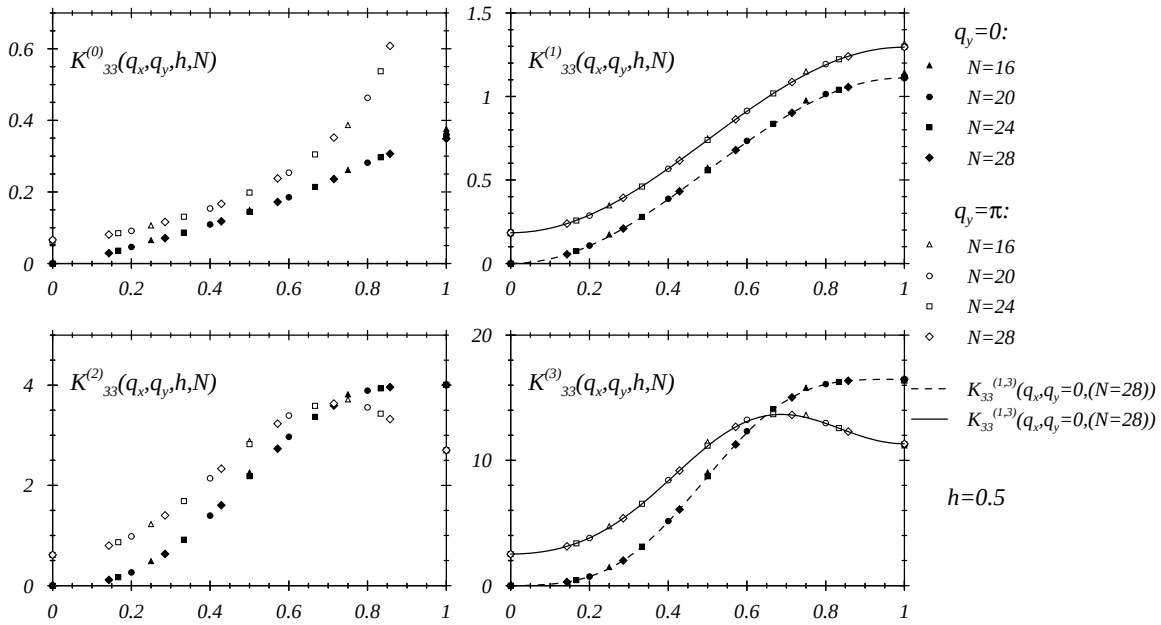

Figure 3.19: Frequency-moments $K^{(n)}(\vec{q}, h, N)$ for $h = 0.5$ an $N = 16, 20, 24, 28$

and their discussion and anew treatment with help of the methods given in the present work will be a topic of the next chapter.

The first systems are 2- and 3-leg zig-zag ladders shown in parts (a) and (b) of Fig. 3.20. The couplings have been chosen according to the choices used in [39]. Variables $J_{i,\pm}$ refer to $J_{i,\pm} = J_i \cdot (1 \pm h)$.

Starting with case (a), the Hamiltonian is simply written as

$$\begin{aligned} H_{(a)} &= J_1 H_0 + 2J_{2,+} \sum_n \left(f_n(4,0) + f_n(4,3)\right) \mathbf{S}_n \mathbf{S}_{n+2} \\ &\quad + 2J_{2,-} \sum_n \left(f_n(4,1) + f_n(4,2)\right) \mathbf{S}_n \mathbf{S}_{n+2} \end{aligned} \tag{3.128}$$

with $J_{2,\pm} = J_2 \cdot (1 \pm h)$ and $H_j = 2\sum_n \mathbf{S}_n \mathbf{S}_{n+j}$ (H_1 being equivalent to the operator formerly named H_0). Using the relations given in Eqns. 3.104 one arrives at

$$H_{(a)} = J_1 H_1 + 2J_2 \sum_n \mathbf{S}_n \mathbf{S}_{n+2} + 2J_2 h \sum_n \left(\cos\frac{\pi}{2} n - \sin\frac{\pi}{2} n\right) \mathbf{S}_n \mathbf{S}_{n+2} \tag{3.129}$$

$$= J_1 H_1 + J_2 H_2 + 2\sqrt{2} J_2 h \sum_n \cos\left(\frac{\pi}{2}(n+1/2)\right) \mathbf{S}_n \mathbf{S}_{n+2}\,, \tag{3.130}$$

i.e. periodic perturbations with $q = \pi/2$ together with second nearest neighbour couplings appear, the choice of $J_{2,+}$ on one leg and $J_{2,-}$ on the other would have resulted in a perturbation $\sim D_2(\pi)$.

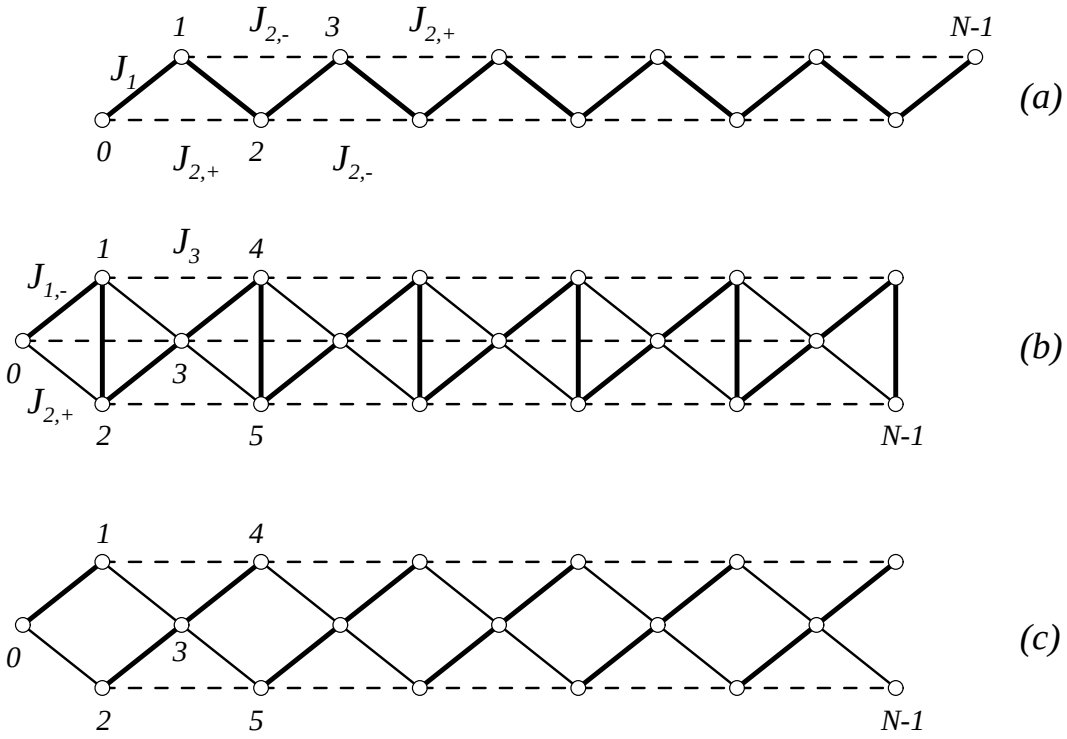

Figure 3.20: Description of zig-zag ladders (a, b) and Kagomé-like 3-leg ladders (c)

Turning now to the 3-leg zig-zag ladder shown in Fig. 3.20 (b), the Hamiltonian reads

$$\begin{aligned} H_{(b)} &= 2J_{1,-} \sum_n \mathbf{S}_n \mathbf{S}_{n+1} + 2J_3 \sum_n \mathbf{S}_n \mathbf{S}_{n+3} \\ &\quad + 2J_{2,+} \sum_n (f_n(3,0) + f_n(3,1)) \mathbf{S}_n \mathbf{S}_{n+2} \end{aligned} \tag{3.131}$$

with $J_{i,\pm} = J_i(1 \pm h)$ and again using Eqns. 3.104 yields

$$f_n(3,0) + f_n(3,1) = \frac{1}{3}\left(2 + \cos\frac{2\pi}{3} n + \sqrt{3}\sin\frac{2\pi}{3} n\right) \tag{3.132}$$

and finally

$$\begin{aligned} H_{(b)} &= J_{1,-}H_1 + J_3H_3 + \frac{2}{3}J_{2,+}\left[H_2 - 2\sum_n \cos\left(\frac{2\pi}{3}(n+1)\right)\mathbf{S}_n\mathbf{S}_{n+2}\right] \\ &= J_{1,-}H_1 + \frac{2}{3}J_{2,+}H_2 + J_3H_3 - \frac{4}{3}J_{2,+}\sum_n \cos\left(\frac{2\pi}{3}(n+1)\right)\mathbf{S}_n\mathbf{S}_{n+2}\,. \end{aligned} \tag{3.133}$$

In this case the additional degree of freedom due to the presence of h is not responsible for the periodic perturbation itself (as it was in the 2-leg case) but serves as an additional free parameter. Here, only for the special choice $h = -1$ the second-nearest neighbour couplings (respectively the corresponding perturbation) vanish. Otherwise, for all non-zero J_2 and $h \neq 1$ the perturbations will be present.

Considering finally in this context the 3-leg ladder with open boundary conditions (obc) for the rungs, we only have to remove the vertical couplings in Fig. 3.20(b) which constitute the periodic rung couplings. We arrive at

$$H_{(b),obc} = H_{(b)} - 2J_{1,-}\sum_n f_n(3,1)\mathbf{S}_n\mathbf{S}_{n+1} \tag{3.134}$$

$$= H_{(b)} - \frac{1}{3}J_{1,-}\left[H_1 + 4\sum_n \cos\left(\frac{2\pi}{3}(n-1)\right)\mathbf{S}_n\mathbf{S}_{n+1}\right] \tag{3.135}$$

$$\begin{aligned} &= \frac{2}{3}(J_{1,-}H_1 + J_{2,+}H_2) + J_3H_3 \\ &\quad -\frac{4}{3}\sum_n\left[J_{1,-}\cos\left(\frac{2\pi}{3}(n-1)\right)\mathbf{S}_n\mathbf{S}_{n+1} + J_{2,+}\cos\left(\frac{2\pi}{3}(n+1)\right)\mathbf{S}_n\mathbf{S}_{n+2}\right] \end{aligned} \tag{3.136}$$

Finally the 3-leg Kagomé-like ladders (part (c) in Fig. 3.20) are obtained by removing the middle leg and all vertical bonds of the 3-leg zig-zag ladder (b). This leads to

$$\begin{aligned} H_{(c)} &= 2J_1\sum_n\left(f_n(3,0) + f_n(3,2)\right)\mathbf{S}_n\mathbf{S}_{n+1} + 2J_2\sum_n\left(f_n(3,0) + f_n(3,1)\right)\mathbf{S}_n\mathbf{S}_{n+2} \\ &\quad +2J_3\sum_n\left(f_n(3,1) + f_n(3,2)\right)\mathbf{S}_n\mathbf{S}_{n+3} \end{aligned} \tag{3.137}$$

$$\begin{aligned} &= J_1H_1 + J_2H_2 + J_3H_3 \\ &\quad -2\sum_n\left\{J_1f_n(3,1)\mathbf{S}_n\mathbf{S}_{n+1} + J_2f_n(3,2)\mathbf{S}_n\mathbf{S}_{n+2} + J_3f_n(3,0)\mathbf{S}_n\mathbf{S}_{n+3}\right\} \end{aligned} \tag{3.138}$$

$$\begin{aligned} &= \frac{2}{3}\left[J_1H_1 + J_2H_2 + J_3H_3\right] - \frac{4}{3}\sum_n\left[J_1\cos\left(\frac{2\pi}{3}(n-1)\right)\mathbf{S}_n\mathbf{S}_{n+1}\right. \\ &\quad \left. + J_2\cos\left(\frac{2\pi}{3}(n-2)\right)\mathbf{S}_n\mathbf{S}_{n+2} + J_3\cos\left(\frac{2\pi}{3}n\right)\mathbf{S}_n\mathbf{S}_{n+3}\right]\,. \end{aligned} \tag{3.139}$$

Here, h-dependences of the couplings have been left out of the formulas, however, their inclusion would again not have affected the nature of the occuring periodic perturbations. As before, the 3-leg ladder case is determined by periodic perturbations with $q = q_c \equiv 2\pi/3$.
It should be added that a change in the numbering of the lattice sites $0, 1, ..., N-1 \to 1, 2, ..., N$ –e.g. used in [216, 217]– simply requires a change $j \to j-1$ in the used terms $f_n(n_u, j)$.
At the end of this part a recent preprint of *Dagotto* (1999) [59] shall be mentioned. It gives an overview of experimental results and theoretical achievements in the study of ladder materials in recent years.

3.5 Special classes II – spin-Peierls systems

In 1993 *Hase et al.* [105] for the first time discovered a spin-Peierls transition in an inorganic material – the cuprate $CuGeO_3$. Due to its much simpler structure (compared with earlier investigated organic materials, see e.g. [126]) and the higher quality and size of single crystals this phenomenon of unusual magnetoelastic transition in quasi 1-dimensional antiferromagnets (insulators) gained new rising attention and wide interest.
Experiments revealed that basic properties of $CuGeO_3$ are in accord with earlier established descriptions of spin-Peierls materials [175, 35, 51, 52]. In particular, the presence of lattice dimerization at low temperatures [115] and the existence of a singlet-triplet gap of magnetic excitations [164] had been established. Deviating from standard spin-Peierls theory [35, 51], however, the consideration of magnetic susceptibility resulted in additionally taking into account frustrating second-nearest neighbour antiferromagnetic spin couplings J_2. The first values suggested have been $\alpha = J_2/J_1 \simeq 0.24$ [43] and $\alpha \simeq 0.36$ [176] – later being improved and corrected towards $\alpha = 0.354(0.01)$ [74]. Since $\alpha > \alpha_c = 0.241167 \pm 5 \cdot 10^{-6}$ [66] this means, that a gap is already present without any dimerization $\sim D_1(\pi)$ leading to a potential spontaneous long-range dimerization of the ground state. One should keep in mind, however, that the opening of a gap due to frustration is rather small in the vicinity of α_c.
In the following, we will not put further weight on still outstanding questions in the above sketched field (temperature dependence of the Heisenberg coupling constants, phonon-induced nature of the lattice dimerization and many other points, see e.g. [211]) but turn our focus to the excitations and formation of magnetization plateaus in case of dimerized and frustrated spin chains. In the next section the respective Hamiltonian and some of its general properties are given and the next chapter contains results for magnetization curves. Following the discussions in case of $CuGeO_3$ we will choose frustration parameters $\alpha = 0.25, 0.3, 0.35$, however, thereby extending the strengths of the dimerized nearest-neighbour coupling (~ 0.03) by far.

3.5.1 Dimerized and frustrated spin chains

In Chap. 4 (Sec. 4.1.5) we will give results for magnetization plateaus of systems described by the Hamiltonian (choosing $J_1 = 1$)

$$\begin{aligned} H &= 2\left\{ J_1 \sum_n (1 + \delta \cdot e^{i\pi n}) \mathbf{S}_n \mathbf{S}_{n+1} + J_2 \sum_n \mathbf{S}_n \mathbf{S}_{n+2} \right\} \\ &= 2J_1 \left\{ \sum_n (1 + \delta \cdot e^{i\pi n}) \mathbf{S}_n \mathbf{S}_{n+1} + \alpha \sum_n \mathbf{S}_n \mathbf{S}_{n+2} \right\} \\ &= J_1 \left(H_0(\alpha) + 2\delta \cdot \sqrt{N} D_1(q = \pi) \right) . \end{aligned} \tag{3.140}$$

In the context of the inorganic spin-Peierls material $CuGeO_3$ this Hamiltonian has been discussed for frustration values α ranging in the interval from closely below (0.24) to well above (0.345) $\alpha_c = 0.2411...$ We will take the course of determining the optimal α-value for $CuGeO_3$ as cause to compare the processes of gap and plateau formation in dimerized spin chains ($D_1(q = \pi)$) in unfrustrated and frustrated spin chains (using the above-mentioned α-values).
In general, not many rigorous results and properties of Hamiltonian 3.140 are known and have been reviewed e.g. in [47] (together with newly obtained results for ground state energies, energy gaps and other quantities in the unmagnetized phase). For $m = 0$ exact results are limited to the lines $\delta = 0$ and $\delta + 2\alpha = 1$. The latter one –exact ground states have been given by *Shastry and Sutherland* [185]– is considered as dividing line between the so-called Néel ($\delta < 1 - 2\alpha$) and spiral ($\delta > 1 - 2\alpha$) phases. In the Néel phase the maximum of the spin-spin SSF $S(q)$ is located at $q_{max} = \pi$ and gradually decreases to $q_{max} = \pi/2$ (for very large α) in the spiral phase. Chitra et al. [47] obtained minimal correlation lengths ξ along the line $2\alpha + \delta = 1$ reflecting highly

disordered ground states. They identified this line as a disorder line separating ground states with $q_{max} = \pi$ and $q_{max} < \pi$.
Finally the special choice $\delta = 1$ can be understood as a regular 2-leg ladder (see Fig. 3.11) with rung couplings $2\delta = 2$ and leg couplings α (a dimerization strength $\delta \neq 1$ would result in additional diagonal couplings). In particular ($\alpha = 0$; $\delta = 1$) is the simple case of independent rungs and can serve as a starting point for perturbation theory for small frustration α.

Chapter 4

Opening of gaps and formation of magnetization plateaus

In this chapter different types of spin-1/2 systems that possibly lead to magnetization plateaus will be discussed. Here, the first aspect will be to present a classification scheme that does allow the prediction of magnetization values of potential plateaus.
For that purpose we map the respective spin systems as already discussed in the last chapter on single Heisenberg chains. These spin chains will carry certain perturbations of their isotropic character due to the respective mapping process. For regular spin systems these perturbations will be periodic ones. In the next section we will therefore begin to study the influence of a single periodic perturbation (with momentum $q_{pert.}$) on the magnetization curve of the spin chain. We will concentrate on the relation between the periodicity of the perturbation $q_{pert.}$ and the soft mode positions $q_{1,3}^{(k)}(m)$ of the unperturbed Heisenberg chain at a given magnetization m –according to an application of the quantization rule of *Oshikawa, Yamanaka and Affleck* [169] to a half-integer spin chain. A spin-S chain Hamiltonian that is invariant under translations of multiples of n sites is predicted to possibly have massive phases –with explicit or spontaneous breaking of translational symmetry– for magnetizations m that fulfill the quantization condition

$$n \cdot (S - m) \quad = \quad \text{integer}\,. \tag{4.1}$$

The soft modes of a spin chain are to be considered the most susceptible parts of the spectrum of the unperturbed chain. The correspondence of $q_{pert.}$ and one of the soft mode positions will be shown to give sufficient conditions for the locations of possible magnetization plateaus and will allow to apply the above given quantization condition from the point of view of the unperturbed chain. On the basis of such a description, however, it will remain an open question to decide, in case of which given possibility a gap/plateau finally will appear.
At the end of the chapter (Sec. 4.3) we will discuss the relationship between the above given quantization condition of Oshikawa, Yamanaka and Affleck –that is based as well on the known manifold of soft modes of the unperturbed chain given by Lieb, Schultz and Mattis (LSM)2.6.2– and the classification scheme that is used in the following. The latter one gives a direct link between the considered perturbation $q_{pert.}$ and the particular longitudinal/transverse soft mode taking part in plateau formation.
For that reason we will finally turn to the second aspect, namely the behaviour of suitably chosen static structure factors (SSFs) under the influence of an applied periodic perturbation. It will be underlined that the mere location of soft modes of the unperturbed Heisenberg chain does not supply sufficient information for an unambiguous prediction of plateaus. Only the investigation and observation of relevant changes in the considered SSFs allows for predictions that will turn out to be in accord with the evaluated plateaus that will be discussed for a variety of examples in the next section.

The next section (Sec. 4.1) will first address general types of periodic perturbations. Then, regular ladder geometries, ladders with competing interactions and ladders with zig-zag- and Kagomé-like geometries will be discussed. Concerning the latter points, DMRG-calculations –by R. M. Wiessner– will be shown. The mapping of these structures on 1-dimensional spin chains (see discussion in the preceding chapter) will be used for plateau predictions in the respective magnetization curves. Moreover, some statistical properties of ladders with competing interactions and their m-dependent ground state energies per site ($E_0(m)/N$) will be discussed. At the end of the section, the formation of plateaus in frustrated spin-Peierls chains (more generally treated by *Totsuka* [200]) at $m = 0$ and $m = 1/4$ is discussed for frustration strengths $\alpha = 0, 0.25, 0.30, 0.35$.
In Sec. 4.2 we will try to leave the partly heuristic position of the plateau discussion of Sec. 4.1 and turn to a consideration of the related background of the formation of plateaus. This will include the sizes of relevant transition matrix elements appearing in static structure factors (SSFs) of unperturbed and perturbed chains. A number of cases of plateau formations (given in the next section) will be analyzed again. It will be exemplified that all plateau formations are accompanied by distinct changes in the SSFs.

4.1 Magnetization curves and plateaus

We will begin this section reconsidering periodic perturbations $2\sqrt{N}X(q)$ that have been discussed in the last chapter:

$$X(q) \quad = \quad S_3(\pi/2),\ D_1(\pi),\ D_1(\pi/2),\ D_2(\pi)$$

– this time using perturbation strengths that are at least an order of magnitude larger than in the context of the scaling solutions discussed earlier. Here, the emergence of magnetization plateaus and the dependence of their widths on periodic perturbation strengths will be discussed. In addition, the presence of 2 different periodic perturbations $-D_1^c(\pi/3) + D_1^c(2\pi/3)$– will be addressed.
We will settle our considerations on the earlier observation, that the appearance of a gap –due to an applied periodic perturbation of momentum $q_{pert.}$– is intimately related to the location of the soft modes of the unperturbed system (H_0) with magnetization m and soft mode momenta

$$q^{(k_3)}(m) = k_3 \cdot \pi(1-2m) \quad ; \quad q^{(k_1)}(m) = k_1 \cdot 2\pi m\,.$$

Plateaus in the magnetization curve of a periodically perturbed system should –if at all– occur at magnetization

$$m_{\text{plateau}}(q, k_3) \quad = \quad \frac{1}{2} \cdot \left(1 - \frac{q_{pert.}}{k_3 \pi}\right) \tag{4.2}$$

$$m_{\text{plateau}}(q, k_1) \quad = \quad \frac{1}{2} \cdot \frac{q_{pert.}}{k_1 \pi} \tag{4.3}$$

with q –the wave number of the periodic perturbation– being equal to one of the soft mode wave numbers $q^{(k_{1,3})}(m)$. While in the discussion of the opening of gaps in the previous chapter mainly $k = 1$-soft modes appeared, we will as well turn to magnetization plateaus related to higher k-values in the course of this chapter. Moreover, we will be led to the necessity of considering both k_1 and k_3 within the given description. Such a situation will appear in the discussion of magnetization plateaus in case of the periodic perturbation $X(q = 2\pi/3) = D_1^c(\pi/3)$. This particular case will as well be taken up again in the discussion of structure factors in Sec. 4.2 and in the final paragraph (Sec. 4.3) where the correspondence of the quantization rule 4.1 and the contributing soft modes will be discussed.

In this section the occurrence of magnetization plateaus and their description according to the scheme of soft mode momenta of the unperturbed chain will be presented. One of the remaining questions, however, "Which soft mode momenta will be the ones belonging to predominantly emerging plateaus?" will be addressed in the following section 4.2.
As another point of particular interest, it remains to be checked to what extent critical exponents ϵ that have been determined for small perturbations (discussing the opening of gaps $\sim h^{\epsilon}$) give adequate descriptions for increasing perturbation strengths.
Again, we will proceed performing finite-size scaling analyzes on the results of finite-chain evaluations. This will be done by means of the BST-algorithm [36] (see App. C). Fig. 4.1 shows typical results for magnetization curves evaluated for small systems and different types of perturbations (type and strength of perturbation are given in the figure). The thick solid lines show the determined plateaus – the remaining parts of these lines are based on the longest chain involved in the respective evaluation and does not represent results of a finite-size analysis. The accuracy of the plateau positions and widths is better than 10^{-3} in general (cf. App. C).

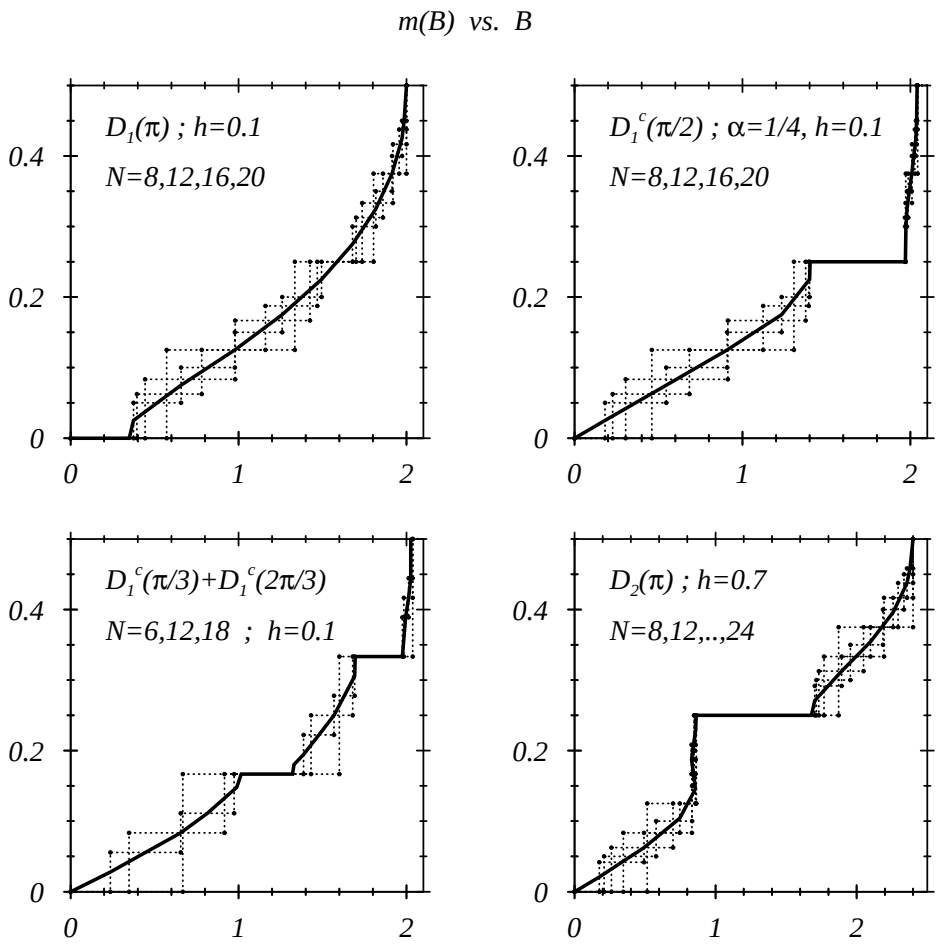

Figure 4.1: Course of plateau determination for various $X(q)$ (see text)

Fig. 4.1 is intended to provide a certain estimation of the N-dependence of plateau formations for some selected perturbation strengths. The then following Figs. 4.2-4.5 show lower and upper bounds and plateau widths for a broader range of strengths of the periodic perturbations.
To begin with, Fig. 4.2 shows the clear appearance of magnetization plateaus ($B_u - B_l > 0$) at $m = 1/4$ with

$$B_u \;=\; \frac{1}{2}\Big(E_0(q_0+\pi, m+1/N) - E_0(q_0, m)\Big) \tag{4.4}$$

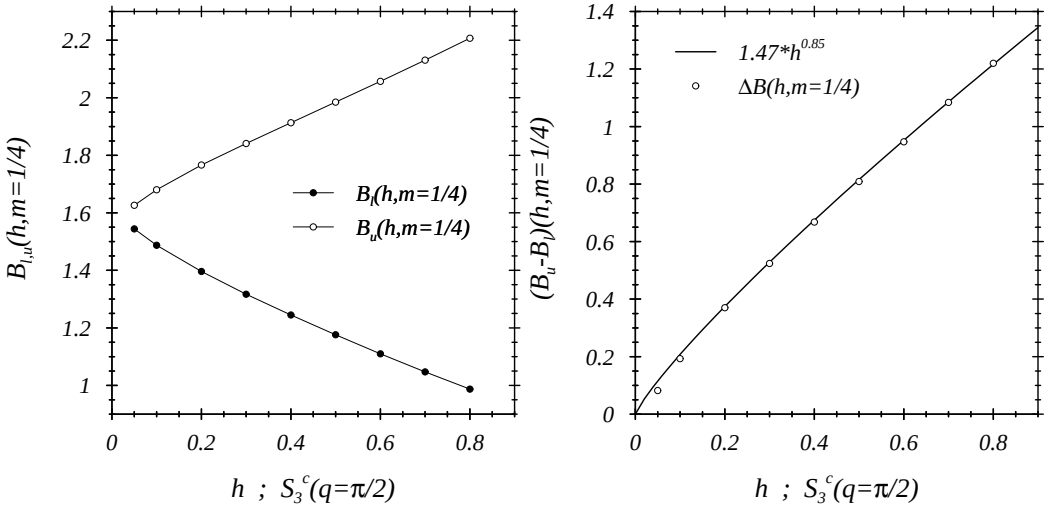

Figure 4.2: Plateau boundaries and width for $S_3^c(q=\pi/2)$, $m=1/4$ ($N=8,12,16,20$)

$$B_l \;=\; \frac{1}{2}\Big(E_0(q_0,m) - E_0(q_0+\pi, m-1/N)\Big) \tag{4.5}$$

for the periodic perturbation $\sim S_3(\pi/2)$. Here, $E_0(q_0,m)$ denotes the ground state energy of $H_0 = 2\sum_n \mathbf{S}_n\mathbf{S}_{n+1}$ in the sector with magnetization m, i.e.

$$B_u - B_l \;=\; \frac{1}{2}\Big(E_0(q_0+\pi, m+1/N) - 2E_0(q_0,m) + E_0(q_0+\pi, m-1/N)\Big)\,. \tag{4.6}$$

The opening of the gap (plateau width $\sim h^\epsilon$, $\epsilon = 0.8101$) has been fitted to the larger coupling strengths with a slightly increased exponent 0.85. The m-value of the plateau is –according to Eq. 4.2– $m=1/4$, i.e. $k_3=1$.

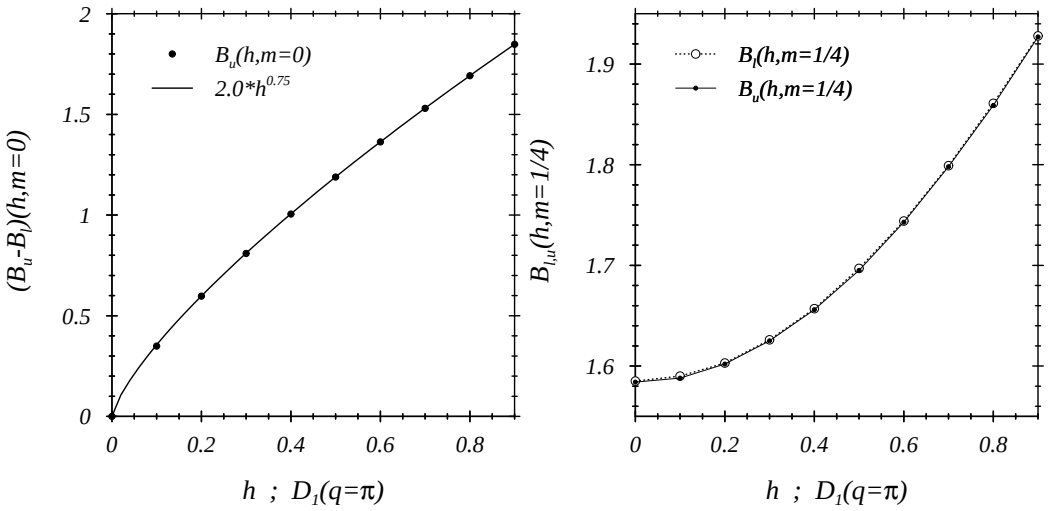

Figure 4.3: Plateau boundaries for $D_1(q=\pi)$, $m=0$, 1/4i ($N=8,12,16,20$)

The following case of a perturbation type $D_1(q=\pi)$ (Fig. 4.3) first shows the magnetization plateau at $m=0$ ($k_3=1$) on the l.h.s. of the figure, and then on the r.h.s. documents the

vanishing width of a potential plateau for $k_3 = 2$ ($m = 1/4$). The given fit $B_u(m = 0) = 2.0 \cdot h^{0.75}$ for the extended range of h-values means in particular, that for $h = 1$ the plateau at $m = 0$ exceeds the whole interval $[0, B_{Sat}]$ with $B_{Sat} = 2$ for $h \leq 2$ (see App. B).

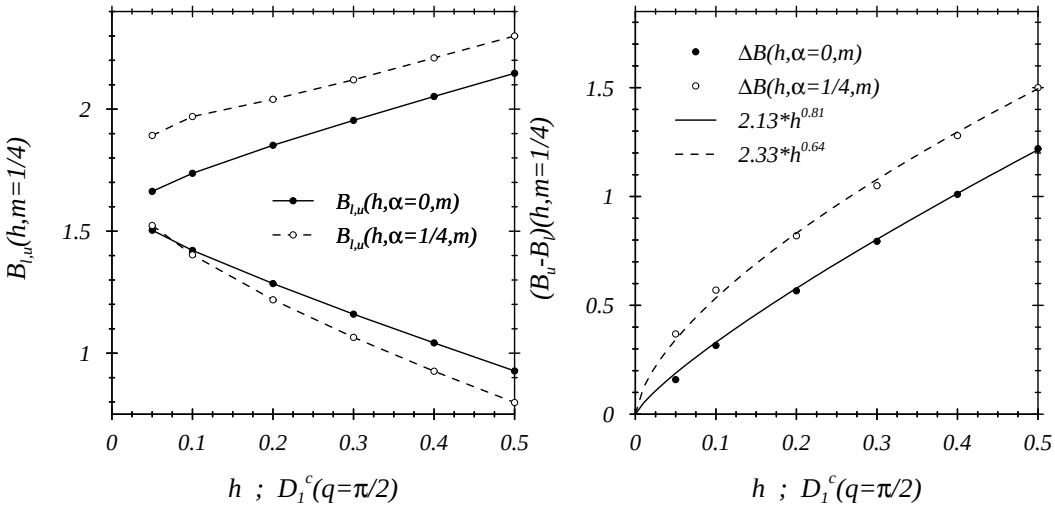

Figure 4.4: Plateau boundaries and widths for $D_1^c(q = \pi/2)$, $m = 1/4$ and $\alpha = 0, 1/4$ ($N = 8, 12, 16, 20$)

A halving of the q-value of the applied perturbation, i.e. choosing $D_1^c(q = \pi/2)$, results in the observation of magnetization plateaus at $m = 1/4$ ($k_3 = 1$). Similar to the last chapter, the 2 cases of frustrations $\alpha = 0, 1/4$ have been considered. The fits for the h-dependence of the belonging plateau widths (gaps) show a good agreement with the exponents that have been determined in the last chapter in the regime of small perturbation strengths (Eqns. 3.101, 3.101. The disturbed curvature of $B_u(h, \alpha = 1/4, m = 1/4)$ (l.h.s. of Fig. 4.4) documents a comparatively bad finite-size behaviour of the numerical data.

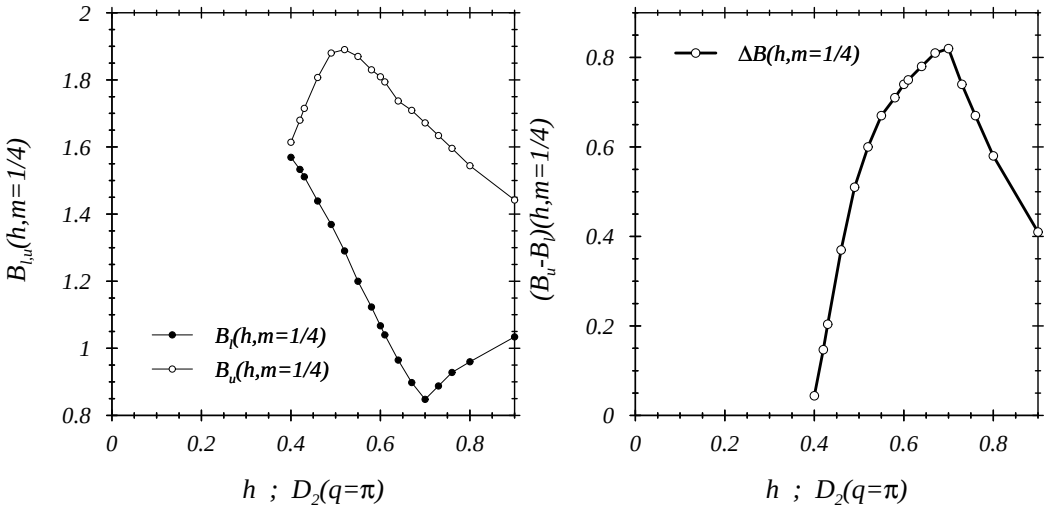

Figure 4.5: Plateau boundaries and width for $D_2(q = \pi)$, $m = 1/4$ ($N = 8, 12, 16, 20$)

We now turn to the first case of a plateau formation related to $k_3 = 2$. Considering $X(q) = D_2(q = \pi)$, no plateau occurs at $m = 0$ –as in the case of $D_1(\pi)$– and only for perturbation strengths exceeding $h \simeq 0.4$ finite-size analysis reveals the opening of a plateau at $m = 1/4$ (Fig. 4.5). The sharp kink in the plateau width can be retraced to the lower plateau boundary. The shown behaviour of $B_l(h, m = 1/4)$ is a typical sign of ground state level crossings. Indeed, as h exceeds the value $h \simeq 0.5$ the alternation of $q_0 = 0, \pi$ of ground state momenta in the whole sequence of magnetization values m starts getting violated ($q_0(m) = \pm\pi/2$ appears for m closely below the saturation value $m = 1/2$). This deviation of ground state momenta proceeds to smaller m-values for increasing h and finally reaches the plateau value $m = 1/4$ almost precisely at $h = 0.7$.
The above discussion can be extended when referring to the quantization rule 4.1 of Oshikawa, Yamanaka and Affleck. The rule states that the $q = \pi$-perturbation on its own cannot account for the observed $m = 1/4$-plateau. An additional spontaneous symmetry breaking is afforded to result in the required symmetry factor $n = 4$. In Sec. 4.2 we will turn again to perturbations $X(q) = D_2(q = \pi)$ and address the h-dependence of various static structure factors (SSFs).

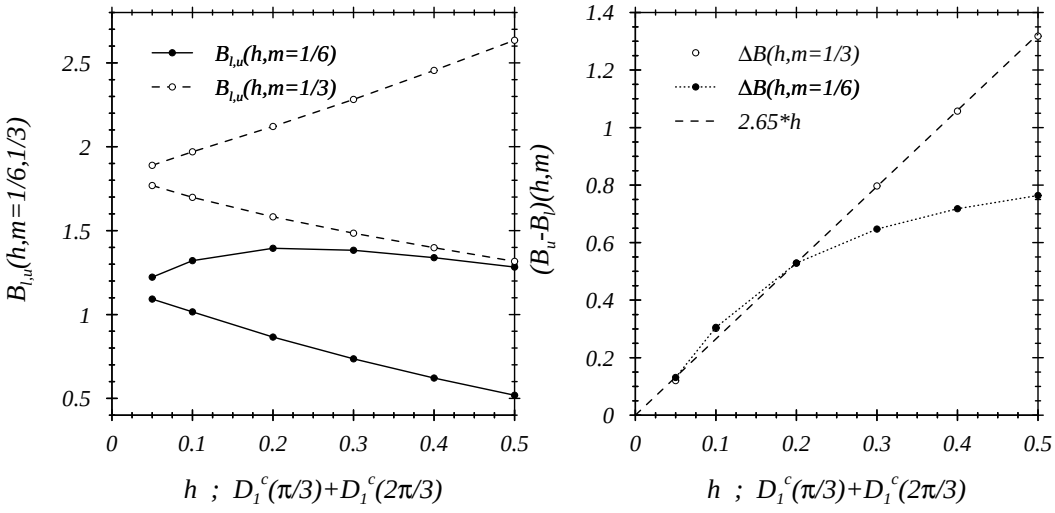

Figure 4.6: Plateau boundaries and widths for $D_1^c(\pi/3) + D_1^c(2\pi/3)$, $m = 1/6, 1/3$

We will now turn to a case that includes a combination of 2 perturbations with different periodicities. Here, one is constrained to a small number of momenta q that still allow for a finite-size analysis when being evaluated on small systems. We chose to consider an equally weighted sum of perturbations $D_1^c(n \cdot \pi/3),\ n = 1, 2$:

$$X(q) \quad = \quad D_1^c(\pi/3) + D_1^c(2\pi/3)\,. \tag{4.7}$$

The evaluation of only 3 system sizes $N = 6, 12, 18$ and the following BST-analysis of plateau widths at $m = 1/6,\ 1/3$ clearly reveals the occurrence of 2 plateaus in the respective magnetization curves (Fig. 4.6, [86]). The opening of the upper plateau ($m = 1/3$) appears to be fairly linear for larger h-values whereas the lower plateau at $m = 1/6$ does not turn out to be sufficiently well described by a single power h^ϵ. Note in addition, that Fig. 4.6 seems to indicate that the development of the lower plateau is dominated by that of the upper one.
In order to get further insight, we will now separately consider both of the above combined periodic perturbations. Figs. 4.7, 4.8 show the resulting pictures for the perturbations $D_1^c(\pi/3)$ and $D_1^c(2\pi/3)$. In case of $D_1^c(\pi/3)$ we observe 2 plateaus at $m = 1/6$ and $m = 1/3$, the latter one is described with $k_3 = 1$. The first one, however, requires to take into account the transverse

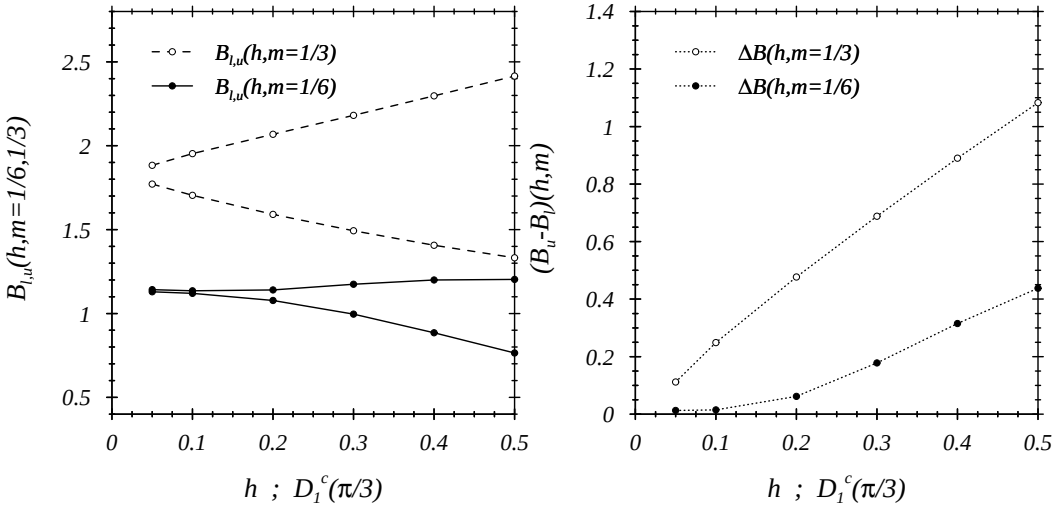

Figure 4.7: Plateau boundaries and widths for $D_1^c(\pi/3)$, $m = 1/6, 1/3$ ($N = 6, 12, 18$)

soft mode momenta $q_1^{(k_1)}(m) = k_1 \cdot 2\pi m$ and is classified by $k_1 = 1$. The periodic perturbation $D_1^c(2\pi/3)$ generates a single plateau at $m = 1/6$ consistently described by $k_3 = 1$.

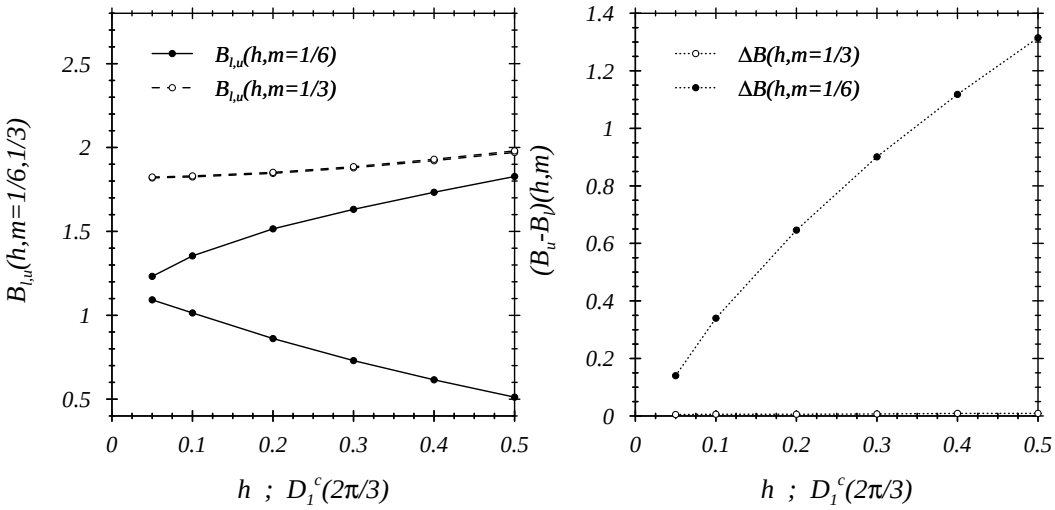

Figure 4.8: Plateau boundaries and widths for $D_1^c(2\pi/3)$, $m = 1/6$ ($N = 6, 12, 18$)

Attempts of giving satisfactory simple fits for the plateau widths in the last cases failed. Their h-dependence is not comparable to the cases discussed before. This in particular led to the decision not to access the scaling properties of the perturbations $D_1^c(\pi/3)$ and $D_1^c(2\pi/3)$ in the regime of small perturbations.

Finally, Fig. 4.9 supplies 2 finite-N examples for the plateau formation in case of the perturbation $D_1^c(\pi/3)$ (for coupling strengths $h = 0.2,\ 0.5$. A BST-analysis of the shown and additional cases led to the plateau widths shown in Fig. 4.7. For further discussions of perturbations with $q = \pi/3,\ 2\pi/3$ the reader is referred to discussions in Sec. 4.2 – addressing the predictability of plateau formations.

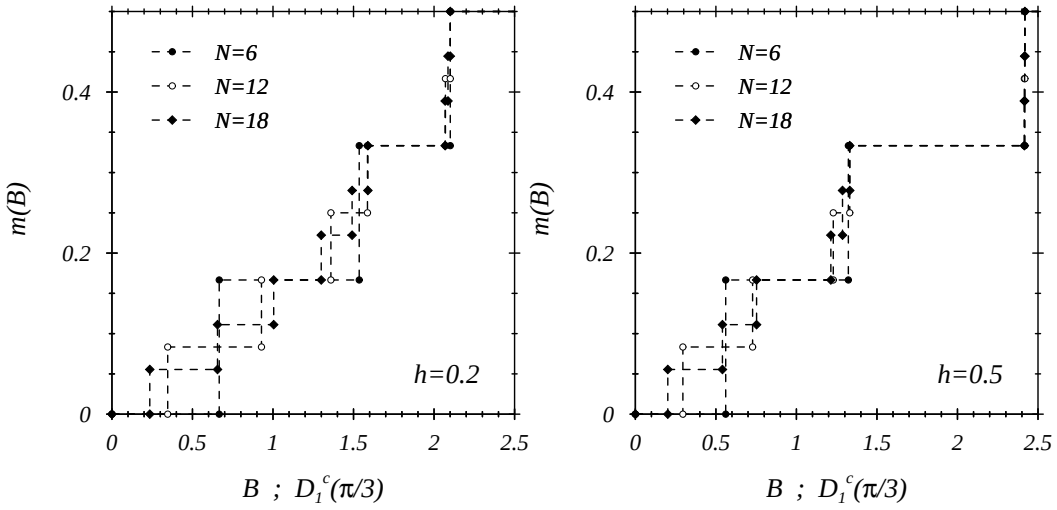

Figure 4.9: Forming of plateaus for $D_1^c(\pi/3)$ for both magnetizations $m = 1/6, 1/3$ ($N = 6, 12, 18$)

We will now briefly return to a point of discussion in Chap. 2, namely the behaviour of ground state energies and their derivatives. Here, we will consider $e_0^{(0)}(m, h, N)$ and $e_0^{(2)}(m, h, N)$ (cf. Eq. 2.30 in Sec. 2.4). In Sec. 2.4 the smooth behaviour of ground state energy and derivatives in case of the unperturbed Heisenberg chain has been documented – Fig. 2.1 shows finite-size data. In order to contrast this behaviour Figs. 4.10, 4.11 show the corresponding behaviour for a Heisenberg chain perturbed by $X(q) = D_2(\pi)$.

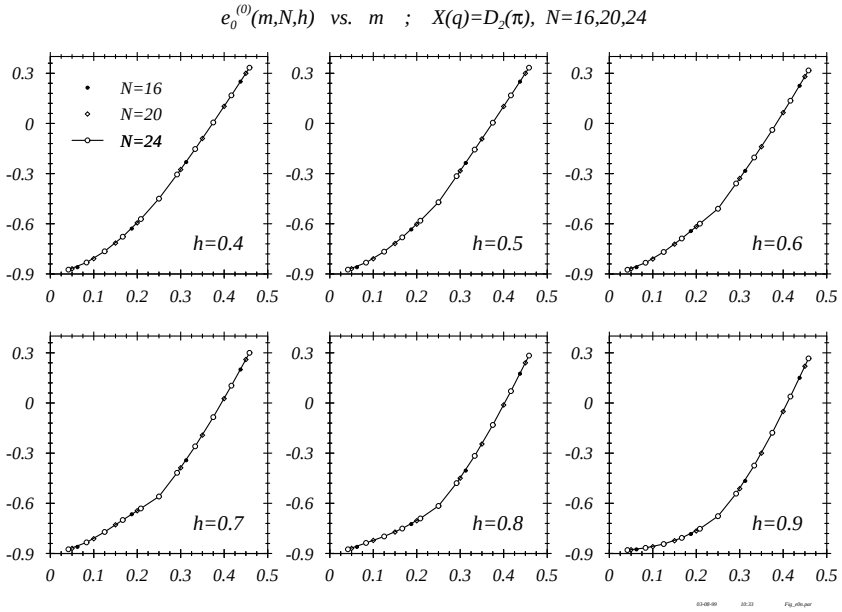

Figure 4.10: $e_0^{(0)}(m, h, N)$ for perturbations $D_2(q = \pi)$ and $h \geq 0.4$

For coupling strengths h that went along with clearly visible magnetization plateaus (see Fig. 4.5) Fig. 4.10 indicates a kink of $E_0(h, m)/N$ at the plateau magnetization $m = 1/4$. This

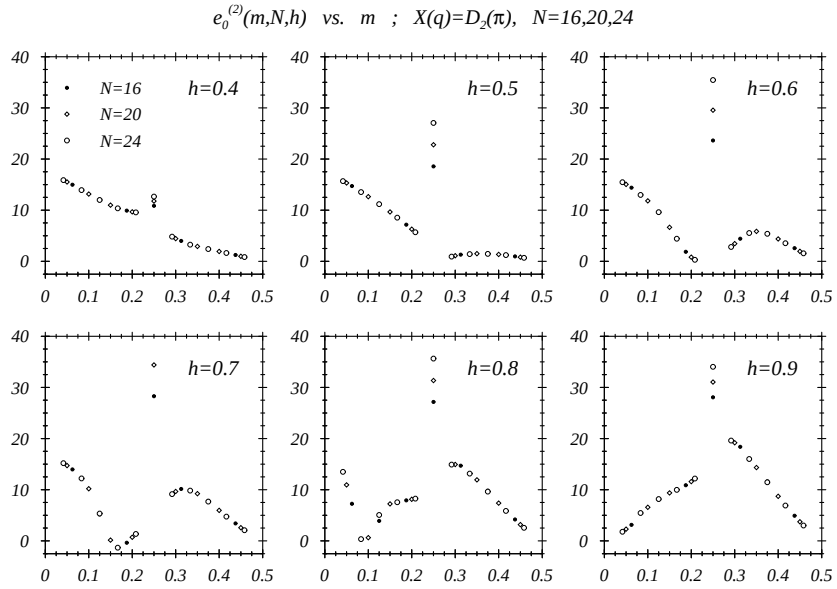

Figure 4.11: Derivative $e_0^{(2)}(m,h,N)$ for perturbations $D_2(q=\pi)$ and $h \geq 0.4$

kink gets much more pronounced when looking at the 2nd derivative (Fig. 4.11). A sharp peak at $m = 1/4$ arises, which is most strongly marked at $h = 0.7$ where the plateau width is maximally developed. Moreover, in the vicinity of this coupling the 2nd derivative of $e^{(0)}(h,m)$ seems to approach negative values indicating the closeness to the boundary (or loss of stability itself) given by stability criteria (cf. Sec. 2.4). These phenomena occurring well apart (below) $m = 1/4$ could not be explained within the analysis of plateau formation and width carried out above.
The consideration of smaller h-values ($h < 0.4$) where no unambiguous formation of plateaus could be observed (see Fig. 4.12) shows no anomalies comparable to the cases $0.4 \leq h \leq 0.9$. Only the 2nd derivative $e_0^{(0)}(m,h,N)$ shows subtlely emerging discontinuities most clearly visible for $h = 0.3$.

4.1.1 Gaps and plateaus for ladder systems

We will now discuss predictions of the location of magnetization plateaus of ladder systems. Therefore, we use the description type (b) being introduced in Sec. 3.4.1. Considering n_l-leg ladders we are concerned with the periodically perturbed Hamiltonian

$$H = H_\perp + H_\perp^{pbc} + H_l \tag{4.8}$$

$$H_\perp = H_0 - 2\sum_n f_n(n_l, n_l-1)\mathbf{S}_n\mathbf{S}_{n+1} \tag{4.9}$$

$$H_\perp^{pbc} = 2\sum_n f_n(n_l,0)\mathbf{S}_n\mathbf{S}_{n+n_l-1} \tag{4.10}$$

$$H_\parallel = 2\sum_n \mathbf{S}_n\mathbf{S}_{n+n_l}\,. \tag{4.11}$$

In the following we will leave out the term $H_\perp^{pbc}$, however, this will not change the occurring types of periodic perturbations of the isotropic Heisenberg chain.

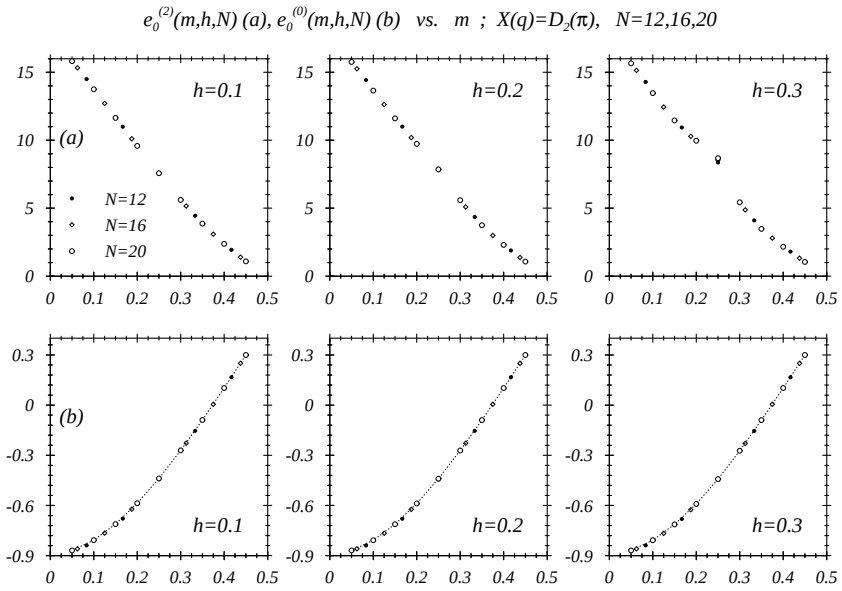

Figure 4.12: Energies and derivatives $e_0^{(0,2)}(m,h,N)$ for perturbations $D_2(q=\pi)$ and $h = 0.1, 0.2, 0.3$

Using the expressions for $f_n(m,j)$ given in Eq. 3.104 and the following generalizations, it turns out that periodic perturbations of type

$$\sum_n \cos(\sin) q_{n_l,j} \mathbf{S}_n \mathbf{S}_{n+1} \quad , \quad q_{n_l,j} = \frac{2\pi}{n_l} j \tag{4.12}$$

with $q_{n_l,j} \leq \pi$ are present. E.g. the Hamiltonian $H = H_\perp + H_l$ for the cases $n_l = 2,3,4$ reads

$$H \;=\; H_0 + H_l - \frac{2}{n_l} \sum_n \mathbf{S}_n \mathbf{S}_{n+1} \begin{cases} (1-\cos\pi n) & , \quad n_l = 2 \\ (1-\cos\frac{2\pi}{3}n + \sqrt{3}\sin\frac{2\pi}{3}n) & , \quad n_l = 3 \\ (1-2\sin\frac{\pi}{2}n - \cos\pi n) & , \quad n_l = 4 \end{cases} . \tag{4.13}$$

An evaluation of possible plateau locations of n_l-leg ladders on the basis of periodically perturbed spin chains (Eqns. 4.2, 4.3) is given in Table 4.1 for ladders with $n_l = 2,3,\ldots,6$ legs. There, we have used the first 2 soft mode momenta $q_{1,3}^{k=1,2}$ for both transverse and longitudinal soft modes – although most of the results in the preceding sections showed that the first longitudinal soft mode in many cases suffices for a classification of magnetization plateaus.

n_l	2	3	4		5		6		
$q_{n_l,j}$	π	$2\pi/3$	$\pi/2$	π	$2\pi/5$	$4\pi/5$	$\pi/3$	$2\pi/3$	π
$k_3=1$	0	1/6	1/4	0	3/10	1/10	1/3	1/6	0
$k_3=2$	1/4	1/3	3/8	1/4	4/10	3/10	5/12	1/3	0
$k_1=1$	(1/2)	1/3	1/4	(1/2)	1/5	2/5	1/6	1/3	(1/2)
$k_1=2$	1/4	1/6	1/8	1/4	1/10	1/5	1/12	1/6	1/4

Table 4.1: Possible plateau positions for n_l-leg ladders refering to soft mode momenta $q_{1,3}^{k=1,2}(m)$

As a first remark, it should be pointed out that the fundamental difference between ladders with

an odd or even number of legs –the gap at $m = 0$ for ladders with an even number of legs– appears quite naturally in our analysis of periodic perturbations.
Second, the occasional appearance of the saturation value $m = 1/2$ (for ladders with an even number of legs, $k_1 = 1$ and $q = \pi$) deserves some correction: In case that all spins are fully aligned, S_z-conserving perturbations cannot alter the momentum $q = 0$ (see Sec. 2.1) of the unperturbed ground state –meaning that the trivial plateau at $m = 1/2$ is of course present in all possible cases (consider Eq. 4.2 for $q = 0$). However, the saturation plateau will be of no further concern for the discussion.
Taking into account that plateaus in many of the considered cases were related to $k_3 = 1$-soft modes, Table 4.2 comprises these "most probable" values. Some more discussion about this will be given in Sec. 4.3 where we will consider the present soft mode description and its relationship to the quantization condition of Oshikawa, Yamanaka and Affleck [169]. The next section, however, will give another interesting example which is not described by these "most probable" values.

n_l	2	3	4	5	6
m	0	1/6	0, 1/4	1/10,3/10	0, 1/6, 1/3

Table 4.2: "Most probable" plateau locations for n_l-leg ladders

Finally it should be stressed that we are sofar in most cases unable to decide whether transverse or longitudinal soft modes are responsible for the formation of a particular plateau. As an exception the periodic perturbation $\sqrt{N}D_1^c(\pi/3)$ may serve where the plateau at $m = 1/6$ could only be described by $k_1 = 1$. As already mentioned, in Sec. 4.2 we will introduce a different approach and consider the behaviour of static structure factors under the influence of applied periodic perturbations. This will suggest a way from the qualitative prediction of possible plateau positions towards quantitative ones.

4.1.2 Ladder systems with competing interactions – spontaneous magnetization

In this section we will discuss spin ladders that have a competition between an antiferromagnetic rung coupling and a ferromagnetic leg coupling [216]. This situation will be contrasted by the wholly antiferromagnetic ladder. Since in this part we are going to present some DMRG-results (cf. [214, 218]) for ladders of up to 5 legs, we expand our discussion considering in addition ladders that as well have open boundary conditions (obc) in the leg direction of the ladders. The ladder Hamiltonian in this case reads (cf. Sec. 3.4.1, note the changed boundary conditions):

$$\begin{aligned} H(J_l, J_r; B) &= 2\left(J_l \sum_{y=0}^{n_l-1} \sum_{x=0}^{n_r-2} \mathbf{S}(x,y)\mathbf{S}(x+1,y) \right. \\ &\quad \left. + J_r \sum_{x=0}^{n_r-1} \sum_{y=0}^{n_l-2} \mathbf{S}(x,y)\mathbf{S}(x,y+1) - B\sum_{x,y} S_3(x,y) \right) . \end{aligned} \tag{4.14}$$

The open boundary conditions for the legs are mainly chosen for reasons of applicability of DMRG calculations. In the following we are going to contrast this choice of boundary conditions by evaluations of smaller systems with periodic boundary conditions for the legs.
Despite of the changed leg-boundary conditions we argue that our analysis of periodic perturbations still holds. In the preceding section we took care of the open ends in the rung direction, effects of open ends of the legs are expected to be less susceptible and disappear in the TDL. In

the course of this section we will comment on the influence of the chosen boundary conditions for the situations of 2- and 3-leg ladders with both competing and purely antiferromagnetic interactions concerning the finite-size dependence of ground state energies per site $e_0(m) = E_0(m)/N$. Before presenting some of the mentioned DMRG results for the above-mentioned ground state energies $e_0(m)$ and magnetizations $m(B)$ we will address some of the basic properties of even- and odd-leg ladders studying 2- and 3-leg ladders of up to 24 sites. Here, we will look at properties of single legs of these ladders (total S_z/leg, total spin S_{tot}/leg), which might support the assessment of a variational ansatz given in [216] (see below). Furthermore, interesting features arising from the magnetization curves will be considered.

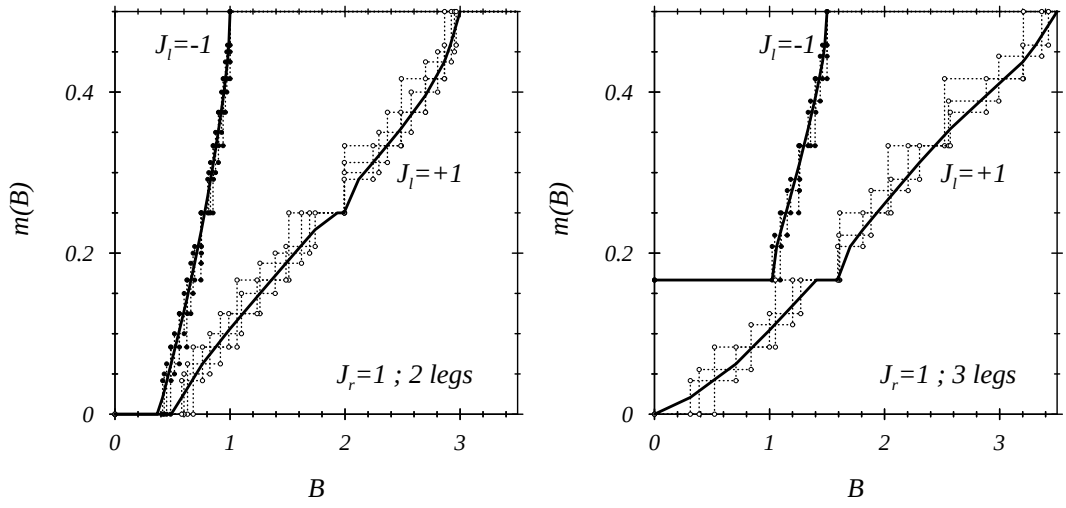

Figure 4.13: Magnetization curves for open 2− and 3−leg ladders with $J_r = 1$, $J_l = \pm 1$

Fig. 4.13 shows magnetization curves for the 2- and 3-leg ladder. Here, the boundary conditions (legs, rungs: obc) have been chosen according to the situation occurring in the DMRG calculations. We contrast the cases $J_l = \pm 1$ keeping $J_r = 1$ fixed. Again we use the BST-algorithm to determine the plateau widths and saturation fields on the basis of the finite-system data ($N = 12, 16, 20, 24$ for $n_l = 2$; $N = 12, 18, 24$ for $n_l = 3$). Otherwise, the shown thick lines represent the Bonner and Fisher curves [32] for the longest used chain ($N = 24$).
The even-leg ladder ($n_l = 2$) shows the expected $m = 0$-plateaus ($k = 1$), however, for the case $J_l = 1$ a small plateau at $m = 1/4$ is present, which again is a non-"most probable" case ($k = 2$). The 3-leg ladders show plateaus at $m = 1/6$, however, no signatures at $m = 1/3$. This again may be seen as a predominance of the longitudinal soft modes for the plateau prediction (see Table 4.1). Even more interesting, the 3-leg ladder with ferromagnetic leg coupling ($J_l < 0$) shows spontaneous magnetization. The ground state energies in the sectors $S_z/N = 0$ up to a limiting value $S_z^*/N = m^*$ are degenerate – the corresponding states all having total spin $S_{tot} = Nm^*$. In [216] it has been shown that this property follows as a consequence of an argument given by *Lieb and Mattis* (1962) [144] in the general context "*Ordering Energy Levels of Interacting Spin Systems*". The considered n_l-leg ladder systems fall in a class of spin systems for which these authors proved the following inequalities (for the lowest energy eigenvalues $E(S_{tot})$ in each S_{tot}-sector):

$$E(S_{tot}+1) \;>\; E(S_{tot}) \qquad \text{for } S_{tot} \geq \frac{1}{2}\cdot n^* \tag{4.15}$$

$$E(S_{tot}) \;>\; E(S_{tot} = n^*/2) \quad \text{for } S_{tot} < \frac{1}{2}\cdot n^*, \tag{4.16}$$

i.e. $E(S_{tot} = n^*/2)$ is the minimal ground state energy for all $0 \leq S_z \leq n^*/2$ leading to a spontaneous magnetization m^* for $n^* > 0$.
While n^* remains zero in ladders with purely antiferromagnetic couplings on rungs and legs, odd-leg ladders with ferromagnetic leg couplings have a non-zero $n^* = N/n_l$ [216] – which means a spontaneous magnetization $m^* = 1/2n_l$ as shown in Fig. 4.13. This does not hold for even-leg ladders.

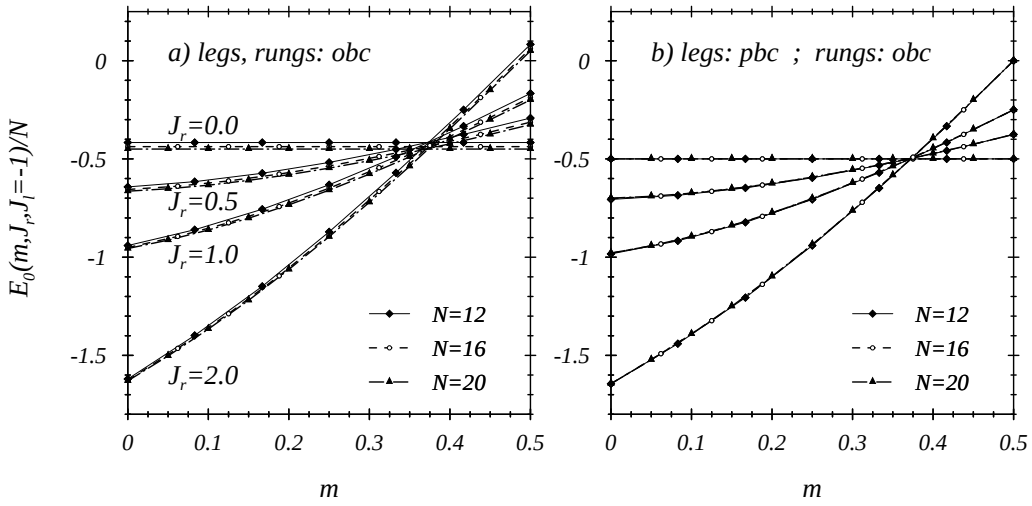

Figure 4.14: Ground state energies per site $e_0(m, J_l = -1, J_r)$ vs. m for 2-leg ladders

The investigation of spin ladder systems with competing interactions disclosed a quite unexpected property of the spin ladders ($n_l = 2, 3, 4$). As exemplified in Fig. 4.15 for a 3-leg ladder, the ground state energies per site $e_0(m, J_r, J_l)$ as a function of the magnetization m for different J_r and a fixed $J_l = -1$ not only show the above-mentioned spontaneous magnetization m^* but in addition a very precise single crossing point of all curves at a higher magnetization value m_x. As will be shown later, this crossing phenomenon does not mean a peculiar property of ladder systems with competing interactions. The same phenomenon is present in purely antiferromagnetic ladders showing the same m_x-value as in case of competing interactions.
Fig. 4.14 shows a similar single crossing point for the case of 2-leg ladders with competing interactions. The 2 Figs. in addition provide a comparison of calculations with open boundary conditions (obc: a)) and periodic boundary conditions (pbc: b)) for the leg direction. It turns out that in case of obc (resembling the DMRG case) finite-size effects are distinctively more pronounced than in case of periodic leg couplings (pbc). The open ends of the legs lead to $1/N$-corrections as can e.g. be seen for the un-coupled legs at $J_r = 0$:

$$\begin{aligned} \text{obc:} \qquad e_0(m, J_r = 0, J_l) &= \left(\frac{1}{2} - \frac{n_l}{N}\right) \cdot J_l \\ \text{pbc:} \qquad e_0(m, J_r = 0, J_l) &= \frac{1}{2} \cdot J_l \,. \end{aligned}$$

DMRG calculations for comparatively large systems led to $e_0(m_x, J_l = -1, J_r) = -1/2$ and $m_x(n_l = 2) \simeq 0.375$, $m_x(n_l = 3) \simeq 0.385$ [216]. Results for a 48-site 3-leg ladder are given in Fig. 4.15 a_2) and in good agreement with Fig. 4.15 b), i.e. results that were obtained from smaller systems using periodic leg-boundary conditions. Figs. 4.14 b), 4.15 b) show that the 2 crossing points ($n_l = 2, 3$) are in good approximation given by $m_x(n_l = 2) \simeq 6/16 = 0.375$ and $m_x(n_l = 3) \simeq 7/18 = 0.388...$

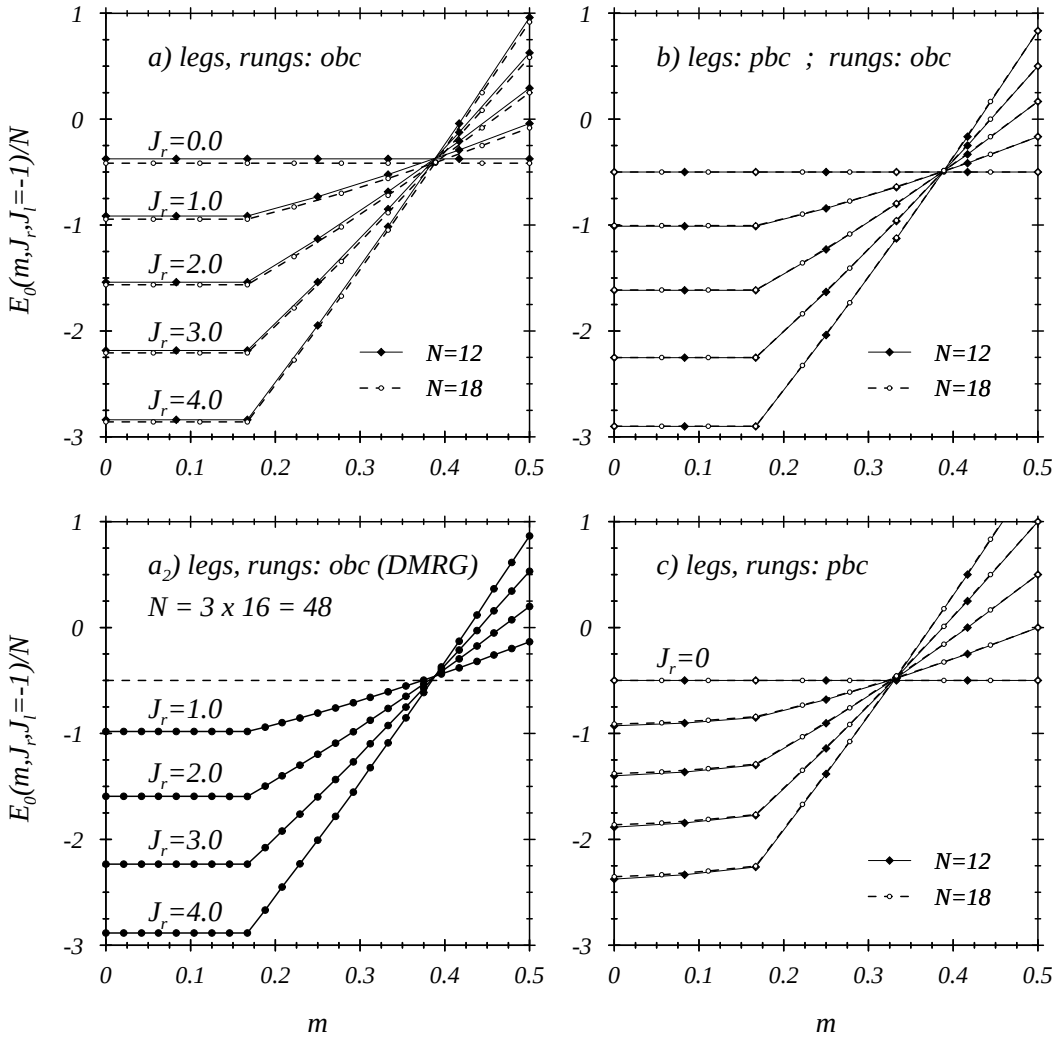

Figure 4.15: Ground state energies per site $e_0(m, J_l = -1, J_r)$ vs. m for 3-leg ladders

Since until now no rigorous explanation could be achieved, the closeness of m_x to the saturation value $m_{sat} = 1/2$ led to an approximate description [216] of the situation starting from the saturation point $m = 0.5$ of the magnetization. (Another description for all considered cases of couplings, however for periodic leg couplings, is given further below.) Owing to the ferromagnetic leg coupling each leg of a ladder below the saturation magnetization is described by applying lowering operators on the fully magnetized legs $|0>$:

$$|leg > (m_{leg} = \frac{1}{2}(1 - k/(N/n_l))) \quad = \quad (S^-_{leg})^k|0> \quad ; \quad S^-_{leg} \equiv \sum_{x=0}^{N/n_l-1} S^-_{x,leg}\,. \qquad (4.17)$$

I.e., the total spin of each leg remains fixed at the saturation value $S_{tot,leg} = N/(2n_l)$ and only the S_z-value is lowered. Moreover, periodic boundary conditions for the leg direction have been chosen in this picture (leading to small deviations that are expected to vanish for increasing N/n_l). Under these assumptions for a variational ansatz for the ground state (based on a superposition of product states), in [216] it was shown that

$$(e_0(m) - e_0(m_x))/J_r \qquad \Big(= m + g(m) \Big) \qquad (4.18)$$

is an almost linear function in m (for $m_x < m < m_{sat}$) with no further dependence on J_r thus explaining the unique crossing point and the linear dependence in m (see Figs. 4.14, 4.15).

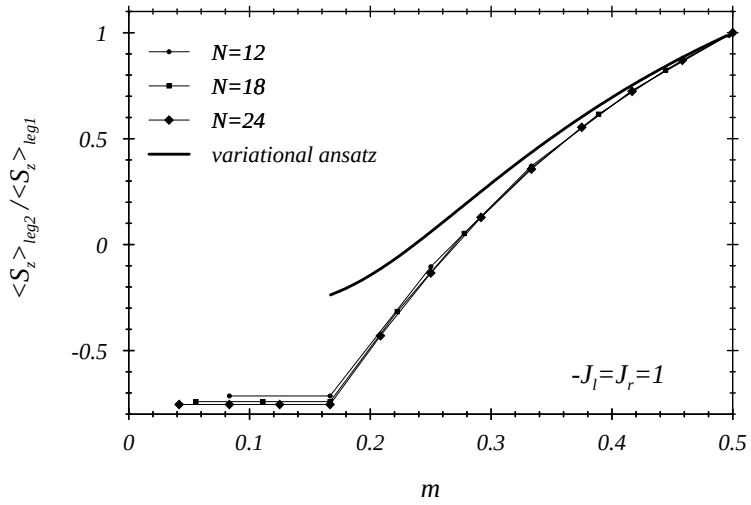

Figure 4.16: Comparison of $< S_z >_{leg\,2} / < S_z >_{leg\,1}$ with a variational ansatz (see text)

The above sketched variational approach has been tested twofold. First, $(e_0(m) - e_0(m_x))/J_r$ was shown to be independent of J_r to a satisfactory level for $m > m_x(n_l)$ [216]. Second, the ratio of S_z-expectation values for the inner and outer legs of a 3-leg ladder ($-J_l = J_r = 1$)

$$\frac{< S_z >_{inner\ leg}}{< S_z >_{outer\ leg}}(m) \quad = \quad \frac{\sum_{x=0}^{N/3-1} < S_z(x, y = 2) > (m)}{\sum_{x=0}^{N/3-1} < S_z(x, y = 1) > (m)} \tag{4.19}$$

have been calculated within the variational ansatz and compared with numerical results for 3-leg ladders (here, $y = 1, 2, 3$ has been used for the numbering of the legs, $1, 3$ denoting the outer ones).

Fig. 4.16 shows results for systems ($N = 12, 18, 24$, obc for legs and rungs) and the variational ansatz and a growing inadequacy becomes apparent for decreasing m. In the following figures (Figs. 4.17,.., 4.19; obc for legs and rungs) results for $< S_{z,tot} >_{leg}$ for finite-N 2- and 3-leg ladders are given. For further comparison, the case $-J_l = J_r = 1$ (solid symbols) is confronted with $J_l = J_r = 1$ (open symbols), i.e. the completely antiferromagnetically coupled ladder.

For 2-leg ladders no difference of expectation values for the 2 legs appears. Expectation values of $< S_{tot} >_{leg\ 1,2}$ (normalized by $(N/n_l) \cdot 1/2 = N/4$) in Fig. 4.17 show that the ground state expectation values $< S_{tot} >_{leg} /(N/2n_l)$ indeed decrease much slower from the saturation value in case of the ferromagnetic leg couplings. The same holds for the 3-leg ladder (Fig. 4.18), where the values for the inner (solid lines) and outer (dotted lines) legs differ. The maximum value of $< S_{tot} >_{leg} /(N/2n_l) = 1$, however, is only retained for the first value $m = 1/2 - 1/N$ below $m_{sat} = 1/2$.

The $< S_z >_{leg}$ expectation values for the 3-leg ladder on the other hand show almost no differences between $J_l = \pm 1$ well above $m_x(3)$ (Fig. 4.19; the 2-leg case gives identical linear behaviour in the whole interval $0 \leq m \leq 1/2$ (r.h.s. Fig. 4.17)). Further below m_x significant differences appear and the onset of the spontaneous magnetization for $J_l = -1$ is clearly indicated by the beginning of plateaus in $< S_{tot} >_{leg}$ and kinks in $< S_z >_{leg}$.

We have seen clear differences in properties of completely antiferromagnetic ladders and those with competing interactions. In the latter case ferromagnetic leg couplings have been considered and it ought to be supplemented that the other case (ferromagnetically coupled antiferromagnetic chains) has been discussed in [39] where unusual behaviour has been reported as well.

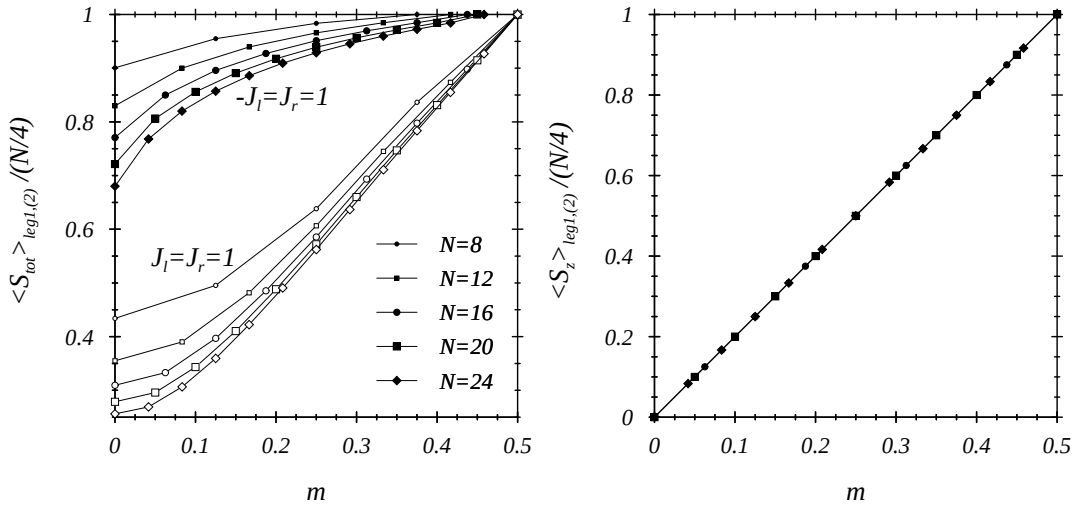

Figure 4.17: Expectation values of S_{tot}, S_z for the legs of a 2-leg ladder

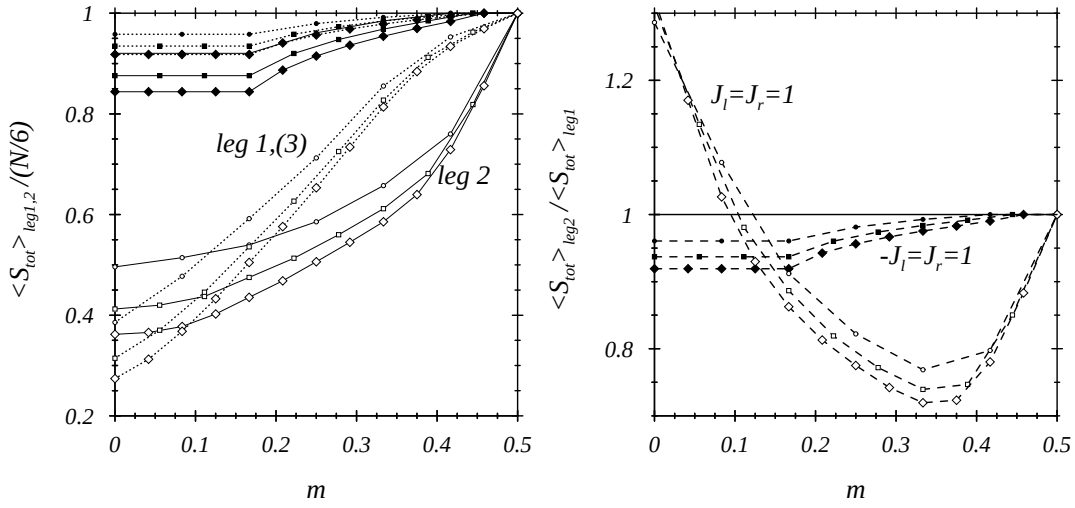

Figure 4.18: Expectation values of S_{tot} for the inner(2) and outer(1,3) legs of a 3-leg ladder

Moreover, a variational ansatz has been discussed that offered an explanation for the single crossing point of the ground state energies per site in case of ferromagnetic leg couplings (Fig. 4.15. Reasons and limitations for the assumptions made in this context have been given and the different situation in case of (antiferromagnetically coupled) ferromagnetic chains has been exemplified in a comparison of the 2 cases $J_l = \pm 1$.

At this place, however, it should be pointed out that in case of purely antiferromagnetic ladders the same feature (single crossing point of energies per site) is present. Fig. 4.20 shows this phenomenon for 2- and 3-leg ladders and $J_l = +1$. Periodic boundary conditions for the leg direction have been applied leading again to very small finite-size dependences.

The shown crossing points again are in fairly good accuracy given by $m_x = 6/16$ ($n_l = 2$), $m_x = 7/18$ ($n_l = 3$) as in case of the ferromagnetic legs (in both cases with obc in rung direction; pbc for the rungs shift the crossing point as shown in Fig. 4.15 c)). For the 3-leg

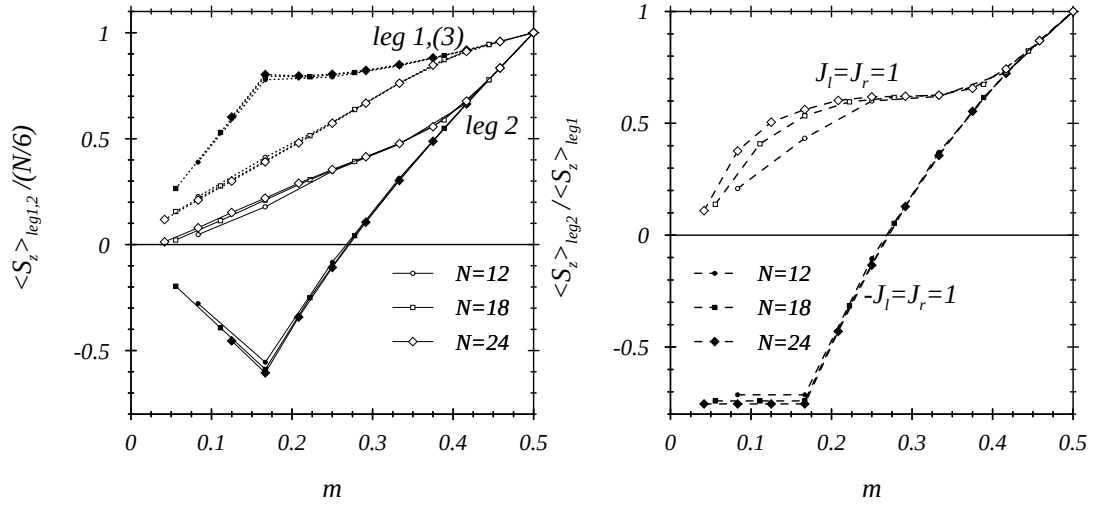

Figure 4.19: Expectation values of S_z for the inner(2) and outer(1,3) legs of a 3-leg ladder

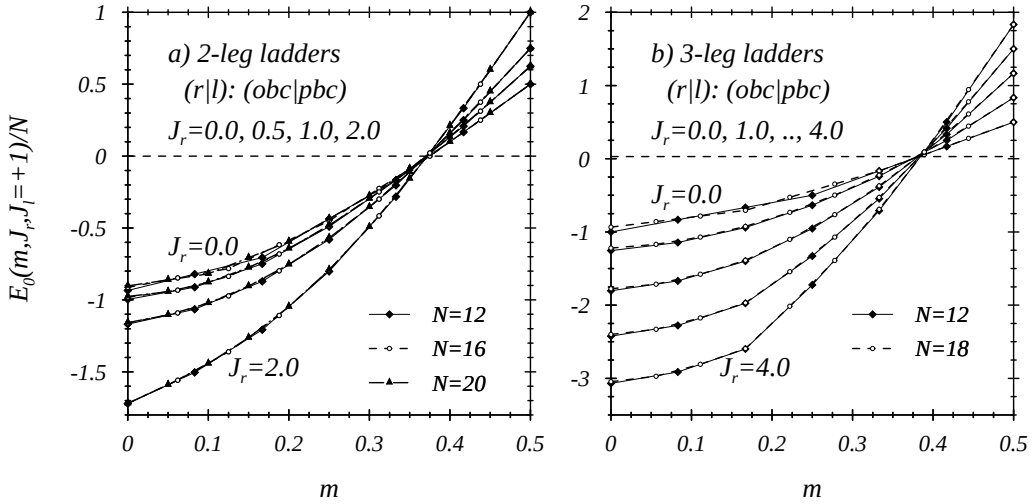

Figure 4.20: Ground state energies per site $e_0(m, J_l = +1, J_r)$ vs. m for 2- and 3-leg ladders

ladders a small non-zero ordinate value ($e_0(m_x, J_l = +1) = 0.03$) has been empirically chosen to optimally locate the crossing point of the shown data. The non-zero value, however, remains questionable. Differences in particular become evident in case of the un-coupled legs. While $e_0(m, J_r = 0, J_l < 0)$ constantly remains at $J_l/2$ (defining the ordinate value of the crossing point), antiferromagnetic leg couplings evolve a non-constant m-dependence even at J_r=0. In this case finite-size effects are clearly visible for $m < m_x$. A number of un-coupled legs does not behave as a single chain in a magnetic field – the total S_z-value has to be distributed on the manifold of legs, which causes an interdependence without existing rung couplings.

We are now going to complete our discussion of the antiferromagnetically coupled ferromagnetic chains (again combined with a comparison of the fully antiferromagnetic ladders) showing in addition the magnetization behaviour of 4- and 5-leg ladders. This will close our discussion of the classification of magnetization plateaus in regular ladder systems with or without competing

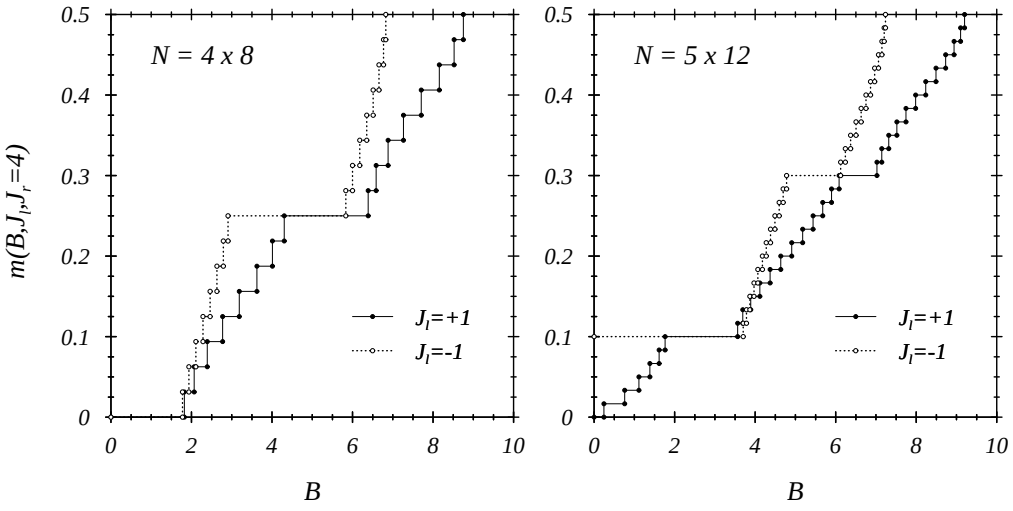

Figure 4.21: DMRG-results for magnetization $m(B)$ of 4- and 5-leg ladders; $J_r = 4$, $J_l = \pm 1$

interactions.
The situation with an even number of legs ($n_l = 4$) first shows the expected gap(plateau) at $m = 0$ and moreover a second gap at $m = 1/4$ as given in Table 4.2. The change from ferromagnetic to antiferromagnetic leg couplings mainly affects the second plateau (position and width). The plateau width decreases despite the increasing saturation field B_{Sat}.
The 5-leg ladder shows the plateau values $m = 1/10,\ 3/10$ as given in Table 4.2 for both types of leg couplings. The situation of ferromagnetic leg couplings ($J_l = -1$) shows a spontaneous magnetization of $m = m^* = 1/(2n_l) = 1/10$ – disappearing for $J_l > 0$ – as discussed earlier. As in the 4-leg ladder case the second plateau decreases and B_{Sat} increases when turning from ferro- to antiferromagnetic leg couplings.

We finally want to offer an alternative explanation/description for the observed singular crossing points of $e_0(m, J_r; n_l, J_l)$. All of the shown cases have in common that $e_0(m)$ behaves to a very high degree of accuracy linear in the relevant regime below $m = 1/2$. We therefore describe the m-dependence of $e_0(m)$ as

$$e_0(m, J_r; n_l, J_l) \quad = \quad e_0(1/2, J_r; n_l, J_l) - 2B_{Sat}(J_r; n_l, J_l) \cdot (1/2 - m) + O\left((1/2 - m)^3\right)$$

(compare Sec. 2.4) – due to the very small finite-size dependences of the shown data (for periodic leg couplings) we omitted the N-dependence in the upper relation. Demanding now the existence of a unique crossing point $(m_x, e_{0,x})$

$$e_0(m_x, J_r; n_l, J_l) \quad = \quad e_0(m_x, J_r'; n_l, J_l) \tag{4.20}$$

we obtain

$$m_x \quad = \quad \frac{1}{2}\left(1 - \frac{e_0(1/2, J_r; n_l, J_l) - e_0(1/2, J_r'; n_l, J_l)}{B_{Sat}(J_r; n_l, J_l) - B_{Sat}(J_r'; n_l, J_l)}\right) + O\left((1/2 - m_x)^3\right) \tag{4.21}$$

$$m_x^{(1)} \quad = \quad \frac{1}{2}\left(1 - \frac{e_0(1/2, J_r; n_l, J_l) - e_0(1/2, J_r'; n_l, J_l)}{B_{Sat}(J_r; n_l, J_l) - B_{Sat}(J_r'; n_l, J_l)}\right). \tag{4.22}$$

Due to the various boundary conditions it is much more convenient to use the numerical results ($e_=(m = 1/2)$ and $B_{Sat} = (E_0(m = 1/2) - E_0(m = 1/2 - 1/N))/2$) then to follow the way of

analytical evaluations as e.g. presented in App. B. An overview of results for $m_x^{(1)}$ for various 2- and 3-leg ladders (all with periodic leg couplings) is given in Table 4.3. The values of $m_x^{(1)}$ all give upper bounds for the crossing points shown in Figs. 4.14, 4.15, 4.20. The smallness of $m_x^{(1)} - m_x$ is consistent with the smallness of the next-to-leading term ($(1/2 - m_x)^3 < 10^{-2}$).

n_l	J_l	legs	rungs	$e_0(m = 1/2)$	B_{Sat}	$m_x^{(1)}$
2	+1	pbc	obc	$+1/2 + 1/4 \cdot J_r$	$2 + J_r$	3/8
2	-1	pbc	obc	$-1/2 + 1/4 \cdot J_r$	J_r	3/8
3	+1	pbc	obc	$+1/2 + 1/3 \cdot J_r$	$2 + 3/2J_r$	7/18
3	-1	pbc	obc	$-1/2 + 1/3 \cdot J_r$	$3/2J_r$	7/18
3	+1	pbc	pbc	$+1/2 + 1/2 \cdot J_r$	$2 + 3/2J_r$	1/3
3	-1	pbc	pbc	$-1/2 + 1/2 \cdot J_r$	$3/2J_r$	1/3

Table 4.3: Crossing point magnetizations $m_x^{(1)}$ for several ladders and boundary conditions

At the end of this consideration we shortly want to turn to the antiferromagnetic 3-leg ladder (J_l, $J_r > 0$) with periodic leg and rung couplings. Here, as shown in Fig. 4.22, for the first time deviations from the existence of single crossing points of ground state energies per site for ladder systems become apparent.

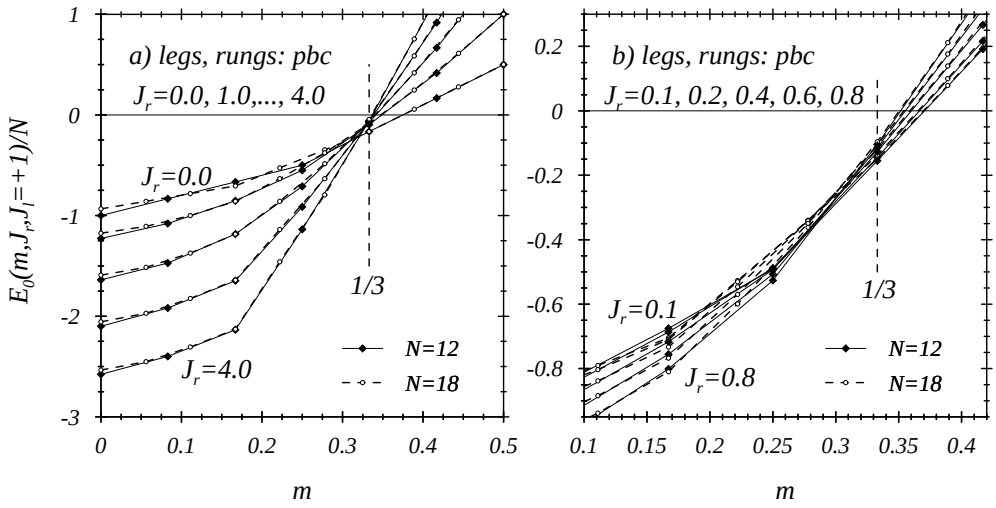

Figure 4.22: Ground state energies per site $e_0(m, J_l = +1, J_r)$ vs. m for 3-leg ladders with both periodic legs and rungs

While for large rung couplings the determined $m_x^{(1)} = 1/3$ again approximates the crossing point from above (Fig. 4.22 a)), small couplings (magnified in Fig. 4.22 b)) do no longer show a unique crossing behaviour with negligible finite-size corrections. This only underlines that the observed phenomenon is not a genuine feature of spin ladder systems.
In summary, it has to be pointed out that the given explanation, while giving a good description of existing crossing points, does not give a definite explanation for the general situation.

In the next section we will turn our attention to the additional "different types of ladder geometries" which have been introduced in Sec. 3.4.2 and again classify magnetization plateaus that

occur in these systems.

4.1.3 Different ladder geometries – a DMRG study

We will close the discussion of spin systems with ladder geometry by applying our prediction scheme for magnetization plateaus to the zig-zag-type and Kagomé-like ladders introduced in Sec. 3.4.2. Following this outline we will first review some recently published DMRG results [217].
In the next paragraph we will discuss the applicability of open leg boundary conditions (which had to be used for the presented DMRG calculations) for the treatment of problems that do require periodic boundaries –or the approach of system sizes that make the choice of boundary conditions rather insignificant. For this purpose the evaluations of 3-leg ladders presented in this section will be carried out again by means of the standard Lanczos techniques applying the required periodic leg boundary conditions. The different finite-size behaviour for both choices of leg boundary conditions will be discussed and documented.
Zig-zag ladders have only recently been investigated by *Cabra, Honecker and Pujol* [39] applying bosonization techniques and numerical evaluations. Here, the appearance of magnetization plateaus will again be considered by mapping the respective Hamiltonians onto 1-dim. spin chains (see Sec. 3.4.2). Compared with the regular ladders that have been treated in the last section, the composition of contributing and perturbed couplings differ. In the following, the Hamiltonians given in Sec. 3.4.2 will be shortly reproduced –together with a classification of potential plateaus and some recently published DMRG results [217] for the respective cases. In addition, the discussion of 2- and 3-leg zig-zag ladders will be supplemented by similar considerations concerning the recently discussed [208] Kagomé-type 3-leg ladder.
We will now give again the Hamiltonians of Sec. 3.4.2 –this time, however, omitting the additional h-dependences of the couplings $J_{1,2}$ for the 3-leg cases. In order to achieve a terse notation we define

$$\bar{D}_r(q,j) \equiv \frac{1}{\sqrt{N}} \sum_{n=0}^{N-1} \cos q(n+j) \cdot \mathbf{S}_n \mathbf{S}_{n+r} \tag{4.23}$$

and refer to the symbols (a)(2-leg zig-zag ladder), (b) (3-leg zig-zag ladder), (b') (3-leg zig-zag ladder with open rung couplings) and (c) (Kagomé-like 3-leg ladder) used in Fig. 3.20. The 4 respective Hamiltonians now read (with $q_3 \equiv \frac{2\pi}{3}$, $q_4 \equiv \frac{\pi}{2}$)

$$H_{(a)} = J_1 H_1 + J_2 \left[H_2 + 2\sqrt{2N} h \bar{D}_2(q_4, 1/2) \right] \tag{4.24}$$

$$H_{(b)} = J_1 H_1 + \frac{2}{3} J_2 H_2 + J_3 H_3 + -\frac{4}{3} J_2 \sqrt{N} \bar{D}_2(q_3, 1) \tag{4.25}$$

$$H_{(b')} = \frac{2}{3}(J_1 H_1 + J_2 H_2) + J_3 H_3 - \frac{4}{3}\sqrt{N} \left[J_1 \bar{D}_1(q_3, -1) + J_2 \bar{D}_2(q_3, 1) \right] \tag{4.26}$$

$$H_{(c)} = \frac{2}{3}(J_1 H_1 + J_2 H_2 + J_3 H_3) - \frac{4}{3}\sqrt{N} \left[J_1 \bar{D}_1(q_3, 2) + J_2 \bar{D}_2(q_3, 1) + J_3 \bar{D}_3(q_3, 0) \right] \tag{4.27}$$

.

The equations show that with increasing complexity periodically perturbed interactions of an increasing number of ranges occur. We now want to apply the scheme of prediction of potential magnetization plateaus as already done for the regular ladder systems. Moreover, these predictions will be accompanied by several calculated (DMRG calculations) magnetization curves as presented in [217]. The application of DMRG algorithms again requires to consider ladders with open leg boundary conditions meaning respective adjustments for the given Hamiltonians. Looking back on the discussion of finite-size effects in the last section –particularly marked in case of obc for the legs– and taking into account the higher complexity (number and ranges of

the periodic perturbations) of the above given Hamiltonians, higher demands on evaluated system sizes for controllable finite-size effects are to be expected. Below, we will give a comparison with Lanczos evaluations using periodic leg boundary conditions for one of the reported DMRG calculations. The important influence of leg boundary conditions will be discussed in the next section.
Concerning magnetization plateaus, we expect –if at all– plateaus in cases where the wave vector q coincides with one of the (longitudinal or transverse) soft mode momenta $q_{1,3}^{(k_{1,3})}(m)$, leading to plateau magnetizations

$$m_{(3)}(k_3) = \frac{1}{2}\left(1 - \frac{q}{k_3\pi}\right) \tag{4.28}$$

$$m_{(1)}(k_1) = \frac{1}{2}\frac{q}{k_1\pi} = \frac{1}{2} - m_{(3)}(k_3 = k_1)\,. \tag{4.29}$$

A first application to the 2-leg zig-zag ladder (an example for the parameters $J_1 = 1$, $J_2 = 2$, $h = 0.6,\ 0.8,\ 1.0$ is shown in Fig. 4.23) leads to

$$q = \frac{\pi}{2} \qquad m_{(3)} = \frac{1}{4},\ \frac{3}{8},.. \qquad k_3 = 1, 2, .. \tag{4.30}$$

$$m_{(1)} = \frac{1}{4},\ \frac{1}{8},.. \qquad k_1 = 1, 2, ..\,. \tag{4.31}$$

Since $\cos\frac{\pi}{2} = \cos\frac{3\pi}{2}$, $\sin\frac{\pi}{2} = -\sin\frac{3\pi}{2}$, one might consider $q = 3\pi/2$ in this particular case as well (in all other cases only multiples of 2π may be added to a given q), leading to

$$q = \frac{3\pi}{2} \qquad m_{(3)} = --,\ \frac{1}{8},.. \qquad k_3 = 1, 2, .. \tag{4.32}$$

$$m_{(1)} = --,\ \frac{3}{8},.. \qquad k_1 = 1, 2, ..\,. \tag{4.33}$$

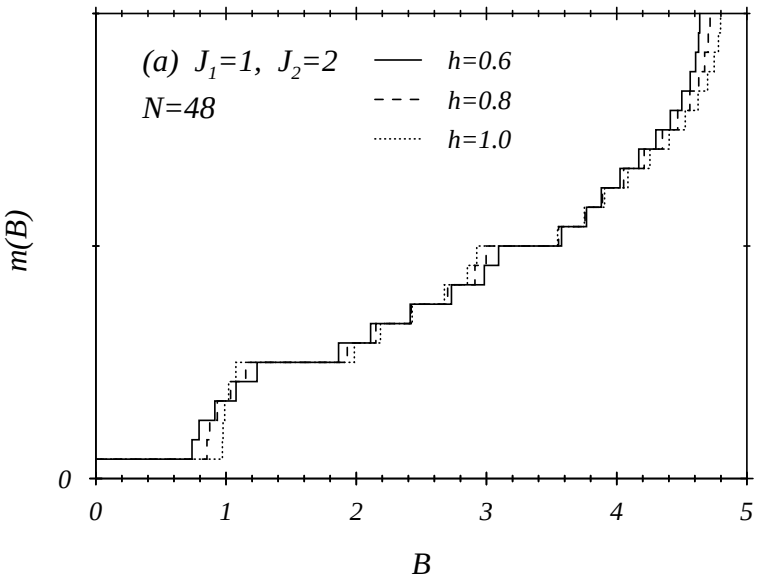

Figure 4.23: $m(B)$ for a 2-leg zig-zag ladder with $J_1 = 1$, $J_2 = 2$ and $h = 0.4,\ 0.6,\ 1.0$

Fig. 4.23 shows two plateaus at $m = 1/8,\ 1/4$, however, no signatures at $m = 3/8$ are visible. The plateau at $m = 0$ is not described by $q = \pi/2$ $(3\pi/2)$. Here, the large $q = 0\,(2\pi)$-contribution J_2H_2 (note $\alpha = J_2/J_1 = 2$) leads to the opening of a gap at $m = 0$ (cf. Chap. 5). The occurrence of the $m = 1/8$-plateau strongly depends on the ratio $\alpha = J_2/J_1 = 2$. Shifting this ratio to

either side results in the vanishing of the plateau. Note that the figure only shows results for a single system size ($N = 48$) to maintain legibility.
The magnetization of a 3-leg zig-zag ladder (Hamiltonian $H_{(b)}$) is shown in Fig. 4.24 (b) for parameters $J_1 = J_2 = 1.5$, $J_3 = 1.0$ and a 3×24-spin ladder. For the finite-size analysis of the (upper) plateau boundaries system sizes $N = 24, 36, \ldots, 96$ have been used.
Applying the prediction scheme for possible plateau formations in presence of a perturbation with $q = q_2 = 2\pi/3$ results in

$$q = \frac{2\pi}{3} \qquad m_{(3)} = \frac{1}{6}, \frac{1}{3}, .. \qquad k_3 = 1, 2, .. \tag{4.34}$$

$$m_{(1)} = \frac{1}{3}, \frac{1}{6}, .. \qquad k_1 = 1, 2, \ldots . \tag{4.35}$$

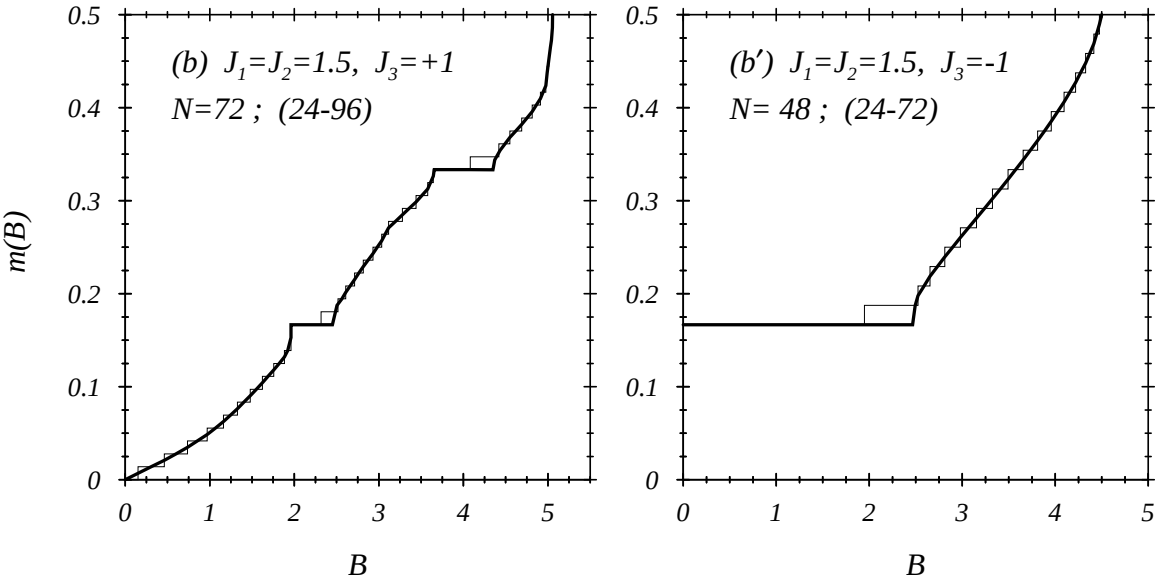

Figure 4.24: $m(B)$ for 3-leg zig-zag ladders with periodic (b) and open (b') rung couplings

Both plateaus are clearly visible in Fig. 4.24 (b). The Bonner and Fisher constructions (cf. Sec. 2.4) for the magnetization curves show rather large finite-size behaviour, requiring the comparatively large system sizes. The different behaviour for periodic leg couplings (using smaller systems) will be considered below.
On this level (calculating $m(B)$), we cannot definitely specify which kind of soft mode is responsible for the plateaus and again we have to refer to Sec. 4.2 for further considerations. In addition, the 3-leg zig-zag ladder has been discussed in [39] (same couplings have been chosen here) for different types of rung boundary conditions (types A, B and C) and the formation of plateaus has been found to react very sensitively on the chosen boundary conditions (no plateau for type B, plateaus at $m = 1/6$ for A and C).
The case of the 3-leg zig-zag ladder with open rung couplings ($H_{(b')}$) consists of periodic perturbations of the same $q_{pert.}$ as Hamiltonian $H_{(b)}$, however with different weights and different contributing coupling lengths of the perturbations. The general analysis of potential magnetization plateaus for $q = q_2 = 2\pi/3$ remains unchanged. For coupling strengths $J_1 = J_2 = 3/4$, $J_3 = 1$ it was shown in [39] that at both magnetizations ($m = 1/6,\ 1/3$ plateaus clearly evolve. In addition, changing from antiferromagnetic to ferromagnetic leg couplings, i.e. $J_3 < 0$, spontaneous magnetization ($m_{spon.} = 1/6$ for $J_1 = J_2 = 3/2,\ J_3 = -1$ has been established, see Fig. 4.24 (b')). In this case, a plateau at $m = 1/3$ is no longer observable.
Finally, we turn to the 3-leg Kagomé-like ladder that already has been discussed in [208] where the authors addressed the question whether the singlet-triplet gap of the Kagomé lattice as well

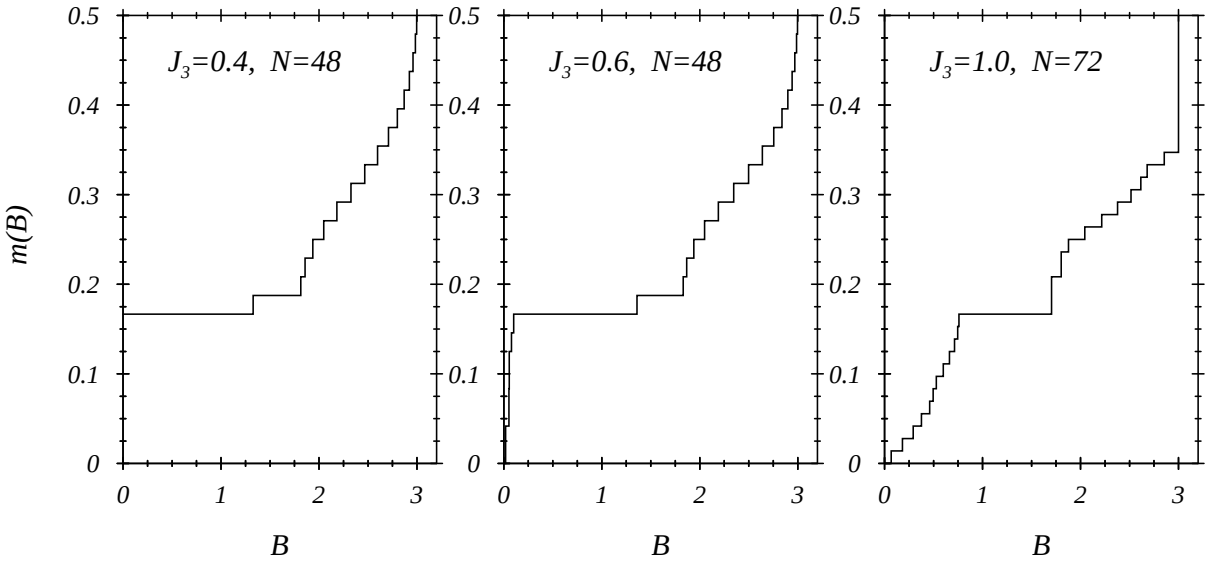

Figure 4.25: $m(B)$ for Kagomé-like 3-leg ladders (c) with $J_1 = J_2 = 1$, $J_3 = 0.4$, 0.6, 1.0

exists for the 3-spin Kagomé-like ladder, i.e. a plateau at $m = 0$ does exist. The observed behaviour, however, has been found to be gap-less in a wide range of coupling strengths [208]. Furthermore, *Azaria et al.* [14] recently discussed a different 3-leg Kagomé-like ladder system. The couplings of Hamiltonian $H_{(c)}$ ($q = q_3 = 2\pi/3$) again result in the prediction of $m = 1/6,\ 1/3$ as possible plateau values. Fig. 4.25 shows magnetization curves for different strengths of the leg coupling J_3. While all cases remain gap-less, an interesting behaviour of the lower plateau ($m = 1/6$) appears. At the lowest considered J_3-value a spontaneous magnetization (or ferrimagnetism) is observed – the plateau beginning at $B = 0$. This B-value changes to $B \simeq 0.1$ when changing from $J_3 = 0.4$ to $J_3 = 0.6$ showing a steep increase of $m(B)$ at $B = 0$. The $m = 1/6$ plateau further decreases when choosing $J_3 = 1.0$. Here, a first hint of the second plateau at $m = 1/3$ appears, followed by an immediate jump of m to the saturation magnetization. The latter phenomenon –a so-called meta-magnetism– has e.g. been discussed in [92]. Like in the earlier presented cases of 3-leg zig-zag ladders certain large finite-size effects at upper plateau boundaries seem to be present (compare with periodic leg coupling evaluations given in the following section).

4.1.4 Open and periodic leg boundary conditions – a comparison

In this part we are going to present results for the earlier given 3-leg evaluations (types (b), (b') and (c)) of the previous section –this time choosing periodic leg boundaries. The same coupling strengths will be chosen to allow for an immediate comparison of the behaviour of both types of boundary conditions.
For this purpose, we will first turn to the finite-size dependences visible in Fig. 4.24 and contrast them with the respective behaviour of ladders with periodic leg boundary conditions. Besides the infinite-N curves (thick lines; shown plateaus resulting from finite-size (BST) analyzes of system sizes out of the ranges given in parentheses in the figure) each part of the figure shows one finite-N magnetization curve (N value as well given in the figure) to illustrate the size of the N-dependences occurring in the performed DMRG calculations. Strong finite-size behaviour appears at the upper plateau boundaries – an effect that is as well observable in the single system results of Fig. 4.25. In particular, for the case $J_3 = 1.0$ in the latter figure the existence of a $m = 1/3$-plateau could not be decided on the basis of the shown data determined with open leg boundary conditions. Experiences out of the comparison of DMRG calculations and calculations

with periodic leg boundary conditions (see e.g. Sec. 4.1.2) may indicate –however, do not prove– that the above-mentioned effects are more likely effects of the applied boundary conditions than genuine effects of the considered perturbations. In the following, we are going to compare the presented 3-leg ladder (types (b), (b') and (c)) magnetization curves with solutions obtained from smaller spin systems and using periodic leg boundary conditions.

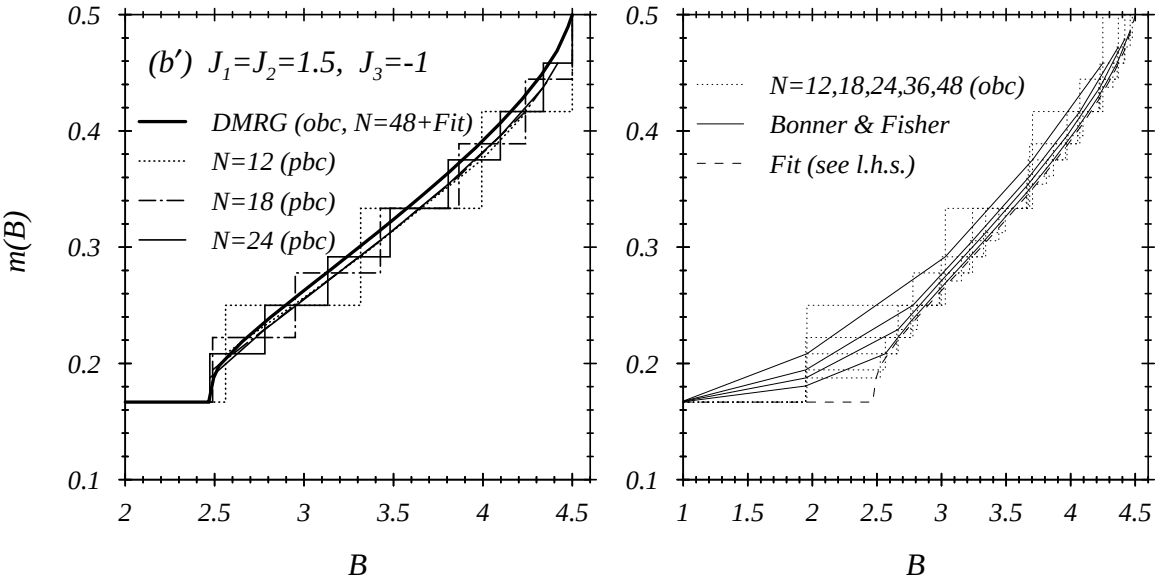

Figure 4.26: Finite-size effects of type-(b') ladders with open and periodic leg boundary conditions

Considering first the 3-leg zig-zag ladder with open rung couplings, the use of periodic boundary conditions for the leg direction indeed considerably "improves" the N-dependence of the magnetization curves as is shown in Fig. 4.26. Here, the $N \to \infty$ DMRG result –shown in Fig. 4.24 (based on $N = 48$ for magnetizations aside from the kink position)– is contrasted with finite-N magnetization curves ($N = 12, 18, 24$) for ladders with periodic leg boundary conditions that were accessible for standard Lanczos diagonalizations. Fig. 4.26 (l.h.s.) shows that the $m = 1/6$-plateau is approached very regularly and to a good degree of approximation even for the small manageable system sizes.

The Bonner-Fisher construction for $m(B)$ ($1/6 < m < 1/2$, $N = 12, 18, 24$) –shown as well on the l.h.s. of Fig. 4.26– already shows good convergence, however, a certain difference to the DMRG result in this regime remains (note that for this interval no finite-size scaling for the DMRG-results of $m(B)$ have been performed). The latter point –together with the finite-size dependence of magnetization curves determined for open leg boundaries– is shown on the r.h.s. of the figure. Open leg boundary conditions clearly enhance finite-size effects and the determination of plateau boundaries (for the given case further supplemented by $N = 72$ data around the kink of the magnetization curve) in the considered example appears to be expensive. The different data shown in the figure clearly favour the case of periodic leg boundary conditions and show that the $N = 48$ magnetization curve still carries small finite-size contributions in the interval $1/6 < m < 1/2$. Moreover, the range ΔB of the finite-size effect shown in Fig. 4.24 (b') appears to be independent of N – its height decreases with increasing N.

Fig. 4.27 now shows similar considerations for the type-(b) (periodic rung couplings) ladder. Again, periodic leg boundaries improve the smallness and direction of finite-size corrections. While both evaluations approximately agree in the course of the magnetization curve between the plateaus and in width and position of the upper plateau, the lower ($m = 1/6$) plateau appears to be somehow shifted to higher B values. The indicated bulge between both plateaus

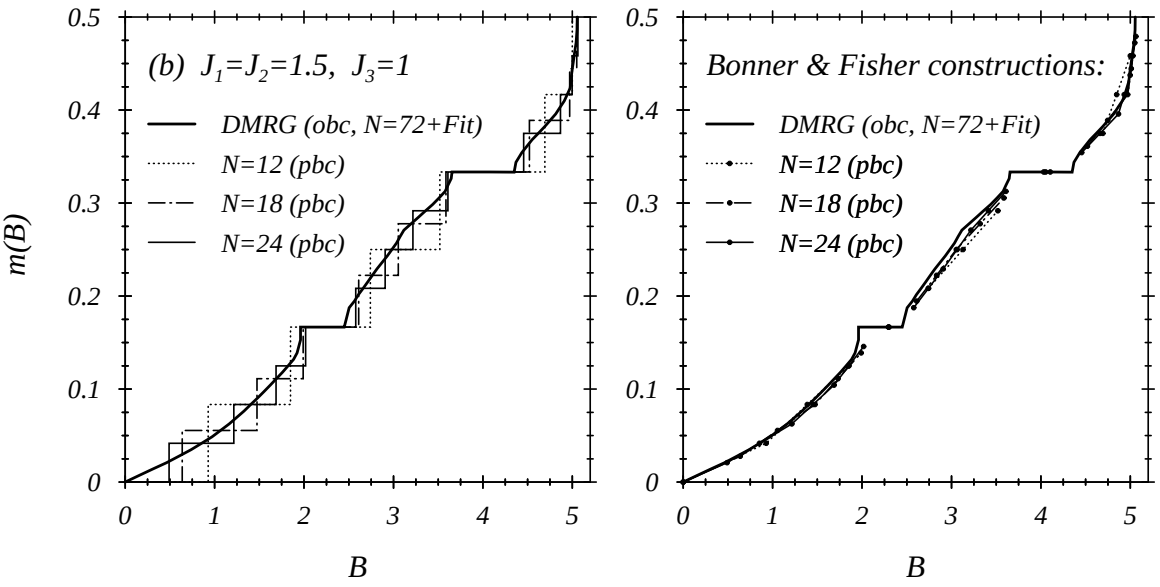

Figure 4.27: Finite-size effects of type-(b) ladders with open and periodic leg boundary conditions

(DMRG result) cannot be commented on the basis of the presented pbc-calculations. In this type-(b) example, as well as in the following type-(c) example, the aforementioned excess of the obc-calculations at the upper plateau is again present (compare Figs. 4.24, 4.25). It should moreover be noted that the number of Lanczos iterations needed to reach the demanded accuracy level (10^{-10} for all cases) considerably increased when turning from open (b')to periodic (b) rung couplings of the zig-zag ladder. The latter effect may be understood as a consequence of the imposed frustration of odd-leg ladders due to the periodic rung couplings.

Turning now again to the three Kagomé cases, Fig. 4.28 at first sight shows that system sizes $N = 12, 18$ are sufficient to give the bounds of the lower ($m = 1/6$) plateau for $J_3 = 0.4, 0.6$. The mentioned obc excesses at the upper plateau bounds do not exist. Calculations for ladders with $N = 24$ spins on one hand show the occurrence of irregular finite-size dependence at the upper bound of the $m = 1/6$ plateau –which corresponds to the larger finite-size effects for $J_3 = 1.0$ for the DMRG calculations. On the other hand, the inclusion of the third system size ($N = 24$) allows for a first finite-size (BST) analysis of the possible existence of a second plateau at $m = 1/3$. While the answer is negative for $J_3 = 0.4, 0.6$ a non-zero plateau exists for $J_3 = 1.0$ –as can as well be immediately seen in the figure. The latter fact only had to be argued on the basis of the performed obc calculations.

As a first summary it remains to be realized that the presented small system calculations with periodic leg boundary conditions not only resulted in the same results as obtained from larger spin systems treated by DMRG evaluations (using open leg boundaries) but moreover avoided the documented finite-size problems occurring for open leg boundaries. In addition, as was shown for the Kagomé-type ladders, pbc calculations proved to be better suited for the check of the existence of the "secondary" plateaus at $m = 1/3$.

The latter judgement of course has to be considered in the context of technical capabilities. While $q_{pert.} = 2\pi/3$ has been rather at the edge of a standard Lanczos diagonalization (three different system sizes are at least needed to assess finite-size dependences in simple cases, DMRG applications can be extended by about one order of magnitude for system sizes and more complex problems can be treated. Nevertheless, the discussed pbc evaluations offer valuable help for the assessment of situations that are no longer treatable with standard Lanczos techniques that allow to apply the important periodic boundary conditions required by the very nature of the discussed problems right from the beginning. The given comparison showed that $O(10^2)$

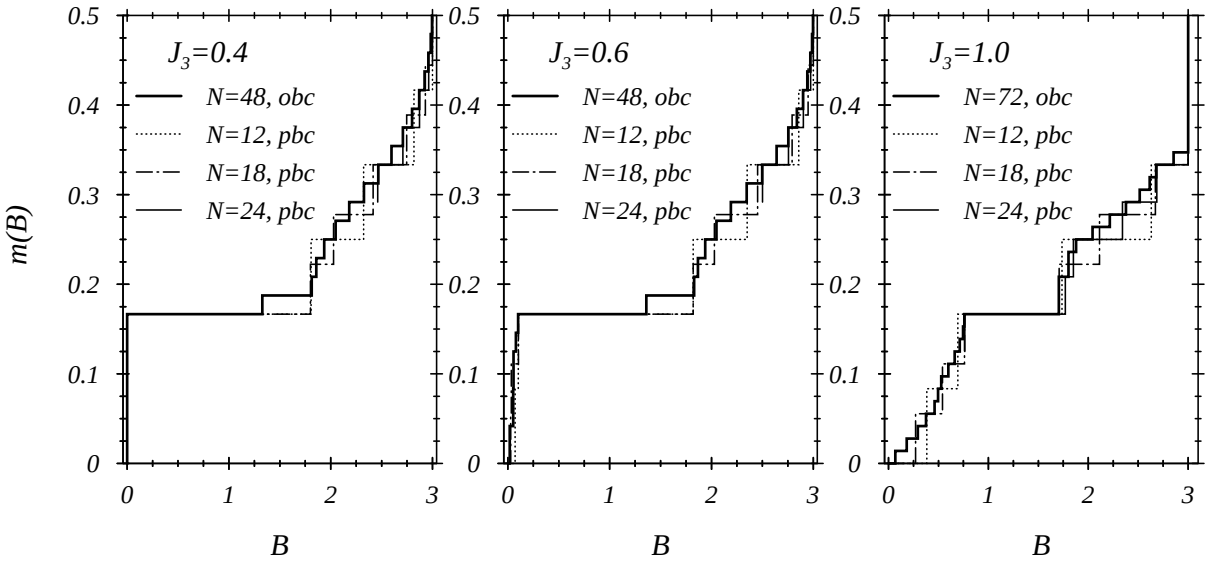

Figure 4.28: Finite-size effects of type-(c) ladders with open and periodic leg boundary conditions

considered spins may not be sufficient to reach in all cases a situation where the applied boundary conditions appear to be sufficiently uninfluential. The upper comparisons may as well support the classification of obc (DMRG) results obtained for above-mentioned cases (e.g. spin-1, -3/2, ..., Hubbard- and $t-J$-models) where similar Lanczos treatments are no longer possible.
The discussion moreover may help to influence endeavours to better and less costly incorporate periodic boundary conditions in DMRG calculations. The necessity of standard (obc) DMRG calculations for the discussed range of problems, however, may be scrutinized.

4.1.5 Gaps and plateaus for the spin-Peierls chain

We will now turn turn to frustrated and dimerized spin chains that have been discussed in the framework of quasi-1-dimensional spin-Peierls materials – in particular $CuGeO_3$ that in 1993 has been reported the first inorganic spin-Peierls material [105]– in Sec. 3.5.
In the present case, we will leave out particular aspects and details of spin-Peierls materials and only consider the periodically perturbed and frustrated 1-dimensional spin-1/2 Hamiltonians that have been found to give proper descriptions for $CuGeO_3$ [43, 176, 74]:

$$H \quad = \quad J_1 \left(H_0(\alpha) + 2\delta \cdot \sqrt{N} D_1(q=\pi) \right) \tag{4.36}$$

choosing $J_1 = 1$ and changing δ to the so far used parameter h. Moreover, we will largely extend the range of the dimerization strength to the interval $0 \leq h < 1$.
We will first consider the opening of the spin-Peierls gap, i.e. the gap at magnetization $m = 0$. Fig. 4.29 shows results of BST-fits (see App. C) based on finite-chain calculations for $N = 8, 12, 16, 20$. The figure includes the earlier obtained results for $\alpha = 0$ (Fig. 4.3) as well as the 3 frustration values ($\alpha = 0.25$, 0.3, 0.35) discussed in Sec. 3.5.
In the un-frustrated case the opening of the gap can be described by a single exponent in the whole interval $0 < h \leq 1$. One should note, however, that the investigation of the scaling behaviour for very small dimerization strengths (compare Sec. 3.3.3 and Fig. 3.9) resulted in a slightly smaller exponent (0.73 instead of 0.75).
The frustrated chains show a drift away from an algebraic increase at smaller dimerization strengths already well below $h = 1$ changing to an almost linear increase. This change is accompanied by a ground state level crossing in the sector $S_z = 1$. The same level crossing

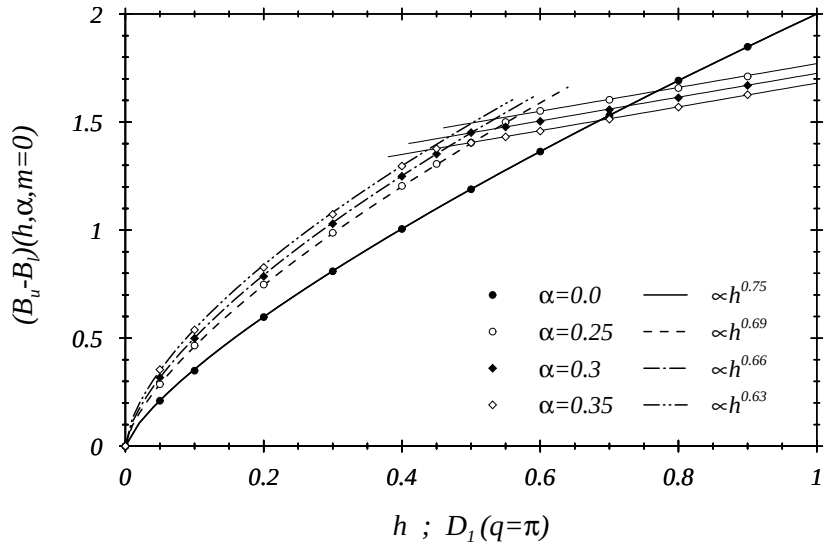

Figure 4.29: $m = 0$ dimer gap ($q = \pi$) for frustrations $\alpha = 0.0,\ 0.25,\ 0.3,\ 0.35$ ($N = 8, 12, 16, 20$)

happens for the un-frustrated chain precisely at $h = 1$. For the regime $h < 0.5$ the data indicate that a growing frustration results in a lowering of the exponent describing the opening of the gap. In the regime of larger dimerization h all curves for $\alpha > 0$ are fitted by straight lines of the same slope. Especially at $h = 1$ these lines seem to approach the value of 2 for the un-frustrated case almost equidistantly – a point that will be considered in a perturbation expansion below.

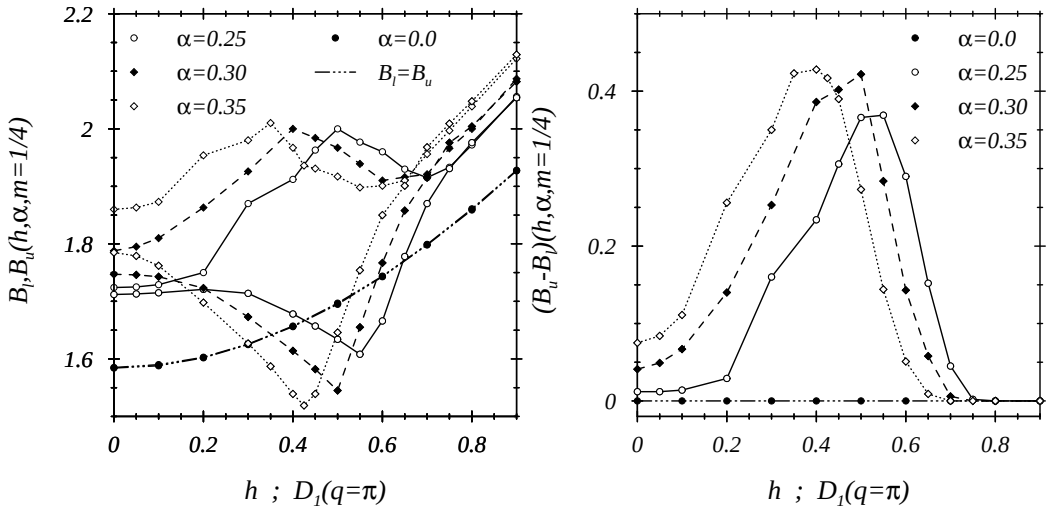

Figure 4.30: $m = 1/4$-dimer gap ($q = \pi$) for frustrations $\alpha = 0.0,\ 0.25,\ 0.3,\ 0.35$ ($N = 8, 12, 16, 20$)

Now, first we will turn to situations of plateaus at a non-zero magnetization. In retrospect to the quantization condition 4.1 it appears that an additional spontaneous symmetry breaking is needed for magnetization plateaus at non-zero magnetization. This spontaneous symmetry breaking is provided by the considered frustrations $\alpha > \alpha_c$ (compare *Totsuka* [200]).
Fig. 4.30 shows that for the considered α-values a second plateau exists for h-values below

$h = 1$ (see figure). The dependence of the $m = 1/4$-plateau on α and h has been discussed in much more detail by *Totsuka* [200] (see phase diagram –Fig. 6– there) using bosonization techniques. The 3 non-zero α-values of Fig. 4.30 and the shown range of perturbation strengths h lie well within the plateau region determined by Totsuka. The entire h-dependence of the plateaus shown on the r.h.s. of Fig. 4.30, however, exceeds the range of Totsuka's treatment.
Using the LSM-predictions given in Eqns. 4.2, 4.3 we can classify the $m = 1/4$-plateaus by $k_1 = k_3 = 2$, i.e. again a case where higher soft mode momenta occur. Quite interestingly, it seems that even in the parameter range discussed for $CuGeO_3$ ($h \leq 0.05$) a second magnetization plateau is predicted. However, considering $J_1 \simeq 80K$ (note the factor of 2 in H) magnetic fields greater than $50\,T$ ($100\,T$) would be required to reach the plateau magnetization $m = 1/4$.
The maximum of each plateau width is characterized by level crossings for the ground state energies in the sectors $m = 1/4,\ 1/4 \pm 1/N$ as is exemplified for $N = 8,\ 12$ in Fig. 4.31 which shows the course of the 2 lowest energies $E_{0,1}(h, m, N)/N$. Again the un-frustrated case (with no second plateau for $h < 1$) is not affected by any level crossing of ground states in that regime. The 2 cases of frustrated systems show level crossings/ lifts of degeneracy at h-values that roughly coincide with the maximum widths of the respective plateaus.

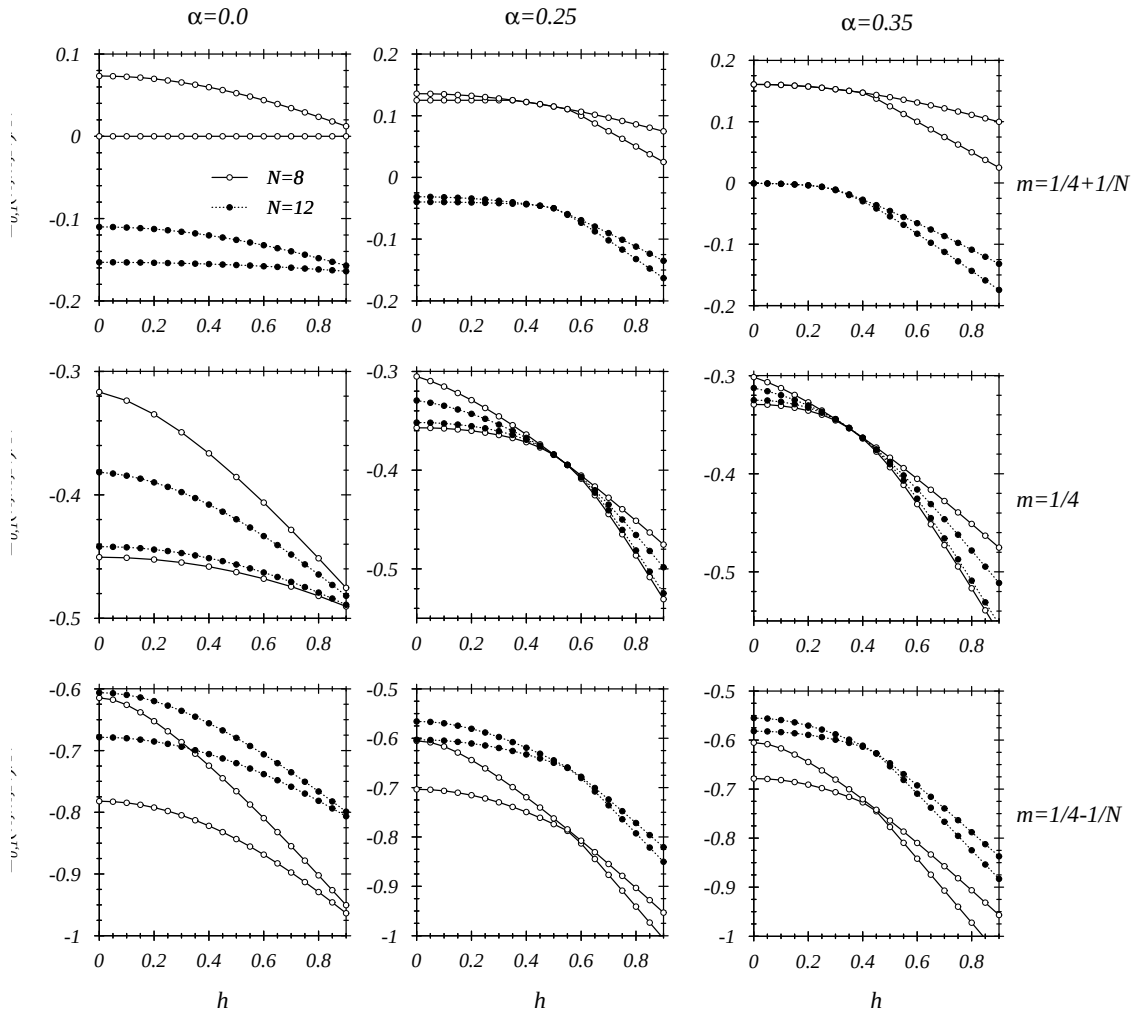

Figure 4.31: Lowest energies $E_{0,1}(h, m, N)$ for $\alpha = 0, 0,\ 0.25,\ 0.35$ and $N = 8, 12$; $D_1(\pi)$

Turning now back to the "spin-Peierls" gap at $m = 0$ we want to reconsider the situation at $h = 1$. In the un-frustrated case consists of $N/2$ un-coupled dimers. A singlet-triplet excitation of a single dimer ($E_{singlet} = -3/4$, $E_{triplet} = 1/4$) affords $\Delta E = 2$ ($J = 1 + h = 2$) resulting in

the gap width shown in Fig. 4.29.
Discussing now the influence of an additional frustration for dimerization strength $h = 1$, we treat the considered frustrations (with ratios $\alpha/(1+h) = \alpha/2 < 1$) as small perturbations for the dimers – now forming the rungs of a 2-leg ladder (see Fig. 4.32). We therefore calculate the gap value $E_{gap} = E_0(S_z = 1) - E_0(S_z = 0)$ up to lowest relevant order perturbation expansion.

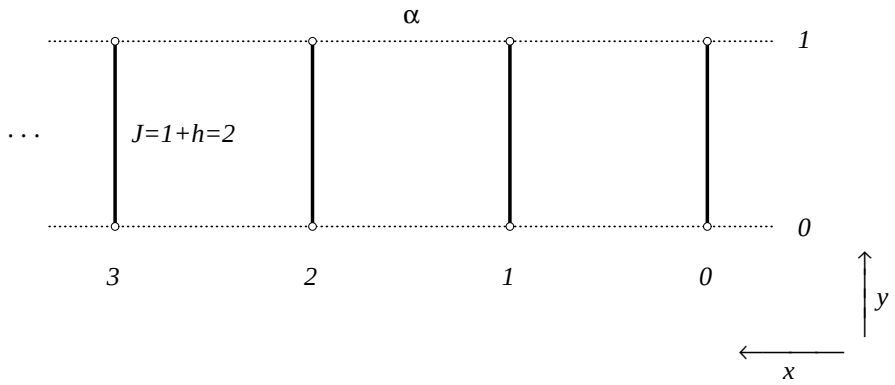

Figure 4.32: Resulting Hamiltonian for the dimerized ($q = \pi$) chain at $h = 1$

For the unperturbed ($\alpha = 0$) ground states in the 2 S_z-sectors we choose

$$\Psi_0(S_z = 0) = \prod_x S_0(x) \tag{4.37}$$

$$\Psi_0(S_z = 1) = \frac{1}{\sqrt{N/2}} \sum_{x=0}^{N/2-1} e^{iq_0 x} T_1(x) \prod_{x' \neq x} S_0(x') \tag{4.38}$$

with S_0, $T_{0,\pm 1}$ denoting the singlet and the 3 triplet states of each rung (thick lines in Fig. 4.32) of the ladder. The calculation of $< \Psi_0(S_z)|H|\Psi_0(S_z) >$ with

$$\begin{aligned} H &= H_{rung} + H_\alpha \\ H_{rung} &= 2\sum_x \underbrace{(1+1)}_{\equiv J} \mathbf{S}(x,0)\mathbf{S}(x,1) = \sum_x H_{rung}(x) \\ H_\alpha &= 2\alpha \sum_x \sum_{y=0}^{1} \mathbf{S}(x,y)\mathbf{S}(x+1,y) = \sum_x H_\alpha(x,x+1) \end{aligned} \tag{4.39}$$

leads to

$$H_{rung}(x)S_0(x) = -\frac{3}{2}JS_0(x) \quad , \quad H_{rung}(x)T_{0,\pm 1}(x) = \frac{1}{2}JT_{0,\pm 1}(x) \tag{4.40}$$

$$\begin{aligned} H_\alpha(x,x+1)S_0(x)S_0(x+1) &= \alpha\Big(T_0(x)T_0(x+1) - T_1(x)T_{-1}(x+1) \\ &\quad -T_{-1}(x)T_1(x+1)\Big) \end{aligned} \tag{4.41}$$

and

$$\begin{aligned} (H_\alpha(x-1,x) + H_\alpha(x,x+1))S_0(x-1)T_1(x)S_0(x+1) &= \\ \alpha\Big(T_1(x-1)S_0(x)S_0(x+1) + S_0(x-1)S_0(x)T_1(x+1)\Big)\,. \end{aligned} \tag{4.42}$$

First, it turns out that $E_0(S_z = 0)$ in 1st order is not changed by H_α (since $< S_0(x)T_j(x) >= 0$). –A second order calculation would result in

$$E_0^{(2)}(S_z = 0, \alpha) \;=\; E_0^{(0)}(0,0)\left(1 + \frac{1}{2}\left(\frac{\alpha}{J}\right)^2\right). \tag{4.43}$$

The 1st order contribution of $E_0^{(1)}(S_z = 1, \alpha)$ reaches its minimum value for the choice $q_0 = \pi$ (see Eq. 4.38) yielding

$$H_\alpha|\Psi_0(S_z = 1, q_0 = \pi) > \;=\; -2\alpha|\Psi_0(1,\pi) > \tag{4.44}$$

and one finally obtains

$$\begin{aligned} E_{gap}^{(1)} &= E_0^{(1)}(S_z = 1, \alpha) - E_0^{(1)}(S_z = 0, \alpha) \\ &= \Big((N/2-1)J(-\frac{3}{2}) + J\cdot\frac{1}{2} - 2\alpha\Big) - NJ(-\frac{3}{2}) \\ &= 2J - 2\alpha \\ &= 2(2-\alpha)\,. \end{aligned} \tag{4.45}$$

Disregarding the pre-factor 2 (definition of H) the leading $(2-\alpha)$-dependence of the energy gap at $h = 1$ is clearly visible in Fig. 4.29 – reaching the shown limit $E_{gap}(\alpha = 0) = 2$ for the limiting case of independent dimers.
The figure implies that the leading linear dependence in α persists down to the level crossing at $h_{l.c.}(\alpha) < 1$. However, we are not going to apply further perturbation calculations to this case but continue our discussion of periodically perturbed spin systems.

In the following section we will leave the field of a mere descriptive analysis of plateau formation when only making the right choice of magnetization m and period of the perturbation q (according to Eqns. 4.2, 4.3). We will determine the actual size of matrix elements $< n|X(q)|0 >$ that are crucial for the shift of ground state energy levels at magnetization values $m^\pm$ in the immediate neighbourhood of a possible plateau at m. Here, static structure factors (SSFs) will turn out to be of importance for the development of magnetization plateaus.

4.2 LSM theorem, structure factors and predictability for the occurrence of plateaus

In this section we want to try to give some further insight into the process of magnetization plateau formation. Throughout our whole discussion the important relationship between a periodically perturbed spin chain and the starting point –the isotropic Heisenberg chain with its massless excitations (at m-dependent positions)– has been emphasized. We therefore first present a survey of a selection of static structure factors $X_{aa,conn.}(q, m, N)$ at different magnetizations (see Fig. 4.33, $m = 1/6,\ 1/4,\ 1/3$):

$$\begin{aligned} X_{aa}(q,m,N) &= < 0|X_a^+(q)X_a(q)|0 > \\ X_{aa,conn.}(q,m,N) &= X_{aa}(q,m,N) - |< 0|X_a(q)|0 >|^2\,. \end{aligned} \tag{4.46}$$

The figure shows the transverse and longitudinal SSFs $S_{11}(q)$, $S_{33}(q)$ that already appeared in Chap. 2 (Sec. 2.5.1) and moreover shows $D_{11}(q)$, $D_{22}(q)$ for the operators $D_{1,2}(q)$. The latter 2 operators have served as well as some of the periodic perturbations discussed in the preceding chapters. The shown lines here and in the following figures are merely for orientation purposes. In case of several system sizes the longest chain data ($N = 24$) is always connected with straight lines allowing to estimate the finite-size behaviour.

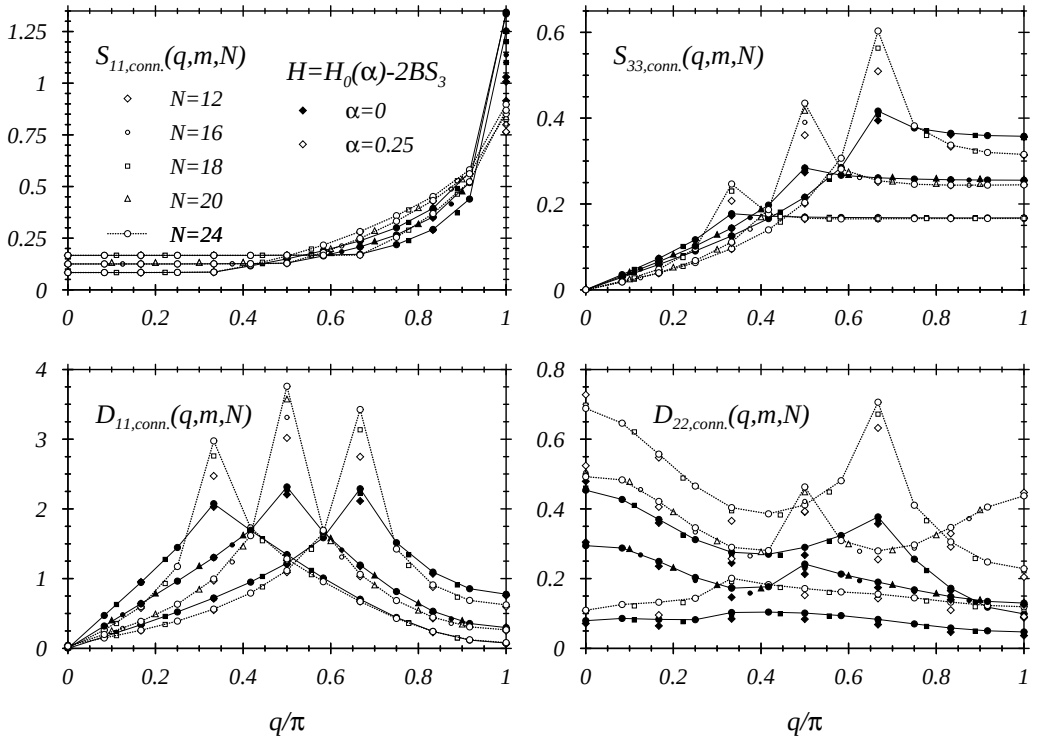

Figure 4.33: Static structure factors of the unperturbed and frustrated ($\alpha = 0.25$) Heisenberg chain for $m = 1/6,\ 1/4,\ 1/3$

In addition, the influence of a second-nearest neighbour coupling J_2 ($J_2/J_1 \equiv \alpha$) has been included for a frustration $\alpha = 0.25$ (open symbols). The assignment of the 3 magnetization values is simply accomplished by identifying the location of the field dependent soft modes ($q_1(m)$ for $S_{11}(q,m)$; $q_3(m)$ for the remaining curves) that mark singularities of the SSFs (the "tiny" singularity of $S_{11}(q)$ at $q = q_1(m)$ has been magnified in Fig. 2.4 for the case $m = 1/4$ – note $S_{++} = 2S_{11} - m$). (See also Chap. 2 for SSFs at zero magnetization that will be addressed further below.)
The η-exponents for the N-dependences of

$$\begin{aligned} S_{11}(q = \pi, N) &\sim N^{1-\eta_1(m)} \\ S_{33}(q = q_3(m)) &\sim N^{1-\eta_3(m)} \end{aligned}$$

have been shown already for general m ($0 \le m \le 1/2$) in Fig. 2.11 obtained from Bethe ansatz (BA) calculations of scaled energy gaps of a 2048-site chain [81]. For the 3 selected magnetizations the exponents are given again in Table 4.4.
Since BA calculations are impracticable for frustrated spin chains, in [86] $\eta_3(m = 1/4, \alpha = 1/4)$ was extrapolated as

$$\eta_3(m = 1/4, \alpha = 1/4) \simeq 0.72$$

and was as well extrapolated for the 3 chosen magnetizations in [91] for a range of frustrations α. For all cases $\eta_3(m, \alpha = 1/4) < 1$ was obtained –however, α must not fall short of 0.25 too far for this property still to hold.
Moreover, in [86] –dealing with $m = 1/4$– it was argued that the N-dependence of $D_{11}(q_3(m), N)$ is governed by the same exponent $\eta_3(m)$ as that of $S_{33}(q_3(m), N)$. For all shown cases –S_{33}, D_{11}, D_{22}– the applied frustration obviously decreases the η-exponents (increases $N^{1-\eta}$) leading to diverging SSFs for $\eta < 1$.

m	1/6	1/4	1/3
$\eta_3(m)\big\|_{q=q_3(m)}$	1.39	1.53	1.68
$\eta_1(m)\big\|_{q=\pi}$	0.72	0.65	0.60

Table 4.4: Critical exponents $\eta_1(m)$, $\eta_3(m)$ for the unperturbed chain with $\alpha = 0$

We will now start to consider the behaviour of $D_{11}(q)$ and $D_{22}(q)$ for the earlier discussed periodically perturbed Hamiltonians

$$H_j(h) \quad \equiv \quad H_0 + 2h \cdot N^{1/2} D_j(\pi) \quad ; \quad j = 1, 2\,, \tag{4.47}$$

assuming that the type of periodic perturbations should be well represented by these SSFs. As presented in Figs. 4.1, 4.3 and 4.5 the Hamiltonians differ in forming magnetization plateaus at $m = 0$ or $m = 1/4$. Here, we will first look at the case of plateau formation at $m = 1/4$ –a process that had been classified as a secondary ($k = 2$) one. This situation will later be contrasted by that of plateaus at $m = 0$ (only formed under the influence of $H_1(h)$, then being a primary ($k = 1$) process.
The above-mentioned SSFs $D_{11}(q)$ and $D_{22}(q)$ (connected parts) for magnetization $m = 1/4$ are shown in Figs. 4.34, 4.35 for 24-site chains, Hamiltonians $H_{1,2}(h)$ and various couplings. It should be noted that the subtraction of disconnected parts only affects momenta $q = 0, \pi$, the SSFs at all other momenta remain unchanged. Moreover, the notation "$r = 0$" in the legends of the figures will be explained below in context with Fig. 4.37. It simply refers to the standard form of SSFs. In addition, open symbols in the following figures have been chosen for perturbations and parameter values showing magnetization plateaus for infinite N. Finally it ought to be mentioned that the lines in the following figures are meant to guide the eye. In particular one should be aware that e.g. in Fig. 4.35 no broad maximum at $q = \pi/2$ exists but a sharp peak.
Looking at the formation of $m = 1/4$-plateaus we have to keep in mind that these have been classified as $k = 2$-plateaus, i.e. we are dealing with $q_{perturbation} = \pi = 2 \cdot q_3(m = 1/4)$. The peaks in the SSFs of the unperturbed chain mark a fundamental susceptibility of the chain at its soft modes, however, the influence of applied perturbations on the singularities at $q(m)$ is crucial. The appearance of an energy gap should involve clear changes in the finite-size behaviour at the soft mode position in the formerly gap-less spectrum.
Figs. 4.34, 4.35 now show important differences for the behaviour of the SSFs in case of $H_1(h)$ and $H_2(h)$. While the peaks of the SSFs at $q_3(m)$ remain almost unchanged under the influence of perturbations $\sim h \cdot D_1(\pi)$, perturbations $\sim h \cdot D_2(\pi)$ result in distinct changes when going beyond a certain finite perturbation strength h. The latter is very well in accord with the finite value of h shown in Fig. 4.5 that is needed to form a detectable plateau – though the observed increases at $q = \pi/2$ are somewhat counterintuitive. The opening of a gap going along with the plateau formation should usually be associated with decreasing singular behaviour (as e.g. shown in D_{11} apart from $q = \pi/2$; compare also the $m = 0$-case, below) –as long as no discrete mode at a continuum border appears. One should keep in mind, however, that even the existence of a δ-like peak (a soft mode in the sector $S_z = N \cdot m$) does not rule out the existence of a gap in neighbouring S_z-sectors resulting in the observed plateau. The peak in $D_{11,conn.}(q)$ at $q = \pi/2$ moreover may be interpreted as a signature of the spontaneous symmetry breaking that is needed to appear in case of $m = 1/4$-plateaus resulting from $q = \pi$-perturbations (see quantization condition 4.1).
As was in addition demonstrated in Fig. 4.3, periodic perturbations $\sim h \cdot D_1(\pi)$ do not give rise to $m = 1/4$-plateaus. We will now change to the situation of frustrated spin chains and consider the case $\alpha = 0.25$. As was shown in Fig. 4.30 (and discussed earlier by *Totsuka* [200]),

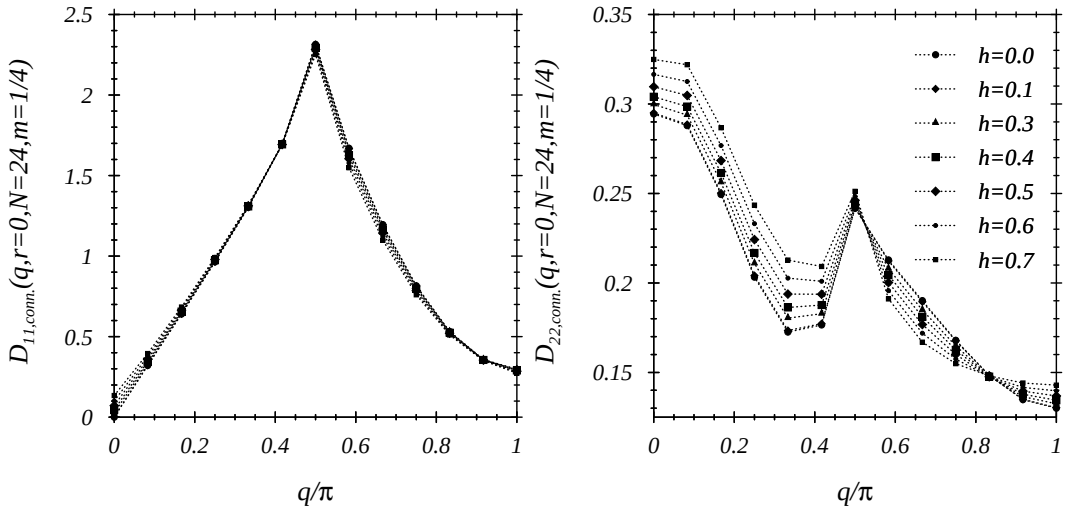

Figure 4.34: $D_{11,22;conn.}(q, N = 24)$ for $H = H_1(h)$, $h = 0.0, 0.3, 0.4, .., 0.7$ and $m = 1/4$

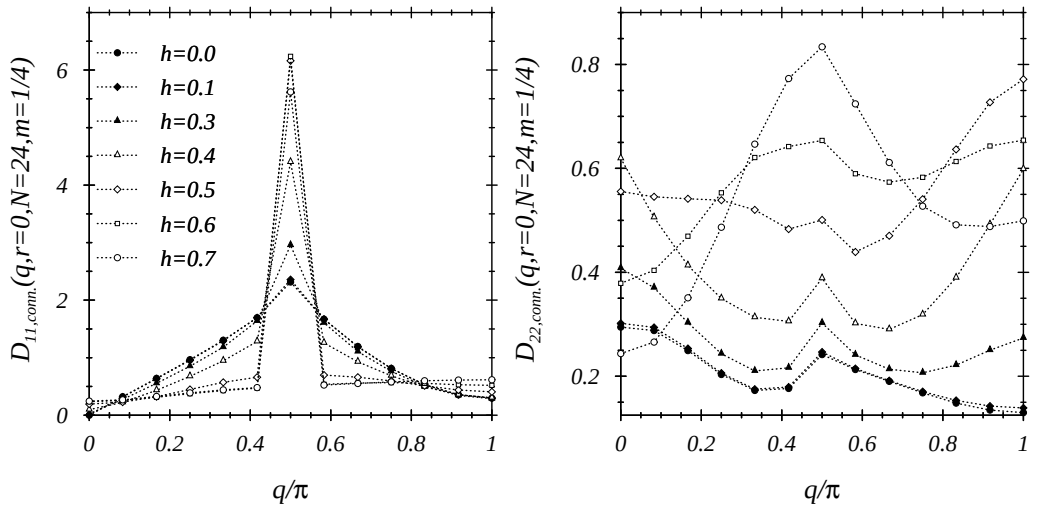

Figure 4.35: $D_{11,22;conn.}(q, N = 24)$ for $H = H_2(h)$, $h = 0.0, 0.3, 0.4, .., 0.7$ and $m = 1/4$

such a frustration leads to the occurrence of $m = 1/4$-plateaus. Looking again at perturbations $\sim h \cdot D_1(\pi)$ –this time of a frustrated chain– Fig. 4.36 demonstrates a clear change in the behaviour of the SSFs. While the situation hardly changes for small h (see development of the plateau in Fig. 4.30), the changes for $\alpha > 0.2$ are again well in accord with the observed plateaus.

Here, some remarks on finite-size behaviour shall be given. Figs. 4.34-4.36 only contain a single system size ($N = 24$) which has been chosen for reasons of clarity. Fig. 4.37 will contain examples of systems $N = 16, 20, 24$ for 2 of the shown cases of SSFs and their finite-size behaviour. It remains to be added, however, that the singular peak of $D_{11}(q = \pi/2)$ shows a strong –almost linear– N-dependence in case of $H_2(h > 0.3)$ that even might be in accord with a single δ-peak at $q = \pi/2$. Such a peak might indicate –as mentioned above– the expected spontaneous symmetry breaking going along with the plateau formation for the considered periodic perturbation.

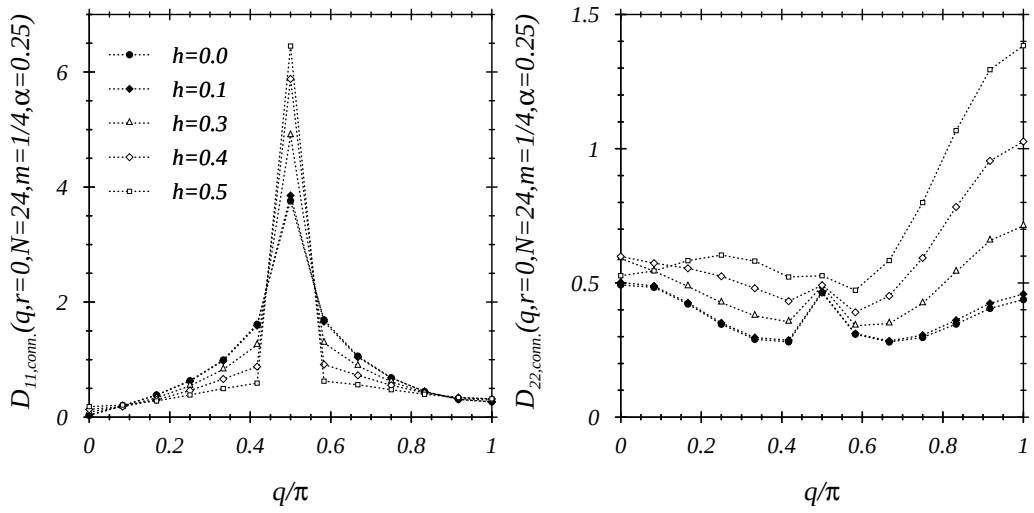

Figure 4.36: $D_{11,22;conn.}(q, N = 24)$ for $H = H_1(h, \alpha = 0.25)$, $h = 0.0, 0.3, 0.4, 0.5$ and $m = 1/4$

At this place, we will briefly address the changed translational symmetry of the periodically perturbed spin chain. The former invariance of the unperturbed Hamiltonian under translations $x \to x+1$ changes to $x \to x+R$, $R = 2\pi/\hat{q}$ for perturbations of momentum $\hat{q}$. Now, R operators $X_r(q)$, $r = 1, 2, \ldots, R$ may be defined that reflect symmetries of the reduced Brillouin zone:

$$X_r(q, N) \equiv \frac{1}{\sqrt{N/R}} \sum_{x=0}^{N/R-1} e^{iqRx} X(Rx + r - 1, N) \tag{4.48}$$

$$X_r(q, N) = X_r(q + 2\pi/R, N) \tag{4.49}$$

and certain degeneracies due to superpositions of momentum eigenstates of the unperturbed chain can be avoided.
Fig. 4.37 gives 2 examples of structure factors being calculated with $X = D_1, D_2$, for the case $\hat{q} = \pi$ (i.e. $R = 2$) with $r = 1(\equiv A)$, $2(\equiv B)$ that have been discussed in this section. The notation $r = 0$ is meant to indicate the standard SSF (Eq, 4.46)). Relations of SSFs for this case e.g. read:

$$X(q) = \frac{1}{\sqrt{2}} \left(X_A(q) + e^{iq} X_B(q) \right) \tag{4.50}$$

$$S_{XX,r=0}(q) = \frac{1}{2} \left(S_{XX,A}(q) + S_{XX,B}(q) \right) + W'_{AB} \cdot \cos q - W''_{AB} \cdot \sin q \tag{4.51}$$

$$W_{AB} \equiv < 0 | X_A^+(q) X_B(q) | 0 > \tag{4.52}$$

with $W' = \Re(W)$, $W'' = \Im(W)$.
Fig. 4.37 shows that the symmetric components (A, B, $S_{nn,A(B)}(\pi/2 - q) = S_{nn,A(B)}(\pi/2 + q)$) allow for a better distinction of peaks less clear visible in the standard SSF (see e.g. discussion in [217]).
Some further examples will be shown below for the following case of $m = 0$-plateaus for $H_1(h)$. Fig. 4.38 displays the connected parts of $D_{11,22}(q)$ for system sizes $N = 12, 16, 20, 24$ and $h = 0.0, 0.1, 0.3, 0.5$ at zero magnetization. The l.h.s. of the figure clearly shows the change of the finite-size behaviour of $D_{11}(q_3(m = 0) = \pi)$ when the perturbation of the system sets in. This type of behaviour is consistent with the opening of a gap and the identification of the η-exponent describing $D_{11}(q = q_3(m), N)$ with $\eta_3(m)$.

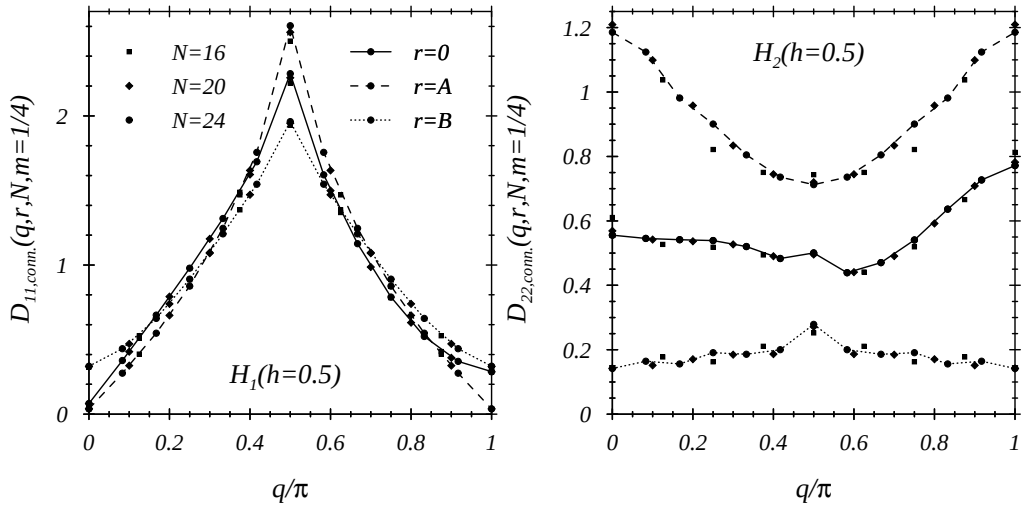

Figure 4.37: Translation-invariant forms (A, B) of selected SSFs in reduced Brillouin zones; m=1/4, $N = 16, 20, 24$

Moreover, the behaviour of the structure factors for $H = H_2(h)$ is as well contained in Fig. 4.38: The increase of h does not result in an observable change of the $h = 0$-structure factors, i.e. for $H = H_2(h)$ the SSFs remain unchanged and coincide with the shown $h = 0$-SSFs for $H = H_1(h)$. Again this gives (strong) evidence that the $h = 0$-situation persists and no magnetization plateau is formed at $m = 0$.

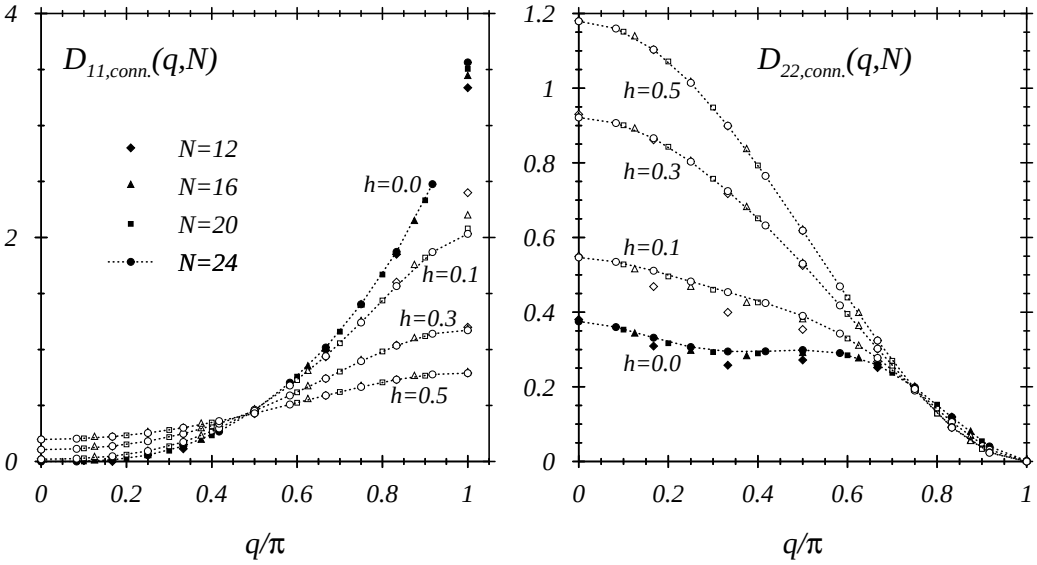

Figure 4.38: $D_{11,22;conn.}(q, N)$ for $H = H_1(h)$, $h = 0.0, 0.1, 0.3, 0.5$ and $m = 0$

Returning to the SSFs for $H = H_1(h)$, Fig. 4.39 gives further examples for both symmetric, sub-lattice-dependent components of $D_{11}(q)$ and $D_{22}(q)$ at zero magnetization.
While $D_{22,A}(q) = D_{22,B}(q)$ holds for all perturbation strengths h, the components (A, B) of $D_{11}(q)$ (l.h.s. of Fig. 4.39) show different behaviour for $h > 0$. The displayed cases ($h = 0.1, 0.3, 0.5$) for both components decrease for increasing h (for the B-component this only holds

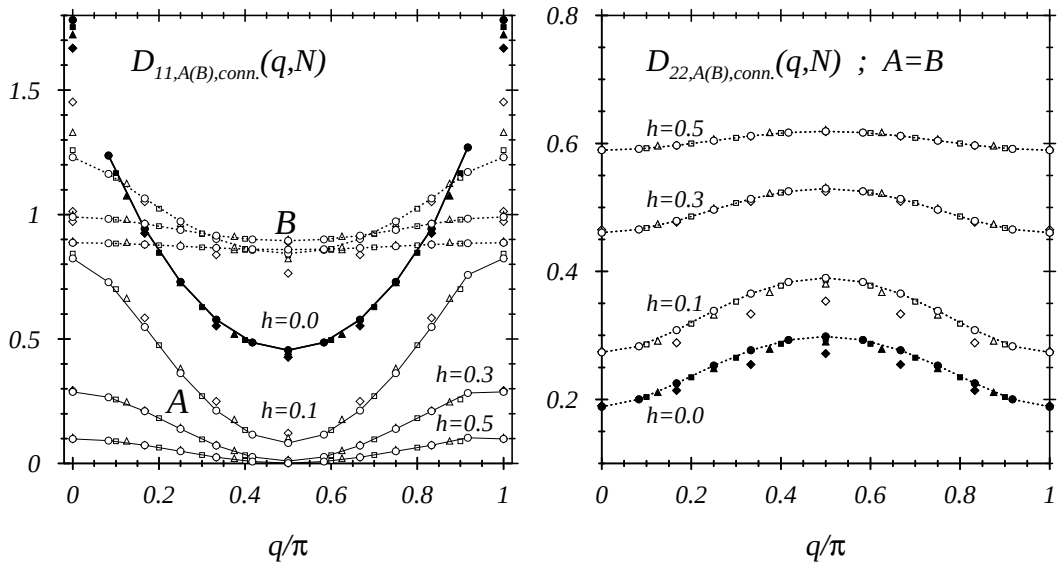

Figure 4.39: $D_{11,22,A(B);conn.}(q,N)$ for $H = H_1(h)$, $h = 0.0, 0.1, 0.3, 0.5$, $m = 0$, N as in Fig. 4.38

close to $q = 0, \pi$). As before, SSF-data of the longest shown chain ($N = 24$) has been connected by auxiliary lines. The former singularity of $D_{11,r=0}(q)$ at $q = \pi$ for the unperturbed chain now appears at $q = 0, \pi$ whereas the occurrence of an approximate crossing point of all $D_{11,r=0}(q)$ close to $\pi/2$ disappeared. Both Fig. 4.38 and Fig. 4.39 clearly demonstrate the influence of periodic perturbations $\sim h \cdot D_1(\pi)$ on the size and shape of the shown SSFs. This together with the absence of any of those changes for the system $H = H_2(h)$ shows again the attachment of the described behaviour and the formation of energy gaps and magnetization plateaus.

We will now conclude our considerations of static structure factors and their predictive powers for the formation of magnetization plateaus by resuming the earlier discussion of periodic perturbations $D_1^c(q_{pert.})$ with momenta $q_{pert.} = \pi/3$ or $q_{pert.} = 2\pi/3$:

$$\begin{aligned} H &= H_1(h, n \cdot \pi/3) \\ &= H_0 + 2h\sqrt{N} D_1^c(n \cdot \pi/3) \quad ; \quad n = 1, 2 \\ D_1^c(q) &= \frac{1}{\sqrt{N}} \sum_{x=0}^{N-1} \cos(qx)\, \mathbf{S}_x \mathbf{S}_{x+1}\,. \end{aligned} \tag{4.53}$$

The evaluation of magnetization curves (Figs. 4.7,4.8) resulted in the observation of a single plateau at $m = 1/6$ for $q_{pert.} = 2\pi/3$, whereas plateaus at $m = 1/6, 1/3$ had been determined for $q_{pert.} = \pi/3$. The plateaus in both cases were found to exist for any non-zero perturbation strength h.
Fig. 4.40 shows $D_{11,conn.}(q)$ for both Hamiltonians $H_1(h, n \cdot \pi/3)$, $n = 1\,(l.h.s.), 2\,(r.h.s.)$ and both magnetizations $m = 1/6, 1/3$ for $h = 0.0, 0.1, 0.3, 0.5$ and system sizes $N = 18, 24$. Finite-size corrections of the shown structure factors appear to be rather small. The figure clearly shows significant changes/decreases of the SSFs in the cases where plateaus are observed. Increasing perturbation strength h results in a decreasing height of the peaks of the SSFs.
In case of the two plateaus for $H_1(h, \pi/3)$ the different behaviour of the decrease of the SSFs for the shown magnetizations bears strong resemblance with the different opening of the plateaus given in Fig 4.7. A comparison of the decreases of the SSFs for the considered Hamiltonians at $m = 1/6$ is as well in a qualitative agreement with the evaluated opening of the respective

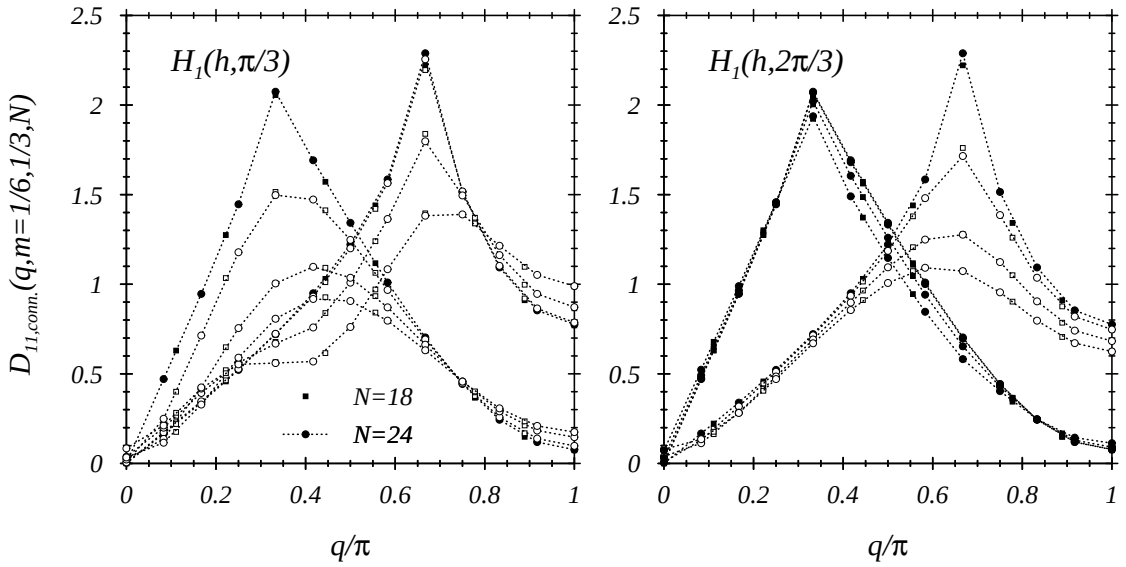

Figure 4.40: $D_{11,conn.}(q,N)$ for $H = H_1(h, n\cdot\pi/3)$, $h = 0.0, 0.1, 0.3, 0.5$, $N = 18, 24$ and $m = 1/6, 1/3$

plateaus. Finally, the subtle changes of $D_{11,conn.}(q = \pi/3)$ for increasing h are also in agreement with the unobserved $m = 1/3$-plateau for $H = H_1(2\pi/3)$.

The absence of the latter plateau is in accord with the quantization rule of Oshikawa, Yamanaka and Affleck [169] that was given at the beginning of the chapter. As long as no additional spontaneous symmetry breaking occurs, the translational invariance $x \to x + 3$ of the ground state of $H_1(2\pi/3)$ does not allow for

$$3 \cdot \left(\frac{1}{2} - \frac{1}{3}\right) \quad = \quad \text{integer}\,. \tag{4.54}$$

We finally want to address the type of the soft mode (longitudinal/transverse) that had to be used for the plateau classification within our scheme. In particular the $m = 1/3$-plateau for $q_{pert.} = \pi/3$ could only be classified by the $k_1 = 1$ transverse soft mode.

A consideration of the longitudinal SSF $S_{33,conn.}(q, N = 18, 24)$ for both $q_{pert.} = \pi/3$, $2\pi/3$ and $m = 1/6$, $1/3$ (Fig. 4.41) shows that the same information of Fig. 4.40 is as well –even in a sharper form– contained in the purely longitudinal structure factor. We therefore can find no immediate connection to transverse SSFs or even their sole importance for the plateau formation at $m = 1/3$.

In this section we have seen that the observation of significant changes in the considered structure factors coincided very well with the occurrences of magnetization plateaus that have been determined in the previous section. This coincidence has been shown for plateaus that open for $h > 0$ and systems that first undergo a spontaneous symmetry breaking at finite h –either due to a frustration (translational invariant second-nearest neighbour coupling) or for the example of a periodically perturbed second-nearest neighbour coupling $\sim h \cdot D_2(q = \pi)$. The latter cases of course do not exhaust the number of possibilities but might serve as representative examples.

We will now compare the presented classification scheme with the quantization condition of Oshikawa et al. [169] and look for general correspondences and counterparts for the transverse soft mode momenta occurring in the present scheme.

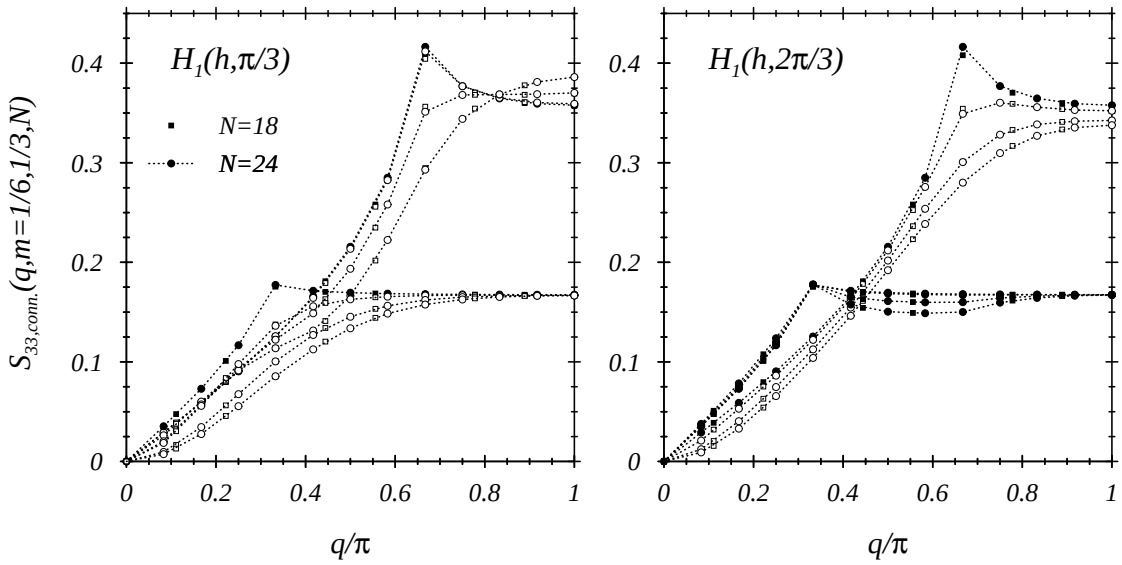

Figure 4.41: $D_{33,conn.}(q,N)$ for $H = H_1(h, n \cdot \pi/3)$, $h = 0.0, 0.1, 0.3, 0.5$, $N = 18, 24$ and $m = 1/6, 1/3$

4.3 Quantization condition and soft mode approach

In this final part of the chapter we are going to discuss the presented method of assigning soft modes of the unperturbed spin-1/2 chain to potentially forming plateaus under the influence of a periodic perturbation. We will consider perturbations with $q_{pert.} = q = 2\pi/n$, $n = 1, 2, 3, 4, 6, 8$ and give a comparison with the predictions of possible magnetization plateaus due to the quantization condition of Oshikawa, Yamanaka and Affleck (OYA) [169] for spin $S = 1/2$.
To this aim, Eqns. 4.55-4.57 first summarize the respective relations for both condition schemes. Here, the integer factor n_{sp} has been added to Eq. 4.55 (OYA) in order to represent the possibility of a spontaneous symmetry breaking ($n_{sp} > 1$) – otherwise $n_{sp} \equiv 1$ results in the known form of the quantization condition. The factor n of $q_{pert.} = q = 2\pi/n$ simply gives the number of required translations to keep the Hamiltonian of the perturbed chain invariant.

$$n \cdot n_{sp} \cdot \left(\frac{1}{2} - m\right) = I \quad ; \quad 1 - 2m = \frac{2I}{n_{sp} \cdot n} \quad , \quad I: \text{ integer} \tag{4.55}$$

$$q_3(m) = k_3 \cdot \pi(1 - 2m) \quad ; \quad 1 - 2m = \frac{2}{k_3 \cdot n} \tag{4.56}$$

$$q_1(m) = k_1 \cdot 2\pi m \quad ; \quad 1 - 2m = 1 - \frac{2}{k_1 \cdot n} \tag{4.57}$$

The following Table 4.5 contains an overview of the predictions resulting from both sets of conditions for magnetizations $0 \leq m < 1/2$. Each q-value in the table shows all possible values of m that are consistent with $n_{sp} = 1, 2$, i.e. $m = j \cdot 1/(2 \cdot n)$, $j = 0, 1, .., n - 1$. As mentioned earlier, the prediction of the trivial saturation plateau $m = 1/2$ can be derived both prediction systems.
At first glance, the table shows correspondences and as well a number of differences that will be addressed in the following. In any case, it first of all demands to realize that both sets of predictions do not coincide – though both having their origin in the soft mode structure of the unperturbed chain (based on LSM [143]).

First, the equations given above show that for $I = 1$ the predictions of OYA coincide with the longitudinal soft mode position $k_3 = n_{sp}$. Relating a certain importance to the smallness of I, this first statement may be considered as supporting our earlier classification of "most probable" plateau locations (see Sec. 4.1.1).

$q_{pert.}$, n	m	n_{sp}	I	k_3	k_1
$q = \frac{2\pi}{1} = 0, \quad n = 1$	0	2	1	2	–
$q = \frac{2\pi}{2} = \pi, \quad n = 2$	0	1	1	1	–
	1/4	2	1	2	2
$q = \frac{2\pi}{3}, \quad n = 3$	0	2	3	–	–
	1/6	1	1	1	2
	2/6	2	1	2	1
$q = \frac{2\pi}{4} = \frac{\pi}{2}, \quad n = 4$	0	1	2	–	–
	1/8	2	3	–	2
	2/8	1	1	1	1
	3/8	2	1	2	–
$q = \frac{2\pi}{6} = \frac{\pi}{3}, \quad n = 6$	0	1	3	–	–
	1/12	2	5	–	2
	2/12	1	2	–	1
	3/12	2	6	–	–
	4/12	1	1	1	–
	5/12	2	1	2	–
$q = \frac{2\pi}{8} = \frac{\pi}{4}, \quad n = 8$	0	1	4	–	–
	1/16	2	7	–	2
	2/16	1	3	–	1
	3/16	2	5	–	–
	4/16	1	2	–	–
	5/16	2	3	–	–
	6/16	1	1	1	–
	7/16	2	1	2	–

Table 4.5: Plateau predictions for spin-1/2 chains: quantization condition vs. presented soft mode assignment

The table moreover shows that the restriction to $I = 1, 2$ correspondingly results in $k_{1,3} = 1, 2$ – which can be shown explicitly for the considered magnetization values. Taking into account higher n_{sp}-values results in $k_3 = n_{sp}$ for $m = 1/2 - 1/(n_{sp} \cdot n)$ (see Eq. 4.56) and vice versa $m = 1/(n_{sp} \cdot n)$ for the respective k_1. The latter in particular means that the presented soft mode assignment method does not result in the same uniform distribution of possible plateau magnetizations as the OYA-condition does. The latter is already indicated in Table 4.5 for the considered $n_{sp} = 1, 2$.
Additional support for the above "small I"-statement, i.e. the prime importance of predictions with a small value of I, may be obtained from the consideration of $m = 0$-plateau predictions. In Sec. 4.1.1 we showed that the existence of $m = 0$-plateaus for even-leg ladders can be retraced

to periodic perturbations with $q = \pi$ (cf. Table 4.1) – at the same time excluding all other (non-zero) q. A translation invariant perturbation ($q = 0, 2\pi, \ldots$, e.g. frustration $\alpha > \alpha_c$) affords a spontaneous symmetry breaking. The OYA-quantization condition –though not being as strict– only gives the same 2 possibilities for the lowest integer $I = 1$ ($I > 0$ for $0 \leq m < 1/2$).
The given table, however, shows as well that the importance of small I –$I = 1$ that is– is only valid for plateaus classified by k_3. In general, including k_1, we obtain:

$$k_3 : \qquad k_3 = n_{sp} \quad , \quad I = 1 \tag{4.58}$$

$$k_1 : \qquad k_1 = n_{sp} \quad , \quad I = \frac{n_{sp} n}{2} - 1 \tag{4.59}$$

with k_1 –in the latter relation– given as integer solution ($k_1 > 0$) of

$$k_1 \quad = \quad \frac{2}{n} \cdot \frac{k_3 n}{k_3 n - 2} \, . \tag{4.60}$$

We may use the comparison given in Table 4.5 to advance the choice of k_3 in favour of k_1 in case of both possibilities occurring at the same magnetization m. The table shows that the latter only happens for few –however in most cases investigated– situations or in the special case of $m = 1/4$ where $q^{(1)}(m = 1/4) = q^{(3)}(1/4)$.
We have to admit, however, that neither the presented discussion of static structure factors nor a decomposition of the considered $\cos q_{pert.} n$ perturbations in single exponentials could give a satisfying reason for the occurrence of transverse soft modes in the presented classification scheme.

It further remains an open question at this place whether the OYA-scheme gives too many possible plateau positions or the presented soft mode oriented classification underestimates the manifold of possibilities. The only possibility within this descriptive discussion of magnetization plateaus would be given in form of a counterexample, i.e. a plateau predicted by OYA and not predicted by the presented formalism. So far, we are neither aware of such a counterexample (among the presented examples and as well among other works dealing with magnetization plateaus in spin-1/2 chains –the latter of course limited to the author's knowledge) nor of any proof of the completeness of the given description. It therefore remains to be summarized that both the OYA as well as the presented scheme to present knowledge give sufficient predictions for the occurrence (of indeed observable) magnetization plateaus, however, both schemes differ in the total number of predicted possibilities for the locations (m-values) of plateaus.

In the following and final chapter of this work we will turn to the remaining class of periodic perturbations for the considered spin chains: chains with translation invariant ($q = (0), 2\pi$) perturbations of the underlying isotropic Heisenberg chain. For a consistent notation we will choose for these cases

$$q_{pert.} \quad = \quad \frac{2\pi}{1} = 2\pi$$

showing that the related ground state –in the absence of spontaneous symmetry breaking– remains invariant under a single translation (i.e. $n = 1$).

Chapter 5

Translation invariant periodic perturbations

5.1 Introduction

As we already announced at different places in course of the previous chapters, we will now turn to the case of translation invariant perturbations of the isotropic Heisenberg chain. Such perturbations –classified as $q = 0$-perturbations– require a spontaneous symmetry breaking to show the formation of a magnetization plateau, i.e. the opening of a related gap (see e.g. discussion of Table 4.5 in Sec. 4.3).
Among the various translation invariant "perturbations" of the spin-1/2 Heisenberg chain

$$H_1 \,(\equiv\, H_0) \;=\; 2\sum_{n=0}^{N-1} \mathbf{S}_n\mathbf{S}_{n+1} \tag{5.1}$$

the 2 most prominent exponents are

a) the XXZ-model

$$H(\Delta) \;=\; H_1 + (\Delta - 1)\cdot 2\sum_{n=0}^{N-1} S_z(n)S_z(n+1) \tag{5.2}$$

$$\equiv\; H_{XX} + 2\Delta\sum_{n=0}^{N-1} S_z(n)S_z(n+1) \tag{5.3}$$

b) the frustrated spin chain

$$H(\alpha) \;=\; H_1 + \alpha\cdot 2\sum_{n=0}^{N-1} \mathbf{S}_n\mathbf{S}_{n+2}\,. \tag{5.4}$$

Both types of models and some of their known properties will briefly be introduced in subsequent paragraphs. Then, we turn to a quite different class of additional translation invariant spin-spin couplings, namely long ranged interactions:

c) kth-nearest neighbour interaction

$$H_k(h) \;=\; H_1 + h\cdot 2\sum_{n=0}^{N-1} \mathbf{S}_n\mathbf{S}_{n+k} \equiv H_1 + h\cdot H_k \tag{5.5}$$

Couplings of the latter type have e.g. been discussed in Sec. 3.4.1 (see discussion of ladder description type (c) – Fig. 3.12) with $k = N/n_l - N$ giving the total number of spins in a n_l-leg ladder.
Another application appears in the approximate modeling of quadratic spin lattices by a 1-dimensional spin chain Hamiltonian with couplings to nearest and k-nearest neighbours ($H_k(h)$). As was shown e.g. in [98] the best approximation is obtained for chain interaction ranges

$$k^2 \quad = \quad N \pm 1\,. \tag{5.6}$$

Examples for $N = 5 \times 5 \pm 1$, e.g. $k = 5$, are given in Fig. 5.11 (see also [221]).

5.1.1 The XXZ-model

A first consequence of the reduced symmetry of the XXZ Hamiltonian 5.2 for $\Delta \neq 1$ compared to the $SU(2)$ symmetric isotropic Heisenberg chain ($\Delta = 1$) is the loss of conservation of total spin ($[H, \mathbf{S}] \neq 0$). This deviation close to the XXX point ($\Delta = 1$) is illustrated in Table 5.1 for the expectation values of the total spin for the 3 lowest –non-degenerate– eigenstates with momenta $q_i = 0, \pi, \pi$ of a $N = 12$ chain at magnetization $m = 0$. For small deviations from $\Delta = 1$ the formerly integer total spin remains retractable and no abrupt changes occur. The total S_z-value for the XXZ Hamiltonian remains a conserved quantity.

Δ	0.85	0.90	0.95	1.00	1.05	1.10	1.15
E_0	0.27824..	0.19852..	0.10777..	0	0.10847..	0.20093..	0.29304..
E_1	1.00573..	1.00265..	1.00068..	1	1.00073..	1.00299..	1.00687..
E_2	0.17866..	0.12343..	0.06435..	0	0.06288..	0.11812..	0.16763..

Table 5.1: "Total spin" of the 3 lowest energy eigenstates of a $N = 12$ XXZ spin chain close to the XXX point

First our short introduction to the case of XXZ-type chains will dwell further on properties already arising in complete diagonalization studies of small spin chains. Fig. 5.1 shows the Δ-dependence of the two lowest energy eigenvalues for momentum eigenvalues $q_n = 2\pi/N, \quad n = 0, 1, .., N/2$ of chains with $N = 8, 10, 12$ spins at zero magnetization.
The figure contains marks for the two best known cases, namely the isotropic Heisenberg chain (XXX, $\Delta = 1$) and the planar XX model ($\Delta = 0$). The latter is distinguished by its complete solvability of its spectrum of eigenvalues by Lieb, Schultz and Mattis [143]. These authors gave solutions for the more general case of the XY model – allowing different couplings for x- and y-spin components. Later, solutions for longitudinal [162] and transverse [192] structure factors for the XX model were given. Fig. 5.1 shows the high degree of degeneracies typical for the XX chain. Similar properties of the XXX chain already have been the subject of Chap. 2.
The XX point moreover is a symmetry point for a particular unitary transformation that relates couplings Δ and $-\Delta$. The application of

$$U_{k=\pi} \quad = \quad e^{i\pi \sum_n n S_z(n)} \tag{5.7}$$

(compare Eq. 2.61) results in

$$U_\pi H(\Delta) U_\pi^{-1} \quad = \quad -H(-\Delta)\,. \tag{5.8}$$

The latter property is of course not visible in Fig. 5.1 since 5.8 relates highest states Δ with lowest states $-\Delta$ and vice versa at fixed magnetization m. However it gives a valuable tool for the discussion of ground state energies.

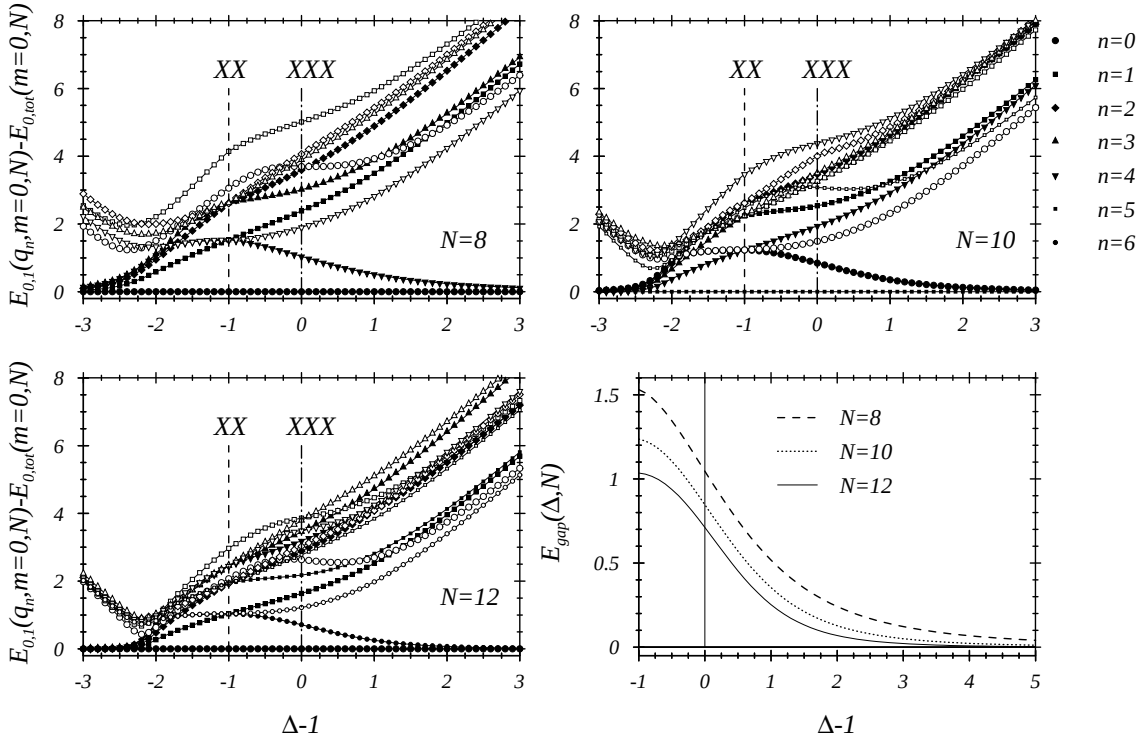

Figure 5.1: 2 Lowest energies $E_{0,1}(q_n, \Delta, N)$ with $q_n = 2\pi n/N$ and E_0 (solid), E_1 (open symbols); $N = 8, 10, 12,\ m = 0$

The figure further shows the onset of "two-fold degenerate" ground states ($|E_0(\Delta, q = 0, N) - E_0(\Delta, q = \pi, N)| \to 0$ for $N \to \infty$, $\Delta > 1$. The exponentially fast disappearance of the energy gap –see lower right of the figure– with the length of the system N often leads to the designation "two ground states" –see below. The isotropic Heisenberg chain ($\Delta = 1$, ground state energy firstly calculated by *Bethe* [22] and *Hulthén* [120]) –the starting point of all presented discussions of perturbed spin-1/2 systems– is located right at a crossing point of two regimes. The application of a generalized Bethe ansatz (*Orbach* [167], *Walker* [209], *des Cloizeaux and Gaudin* [49]) led to analytical solutions for $-1 < \Delta \leq 1$ (with unique ground states), while the ground state is 2-fold degenerate for $\Delta > 1$ with an energy gap (indicated by the small system results) above. A number of proofs and detailed calculations is furthermore given by *Yang & Yang* [220]. In the Ising limit of large Δ the system ground state has classical Néel order whereas it has ferromagnetic order for all $\Delta \leq -1$. Precisely at $\Delta = 1$ a Kosterlitz-Thouless [137] transition from the gap-less regime with unique ground states ($-1 < \Delta \leq 1$) to 2-fold degenerate, Néel-ordered ground states with an energy gap above takes place.

The size dependence of the energy difference between the above-mentioned almost degenerate ground states –at $\Delta = 1 + 0$– is rather subtle and the algebraic type of description used in previous chapters does not apply. A study of one of the two relativistic continuum limits of the model has been given by *Hauer et al.* [106]. For the Hamiltonian

$$H \quad = \quad \frac{1}{\pi}\left(H(\Delta) - \frac{N}{2}\Delta\right) \quad , \quad \Delta = \cosh\gamma > 1 \tag{5.9}$$

and in the limit $\gamma \to 0$, $N \to \infty$, $a \to 0$ (finite $L = N \cdot a$) these authors showed that the limiting

massive relativistic theory with mass M,

$$\frac{4}{a}e^{-\pi^2/2\gamma} \quad \rightarrow \quad M\,,$$

leads to a finite but (in the length L of the system) exponentially small energy difference

$$\Delta E_0 \quad = \quad \left(\frac{8M}{\pi L}\right)^{1/2} e^{-LM} \tag{5.10}$$

of the two "ground states".
Besides the basic spin-1/2 XXZ Hamiltonian (Eq. 5.2 and numerical examples in this paragraph) XXZ-type models have been discussed with an additional next-nearest-neighbour coupling (see e.g. [92, 113] and references therein) or/and higher quantum spin (see e.g. [112], $S = 1$). We will not proceed further into this direction but turn to a brief introduction and discussion of the second basic translation invariant perturbation of the (spin-1/2) Heisenberg chain: Spin frustration via next-nearest-neighbour (NNN) couplings.
We will meet the case of frustrated Heisenberg chains as another example of spin chains with translation invariant Hamiltonians that show the opening of gaps in a not purely algebraic way in the next section. Later we furthermore will explicitely take up the example of a translation invariant 2-leg ladder Hamiltonian to address the problem of finding scaling solutions for a translation invariant spin system.

5.1.2 Frustrated spin chains

The $S = 1/2$ antiferromagnetic Heisenberg chain with next nearest neighbour (NNN) interactions is a typical example of spin systems with competing interactions. Positive α (see Hamiltonian 5.4 change (*frustrate*) a Néel-type order of spins caused by the antiferromagnetic H_0. Increased α leads to substantial changes for the ground state and lowest excitations of the spin chain. For zero magnetization this is exemplarily showed for system sizes $N = 8, 10, 12$ in Fig. 5.2. Since the Hamiltonian with additional NNN couplings still has conserved total spin (and e.g. total S_3), the figure shows the lowest $E(q_n, S)$ for all $q_n = 2\pi n/N$ and total spin $S = 0$, 1. The figures first of all show that the ground state of frustrated spin chains at $m = 0$ either have $q_0(\alpha) = 0$ or $q_0(\alpha) = \pi$ –for small $\alpha < 0.5$ following Marshall's sign rule [151] (see e.g. Sec. 2.1). At $\alpha = 0.5$ a particular situation with exactly solvable ground state –first given by *Majumdar and Gosh* [148, 149, 150]– occurs. Here, the ground state is a twofold degenerate pure dimer state (spin singlet pairs, 'valence bonds') and $H(\alpha)$ has the special property

$$H(\alpha = 1/2) \quad = \quad \frac{1}{2}\sum_n \left(\mathbf{S}_n + \mathbf{S}_{n+1} + \mathbf{S}_{n+2}\right)^2 + const. \tag{5.11}$$

meaning that for the two ground states the sum of any three neighbouring spins is $S = 1/2$ (for further discussion see e.g. [5]).
The number of solvable models with competing interactions has later been enlarged by *Shastry and Sutherland* [185] considering a "*dimerized next-neighbor antiferromagnetic chain*" (see Hamiltonian (3.140)). The additional presence of a dimerization $\delta \cdot \sqrt{N} D_1(\pi)$ leads to exactly known ground states for $\delta + 2\alpha = 1$. *Affleck,Kennedy, Lieb and Tasaki* (AKLT) [4] later showed the existence of a gap between the two ground states and the first excited state at the Majumdar-Gosh point ($\alpha = 0.5$) in the TDL.
Starting from $\alpha = 0.5$ the ground state of a $N = 4n + j \cdot 2$ ($n \in \mathbb{N}$, $j = 0, 1$) chain changes its momentum for another $(N-2j-4)/4$ times (see also [193]). While $\alpha = 0.5$ and as well the large-N limit of α_c (see below) are finite and fixed values, the values $\alpha_2(N)$ (uppermost α with twofold degenerate ground state) as well as $\alpha_u(N)$ ($q = \pi/2$ becoming the lowest excitation for $N = 4n$)

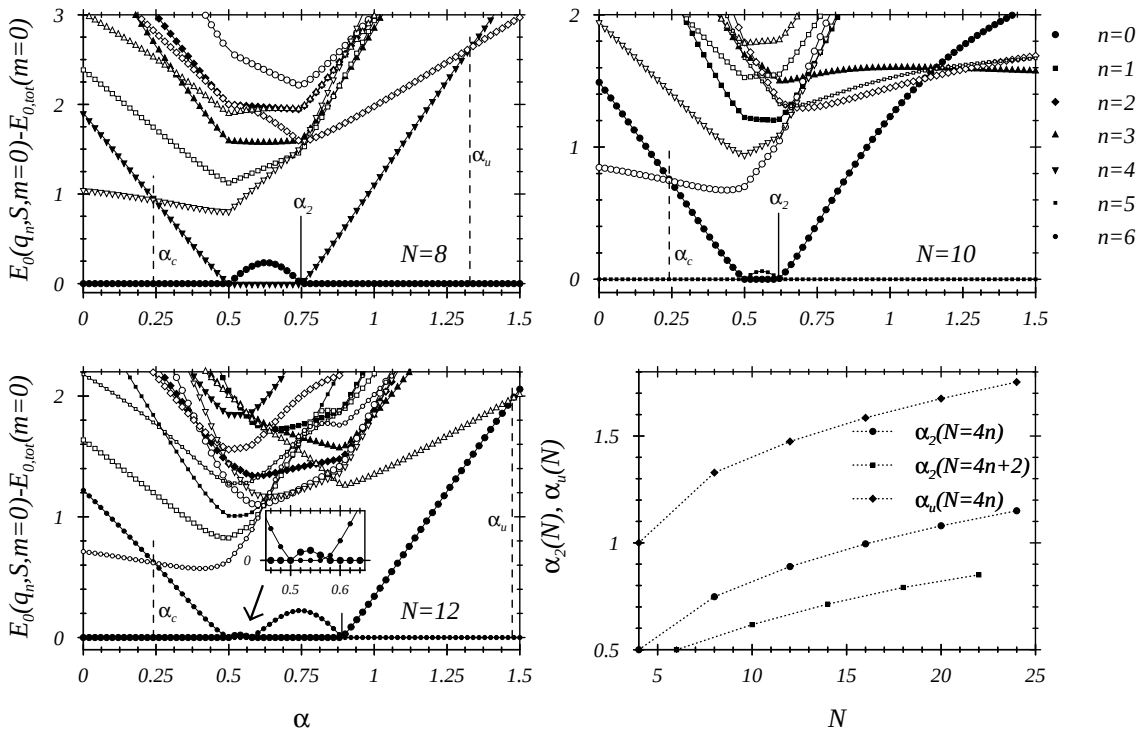

Figure 5.2: Lowest energies $E_0(q_n, S, \alpha, N)$ with $q_n = 2\pi n/N$ and $S = 0$ (solid), $S = 1$ (open symbols); $N = 8, 10, 12$, $m = 0$

diverge (see lower right of Fig. 5.2), meaning that no further finite singular point in the phase diagram of frustrated spin chains exists, i.e. no finite upper boundary of the dimer phase in the TDL is to be expected. Though the number of exact degeneracies in the interval $[0.5, \alpha_2(N)]$ increases proportional to N, a finite-size study of $\max|E_0(q = \pi, \alpha) - E_0(q = 0, \alpha)|(S = 0)$ leads to the assumption of the two states $(q = 0, \pi)$ becoming degenerate in the thermodynamic limit (TDL).

The determination of the onset of the dimer phase ($\alpha = \alpha_c$) started in 1982 with *Haldane* [99] and the up to now best approximation ($\alpha_c = 0.241167 \pm 0.000005$) has been given by *Eggert* [66] in 1996. The latter value is shown in Fig. 5.2. The point of degeneracy of the lowest $S = 0$ and $S = 1$ excitation –the fluid-dimer transition point– for the considered small systems already approaches α_c very well (for more and quantitative details see App. C).

The shown figures moreover give some information concerning structure factors of frustrated spin chains. While the system for small α ($0 \leq \alpha < \alpha_c$) stays in the *spin liquid* phase showing singlet-triplet excitations ($\Delta S = 1$) as lowest ones, increasing α leads to the shown changes in lowest $S = 0$ and $S = 1$ excitations. For the $S_{33}(q, \alpha)$ SSF –SSFs will not be further discussed in detail here– the maximum shifts from $q = \pi$ towards $q = \pi/2$ for increasing α. The latter shift is accompanied by the change of the lowest $\Delta S = 1$ excitation from $\Delta q = \pi$ to $\Delta q = \pi/2$ (reflecting the decoupling of the chain in two subsystems of twice the unit length for large α.

Considering the competing interaction of strength α as a perturbation of the critical Heisenberg chain an important effect not visible in Fig. 5.2 arises. The spin chain remains gap-less for $\alpha < \alpha_c$ and then a very small gap opens in a non-algebraic form. A scaling starting near a line of unstable fixed points motivated *Haldane* [99] to an approximation of the dimerized spin chain with the sine-Gordon (SG) field theory [60] resulting in a critical scaling behaviour of dimer gap,

order parameter and inverse correlation length as

$$(\alpha - \alpha_c)^{1/2} \exp[-a/(\alpha - \alpha_c)] \quad ; \quad \alpha > \alpha_c \,. \tag{5.12}$$

A similar behaviour ($E_{gap} \sim \exp[-a/(\alpha - \alpha_c)]$) was discussed by *Chitra et al.* [47]. These authors remarked that even calculations for 300 spins (DMRG) result in gaps indistinguishable from zero for $\alpha \lesssim 0.3$. These unfavourable conditions hindered earlier attempts of determining α_c by direct observation of the opening gap (see e.g. [193]). Again this shows differences to the behaviour of periodically perturbed spin chains discussed in Chap. 3: There is neither a $\alpha \leftrightarrow -\alpha$ symmetry in the behaviour of frustrated chains, nor does the opening of the gap (at $\alpha_c > 0$!) admit a description by the earlier used scaling variables.

Antiferromagnetic Heisenberg chains with competing NNN interactions (frustration) in a homogeneous external magnetic field (i.e. $m > 0$) are not known to show further gaps in their spectra. Their ground states –shown in Fig. 5.3 for $m = 1/4$ and $N = 8, 12$– are no longer restricted to momenta $q_0(\alpha) = 0, \pi$. This latter fact will of course show its influence on the shape of structure factors for varying α. Again, we will keep these and other topics beyond the range of this introductory part of well established translation invariant perturbations of the underlying critical Heisenberg chain.

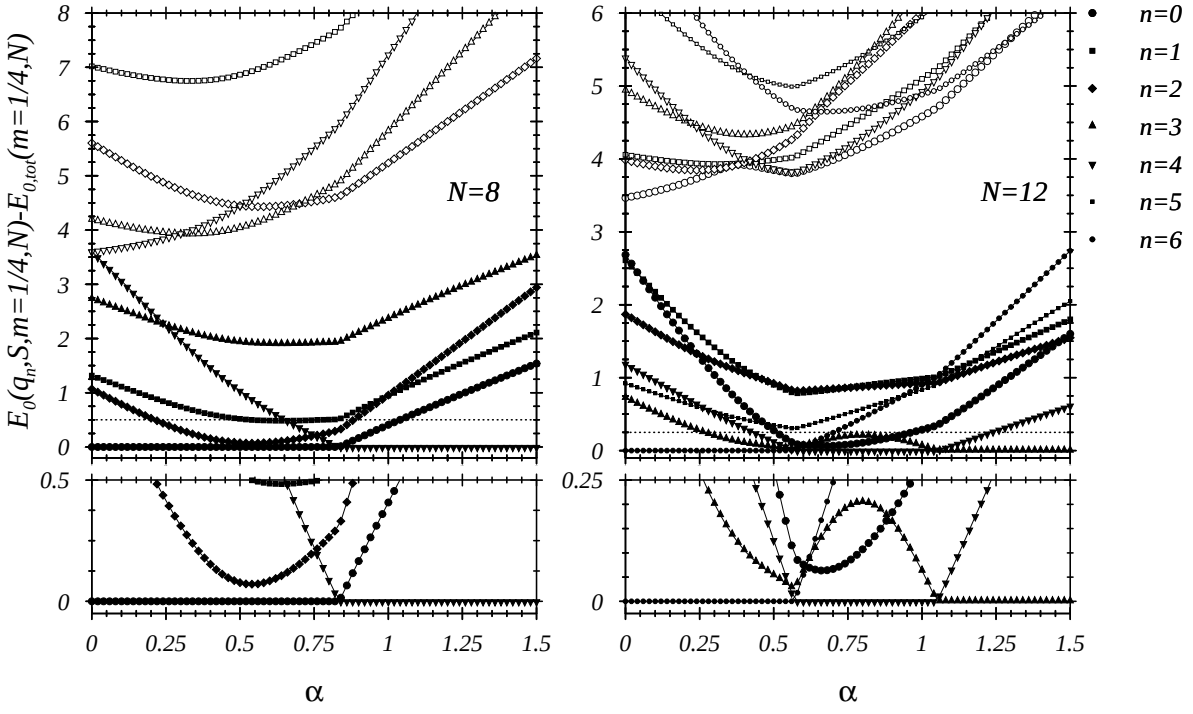

Figure 5.3: Lowest energies $E_0(q_n, S, \alpha, N)$ with $q_n = 2\pi n/N$ and $S = mN$ (solid), $S = mN + 1$ (open symbols); $N = 8, 12$, $m = 1/4$

Fig. 5.3 shows separate magnifications of the low excitation parts of the considered systems. These show that not really the number of degeneracies of the $m = 0$ ground state is present (however, a $q = \pi/2$ excitation approximately approaches the ground state energy at a single α value.

As a final remark we want to note that for the shown $m = 1/4$ cases the lowest excitations with total spin $S = Nm$ and $S = Nm + 1$ seem to be well separated. This separation is a consequence of the chosen quantity that is plotted. For $m \neq 0$ the shown energy differences –though all quantities are shown for the same S_z– are affected by different Zeeman terms for

different total spin, meaning that energies for $S = Nm + 1$ are shifted upwards by a single (N dependent) Zeeman contribution compared to those with $S = Nm$.
In the following paragraph we will turn to different types of translation invariant "additives" (perturbations) of the Heisenberg chain. These will contain $O(N)$ or $O(N^{1/2})$ ranges of spin couplings – couplings that on first sight do not allow the use of the LSM theorem [143] e.g. to pinpoint soft mode positions in gap-less systems.

5.1.3 Macroscopic coupling ranges of additional interactions

A first type of long coupling ranges appeared in Sec. 3.4.1 in type (c) of the discussed ladder parameterizations. n_l-leg ladders had been mapped on a single spin chain in such way that the rung couplings of the ladder were given by spin couplings of range N/n_l. A translation invariant type of such spin systems will be considered for 2- and 3-leg ladders in the next section. The relation of such parameterizations to the earlier discussed ladder representations based on periodically perturbed chains will be discussed.
We will then briefly discuss the problem of scaling solutions at the example of translation invariant formulations of spin ladders. We will not be able to present sufficient scaling behaviour, however elucidate the changed initial conditions needed for the evolution equations 3.2 as well as the inaccessibility of purely algebraic combinations of scaling variables.
At the end of this chapter we will address another type of translation invariant perturbations: systems with helical boundary conditions (see Sec. 5.4. Such boundary conditions allow an approach to 2-dimensional systems [98]. We will comment on a very precise statement about the onset of staggered (sub-lattice) magnetization when starting to couple chains to form a 2-dim. matrix [83].
This will end our study of (periodically) perturbed spin-1/2 critical antiferromagnetic Heisenberg spin systems.

5.2 Translationally invariant coupled chains

In this section we are going to consider the case of spin ladders that are given as a translationally invariant spin system (chain). The respective Hamiltonian of a n_l-leg ladder has been introduced in Sec. 3.4.1 (there given for $J_{leg} = J_{rung} = 1$) as:

$$\begin{aligned} H_{tr.\,inv.}(J_{leg}, J_{rung}, n_l) &= H_1 + H_{N/n_l} \\ &= 2\sum_n \left\{ J_{leg} \cdot \mathbf{S}_n \mathbf{S}_{n+1} + J_{rung} \cdot \mathbf{S}_n \mathbf{S}_{n+N/n_l} \right\} \qquad (5.13) \\ &= 2J_{rung} \cdot \sum_n \left\{ \mathbf{S}_n \mathbf{S}_{n+N/n_l} + \frac{J_{leg}}{J_{rung}} \cdot \mathbf{S}_n \mathbf{S}_{n+1} \right\} \qquad (5.14) \end{aligned}$$

with

$$\begin{aligned} J_1^{tr.\,inv.} &= J_{leg} \qquad (5.15) \\ J_{N/n_l}^{tr.\,inv.} &= J_{rung}\,. \qquad (5.16) \end{aligned}$$

The resulting Hamiltonian has been visualized in Fig. 3.12 (type (c) for the case of a 2-leg ladder. In the present discussion we are not going to subtract long range terms (see term ($*$), Eq. 3.113) but keep the translation invariant form of H.
The following discussion of 2- and 3-leg ladders described by Hamiltonian 5.13 will underline the equivalence of the different ways of ladder descriptions and parameterizations discussed in Sec. 3.4.1. In particular we will refer to the classification of magnetization plateaus – this time related to periodic perturbations with $q_{pert.} = 2\pi$.

So far, n_l-leg ladders have been discussed as periodically perturbed spin chains with $q_{pert.} = 2\pi/n_l$ (see previous chapters 3 and 4 for further information). The following equations for periodically perturbed 2- and 3-leg ladders already contain the choice $h = 1.0$ necessary to prevent diagonal couplings in the considered ladder –compare Sec. 3.4.1.

- 2-leg ladder

$$H = 2J_1 \sum_n \Big[2f_n(2,0) \cdot \mathbf{S}_n \mathbf{S}_{n+1} + \alpha_2 \cdot \mathbf{S}_n \mathbf{S}_{n+2} \Big] \tag{5.17}$$

- 3-leg ladder

$$\begin{aligned} H = 2J_1 \sum_n \Big[& (1 - f_n(3,2)) \cdot \mathbf{S}_n \mathbf{S}_{n+1} \\ & + f_n(3,0) \cdot \mathbf{S}_n \mathbf{S}_{n+2} + \alpha_3 \cdot \mathbf{S}_n \mathbf{S}_{n+3} \Big] \end{aligned} \tag{5.18}$$

In the following, we will turn to translation invariant systems (Hamiltonian 5.14, $n_l = 2, 3$) that form the closest approximation of the perturbed systems described above.

5.2.1 2-leg ladders

The translation invariant 2-leg ladder has the special property –like other 2-leg ladders as well– that the periodic rung boundary conditions given by the Hamiltonian 5.13 are equivalent to open rung couplings of double strength. This particular property allows to identify

$$H_{tr.\,inv.}(J_{leg}, J_{rung}, n_l = 2) = J_1 \cdot \Big(H_0(\alpha) + 2h\sqrt{N} D_1(\pi) \Big) \tag{5.19}$$

with

$$J_1 \equiv J_{rung}|_{h=0} \tag{5.20}$$

$$\alpha \equiv \left. \frac{J_{leg}}{J_{rung}} \right|_{h=0} . \tag{5.21}$$

We are therefore in the position to identify Hamiltonian 5.13, 5.14 ($n_l = 2$) –up to the additional boundary terms ($*$), Eq. 3.113– with the spin-Peierls Hamiltonian 4.36 discussed in Sec. 4.1.5. There, the frustration $\alpha = J_2/J_1$ expressed the strength of the leg coupling of the 2-leg ladder and has been discussed for $\alpha = 0.0, 0.25, 0.30, 0.35$.
Fig. 5.4 shows the results of BST studies (see App. C) for the widths and locations of possible magnetization plateaus at $m = 0$ and $m = 1/4$. The $m = 0$ plateau is clearly present and for $J_{rung} \gtrsim 1, .., 2$ -i.e. $\alpha \lesssim 0.5, .., 1$– an almost linear increase ($\sim J_{rung}$) of $B_u(m = 0, J_{rung})$ –i.e. the plateau width– appears:

$$B_u(m = 0, J_{rung}; J_{leg}) = J_{rung} \cdot \left(2 - \frac{J_{leg}}{J_{rung}} \right) = J_{rung} \cdot (2 - \alpha) \ . \tag{5.22}$$

Such a behaviour was shown to hold in the spin-Peierls case for $h = 1.0$ as well, see Sec. 4.1.5, Eq. 4.45. The vertical line in Fig. 5.4 at $J_{rung} = 4$ refers to one of the frustration values ($\alpha = 0.25$) displayed in Fig. 4.29. Up to an overall pre-factor ($J_{rung} = 4$) both figures give the same result for the plateau width and its leading α-, J_{leg}/J_{rung}-dependence which had to be expected based on the freedom of description of the spin system. The repeatedly mentioned additional terms ($*$) in the translation invariant description seem to be of the expected insignificance and do not cause substantial differences for both types of descriptions. The shown range of linear behaviour

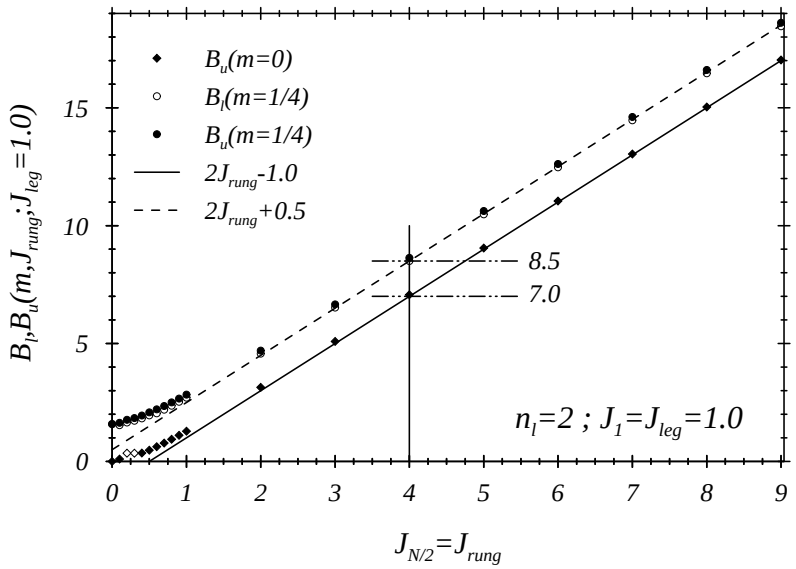

Figure 5.4: J_{rung}-dependence of $m = 0$- and $m = 1/4$-plateaus for translation invariant 2-leg ladder with $J_{leg} = 1.0$; $(N = 8, 12, 16, 20, (24))$

of $B_u(m = 0, J_{rung})$ moreover seems to indicate a rather large α interval that is well described by the lowest order perturbation theory discussed in Sec. 4.1.5.

The same degree of correspondence between both types of description is present for the second plateau ($m = 1/4$) that has first been discussed in Sec. 4.1.5 for perturbation strengths $0 \leq h \leq 1$. Its non-existence is concurringly shown in Figs. 4.30 ($h = 1.0$) and 5.4. The latter figure in addition shows the same linear J_{rung} dependence of $B_u(m = 0)$ and $B(m = 1/4)$. Both lines in parallel increase with $B(m = 1/4) - B_u(m = 0) \simeq 3/2$.

The plateau predictions discussed in the last chapter result in $n_{sp.} = k_3 = 2$ for $q_{pert.} = 2\pi$ ($n = 1$) and $m = 0$. A possible plateau at $m = 1/4$ would have to be classified by $n_{sp.} = k_3 = 4$. The open symbols used for $B_u(m = 0, J_{rung})$ for small J_{rung} symbolize cases of insufficient accuracy of the actual BST fits. The above-mentioned predictions of spontaneous symmetry breaking are moreover consistent with determinations of ground state momenta for varying m. For all shown $J_{rung} > 0$ the $m = 0$ ground state has momentum $q = \pi$, while for $m = 1/4$ although no plateau is present the ground state has momentum $q = \pi/2$.

5.2.2 3-leg ladders

In case of the translation invariant 3-leg ladder no direct periodically perturbed analogue has been discussed earlier in this work. It is obvious, however, that the preparation of the respective 3-leg ladder affords periodic changes of nearest and next-to-nearest neighbour couplings with $q_{pert.} = 2\pi/3$ –see e.g. the discussion of different 3-leg ladder geometries in Sec. 4.1.3. We are therefore led to examine the appearance of magnetization plateaus at $m = 1/6$ and $m = 1/3$.

Fig. 5.5 shows the respective BST results for plateau widths of the 3-leg ladder. Again, the lower ($m = 1/6$) of the two investigated plateaus clearly emerges (for $J_{rung}/J_{leg} > 1$), whereas no definite identification of a finite $m = 1/3$ plateau is possible. Moreover, the narrow shaded regime in the figure has to be identified with the rather low BST accuracy for the extrapolations of the $m = 1/3$ plateau. The unobserved $m = 1/3$ plateau is consistent with earlier discussions of $q_{pert.} = 2\pi/3$ perturbations. In all discussed cases only the $m = 1/6$ plateau had been confirmed. The two thick horizontal marks at $J_{rung} = 0$ moreover mark the positions of $B(m = 1/6, 1/3)$ for the unperturbed Heisenberg chain (Bonner & Fisher construction, see e.g. Sec. 2.4).

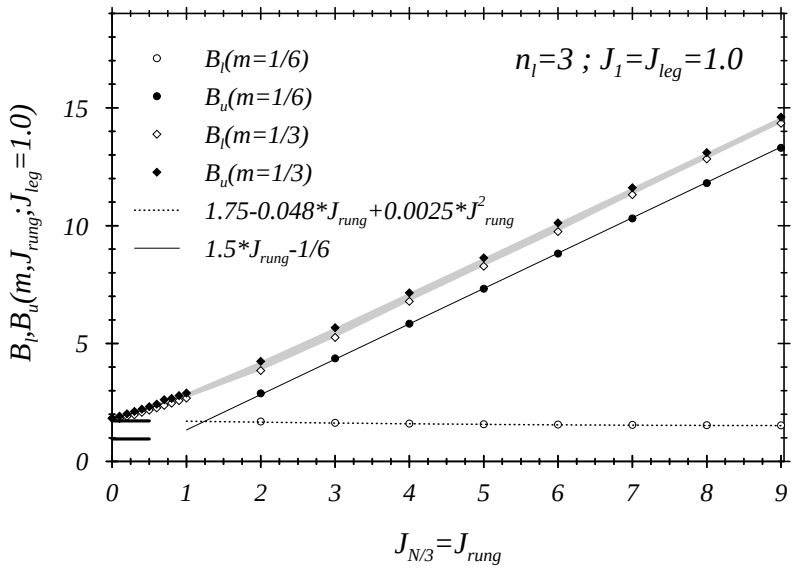

Figure 5.5: J_{rung}-dependence of $m = 1/6$- and $m = 1/3$-plateaus for translation invariant 3-leg ladder with $J_{leg} = 1.0$; $(N = 6, 12, 18, 24)$

Definite statements concerning the existence and width of the $m = 1/6$ plateau for small J_{rung}/J_{leg} are not possible on the basis of the considered system sizes. The linear behaviour of $B_u(m = 1/6)$ for larger J_{rung}/J_{leg} (as well as the almost linear behaviour of $B_l(m = 1/6i)$) again points to lowest order effects in J_{leg}/J_{rung} as in case of $B_u(m = 0)$ for the 2-leg ladder (see Eq. 5.22). Here, we do not want to pursue this line further.
Now, we rather want to turn to the more complex situation of weakly, translationally invariant coupled chains. At the example of the 2-leg ladder we will briefly present the changed starting point (initial conditions for the evolution equations 3.2.2) and the problems arising when looking for scaling solutions in the regime of small perturbations (chain couplings) h.
In addition, the application of the Lieb-Schultz-Mattis (LSM) construction (see Sec. 2.6.2) to spin systems with longer ranges ($O(N^\beta)$, $\beta = 1/2$, 1, see below) of couplings will be discussed.

5.2.3 Evolution equations, scaling and opening of gaps in (weakly) coupled chains

We will now return to the particular case of the translation invariant 2-leg ladder already discussed in Sec. 5.2.1. First we will discuss lowest excitations and quantum numbers for a broader range of inter-chain couplings in some detail, and then further address the situation of weakly coupled chains.
Considering the case of zero magnetization and using the Hamiltonian

$$H = H_1 + h \cdot H_{N/2} \quad ; \quad H_k \equiv 2 \sum_n \mathbf{S}_n \mathbf{S}_{n+k} \,, \tag{5.23}$$

i.e. $h = J_{rung}/J_{leg}$, Fig. 5.6 gives results for the lowest excitations $E_1(h, S)$ with total spin $S = 0, 1$ for $N = 8, 10, 12$ and magnetization $m = 0$. Momenta of the respective eigenstates are classified by $q_n = 2\pi n/N$. The ground state –with energy $E_0(h, q_0, S = 0)$– changes its momentum at the $S = 0$ soft mode position h_S ($E_1(h, S = 0) - E_0(h, S = 0) \to 0$ for $h = h_S$):

$$q_0(N) \;=\; \left\{ \begin{array}{l} 0 \\ \pi \end{array} \right. \quad \text{for} \quad \left\{ \begin{array}{l} h < h_S(N) \\ h > h_S(N) \end{array} \right. \;. \tag{5.24}$$

Since the operator $H_{N/2}$ conserves total spin and momentum, the study of opening gaps (plateaus) is restricted to coupling regimes where the ground state already underwent a change $\Delta q = \pi$ of its momentum with respect to the momentum of the unperturbed chain symbolizing the spontaneous breaking of symmetry (see discussion in Sec. 5.2.1). The latter change of momentum does not take place at $h = 0^+$ for all finite N e.g. as in case of $D_1(\pi)$ for the spin-Peierls gap but at the finite $h_S(N)$. We will yet firstly stick to the standard form and application of the evolution equations.

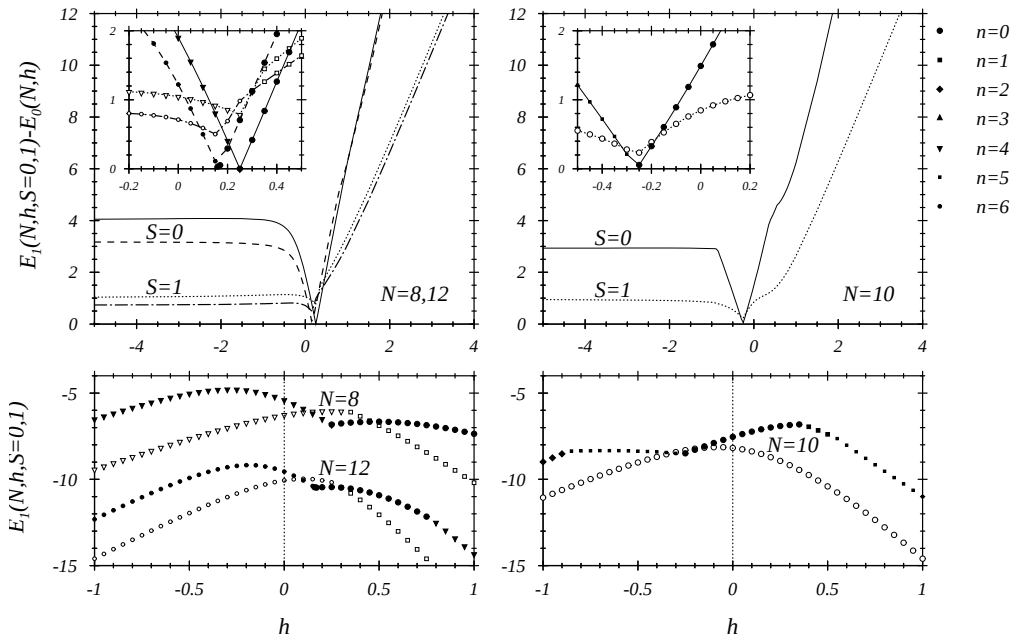

Figure 5.6: Lowest excitations $E_1(S = 0, 1; h)$ for translation invariant 2-leg ladders ($N = 8, 10, 12$) at $m = 0$

In the displayed interval ($-5 \leq h \leq 5$) $E_1(h, S = 1, m = 0)$ as well only changes its momentum once. Besides the narrow region around $h_S(N)$ –and in particular at $h = 0$– the lowest excitation of the ladder is of singlet-triplet ($\Delta S = 1$) character. For systems with $N = 4n$, $4n+2$ this region differently extends from $h = 0$ to $h < 0$, $h > 0$. The lowest $S = 0$ excitations $E_1(N, h, m = 0)$ –shown in Fig. 5.6– furthermore differ for almost all h and N by $\Delta q = \pi$ from $q_0(N, h, m = 0)$, which means that $E_1 - E_0$ does not represent an excitation ω_{01} of the momentum conserving $H_{N/2}$ with

$$\omega_{10}(N, h, m) \equiv E_1(h, m; q_0(h, N, m)) - E_0(h, m; q_0(h, N, m)) \tag{5.25}$$

(further details are given in Fig. 5.10 below).
The evolution equations 3.2 need the first derivative of $E_0(N, h)$ at $h = 0$ as one essential initial condition for the description of the evolution of energies and matrix elements under the influence of a perturbation of strength h. Following Sec. 3.2.1 we obtain

$$\frac{d}{dh}E_0(N, h) = < 0|H_{N/2}|0 > \equiv T_{00}(h) \tag{5.26}$$

$$= N \cdot < 0|\mathbf{S}_0\mathbf{S}_{N/2}|0 > \equiv N \cdot t_{00}(h)\,. \tag{5.27}$$

A first overall picture of $T_{00}(N, h, m)/N$ for a broader range of perturbation strengths h (and magnetization $m = 0$) is given on the l.h.s. of Fig. 5.7.

The figure resembles that for $|h| \gg 1$ the rungs are in a $S_{rung} = 1$ ($h \ll -1$) or $S_{rung} = 0$ ($h \gg 1$) state and furthermore that at $h = 0$ the derivative of $E_0(N, h, m = 0)$ is unequal to zero.

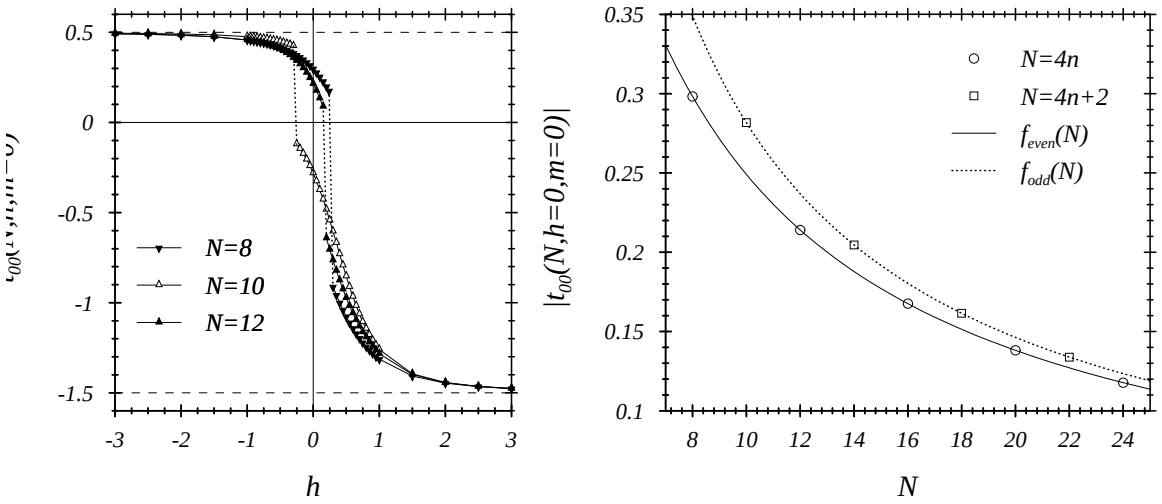

Figure 5.7: First derivative of $E_0(N, h)/N$ for system sizes $N = 8, 10, 12$, $|h| \leq 3$ (l.h.s.) and fits to the N-dependence of $t_{00}(N, h = 0)$ (r.h.s.)

For growing $|h|$ a dominant exponential h-dependence of $t_{00}(N, h, 0)$ becomes apparent. A large-N extrapolation of finite-N data to a simple description combining algebraic behaviour for $|h| \ll 1$ and the shown saturation for large $|h|$:

$$t_{00}(h, 0) \quad = \quad a + b \cdot e^{-c \cdot |h|^d} \tag{5.28}$$

led to the two sets of parameterizations for negative h given in Table 5.2 –depending on keeping $t_{00}(-\infty, 0)$ fixed ($= 1/2$) or adjustable. System sizes of up to $N = 24$ and perturbations $-3 \leq h \leq 0$ entered the extrapolations.

a_i	b_i	c_i	d_i
0.49	0.516	2.984	0.671
1/2	0.533	2.762	0.635

Table 5.2: Parameterizations $a_i + b_i \cdot e^{-c_i \cdot |h|_i^d}$ for the large-N behaviour of $t_{00}(N, h, m = 0)$; $h < 0$

The quality of the exponential fits, however, does not allow for reasonable applications in the range of small h addressing the scaling behaviour of the two weakly coupled legs.
The above discussion furthermore shows that the direct extension from $h = 0$ to finite h considers ladder systems with unchanged ground state momentum ($q_0(m = 0) = \pi \cdot N/2$), i.e. the evolution equations in their originally given form do not apply to the interesting case of the potential formation of magnetization plateaus for small inter-chain coupling.
We continue considering the N-dependence of $t_{00}(N, h = 0, m)$, i.e. the unperturbed (initial) situation. The r.h.s. of Fig. 5.7 shows results of fits $f_i(N)$ separately performed for "even" ($N = 4n$) and "odd" ($N = 4n + 2$) N. The two resulting functions $f_i(N)$ are given by

$$\begin{aligned} f_{even}(N, m = 0) &= \frac{1}{N} \cdot (1.9248 + 0.2974 \cdot \log(N - 3.2920)) \\ f_{odd}(N, m = 0) &= \frac{1}{N} \cdot (2.4962 + 0.0582 \cdot N^{0.5788}) \,, \end{aligned}$$

suggesting a different leading large-N behaviour

$$t_{00}(N, h=0, m=0) \quad \stackrel{N\to\infty}{\longrightarrow} \quad \frac{(\log N)^{\kappa}}{N} \quad , \quad N = 4n \tag{5.29}$$

$$t_{00}(N, h=0, m=0) \quad \stackrel{N\to\infty}{\longrightarrow} \quad N^{-\kappa'} \quad , \quad N = 4n+2 \tag{5.30}$$

for the two classes $N = 4n$ and $N = 4n + 2$. A similar treatment of the situation $m = 1/N$ led us to fits of comparably good quality –this time given by single powers of $1/N$:

$$\begin{aligned} f_{even}(N, m = 1/N) &= \frac{1}{N} \cdot \left(1.3814 + 4.2012 \cdot N^{-1} - 7.1338 \cdot N^{-2}\right) \\ f_{odd}(N, m = 1/N) &= \frac{1}{N} \cdot \left(-1.3820 + 1.0544 \cdot N^{-1} + 7.1848 \cdot N^{-2}\right) . \end{aligned}$$

The presented fits of course do not represent rigorous statements on the analytical form of the finite-size behaviour of $t_{00}(N, h, m)$, however give first indications of peculiarities for the $m = 0$-case.
The expectation value $T_{00}(h)$ is shown in Fig. 5.8 for a narrow region around $h = 0$. Both parts of the figure again show the different behaviour of the two sets $N = 4n$ and $N = 4n + 2$. In addition, the figure shows for both cases the dominant linear component in h for the behaviour of $T_{00}(N, h)$. Odd powers of the perturbation strength did not appear for periodically perturbed systems –compare e.g. discussion of Eqns. 3.46, 3.47 in Chap. 3.

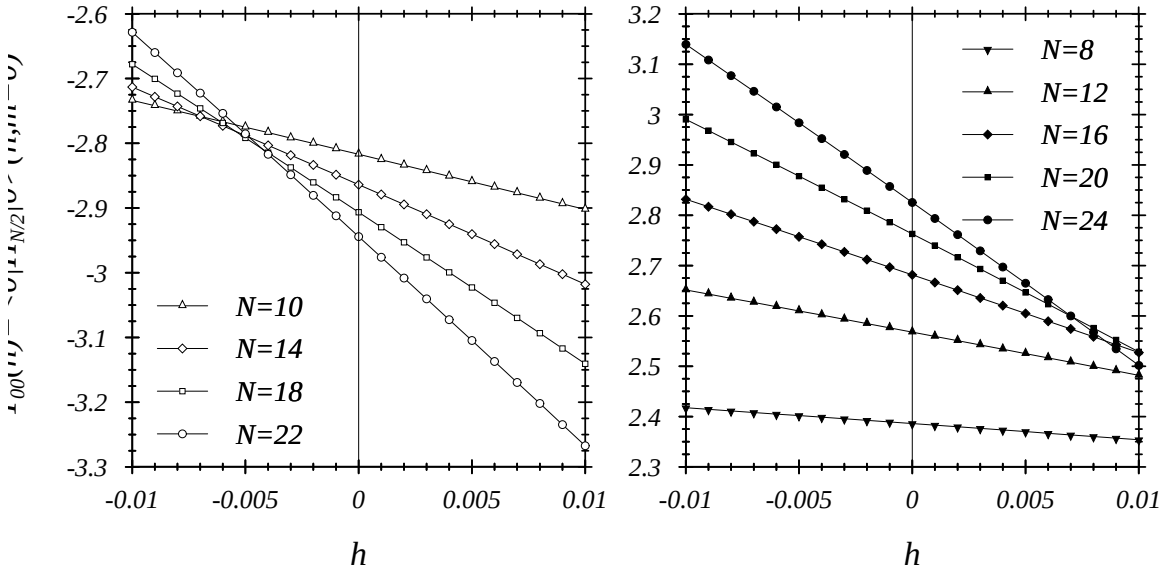

Figure 5.8: First derivative of $E_0(N, h)$ for system sizes $N = 8, 10, \ldots, 24$, $|h| \leq 0.01$

We are now going to sketch parts of the scaling behaviour and comment on limitations of a more general treatment discussing the two magnetizations $m = 0$ ($S_z = 0$) and $m = 1/N$ ($S_z = 1$). We will first present the scaling of $T_{00}(N, h, m)$ for perturbation strengths h fulfilling $-(-1)^{N/2}|h| = h$, i.e. negative h for $N = 4n$ and vice versa for $N = 4n + 2$ (e.g. the low-h regions without crossings shown for $m = 0$ in Fig. 5.7). The latter means that we avoid entering the regime of the (spontaneously) changed ground state momentum ($q_0(N) : 0 \leftrightarrow \pi$) for $m = 0$. Then, we will end this paragraph with some brief remarks concerning the discussion of $\Delta q = \Delta S = 0$ excitations caused by the translation invariant perturbation $H_{N/2}$.
Fig. 5.9 shows results of optimization processes for the determination of scaling exponents ϵ that allow for a scaling plot of the different system sizes at the respective magnetization as a function of the scaling variable $x = N|h|^{\epsilon}$. Table 5.3 gives the results of the interpolations of

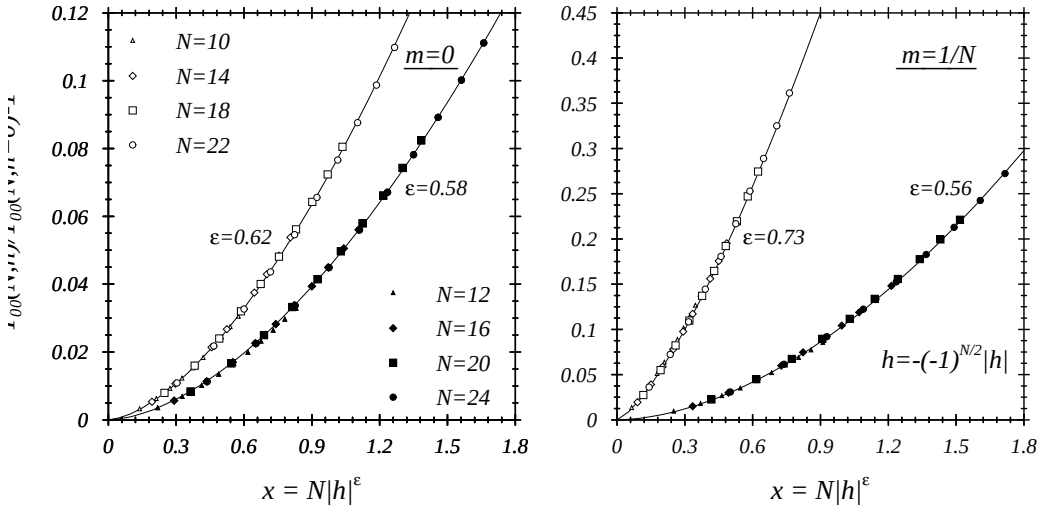

Figure 5.9: Scaling of $T_{00}(N,h,m)$ versus scaling variable $x = N|h|^\epsilon$ for $N = 4n$, $4n+2$ and $m = 0,\ 1/N$

the data that are as well shown in Fig. 5.9 as solid lines. The given values strongly emphasize a leading

$$\frac{T_{00}(x,m)}{T_{00}(0,m)} - 1 \quad \sim \quad x^{1/\epsilon(m)}$$

behaviour for small x again giving the aforementioned linear h-dependence for fixed N. $\epsilon(m)$ as well depends on the two classes of chain lengths $N_{even} = 4n$, $N_{odd} = 4n+2$. The considered 2 m values seem to indicate a growing divergence of $\epsilon_{odd/even}(m)$ for growing m, however, offer no proof.

m	N	ϵ_i	a_i	b_i	$1/b_i$
0	$4n$	0.58	0.047	1.70	0.588..
0	$4n+2$	0.62	0.0753	1.62	0.617..
$1/N$	$4n$	0.56	0.104	1.79	0.558..
$1/N$	$4n+2$	0.73	0.520	1.37	0.729..

Table 5.3: Fits $f_i(x) = a_i \cdot x^{b_i}$ given as solid lines to the scaled data (exponents ϵ_i) in Fig. 5.9

Several attempts have been made to yield a consistent scaling description of the h-dependence of the ground state energy, its first and second derivative and as well as the lowest excitation $\omega_{01}(N,h,m)$. N-dependent shifts of the zero positions of the applied scaling, combinations of algebraic and exponential h-dependences and further modifications have been tested. In none of these attempts, however, a consistent scaling description could be obtained. Furthermore it turned out, that by no means a satisfying analytical treatment nor verification of scaling solutions –as presented in Sec. 3.2.3 for the example of a longitudinal staggered field– was feasible. Definite answers on the opening of gaps and plateaus for small h –like in case of the BST extrapolations in Secs. 5.2.1, 5.2.2– could not be obtained.
We will not pursue the variety of briefly mentioned investigations any further at this place but end the paragraph with some final remarks on the complex situation of lowest non-zero excitations with $\Delta q = \Delta S = 0$.

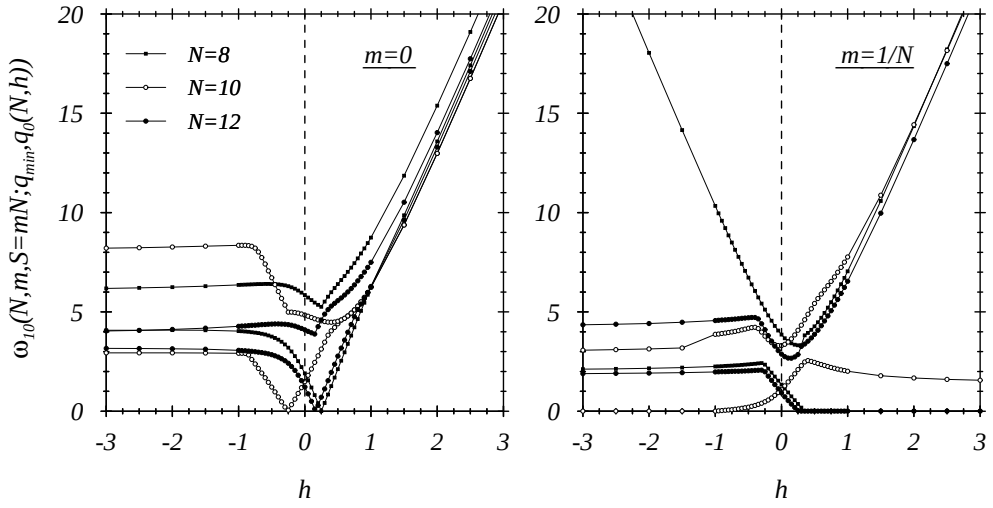

Figure 5.10: Lowest excitations $E_1(N, h, m, S == m \cdot N; q)$ for optimal q and $q = q_0(N, h, m)$, i.e. $\Delta q = \Delta S = 0$ excitations; $N = 8, 10, (12)$

Fig. 5.10 shows for $N = 8, 10, 12$ at $m = 0, 1/N$ the courses of the lowest excitations

$$\begin{aligned} \Delta E_{i0}(N, h, m, S = mN; \Delta q_{i0}, \Delta S = 0) &= E_i(N, h, m, S = mN; q_i) \\ &\quad -E_0(N, h, m, S = mN; q_0) \quad ; \quad i = 1, 2\,. \end{aligned}$$

While $i = 1$ refers to the absolute lowest excitation of $\Delta S = 0$-type (for $m = 0$ also given in Fig. 5.6), $i = 2$ denotes the sub-class of lowest excitations additionally fulfilling $\Delta q = 0$, i.e. $q_2 = q_0$. Both energies are given by same symbols and are to be distinguished using $E_2(h) \geq E_1(h)$. The ground state momentum only changes once (as function of h) for both values of magnetization m. For $m = 1/N$ the changes are $\pi \to \pm 2\pi/N$ $(N = 4n)$ and $0 \to \pm(\pi - 2\pi/N)$ $(N = 4n + 2)$ – characterized by $E_1(h) = 0$ in the figure.

The l.h.s. of the figure $(m = 0)$ shows the almost linear behaviour of $(E_2 - E_0)(h)$ at those $h_0(N)$ where the ground state changes its symmetry pointing at a possible description through

$$\frac{\omega(h - h_0(N))}{\omega(-h_0(N))} - 1 \quad \sim \quad \tilde{x}^{1/\epsilon} \quad ; \quad \tilde{x} = N|h - h_0(N)|^{\epsilon}\,.$$

In any case, the figure demonstrates a complicate pattern of finite-size dependent changes in quantum numbers and lowest excitations not at but close to $h = 0$ that cause the problems within a consistent scaling description of weakly coupled chains.

The described scaling problem is yet an unsettled one and requires further investigation. At this place, however, we will not proceed any further and do content ourselves with the explanation of some of the details that have to be addressed by a following analysis.

We will now leave the field of scaling ansatzes and theories and turn to the discussion of another technical tool that can offer some insight –as well as giving new directions– for further discussions and investigations of magnetization phenomena (in particular plateaus). In the next section the soft mode investigation scheme of *Lieb, Schultz, Mattis* (LSM) [143] is applied to spin chains with long-range couplings. These will be translation invariant ladder Hamiltonians as well as translation invariant (approximate) square lattices of spins.

5.3 LSM application to spin chains with long ranges of spin couplings

In this paragraph we want to consider applications of the construction of Lieb, Schultz, Mattis (LSM) [143] –introduced in Sec. 2.6.2– to spin chains with far reaching interactions. Right at the beginning it should be stressed that the following results do not claim the status of rigorous and final proofs. They rather intend to show relations to other statements concerning the existence of magnetization plateaus in the respective spin systems. Moreover, the presented discussion of two-dimensional spin systems only covers some aspects of a still ongoing investigation.
We will start discussing translation invariant n_l-leg ladder Hamiltonians (coupling range N/n_l, i.e. $O(N)$ for the up to now discussed ladder types) [86]. Later we will turn to spin systems with helical boundary conditions that will be briefly commented in the final section of this chapter.
In the following we will use translation invariant ladder Hamiltonians in the form

$$H(h) = H_1 + h \cdot H_\tau \quad ; \quad H_m \equiv \sum_n \mathbf{S}_n \mathbf{S}_{n+m} \tag{5.31}$$

with $\tau = N/n_l$ and $h = J_{rung}/J_{leg}$. Redoing the analysis of LSM (see also [86]) now leads to the energy difference $\Delta E_k =< 0|U_k H U_k^{-1} - H|0 >$:

$$\begin{aligned}
\Delta E_k \;=\; & (\cos(k)-1)\cdot \underbrace{\sum_n < 0|\left(S_x(n)S_x(n+1)+S_y(n)S_y(n+1)\right)|0>}_{O(N)} \\
& + (\cos(k\tau)-1)\cdot h \cdot \underbrace{\sum_n < 0|\left(S_x(n)S_x(n+\tau)+S_y(n)S_y(n+\tau)\right)|0>}_{O(N)} \\
& + \sin(k)\cdot \underbrace{\sum_n < 0|\left(S_x(n)S_y(n+1)-S_y(n)S_x(n+1)\right)|0>}_{=<I>} \\
& + \sin(k\tau)\cdot h \cdot \underbrace{\sum_n < 0|\left(S_x(n)S_y(n+\tau)-S_y(n)S_x(n+\tau)\right)|0>}_{=<II>}
\end{aligned} \tag{5.32}$$

with $k = 2\pi \cdot j/N$, $j = 1, 2, \ldots$. Using the separate conservation of the total S_z for H_1 and H_τ ($[H(h), S_z] = 0$ holds as well), i.e.

$$< I > \;=\; < 0|[H_1, S_z]|0 >= 0 \tag{5.33}$$

$$< II > \;=\; < 0|[H_\tau, S_z]|0 >= 0\,, \tag{5.34}$$

it only remains to establish the vanishing of the first two lines of the equation. The factor $[\cos k\tau - 1] = [\cos(2\pi j/n_l) - 1]$ only vanishes for $j = n \cdot n_l$ which as well leads to the decay of the first part (H_1 contribution) as $\sim O(N^{-1})$.
We now want to address the above-mentioned link to plateau predictions for translation invariant ladder systems. The presented calculations do not provide states $|j >= |k(j) >= U_k(j)|0 >$ that are degenerate with the ground state in the TDL for j-values $j = 1, 2, .., n_l - 1$ ($k = 2\pi \cdot j/N$). Taking now into account the momentum p_j of the state $|k(j) >$ (see e.g. Sec. 2.6.2):

$$p_j \;=\; p_0 + j \cdot \pi(1 - 2m) \tag{5.35}$$

one notices that situations of particular interest ($p_j = p_0 + n \cdot 2\pi$), i.e. a complete loss of degeneracy, occur for $p_j - p_0 = n \cdot 2\pi$ leading to

$$j \cdot \left(\frac{1}{2} - m\right) \;=\; n \,=\, \text{integer}\,. \tag{5.36}$$

The latter equation is equivalent to the quantization condition 4.1 of Oshikawa, Yamanaka and Affleck [169] for $S = 1/2$. It should be noted, however, that the factor j must not be interpreted as describing the explicit symmetry breaking given by the Hamiltonian –which simply would give $n = 1$– but has to be interpreted as $j = n \cdot n_{sp} = n_{sp}$ (see also Chaps. 4, 5).
Furthermore the reader should be reminded that the above statement is by no means a rigorous one. It should however serve as an additional approach to the phenomenon of the opening of gaps and formation of magnetization plateaus. Spontaneous breaking of symmetry, the occurrence of a complete lifting of ground state degeneracy (obtained from the above given LSM soft mode scheme) and the appearance of magnetization plateaus have been presented in a unique picture free of immediate contradictions.

We finally want to address the Hamiltonian $H_{hel.}(\alpha, k)$ (Eq. 5.44) as a further example of a spin system exposed to a translationally invariant perturbation. The helical boundary conditions (cf. Fig. 5.11 and Sec. 5.4 for further discussion) allow for an approximate treatment of a square lattice of Heisenberg spins. In the present section we again want to apply the LSM scheme and want to figure out possibilities for the occurrence of soft modes or a spontaneous symmetry breaking accompanying the formation of magnetization plateaus. Here, as well as in the next section, we will restrict on the outlines of a still ongoing study of magnetization phenomena in two-dimensional spin-1/2 systems.
The application of LSM and the evaluation of the energy difference $\Delta E_q =< 0|U_q H U_q^{-1} - H|0 >$ –using $q = 2\pi \cdot j/N$ and omitting the pre-factor 2 of Hamiltonian 5.44– results in

$$\begin{aligned}
\Delta E_q &= (\cos(q) - 1) < H_1^{\perp} > + (\cos(kq) - 1) < H_k^{\perp} > \qquad (5.37)\\
&\quad + \alpha \cdot \Big[(\cos(q(k-1)) - 1) < H_{k-1}^{\perp} > + (\cos(q(k+1)) - 1) < H_{k+1}^{\perp} > \Big] \\
&= (\cos(q) - 1) < H_1^{\perp} > + (\cos(kq) - 1) < H_k^{\perp} > \\
&\quad + \alpha \cdot \Big[(\cos(kq)\cos(q) - 1) \Big(< H_{k-1}^{\perp} > + < H_{k+1}^{\perp} > \Big) \\
&\qquad + \sin(kq)\sin(q) \Big(< H_{k-1}^{\perp} > - < H_{k+1}^{\perp} > \Big) \Big] \qquad (5.38)
\end{aligned}$$

with

$$< H_a^{\perp} > \equiv \sum_n < 0|S_x(n)S_x(n+a) + S_y(n)S_y(n+a)|0 > \, . \qquad (5.39)$$

and $|0 >$ denoting the ground state for the considered magnetization m.
Not all of the four q-dependent factors in Eq. 5.38 show the required $O(N^{-(1+\delta)})$ $(\delta > 0)$ behaviour to result in $\Delta E_q \to 0$ for an appropriately chosen q and $N \to \infty$. The latter condition, however, can be fulfilled when using the transformation properties of H_1, H_k with respect to the permutation

$$Q : \qquad x \to 1 + (x-1) \cdot k \, . \qquad (5.40)$$

The latter permutation transforms horizontal into vertical nearest neighbours (and vice versa):

$$Q H_1 Q^+ = H_k \qquad , \qquad Q H_k Q^+ = H_1 \, , \qquad (5.41)$$

however leave the Hamiltonians H_{k-1}, H_{k+1} with the diagonal couplings invariant. Relation 5.41 yields

$$\begin{aligned}
\Delta E_q &= (\cos(kq)\cos(q) - 1) \Big[\frac{1}{2} \Big(< H_1^{\perp} > + < H_k^{\perp} > \Big) + \alpha \cdot \Big(< H_{k-1}^{\perp} > + < H_{k+1}^{\perp} > \Big) \Big] \\
&\quad - (1 - \cos(q))\,(1 - \cos(kq)) \, \frac{1}{2} \Big(< H_1^{\perp} > + < H_k^{\perp} > \Big) \\
&\quad + \alpha \cdot \sin(kq)\sin(q) \Big(< H_{k-1}^{\perp} > - < H_{k+1}^{\perp} > \Big) \qquad (5.42)
\end{aligned}$$

and here the last two lines of Eq. 5.42 may be chosen to vanish in the limit $N \to \infty$, $k = \sqrt{N \pm 1}$. What remains is the so far unprecedented situation of bringing the whole expression to vanish by fulfilling the final implicit condition for the size of the applied frustration value α, namely

$$\alpha \;=\; -\frac{1}{2}\frac{< H_1^{\perp} > + < H_k^{\perp} >}{< H_{k-1}^{\perp} > + < H_{k+1}^{\perp} >} \,. \tag{5.43}$$

We will return to Eq. 5.43 in the final part of the following section and present some first provisional results from an ongoing study of the immediate vicinity of the boundaries of magnetization plateaus and the interpretation of soft modes in 2-dimensional spin-1/2 systems using LSM constructions, static and dynamical structure factors as well as frequency-moments of the latter in our discussion of extensions to 2-dimensional spin-1/2 systems (Sec. 5.4.3).

5.4 Two-dimensional antiferromagnetic spin-1/2 systems

In this final section we will approach two-dimensional (quadratic) Heisenberg spin systems as well as the transition from one-dimensional spin chains to two-dimensional spin lattices. This will be mainly done in a parameterization using helical boundary conditions that will be introduced and defined in the next paragraph. The latter description/mapping of spin systems and its relation to quadratic spin lattices will be commented.
We will further present a discussion of staggered magnetizations $m_{stagg.}$ that play an important role for the discrimination one- or two-dimensional behaviour of a spin system (see Sec. 5.4.2). A study of the first derivative of $m_{stagg.}$ –strictly speaking: $m^2_{stagg.}$– for the cross-over from uncoupled chains to a two-dimensional matrix of nearest-neighbour coupled spins will be reviewed as a further application of helical boundary conditions. In particular, the development of a non-zero $m_{stagg.}$ for increasing lateral spin couplings and the determination of the precise size of $J_{lateral}$ at the transition point $m_{stagg.} = 0$ – $m_{stagg.} > 0$ will be addressed.
The final paragraph (Sec. 5.4.3) will be used for a presentation of first results concerning the meaning of relation 5.43 for the formation of magnetization plateaus in frustrated two-dimensional spin lattices. These aspects will be accompanied by the presentation of selected magnetization curves that may serve as first building blocks of evidence for plateau formations since no theoretical scheme has been presented yet.

5.4.1 Spin systems with helical boundary conditions

The following Hamiltonian (depicted for $N = k^2 \pm 1$, $k = 5$ in Fig. 5.11) gives an approximate square lattice $(H_1 + H_k)$ with an additional square lattice $(H_{k-1} + H_{k+1})$ forming the diagonal bonds of the previous.

$$\begin{aligned} H_{hel.}(\alpha, k) &= 2\sum_n \mathbf{S}_n \cdot (\mathbf{S}_{n+1} + \mathbf{S}_{n+k}) + \alpha \cdot 2 \sum_n \mathbf{S}_n \cdot (\mathbf{S}_{n+k-1} + \mathbf{S}_{n+k+1}) \\ &= H_1 + H_k + \alpha\,(H_{k-1} + H_{k+1}) \end{aligned} \tag{5.44}$$

Helical boundary conditions translate into a quantization of a 2-dimensional wave vector $\vec{q} = (q_x, q_y)$ via

$$q_x = \frac{2\pi}{N} \cdot n, \qquad q_y = \frac{2\pi}{N} \cdot k \cdot n, \quad n = 0, \ldots, \frac{N}{2}\,, \tag{5.45}$$

which deviates from the usual periodic boundary conditions.
The degree and quality of approximations of square lattices of systems $H_1 + H_k$ was first discussed in [98] and comparisons with results obtained directly from systems with periodic boundary conditions were performed.

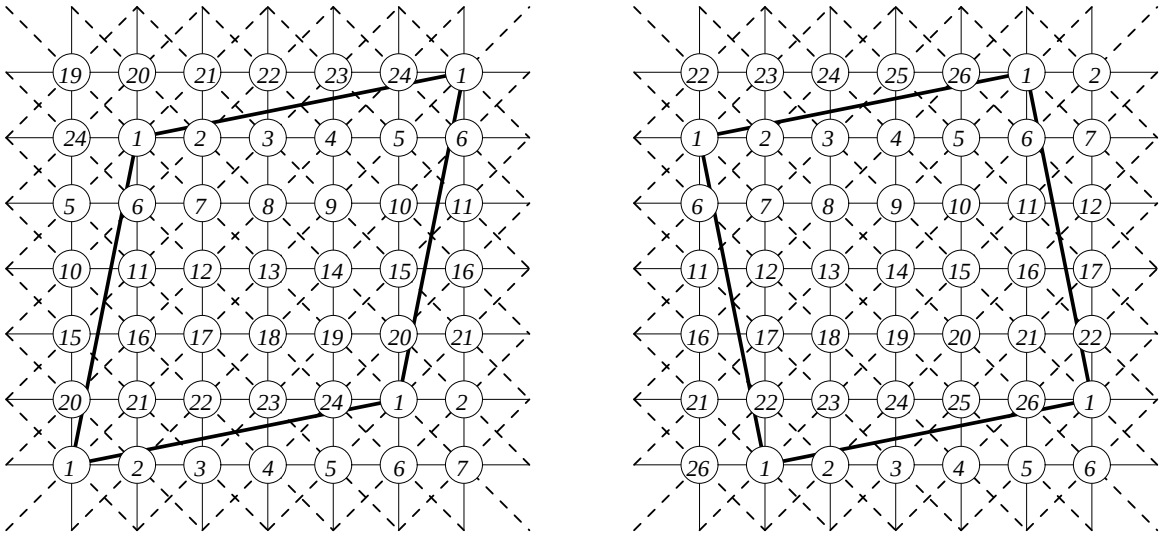

Figure 5.11: Square lattices with helical boundary conditions for $k = 5$: $N = k^2 \pm 1 = 24$ (left), 26 (right); dashed lines: frustrating couplings – see text

The influence of frustrating diagonal couplings have e.g. been discussed by means of diagonalizations of $N = 16, 20$ *Dagotto, Moreo* [55], 4×4 and 6×6 lattices (*Schulz, Ziman* [183]) or applications of helical boundary conditions (*Yang, Mütter* [221]). The final two papers concentrated on characteristics of critical behaviour in two dimensions, ground state ordering as well as the α-dependence of the position of extrema of static structure factors. It should be noted that the smaller 4×4-system is known [70] to be interfered in its meaning as a further square lattice with at the same time representing the smallest 4-dimensional ($N = 2^4$) system with periodic boundary conditions. The latter property gives rise to certain symmetries (degeneracies) that are not genuine for two-dimensional (square) spin lattices.

We will return to 2-dimensional behaviour, existence of gaps and related spontaneous breaking of symmetry in part 5.4.3. There, we will present first results based on the α-fixing given by Eq. 5.43 and some magnetization curves. Before, we will remark on the transition from one-dimensional behaviour with zero staggered magnetization to two-dimensional spin systems with a finite staggered magnetization. Increasing the coupling strengths J_k of $H = J_1 H_1 + J_k H_k$ from zero, in [83] the onset value $J_{k,0}$ of non-zero staggered magnetization has been determined [83] to be located at $J_{k,0} = 0$. The latter result, however, is not un-contradicted and some references will be given.

5.4.2 Sub-lattice magnetization at the $1d - 2d$ transition

In this section we want to recall a recent study [83] of spin systems with helical boundary conditions to determine the size of lateral spin couplings for the point of appearance of a non-zero staggered magnetization $m_{stagg.}$. The $N \to \infty$ limit of the latter quantity,

$$m^2_{stagg.} \;=\; \frac{1}{N} < 0|\mathbf{S}^+(\pi)\mathbf{S}(\pi)|0 > = \frac{1}{N^2} \sum_{mn} e^{i\pi(m-n)} < 0|\mathbf{S}(m)\mathbf{S}(n)|0 > , \qquad (5.46)$$

has earlier been determined in [98] for an approximate two-dimensional lattice ($\Theta = 0$ in the following Hamiltonian)

$$H(\Theta) \quad = \quad \frac{1}{2}(1+\Theta)\cdot H_1 + \frac{1}{2}(1-\Theta)\cdot H_k \quad , \quad H_j \equiv 2\sum_n \mathbf{S}(n)\mathbf{S}(n+j)\,, \tag{5.47}$$

by an extrapolation from finite helical systems. The obtained $m_{stagg.} \simeq 0.25..0.3$ appeared to be in reasonable agreement with results obtained from extrapolations of square lattices ($m_{stagg.} \simeq 0.2765$) [183].
The staggered magnetization should not be put in direct relation to the z-component magnetization m considered sofar. Its importance for the discussion of antiferromagnetic spin systems emerges more clearly when e.g. considering its homogeneous $q = 0$ counterpart $m_{hom.}$

$$m^2_{hom.} \quad = \quad \frac{1}{N} < 0|\mathbf{S}^+(q=0)\mathbf{S}(q=0)|0 > = \; S(S+1)\,. \tag{5.48}$$

While the total spin S of the ground state of an antiferromagnetic spin system (cf. e.g. [144]) is zero for all dimensions, the staggered magnetization $m_{stagg.}$ offers an interesting dependence on the dimensionality of the antiferromagnetic Heisenberg system. $m_{stagg.}$ is known to be zero for 1d-Heisenberg chains, the known long-range behaviour

$$\lim_{x\to\infty} < 0|\mathbf{S}_0\mathbf{S}_x|0 > \quad \sim \quad (-1)^x \cdot \frac{1}{x} \tag{5.49}$$

is insufficient to conclude for a non-zero $m_{stagg.}$, and non-zero for $d \geq 3$ (in each case for $N \to \infty$). The study of $m_{stagg.}$ and antiferromagnetic ordering in 2d-spin systems –the latter point in particular stimulated by the advent of high-temperature superconductivity [20]– as well led to a finite staggered magnetization. The reduction of $m_{stagg.}$ from its classical value $m_{stagg.} = S$ –due to zero point quantum fluctuations–has been investigated by means of spin wave theory [10, 138], perturbation theory [61, 170, 121], on small systems [165, 183, 98] as well as experimentally [219, 210] (considering the quasi-two-dimensional systems K_2NiF_4, K_2MnF_4, Rb_2MnF_4).
Introducing now lateral couplings of variable strength, the onset of a non-zero staggered magnetization has been again treated with several techniques. In most cases, spin wave theories, mean field approaches (reference see e.g. [122]) as well as e.g. a "heuristic" renormalization group argument (*Affleck, Gelfand, Singh* [7]) resulted in onset values $J_{lateral}/J_{chain} \lesssim O(10^{-2})$ leading to the suggestion $m_{stagg.}(J_{lateral}) \neq 0$ for all $J_{lateral} > 0$. It should be mentioned, however, that a recent study [122] –based on a Green's function approach and finite-lattice Lanczos diagonalizations (of up to $N = 36$ sites– arrived at a considerably larger threshold value of $J_{lateral}/J_{chain} \simeq 0.2$. –It finally should be added that investigations of particular systems with non-integer or fractal dimensionality between one and two (e.g. non-translational *Sierpiński* lattices of dimension $d = \ln 3/\ln 2 \simeq 1.58$; *Tomczak, Ferchmin, Richter* [190]) led to disordered ground states –i.e. zero staggered magnetization– and further to the speculation that Heisenberg antiferromagnets on fractal lattices quite generally may not order below dimension two.
In the following we will instead give a brief review of an investigation ([83]) giving strong evidence to the before-mentioned suggestion of an onset of finite staggered magnetizations (in translational lattices) for all $J_{lateral} > 0$.
In [83] the dimensional behaviour of the staggered magnetization was investigated via the Θ-dependence $-m_{stagg.}(\Theta)$– of the helical spin system 5.47. The Θ-evolution of eigenvalues $E_n(\Theta)$, eigenvectors $|\Psi_n(\Theta) >$ and of matrix elements of hermitian operators $O(\Theta)$ was presented, resulting in

$$\frac{d}{d\Theta} m^2_{stagg.}(\Theta) \quad = \quad -\frac{2}{N}\sum_{n\neq 0} \frac{< \Psi_n(\Theta)|(H_1 - H_k)/2|\Psi_0(\Theta) >}{\omega_n(\Theta)} \cdot M_n(\Theta,\pi) \tag{5.50}$$

$$= \quad -\frac{1}{N}\sum_p \left(e^{-ip} - e^{-ipk}\right) \underbrace{\sum_{n\neq 0} \frac{(\underline{\underline{2}}) \cdot M_n(\Theta,p)M_n(\Theta,\pi)}{\omega_n(\Theta)}}_{\equiv \quad \Sigma(\Theta,p,\pi,N)} \tag{5.51}$$

with

$$\omega_n(\Theta,N) = E_n(\Theta,N) - E_0(\Theta,N) \tag{5.52}$$

$$M_n(\Theta,p,N) = <\Psi_n(\Theta)|\mathbf{S}(-p)\mathbf{S}(p)|\Psi_0(\Theta)> \tag{5.53}$$

$$= \frac{1}{N}\sum_{l,l'} e^{-ip(l-l')} <\Psi_n(\Theta)|\mathbf{S}(l)\mathbf{S}(l')|\Psi_0(\Theta)> \ . \tag{5.54}$$

Note in particular, Eq. 5.50 showing the independence of the given derivative with respect to the chosen prefactor of Hamiltonian 5.47. In the following, we will maintain definition 5.47 without further explicitly marking the respective factor $(\underline{\underline{2}})\cdot$.
The latter equation in particular leads to

$$\sum_p e^{-ipj} M_n(\Theta,p) = \sum_l <\Psi_n(\Theta)|\mathbf{S}(l)\mathbf{S}(l+j)|\Psi_0(\Theta)> \tag{5.55}$$

and important sum rules like

$$\sum_p M_n(\Theta,p,N)\Big|_{n\neq 0} = \sum_p \Sigma(\Theta,p,p',N)\Big|_{n\neq 0} = 0 \tag{5.56}$$

$$<\Psi_n(\Theta)|H(\Theta)|\Psi_0(\Theta)>\Big|_{n\neq 0} = \sum_p \left[(1+\Theta)e^{-ip} + (1-\Theta)e^{-ipk}\right] M_n(\Theta,p)\Big|_{n\neq 0}$$

$$= 0\,. \tag{5.57}$$

The first sum rule has been portrayed in App. A where its importance as a check for applications of the recursion method was discussed.

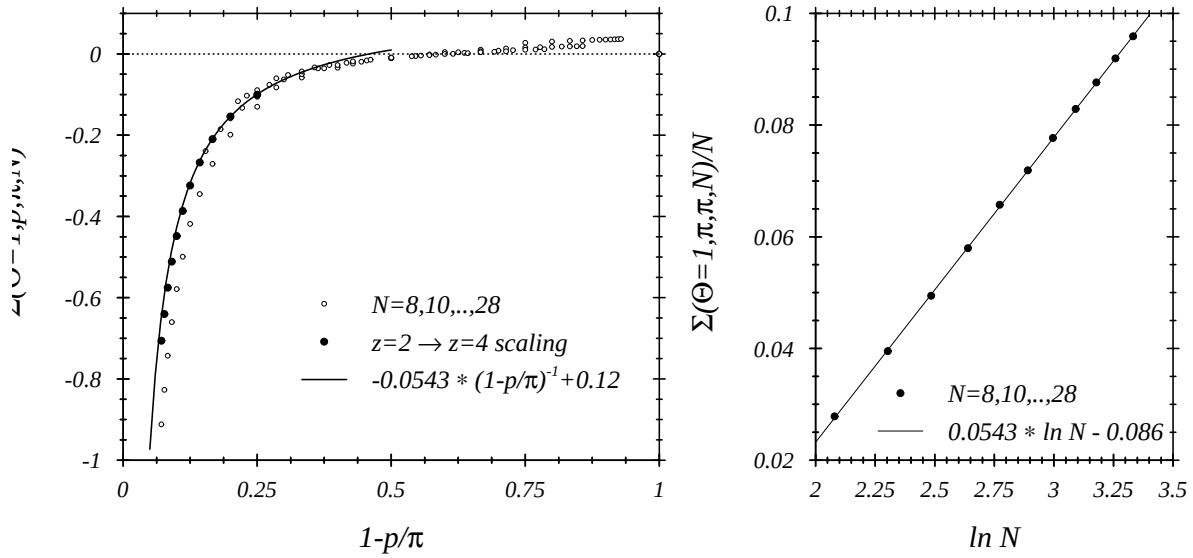

Figure 5.12: l.h.s.: $\Sigma(1,p,\pi,N)$ for $N = 8,10,..,28$ (open symbols), finite-size fits (solid symbols; see text) and prediction 5.59 (solid line); r.h.s.: corresponding fit 5.58 for $\Sigma(1,\pi,\pi,N)/N$

A more significant importance fell to sum rule 5.57 for the determination of the $N \to \infty$ behaviour of $\Sigma(1,p,\pi,N)$ in the limit $p \to \pi$. The sum rule allowed to transfer (see [83]) the

clear logarithmic dependence of $\Sigma(1,\pi,\pi,N)/N$:

$$\Sigma(1,\pi,\pi,N)/N \quad \stackrel{N\to\infty}{\longrightarrow} \quad A\ln\frac{N}{N_0} \tag{5.58}$$

(see r.h.s. of Fig. 5.12; $A = 0.0542(5)$, $N_0 = 4.853(6)$) to

$$\Sigma(1,p,\pi,N) \quad \stackrel{p\to\pi}{\longrightarrow} \quad \frac{-A}{1-p/\pi}\,. \tag{5.59}$$

The latte prediction is supported by a finite-size scaling analysis whose results are additionally shown in Fig. 5.12 (l.h.s.). The controlled behaviour (smallness) of finite-size effects of $\Sigma(1,p,\pi,N)$ for momenta p away from the singularity ($p=\pi$) allows the discussion of a combined limit:

$$p\to\pi, \qquad N\to\infty, \qquad z\equiv(1-p/\pi)\cdot N \quad \text{fixed} \tag{5.60}$$

leading to the scaling ansatz

$$\Sigma(1,p,\pi,N) \quad = \quad \Sigma(1,p,\pi,\infty)\cdot G(z)\,. \tag{5.61}$$

Similar ansatzes had earlier been used for the study of the singular behaviour of static structure factors of Heisenberg chains [127, 128]. Here, the application of scaling ansatz 5.61 to the determination of the solid points ($N = 16, 20, .., 56$, $z = 4$) in the left.-hand part of the figure uses

$$\Sigma(1,p,\pi,2N) = \frac{G(4)}{G(2)}\cdot\Sigma(1,p,\pi,N) \quad ; \quad \frac{G(4)}{G(2)} = \frac{\Sigma(1,p,\pi,2N')}{\Sigma(1,p,\pi,N')} \tag{5.62}$$
$$p = \pi - \frac{2\pi}{N} \qquad .$$

The weak "N-dependence" of $G(4)/G(2)$ as well as its extrapolated $N\to\infty$ limit are illustrated in Table 5.4. The obtained scaling result is already close to the predicted behaviour 5.59.

$2N$	$\Sigma(1,z=4,\pi,2N)$	N	$\Sigma(1,z=2,\pi,N)$	$\frac{\Sigma(1,z=4,\pi,2N)}{\Sigma(1,z=2,\pi,N)} \rightsquigarrow \frac{G(4)}{G(2)}$
16	-0.10552295	8	-0.12983263	0.81276142
20	-0.15869572	10	-0.19882874	0.79815282
24	-0.21198842	12	-0.27062879	0.78331807
28	-0.26698573	14	-0.34482702	0.77425988
BST extrapolation:				**0.76560**

Table 5.4: Remaining N-dependence of the scaling coefficient $G(4)/G(2)$; BST(see App. C)-extrapolation value

The obtained singularity 5.59 finally yields the leading contribution to the investigated derivative of $m^2_{stagg.}(\Theta)$ at $\Theta = 1$:

$$\left.\frac{d}{d\Theta}m^2_{stagg.}\right|_{\Theta=1} \quad \stackrel{N\to\infty}{\longrightarrow} \quad -\frac{A}{2}\ln N\,, \tag{5.63}$$

i.e. meaning that the turning away from the 1-dimensional ($m_{stagg.} = 0$) behaviour takes place at $\Theta = 0^+$. It is important to recapitulate that the use of the (rigorous) sum rule 5.57 decisively enforced the latter result. Finite-size evaluations of the derivative of $m^2_{stagg.}(\Theta)$ alone –as well discussed in [83]– would under no circumstances have been sufficient to reach this result.

The latter remark might help to elucidate the ongoing and still unsettled discussion (see above) concerning the starting point (size of the lateral couplings) of a non-zero staggered magnetization. The result of the above briefly sketched study strongly favours the exceptional situation of the truely 1-dimensional spin chain ($\Theta = 1$).
We finally want to add some errata not impairing the general result to [83]: 1. a missing prefactor 1/2 on the r.h.s. of Eq. (3.5); 2. a mis-typed y-label in FIG. 1 of the publication (compare Fig. 5.12); N_0 given in Eq. (3.11) should be read as N_0^A; 3. the matrix elements given in Table 1 have to be doubled to give values consistent with prior definitions.

5.4.3 Opening investigation of formations of magnetization plateaus in two dimensions

In this final paragraph of the present work some preliminary aspects, forming in part the basis or starting point of a current investigation, shall be discussed. In Sec. 5.3 we applied the original argument of Lieb, Schultz and Mattis [143] to certain spin chains/systems with long range interactions. In case of n_l-leg ladders we arrived at the quantitzation rules [168] for the occurrence of magnetization plateaus requiring a complete loss of degeneracy, i.e. $p_j - p_0 = n \cdot 2\pi$ for the momentum p_j of the obtained state $U(k(j))|0>$.
Subsequently, we obtained for the Hamiltonian $H_{hel.}(\alpha)$ (5.44) the following condition to hold for the existence of a soft mode in the sense of LSM:

$$\alpha \;=\; -\frac{1}{2} \cdot \frac{< H_1^{\perp} > + < H_k^{\perp} >}{< H_{k-1}^{\perp} > + < H_{k+1}^{\perp} >} \equiv -\frac{1}{2} \cdot \frac{f_{1,k}}{f_{k-1,k+1}} \,. \tag{5.64}$$

In the following we will give some first discussion of the meaning of the latter equation and numerical data will be presented that indicate the non-existence of a solution. We will not, however, proceed at this place to further investigations on the existence and nature of soft modes at the ends of magnetization plateaus. The latter will be left to a future publication [160].

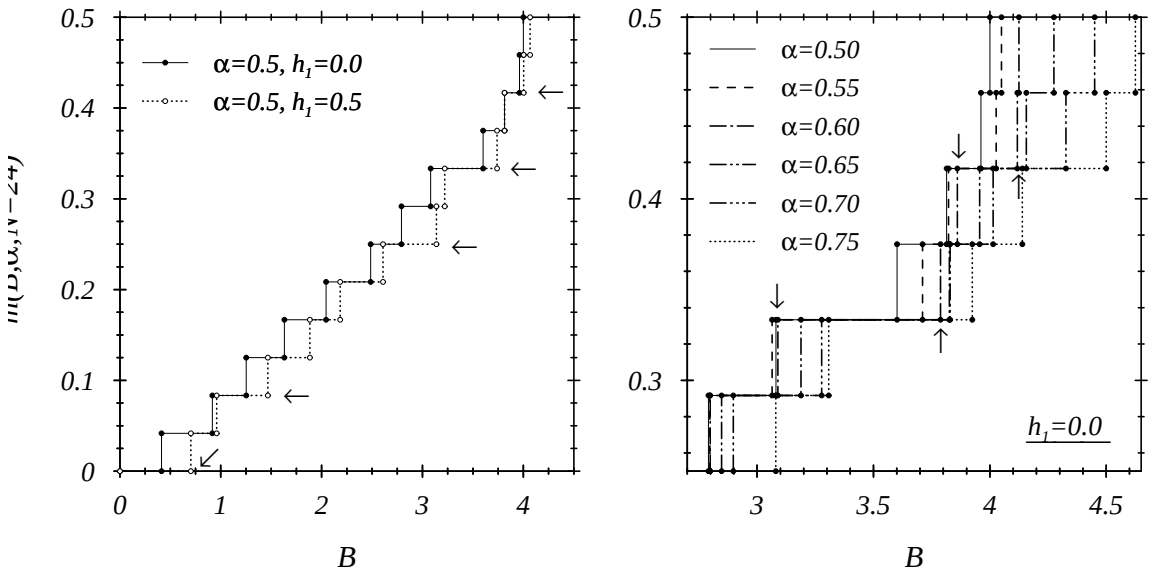

Figure 5.13: Magnetization curves for $N = 5^2 - 1 = 24$ ($k = 5$), $\alpha = 0.5$ and periodic perturbations $h_1 = 0$, 0.5 (l.h.s.) as well as different α, $h_1 = 0$ for $m = 1/3$, 5/12 (r.h.s.)

Considering first the shape of magnetization curves of systems described by Hamiltonian $H_{hel.}(\alpha, k)$ (5.44), a frustration value $\alpha = 0.5$ has been chosen guided by earlier investigations of $4 \times 4-$,

$6 \times 6-$ square lattices (*Schulz et al.* [183, 184]), as well as helical spin lattices (*Yang, Mütter* [221]). The l.h.s. of Fig. 5.13 shows the total magnetization curve –$\alpha = 0.5$, $N = 24$, helical boundary conditions– for both the translation invariant Hamiltonian 5.44 as well as a "uniaxially" perturbed system:

$$H = H_{hel.}(\alpha, k) + h_1 \cdot H_1(\pi) \tag{5.65}$$

$$H_1(\pi) = 2 \sum_n e^{i\pi n} \mathbf{S}_n \mathbf{S}_{n+1} \,. \tag{5.66}$$

The latter magnetization curve –evaluated for $h_1 = 0.5$– has been empirically used to guide first estimates on the position of possible magnetization plateaus (see arrows). The small number of system sizes that can be treated numerically offers scarce possibility for the kind of extrapolations used for one-dimensional systems. Evaluations of helical $k = 7$ ($N = 48$) systems are confined to rather large m. Due to the long coupling ranges, DMRG calculations are limited to similar system sizes and the finite-size behaviour of their different boundary conditions still has to be classified.

The r.h.s. of Fig. 5.13 moreover shows the α-dependence for the two highest plateau candidates ($m = 1/3,\ 5/12$) for a range of frustrations $\alpha = 0.5,\ 0.55,\ \ldots,\ 0.75$ of the translation invariant $N = 24$ ($k = 5$) lattice. For the used discretization of α the magnetization step at $m = 1/3$ appears broadest for $\alpha = 0.6$. The same α value only leads to a relative maximum of the step width at $m = 5/12 = 0.41\overline{6}$. Further increase in α leads to a further increase of the saturation field $B(m = 1/2, \alpha, k) = B_{sat.}(\alpha, k)$ starting from $B_{sat.} = 4$ for $\alpha \leq 0.5$.

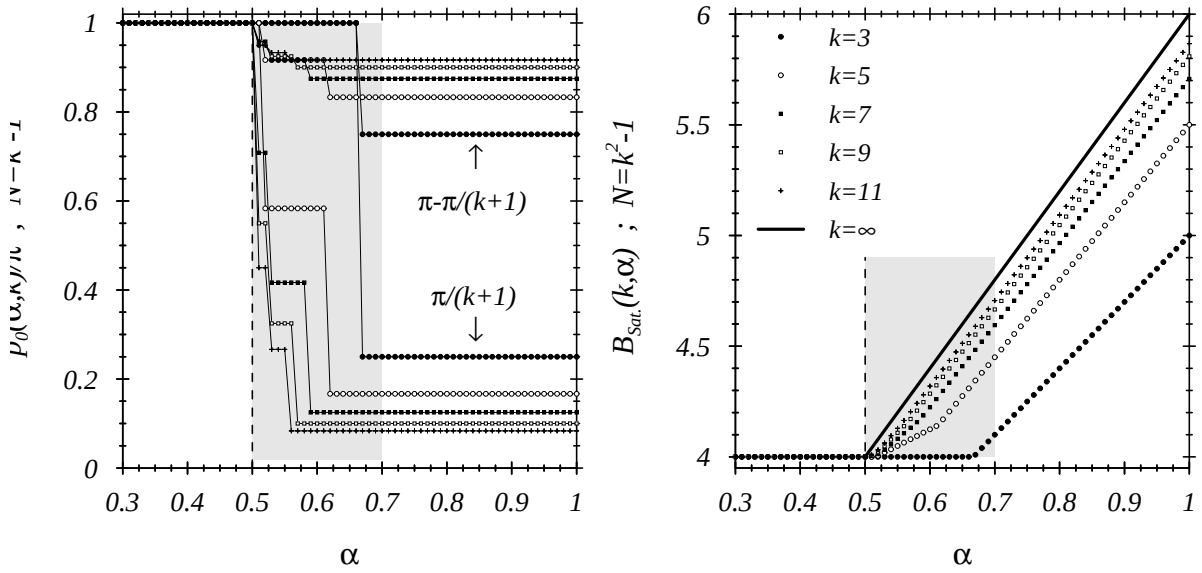

Figure 5.14: Minimum position $p = p_0(k, \alpha)$ of $E_0(S_z = N/2 - 1, p; \alpha, k)$ and saturation field $B_{Sat}(\alpha, k)$ for $H_{hel.}(\alpha, k)$, $N = k^2 - 1$

An analytical evaluation of the saturation field $B_{Sat}(\alpha, k)$ –cf. App. B– leads to

$$\begin{aligned} B_{Sat}(\alpha, k) &= \frac{1}{2} \max_p \Big[E_0(S_z = N/2; \alpha, k) - E_0(S_z = N/2 - 1, p; \alpha, k) \Big] \\ &= 2(1 + \alpha) - \cos p_0 - \cos k p_0 - 2\alpha \cos k p_0 \cos p_0 \,. \end{aligned} \tag{5.67}$$

Fig. 5.14 shows the α- and N-dependence of the maximum value p_0 and the respective $B_{Sat}(\alpha, k)$ for systems $N = k^2 - 1$. The shaded region ($0.5 \leq \alpha \lesssim 0.7$) denotes a cross-over region for the change $p_0 = \pi$ ($\alpha < 0.5$) $\rightarrow$ $p_0 = 0; \pi$ ($\alpha > 0.5$). The width shrinks for increasing N and

disappears in the TDL. The thick solid line on the r.h.s. of the figure gives the $k \to \infty$ result of B_{Sat} for $N = k^2 \pm 1$. $N = k^2 + 1$ gives similar finite-k results for $p_0(\alpha, k)$ with $\pi \cdot (k+1)/N$ instead of $\pi/(k+1)$ for $\alpha \gtrsim 0.7$.

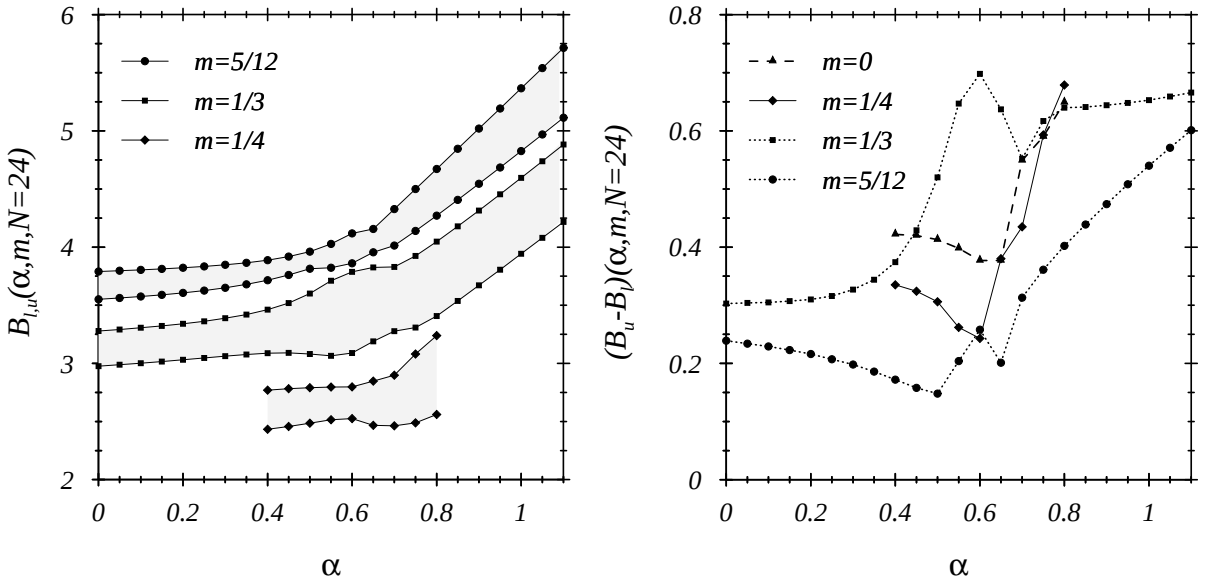

Figure 5.15: Magnetization step boundaries and widths at $m = 0, 1/4, 1/3, 5/12$ for a 24-site ($k = 5$) system and varying frustrations α

The type of cross-over may be compared with the findings of Schulz an Ziman [183] for frustrated Heisenberg models in two dimensions. Finite-size analyses on 4×4 and 6×6 lattices ($m = 0$) resulted in the existence of an intermediate phase without magnetic long-range order (LRO) for $0.4 < \alpha < 0.65$ between an ordered phase ($\alpha < 0.4$, $\vec{p} = (\pi, \pi)$) and a collinear phase ($\alpha \gtrsim 0.65$, $\vec{p} = (0, \pi)$, $(\pi, 0)$). Though the width of the cross-over region in the helical one-magnon case disappears in the TDL, the ground state momenta for the two remaining regimes resemble the respective results of [183].

We further present in Fig. 5.15 a combined overview of the α-dependence of the $m = 0$, $1/4$, $1/3$, $5/12$ magnetization step widths for a $N = 5^2 - 1$ helical spin system. Both, the step widths for $m = 1/3$ and $m = 5/12$ show a relative maximum at $\alpha \simeq 0.6$. Further studies concentrate on additional characteristica capable of providing information on level crossings, symmetry breaking and plateau formation. Two elements of such studies are given by static longitudinal and transverse structure factors as well as frequency moments (cf. Sec. 2.6.6) of dynamical structure factors. The first frequency moment is e.g. related to the first derivative $d\,E_0(\alpha)/d\alpha$ and further moments are to be considered to check for peculiarities of the spectral width when crossing a potential plateau value of α. First studies of static structure factors already resulted in significant changes for the courses of the $p = \pi$ and $p = \pi/6$ components (the helical $k = 5$ analogues of the quadratic LRO (π, π)- and collinear $(\pi, 0)$-,$(0, \pi)$-phases). We will not follow these investigations any further at this place.

We however finally turn to the condition given by Eq. 5.64 and present results for $N = 24$ and various m in Fig. 5.16 as well as a comparison of $N = 24, 48$ (helical) and $N = 36$ (square lattice) results for $m = 5/12$ –the latter allowing for a basic assessment of finite-size and boundary effects.

First it appears that the given data indicate the existence of a solution of Eq. 5.43 (crossing of the dashed line (l.h.s.) or zero (r.h.s.) in Figs. 5.16, 5.17) in no conclusive way. Increasing deviations occur for decreasing m.

The two different helical spin systems ($k = 5, 7$) compared for $m = 5/12$ do not give evidence for

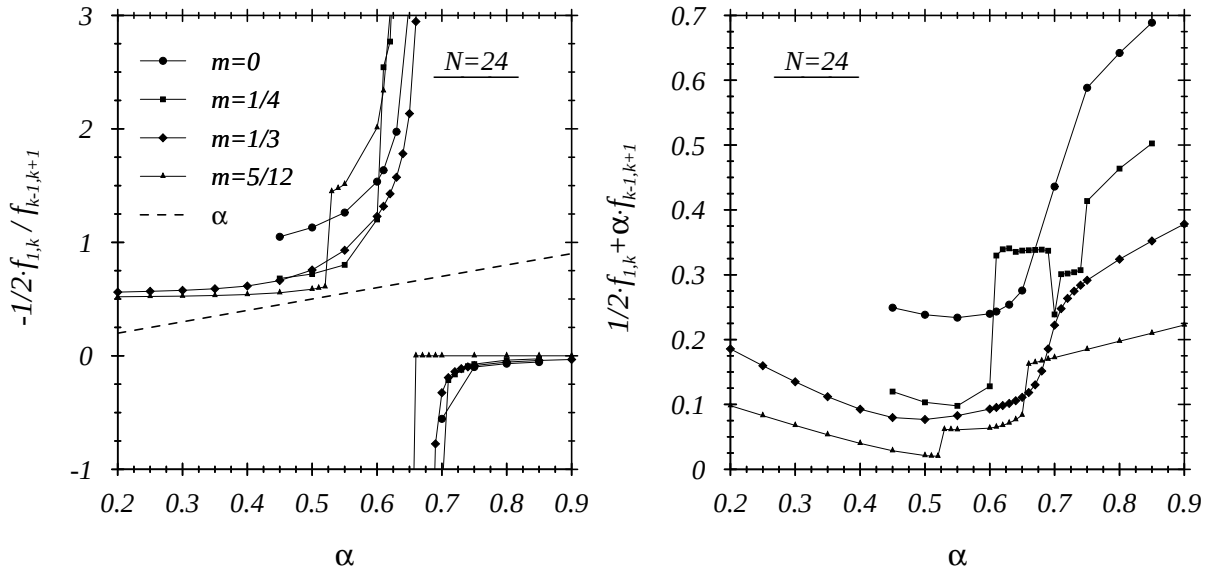

Figure 5.16: $f_{1,k}/f_{k-1,k+1}$ and $f_{1,k} + \alpha \cdot f_{k-1,k+1}$ for the helical $N = 24$ ($k = 5$) system; $m = 0, 1/4, 1/3, 5/12$

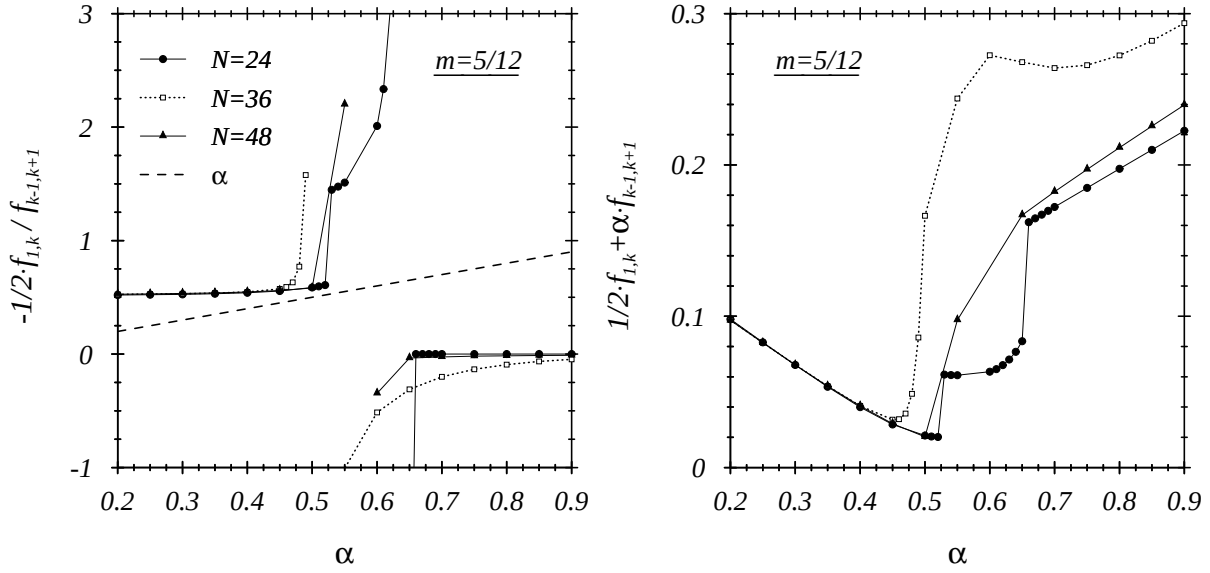

Figure 5.17: $f_{1,k}/f_{k-1,k+1}$ and $f_{1,k} + \alpha \cdot f_{k-1,k+1}$ for helical ($k = 5, 7$) sytems at $m = 5/12$; in addition: quadratic 6×6-lattice

finite-size effects closing the remaining gaps. Similar evaluations for the 6×6 spin lattice –though not directly addressed by the evaluations leading to 5.43– almost lead to identical behaviour of the shown coefficients for $\alpha \lesssim 0.4$. All shown data have in common an almost linear behaviour for $\alpha \lesssim 0.4..0.5$ and $\alpha \gtrsim 0.6$, again pointing to the phases obtained by Schulz and Ziman.
At this place we will not further continue the presented start of a study that not only concentrates on magnetization plateaus in two-dimensional spin systems but quite generally addresses DOS and soft mode phenomena at the edges of forming plateaus [160] that will possibly help to address and explain a manifold of newer experiments on the magnetization of approximately 2-dimensional spin-1/2 antiferromagnets.

Chapter 6

Summary, conclusions and outlook

In the present work we investigated and discussed the behavior of ground states of antiferromagnetic spin-1/2 Heisenberg systems under the influence of periodic or translation invariant external fields and perturbations. Mostly the corresponding field- or perturbation-terms have been added to the symmetric, translation invariant Hamiltonian of the antiferromagnetic Heisenberg chain and their particular impact on excitation energies and matrix elements were studied. A point of major importance was the investigation and classification of magnetization plateaus and their relation to level crossings, symmetry changes or spontaneously broken symmetries.

The guiding importance of the unperturbed Heisenberg chain has been particularly emphasized by the extended introductory discussion in **Chapter 2**. Special attention has been laid on the criticality, i.e. the existence of zero-energy excitations (*soft modes*), of the unperturbed chain which is getting manifest in a singular behaviour of static and dynamic correlation functions (structure factors) at the well-defined positions (momenta) of the soft modes. Particular emphasis was given to a proof of the existence of soft modes in the antiferromagnetic Heisenberg chain by *Lieb, Schultz, Mattis* [143] in 1961. The general idea and technique of the respective proof reappeared in different parts of the work and has been used in discussions of eventual formations of magnetization plateaus in differently perturbed spin systems.
Furthermore, an informal discussion of applications of *Conformal Field Theory* (CFT) to the approximate determination of critical exponents of correlation functions based on numerical evaluations of finite spin systems has been given and different models/approximations for the dynamical structure factor of the Heisenberg chain at zero magnetization have been reviewed.
In the remaining part of the chapter, the concept of frequency-moments and related sum rules [116, 158] has been discussed. Their technical importance was exemplarily presented for the valuation of ansatzes for the dynamical structure factor (at zero magnetization [158, 80, 132]) and in addition the application of frequency-moments in cases of non-zero magnetization has been introduced.
Finally, the important aspect of evaluation and extrapolation of magnetization curves shall not remain unmentioned. While Chapter 2 only addresses the topic of smooth magnetization curves of the isotropic Heisenberg chain –as well as the introduction of the important *Bonner and Fisher* [32] technique to obtain rather smooth finite-N magnetization curves–, subsequent chapters and appendices apply and explain extrapolation schemes neccessary for the manifestation of finite remaining step widths (plateaus) in the thermodynamic limit (number of spins $N \to \infty$).
For further details and publications concerning this and the following chapters the reader is generally referred to the respective chapters.

Turning away from the isotropic spin-1/2 chain, **Chapter 3** introduced several classes of perturbations (periodic tranverse or longitudinal fields, additional periodic dimer-like Hamiltonians,...) perturbing the initial Heisenberg chain with a strength h. The response of the Heisenberg chain with respect to such perturbations, i.e. the changes of excitation energies and transition ma-

trix elements, was shown to be governed by a complete, however complicate, set of differential equations, the so-called *evolution equations*.

In this work the study of periodic perturbations concentrated on the most susceptible effect, namely the correspondence of the wave number (vector) of the perturbation and the location of the soft mode(s) of the unperturbed chain. The dominant and clearest detectable effect that may arise in such cases is the loss of criticality, i.e. the opening of a gap in the excitation spectrum.

The latter effect, as well as the behaviour of related energies and matrix elements, has first been studied for several types of perturbations in the limit of small perturbation strengths h. Exemplarily, the existence of a scaling solution consistently fulfilling the general set of differential equations could be shown [84] and provided with good numerical evidence. The particular scaling limit allows –in leading order– the determination of the x^{α_i}-dependence (scaling variable $x = Nh^{\epsilon}$) of essential quantities (gap, lowest excitations,..). It is important to note that the interrelation to the exact evolution equations (logarithmic corrections of the initial conditions had to be omitted) results in *non-perturbative*, non-integer exponents for perturbation strength h and system length N. Comparisons with different predictions/determinations (e.g. CFT) were performed and partially good correspondence was achieved. The lacking consideration of logarithmic or other non-algebraic corrections, however, makes a similar discussion connecting evolution equations and scaling solutions in more advanced cases where the neglect of these contributions no longer seems tenable impracticable.

It should be added that the unperturbed chain not only establishes the initial conditions for the description of the perturbed system. The exponent describing the opening of the respective energy gap can furthermore be traced back to the critical η-exponents of the static structure factors of the unperturbed chain.

A number of periodic perturbations and some of their combinations were investigated before the range of description was opened to include a field of broader current interest: the formation of magnetization plateaus in various and in particular ladder-type spin systems. Magnetization plateaus are an unambiguous fingerprint of the opening of a gap in the formerly continuous spectrum of the unperturbed Heisenberg system. As a preparation of the detailed discussion of plateaus in Chapter 4, different ladder types and the ambiguities for mappings of these structures on one-dimensional spin chains –a unifying concept of description– have been discussed. Furthermore, the magnetic spin-Peierls Hamiltonian i.e. without phononic parts has been introduced as an example of a periodically perturbed spin-1/2 chain.

The presented Hamiltonians for regular ladders with n_l legs in particular showed the interesting dichotomy of either representing the system by a translation or non-translation invariant Hamiltonian. The related aspect of a spontaneous breaking of symmetry was addressed in subsequent chapters.

Chapter 4 has been devoted to the analysis of magnetization plateaus in periodically perturbed spin-1/2 chains. The investigation covered the basic types of perturbations formerly discussed in the framework of small perturbations in Chapter 3 as well as the different types of ladders introduced there. Infinite-N extrapolations of the finite system evaluations of magnetization curves were performed (BST extrapolations; discussion and examples see App. C) and the obtained plateaus were shown to be covered by both the quantization rule of *Oshikawa, Yamanaka and Affleck* (OYA) [168, 169] and a further soft mode approach [85, 86] presented in this work. The latter approach is based on the immediate correspondence of a soft mode position $q^{(k)}(m)$ of the unperturbed chain and the q-value of the considered perturbation. In most of the considered cases the longitudinal soft modes of the Heisenberg chain proved to be adequate for the prediction of the magnetizations of possible plateaus.

In particular, the presented scheme for plateau predictions –based on a short-range ladder representation with periodically perturbed couplings [86]– directly leads to the basic difference of

ladders with even and odd numbers of legs: As discussed by *Dagotto and Rice* [58] for the first time, even-leg spin-1/2 ladders show a magnetization plateau at zero magnetization ($m = 0$). Investigations showed that perturbation components with $q_{pert.} = \pi$ –only occurring in even-leg ladders– are responsible for this particular gap/plateau. A similar perturbation is e.g. present in the spin-Peierls chain (see Sec. 4.1.5) equally leading to a plateau formation at $m = 0$ for non-zero perturbations.

In the course of the chapter different variants and courses of plateau formations were studied: (a) immediate opening of a gap/plateau with beginning perturbation, (b) finite threshold value h_c for (observable) plateau, (c) requirement of additional (translationally invariant) coupling. The different types of plateaus were classified with respect to the order of the soft mode required for the prediction in the latter approach. The cases (b) and (c) were shown to be cases that need the occurrence of a spontaneous symmetry breaking prior to the plateau formation – again in accordance to OYA.

This chapter as well gave examples for the behaviour of ground state energies and their (2nd) derivatives in and around situations of plateau formation. Examples for the spin-Peierls chain with zero and non-zero frustration in particular underlined the importance of level crossings for a plateau formation. Extrapolations for larger N (Fig. 4.30) showed the opening of a $m = 1/4$-plateau for the spin-Peierls system beginning at frustrations $\alpha \simeq 0.25$ in accord with *Totsuka's* [200] $\alpha_{threshold} = \alpha_c = 0.2411\ldots$. Perturbation expansions for the $m = 0$, small α case later served as orientation for the discussion of translationally invariant 2-leg ladders.

The discussion of ladder systems furthermore contained studies of various combinations of anti- and ferromagnetic rung and leg couplings. While the change to ferromagnetic leg couplings (antiferromagnetic rungs) led to the occurrence of a spontaneous magnetization for ladders with an odd number of legs [216] other plateau features for both odd and even leg numbers proved to be remarkably stable in their occurrence. An equally continuous appearing phenomenon was shown for the ground state energies per site that formed to good approximation singular crossing points ($m = m_x$) for arbitrary rung couplings, J_{leg} fixed. The latter phenomenon was described using the approximately linear behaviour of the magnetization curve $m(B)$ in the regime of m_x close to $m = 1/2$ as earlier exemplified for the unperturbed Heisenberg chain in Sec. 2.4. Correspondingly, we gave some discussion of the basics of a variational ansatz that had been used earlier [216] for an explanation of the crossing phenomenon.

Furthermore, the discussion of magnetization curves of ladder systems repeatedly referred to results contributed by applications of the Density Matrix Renormalization Group (DMRG) technique [212, 214, 218] (the latter performed by R. M. Wießner [216, 217]). This technique allows the approximate treatment of spin systems up to ($O(10)$) larger than those accessible by Lanczos diagonalizations. Since the used DMRG technique affords the employment of a different kind of boundary conditions for the treated chains (open instead of periodic ones), the presentations of DMRG results have at the same time been used for a comparison of the effects of the changed boundary conditions – an inappropriate change that in the given context is only determined by its function. The application of this numerical technique on spin systems that are intimately related (in their unperturbed state) to critical Heisenberg chains consequently affords the DMRG data being obtained from sufficiently large systems keeping the influence of the open ends of controllable/negligible size. We therefore contrasted in Secs. 4.1.2-4.1.4 standard Lanczos evaluations applying periodic boundary conditions to the investigated spin chains or ladders with those of DMRG using open chain or leg boundary conditions. The comparisons clearly showed the expected higher suitability and better convergence of calculations with periodic boundary conditions. Periodic chains or ladder systems of up to 24 sites not only proved to show all the plateaus given by DMRG applications, their respective finite-size behaviour turned out to be superior to that of open ended systems of up to quadruple length. In one of the given comparisons (Kagomé-like 3-leg ladder) evaluations with periodic boundary conditions for the first time allowed for a definite identification of secondary plateaus (cf. Secs.

4.1.3, 4.1.4). The given Lanczos evaluations should in any case be used as a support for the interpretion and classification of DMRG results in cases of complex problems (e.g. multi-leg ladders, spin $S > 1/2$, ...) that do no longer allow for finite-size analyses of Lanczos or similar results.

We then proposed an opportunity to overcome the mere status of predictability of magnetization plateaus in a consideration of correlation functions for a variety of earlier discussed cases of plateau formation. Static spin and dimer structure factors were –for *all* considered cases– shown to develope significant increases at soft mode positions related to observed plateaus while the maxima at the uninvolved former soft modes remained almost unchanged. It is important to recapitulate that not the very extremum of static structure factors of the unperturbed chain at a soft mode position already gives reliable information about plateau formation but the study of its behaviour under the influence of the perturbation.

Finally we presented a comparison of the two discussed and applied plateau prediction schemes (OYA, soft mode approach). The OYA quantization rule was shown to give a higher number of possible plateau magnetizations, however, no example or counterexample could be given for a possible distinction of the predictive powers of both schemes.

In **Chapter 5** the investigation switched to spin systems with translationally invariant perturbations. At the beginning, two well known examples of "translationally invariant perturbed" spin-1/2 chains –the XXZ chain and chains *frustrated* by next-to-nearest neighbour interactions– have been introduced emphasizing the different (compared with periodically perturbed chains) algebraic behaviour of certain characteristic quantities. The opening of a gap beginning at finite frustration values $\alpha = J_2/J_1$, however, should not be considered characteristic and exclusively present for this type of perturbation – note e.g. the opening behaviour of the $m = 1/4$ plateau for the periodic perturbation $D_2(\pi)$ (Fig. 4.5). The unifying aspect, instead, may be seen in the assessed soft mode ($k = 2$) for both cases, i.e. showing a link between secondary soft modes for a periodic perturbation and the $k = 2$ needed for the description of the spontaneous symmetry breaking leading to a $m = 0$ plateau for the translation invariant system.

The consideration then turned to the earlier mentioned dichometry arising from the capriciousness of choosing periodic or translationally invariant perturbations for the representation of the same spin ladder. For 2-leg ladders, the ambivalence of both types of description was shown in detail. The equally discussed 3-leg ladder had no immediate counterpart in the 3-leg ladders discussed in Chapter 4 where different rung boundary conditions had been considered. Both, the 2-leg and 3-leg ladders showed clearly formed plateaus at $m = 0$, $m = 1/6$ respectively, for $J_{rung} \gtrsim J_{leg}$, whereas plateaus at $m = 1/4$ ($m = 1/3$ respectively) were unobservable. The latter phenomenon again was in accord with earlier findings for the respective systems with periodic perturbations. BST extrapolations for plateau widths of the first group of plateaus and weak rung couplings, however, did not allow for any conclusive statements.

In the following, an application of the scaling treatment –given in Secs. 3.2.3, 3.2.4– to the situation of weakly and translationally invariant coupled chains (legs) was touched on. The change at the situation of initial conditions for the evolution equations (Secs. 3.2-3.2.2) and the different behaviour of "perturbed" systems was discussed for the example of a 2-leg ladder. Satisfactory scaling solutions (e.g. for a possible gap or plateau) have not been obtained until now and a definite description therefore had to be left open. The general practicability of a scaling treatment of the earlier described form (longitudinal perturbation $\sim S_3(\pi)$) for more advanced and complicate situations is questionable.

The remaining part of the chapter treated –or supplied preparations for the following treatment– physical aspects of more than one-dimensional Heisenberg antiferromagnets. The concept of spin systems with helical boundary conditions was recapitulated and used as an approximate description of two-dimensional spin systems. Before, the existence of long-range spin couplings –arising in the prior ladder parameterizations and as well in the helical spin Hamiltonians–

have been analyzed following the outlines of the original *Lieb, Schultz, Mattis* theorem [143] addressing the existence of soft modes in Heisenberg antiferromagnets. The latter consideration on one hand reproduced (no solid rigorousity was intended nor obtained) the earlier given plateau quantization rules ([168]) for spin ladders, on the other hand resulted in a particular condition for the ratio (α) of diagonal and orthogonal coupling strengths of the considered spin lattice.

Before finally turning to a potential decision on the existence of a solution for the latter condition, a further application of helical boundary conditions, namely the determination of the onset of a non-zero staggered magnetization of laterally coupled isolated chains, was given ([83]). The exploitation of a rigorous sum rule (energy conservation rule) allowed to delimit/overcome certain finite-size effects to locate the mentioned onset immediately at the one-dimensional chain expressing its exceptional situation in the dimensionality of Heisenberg spin systems. As was already set out in Sec. 5.4.2, the latter position is not generally accepted.

The following and initial discussion of magnetization plateaus in frustrated two-dimensional spin systems –mainly the helical approximation of square lattices– has essentially been limited to Lanczos diagonalizations of $N = 24$ spins ($k = 5$, see Sec. 5.4.1) covering the whole range of magnetizations $0 \leq m \leq 1/2$ and smaller manageable regimes of m (below saturation $m = 1/2$) for the larger helical $k = 7$ ($N = 48$) and the quadratic $N = 6 \times 6$ system. The presented considerations have not been intended to represent solid arguments concerning the existence of plateaus but offer first indications. The given sequences of magnetization curves for the helical $N = 24$ system at varying frustrations resulted in characteristic α-dependences of magnetization step widths for selected values of m. Beforehand, the latter selection had been given additional support by considering the influence of a periodic perturbation of the spin coupling in x-direction of the spin lattice. The most susceptible points (frustration values) for the step widths of the translationally invariant system turned out to be at $\alpha \simeq 0.6$. Referring to the earlier investigation of quadratic spin systems (*Schulz an Ziman* [183]), this α-value coincides with the cross-over region between two ordered phases of the frustrated lattice: $|\vec{p}_0 = (\pi, \pi)| \ldots |\vec{p}_0 = (0, \pi), (\pi, 0)\,|$. Such a change of symmetry forms an important characteristic for the process of plateau formation.

The following discussion of the particular α-condition originating from the LSM application to systems with helical boundary conditions showed that the condition was unrealizable for any m well apart from $m = 1/2$. The shown approach of the required zero (see Sec. 5.4.3) with increasing m is consistent with the obtainable existence of a solution in the one-magnon ($S_z = N/2-1$) sector. Evaluations for $N = 48$ spins in addition widely excluded finite-size effects responsible for the observed unrealizability of the condition. Furthermore, evaluations for the quadratic 6×6-lattice resulted in good correspondence for small frustrations and comparable behaviour for large α. Although they did not provide solutions for the remaining $m < 1/2-1/N$, the corresponding evaluations again showed the existence of a cross-over regime –around $\alpha = 0.6$– between two well-behaved regimes.

The incomplete status of the latter paragraph directly leads up to the first part of the **Outlook** addressing ongoing and intended further projects following the sequence of investigations described in the presented work.

At present, further evaluations of longitudinal and transverse static structure factors and respective frequency-moments are being performed and the smaller 4×4-lattice is to be included in further studies. In particular, the non-monotonic α-dependence of lower and upper boundaries of the described magnetization steps (again for $\alpha \simeq 0.6$) will be investigated. Moreover, it remains to be decided to further enlist the support of DMRG calculations. They at least provide evaluations of all magnetization sectors

The behaviour of magnetization curves close to plateaus (e.g. the algebraic dependence $m \sim |B - B_{l,u}|^{1/n}$ at the plateau boundaries) has not been particularly emphasized in this work. Investigations close to B_{Sat} (*Schmidt et al.* [178]) resulted in a different exponent n for α

approaching $\alpha = 0.5$ (*Majumdar-Gosh point* [148, 149]) in a frustrated chain (different n for $\alpha \neq 0.5$ ($n = 2$) and $\alpha = 0.5$ ($n = 4$)) and *Cabra et al.* [39] gave an analytical treatment of one- and two-spin wave excitations for the transition to saturation for 2-leg zig-zag ladders. Respective *Taylor* expansions clearly relate changes of n to the discontinuation of particular components. General considerations of the analytical behaviour of magnetization functions in the surroundings of plateaus mark a further intention.
It further appears that there still remains a certain need of clarification of the nature of soft modes. This as well rises the problem of classification of certain measured (susceptibility) singularities as e.g. the assignment of transverse soft modes (cf. e.g. Figs. 4.7, 4.40 and related discussion) in the described soft mode approach.
It then remains the possibility of leaving the field of spin-1/2 Heisenberg systems and extend the performed investigations to spin models with higher spin and/or include itinerant fermion models like $t-J$ or Hubbard systems (see e.g. [16]). Such models offer the possibility to discuss plateau formations in chemical potentials. It has to be taken into account, however, that the preparation of the needed critical initial systems can considerably narrow down the parameter space of these systems.
The fractional character of systems showing magnetization plateaus finally brought the physics of quantum-Hall systems closer to the physics of one-dimensional quantum phenomena. The question arose whether suitably chosen one-dimensional systems –e.g. Hubbard chains– do allow for a qualitative mapping of certain characteristics of quantum-Hall systems (see e.g. [76]). A discussion of these aspects will of course afford the prior study of the before-mentioned classes of (spin) systems.

Appendix A

The recursion method

A.1 Description of the method

In the following a numerical technique is described that is used to evaluate products of matrix elements of type

$$f_{BA}(q,n) \;=\; <0|B^{+}(q)|n><n|A(q)|0>$$

and as well the related energy differences $\omega_{0n} \equiv \omega_n = E_n - E_0$ approximately. Hereby, $|0>$ and $|n>$ denote the ground state and excited states (n) of a given spin Hamiltonian of a translation invariant N-site system.
First, the case $B = A$ that is required for the calculation of DSF-components $f_{AA}(q,n,N)$ of

$$f_{AA}(q,\omega,N) \;=\; \sum_n \underbrace{|<n|A(q,N)|0>|^2}_{f_{AA}(q,n,N)} \cdot \delta(\omega - \underbrace{(E_n(q,N) - E_0(q_0,N))}_{\omega_n(q,N)}) \tag{A.1}$$

will be considered. For simplicity the variables q, N will not be given explicitely. The Laplace transform of $f_{AA}(\omega)$ reads

$$f_{AA}(\tau) \;=\; \sum_n e^{-\omega_n \tau} |<n|A|0>|^2 \tag{A.2}$$

$$\;=\; <0|A^{+} e^{-(H-E_0)\tau} A|0> \equiv <f_0|f(\tau)> \tag{A.3}$$

with $|f_0> = A|0>$ and $|f(\tau)>$ fulfilling

$$\frac{\partial}{\partial \tau}|f(\tau)> \;=\; -\bar{H}|f(\tau)> \qquad (\bar{H} \,=\, H - E_0). \tag{A.4}$$

Now, a Gram-Schmidt construction is used (see also [207]) to form an orthogonal set of states $\{|f_k>\}$, namely

$$|f_{k+1}> \;=\; \bar{H}|f_k> - a_k|f_k> - b_k^2|f_{k-1}> \tag{A.5}$$

$$a_k = <f_k|\bar{H}|f_k> / <f_k|f_k> \quad ; \quad k = 0,1,2,..,L-1 \tag{A.6}$$

$$b_k^2 = <f_k|f_k> / <f_{k-1}|f_{k-1}> \quad ; \quad k = 1,2,..,L-1 \quad , \; b_0^2 \equiv 0 \tag{A.7}$$

and $|f(\tau)>$ is given by

$$|f(\tau)> \;=\; \sum_{k=0}^{L-1} D_k(\tau)|f_k> . \tag{A.8}$$

L denotes the dimension of the Hilbert sub-space, i.e. the number of states $|n>$ leading to nonzero matrix elements $<n|A|0>$. The upper differential equation leads to

$$\sum_k \dot{D}_k(\tau)|f_k> \;=\; -\sum_k D_k(\tau)\Big\{|f_{k+1}> + a_k|f_k> + b_k^2|f_{k-1}>\Big\} \tag{A.9}$$

or in matrix notation $\dot{\vec{\mathbf{D}}} = -\mathbf{M}\vec{\mathbf{D}}$ with $\mathbf{M}$ being a tridiagonal (non-symmetric!) $L \times L$-matrix with eigenvalues ω_n and eigenvectors $\vec{e}_n$. The eigensolutions $v_k(\tau)$ of the set of linear differential equations read $v_k(\tau) = v_k^0 e^{-\omega_k \tau}$ leading to

$$D_k(\tau) \;=\; \sum_n (\vec{e}_n)_k v_n^0 e^{-\omega_n \tau}. \tag{A.10}$$

Here, the v_k^0 are given by the initial condition $\vec{\mathbf{D}}(\tau = 0) = (1, 0, 0, ..., 0)^T$ yielding for $f_{AA}(\tau)$

$$f_{AA}(\tau) = D_0(\tau) < f_0|f_0> \;=\; \sum_n e^{-\omega_n \tau} v_n^0 (\vec{e}_n)_0 < f_0|f_0> \tag{A.11}$$

i.e. $|<n|A|0>|^2 = v_n^0(\vec{e}_n)_0 < f_0|f_0>$. It should be noted that the eigenvalues of M are real, however, the non-symmetrical structure of $\mathbf{M}$ does not require the $\vec{e}_n$ to be orthogonal. The approximation in the described scheme is given by the fact that the numerical treatment does not allow for generating the whole set of L orthogonal states. The number of iterations in A.5 is reduced to $\tilde{L}$, the matrix M truncated to $\tilde{L} \times \tilde{L}$ and the presented evaluation is performed on this reduced set of states.

Now we turn back to the more general expression given at the beginning of the appendix. Expressions of type A.1 are contained in

$$< g|f(\tau) > \;=\; < g|e^{-\tau \bar{H}}|f_0 > \tag{A.12}$$

$$\;=\; \sum_n e^{-\omega_n \tau} < 0|B^+|n >< n|A|0 > \tag{A.13}$$

with $|f_0 >= A|0 >$, $|g >= B|0 >$, A and B acting on the same space. Using the series representation (A.8) of $|f(\tau) >$ we obtain

$$< 0|B^+|n >< n|A|0 > \;=\; \sum_k v_n^0 (\vec{e}_n)_k < g|f_k > \tag{A.14}$$

which contains the transition probabilities $|<n|A|0>|^2$ for the choice $B = A$.

The described method was developed independently, howewer it is closely related to the earlier proposed method of *Gagliano, Balseiro* [89] of computation of real-frequency correlation functions in finite systems at zero temperature. Both methods make use of the ground state vector $|0>$ and energy E_0 of a given finite system (using e.g. Lanczos techniques [53]) and coefficients a_k, b_k^2 (A.6). They formally differ in the way of extracting energies and matrix elements (continued fraction vs. differential equations) from the input data, howewer, make use of the same input.

A.2 Accuracy of the method

The reliability of the recursion method –as well as its shortcomings– have been investigated by various methods and techniques.

DSF $S_z(q,\omega,N=16)$; $q=\pi/2,\pi$

n	$\omega_n(q,N=16)$	$\mathrm{w}_n(q,N=16)$		
1	3.3806613858893	8.603551483282	$\cdot10^{-1}$	
2	4.197135363571	1.288323108707	$\cdot10^{-1}$	
3	4.59757074255	6.12984208	$\cdot10^{-3}$	$q=\pi/2$
4	4.73871528573	1.48596359	$\cdot10^{-3}$	
5	4.902809151	9.727121	$\cdot10^{-5}$	$S_z(q=\pi/2,N=16)=$
6	5.35132697	1.723352	$\cdot10^{-4}$	0.6794375761266
7	5.8903	3.01	$\cdot10^{-4}$	
8	5.9	1.875	$\cdot10^{-3}$	
9	6.47	8.	$\cdot10^{-5}$	
1	0.540379364500	8.01345217378	$\cdot10^{-1}$	
2	2.79206117219	1.4109158151475	$\cdot10^{-1}$	$q=\pi$
3	4.668596605332	4.6691968837931	$\cdot10^{-2}$	
4	5.475947091450	1.636197084	$\cdot10^{-4}$	$S_z(q=\pi,N=16)=$
5	5.9070165813	1.044901942	$\cdot10^{-2}$	4.292303508279
6	5.994081	1.03778	$\cdot10^{-6}$	
7	6.573253	1.55186	$\cdot10^{-4}$	
8	6.80283	6.702	$\cdot10^{-5}$	
9	7.1	$\mathcal{O}(10^{-7})$		

Table A.1: Comparison: Recursion Method – Complete Diagonalization

In case of the DSF of the unperturbed Heisenberg chain (cf. Sec. 2.6) results have been compared with complete diagonalization results [72, 79, 81] and Bethe Ansatz calculations [133]. Table A.1 shows results for the first nine excitations $\omega_n(q)$ and matrix elements $w_n(q) = |<n|S_z(q)|0>|/<0|S_z(-q)S_z(q)|0>$ of the DSF $S_z(q,\omega)$ for a 16-site chain with no external field for 2 values of q. Only those digits are displayed that agree with complete diagonalization data.
The shown data (as well as all the remaining q-values of the chain) can be taken as an example for a more general situation discussed in [79, 81]: The recursion method gives reliable results with high accuracy ($\sim 10\ldots14$ digits) for the first few excitations if these carry the dominant part of spectral weight.
If considerable contributions do occur at much higher excitations (see e.g. [81]) the smallness of $\tilde{L}$ does not allow for a satisfying evaluation of these contributions. However, even in these cases the lowest excitation and its matrix element are obtained with high precision. Since this excitation is the most influential one for dynamical properties, the recursion method remains a useful tool even in such situations.

Moreover, in certain cases sum rules can be used as a global criterion for the degree of validity of recursion results. As an example for calculations of the $<0|B^+(q)|n><n|A(q)|0>$-type within the recursion method we consider an application of sum rule 5.56 for the choice $\Theta=1$ (cf. Sec. 5.4.2):

$$\Sigma(1,p,q,N) \;=\; \sum_{m\neq0}\frac{1}{E_m-E_0}<0|\mathbf{S}(-p)\mathbf{S}(p)|m><m|\mathbf{S}(-q)\mathbf{S}(q)|0>, \qquad (A.15)$$

i.e. a summation of matrix elements where the states $|m>$ are required to have the same total

spin and momentum as the ground state $|0>$ to give non-zero contributions (see also discussion in Sec. 5.4.2):

$$\sum_p \Sigma(1,p,q,N) = \sum_{n=0}^{N-1} \Sigma\left(1, p=\frac{2\pi}{N}\cdot n, q, N\right) \tag{A.16}$$

$$= \sum_{m\neq 0} \underbrace{\sum_p M_m(1,p)}_{= N\cdot S(S+1)\cdot\delta_{m,0}} \frac{M_m(1,q)}{\omega_m(1)} \tag{A.17}$$

$$= 0 \qquad \text{for} \quad m \neq 0 \tag{A.18}$$

(cf. [83], Sec. 5.4.2). Table A.2 shows results for $\sum_p \Sigma(p,q,N=20)$ with $|0>$ being the ground state of a 20-site nearest-neighbor Heisenberg chain at zero magnetization. Moreover, the table shows results for three different truncation numbers $\tilde{L}$ used in the recursion algorithm, i.e. the given sum rule can as well be used to optimize the parameters for the algorithm.
The static structure factors (SSFs) of the earlier discussed examples do not serve as a computational test of the recursion method. They only form initial conditions (given via $A|0>$) and $\sum_n \mathrm{w}_n = 1$ by construction.
Finally, it should be added that the described method only uses the constraint $\sum_n \mathrm{w}_n(q) = 1$, however, not $\mathrm{w}_n(q) \geq 0$. The latter conditions are usually fulfilled to very high accuracy and they are used as a limitation for the value $\tilde{L}$ which tends to be about $20 \ldots 40$ as long as $\tilde{L} < L$.
In summary, the recursion method is limited to the approximate determination of a finite number ($\tilde{L}$) of excitations caused by the considered operator A. The optimal truncation number $\tilde{L}$ is limited by numerical precision of the recursion process and the size L of the Hilbert space (depending on system size N and the considered operator A).

q/π	$\Sigma(1,0,q,N)+\Sigma(1,\pi,q,N)$	$\sum_{p\neq 0,\pi}\Sigma(1,p,q,N)$	$\sum_p \Sigma(p,q,N)$	
0.100	$0.17678495288824E-01$	$-0.17678495342919E-01$	$-0.5410E-10$	
0.200	$0.86810293873461E-02$	$-0.86810294164457E-02$	$-0.2910E-10$	
0.300	$0.40681950717119E-02$	$-0.40681961695584E-02$	$-0.1098E-08$	
0.400	$0.50030193195723E-04$	$-0.50029992915329E-04$	$0.2003E-09$	
0.500	$-0.50673764697107E-02$	$0.50673767434741E-02$	$0.2738E-09$	$\tilde{L}=20$
0.600	$-0.13606385253498E-01$	$0.13606384885101E-01$	$-0.3684E-09$	
0.700	$-0.31364290001213E-01$	$0.31364294572298E-01$	$0.4571E-08$	
0.800	$-0.79347860219535E-01$	$0.79347862698623E-01$	$0.2479E-08$	
0.900	$-0.28949125375861E+00$	$0.28949125564118E+00$	$0.1883E-08$	
1.000	$0.77679883152275E+00$	$-0.77679883152298E+00$	$-0.2275E-12$	
0.100	$0.17678495313556E-01$	$-0.17678495313198E-01$	$0.3585E-12$	
0.200	$0.86810293867244E-02$	$-0.86810293885494E-02$	$-0.1825E-11$	
0.300	$0.40681954558274E-02$	$-0.40681954719143E-02$	$-0.1609E-10$	
0.400	$0.50030431580794E-04$	$-0.50030430849441E-04$	$0.7314E-12$	
0.500	$-0.50673764199077E-02$	$0.50673764188729E-02$	$-0.1035E-11$	$\tilde{L}=25$
0.600	$-0.13606386170858E-01$	$0.13606386197690E-01$	$0.2683E-10$	
0.700	$-0.31364291524992E-01$	$0.31364291551446E-01$	$0.2645E-10$	
0.800	$-0.79347859109161E-01$	$0.79347859112591E-01$	$0.3430E-11$	
0.900	$-0.28949125312430E+00$	$0.28949125312952E+00$	$0.5228E-11$	
1.000	$0.77679883152273E+00$	$-0.77679883152305E+00$	$-0.3214E-12$	
0.100	$0.17678495313832E-01$	$-0.17678489474219E-01$	$0.5840E-08$	
0.200	$0.86810293863549E-02$	$-0.86810640209939E-02$	$-0.3463E-07$	
0.300	$0.40681954586067E-02$	$-0.40681863881122E-02$	$0.9070E-08$	
0.400	$0.50030436287957E-04$	$-0.50081692596133E-04$	$-0.5126E-07$	
0.500	$-0.50673764180295E-02$	$0.50675162011048E-02$	$0.1398E-06$	$\tilde{L}=30$
0.600	$-0.13606386183473E-01$	$0.13606328125024E-01$	$-0.5806E-07$	
0.700	$-0.31364291540077E-01$	$0.31364610656580E-01$	$0.3191E-06$	
0.800	$-0.79347859097145E-01$	$0.79347656407129E-01$	$-0.2027E-06$	
0.900	$-0.28949125311789E+00$	$0.28949124997464E+00$	$-0.3143E-08$	
1.000	$0.77679883152272E+00$	$-0.77679883152307E+00$	$-0.3445E-12$	

Table A.2: Sum rule 5.56 for $\Sigma(\Theta=1,p,q,N=20)$, $S_z=0$ and different iteration numbers $\tilde{L}$

Appendix B

Magnetic saturation fields B_{Sat} for various spin chains

B.1 Calculation of B_{Sat}

As being discussed in Sec. 2.4 the saturation field B_{Sat} for Hamiltonians that do conserve the total S_z value (positive curvature of $M(B)$ in the vicinity of B_{Sat} is assumed) is given by

$$2B_{Sat} \;=\; \left.\frac{d\epsilon_0(m)}{dm}\right|_{m=1/2} = E_0(S_z = N/2) - E_0(S_z = N/2-1) \tag{B.1}$$

with $\epsilon_0(m) = E_0(m = S_z/N)/N$. The factor 2 in B.1 accounts for the overall factor of 2 in the Hamiltonian (s. below).
The upper relation shall now be demonstrated for cases of periodic spin-1/2 chains

$$H_0(B,\alpha) \;=\; 2\sum_{i=0}^{N-1}\Big(\mathbf{S}_i\mathbf{S}_{i+1} + \alpha\mathbf{S}_i\mathbf{S}_{i+2} - BS_{z,i}\Big) \tag{B.2}$$

that are perturbed by $D_j^c(q)$ (cf. Sec. 3.1), namely

$$H_{j,q}(B,\alpha,\delta) \;\equiv\; H_0(B,\alpha) + 2\delta N^{1/2} D_j^c(q)\,, \tag{B.3}$$

with $j = 1, 2$ and $p = \pi, \pi/2$ will be considered. Here, we exchanged the general strength h of the periodic perturbation by the more frequently used δ in case of dimer-like perturbations.
Choosing system sizes $N = 2n$ for $q = \pi$ and $N = 4n$ for $q = \pi/2$ ($n \in \mathbb{N}$) all 4 cases have ground state energies $E_0(S_z = S_z^{tot} = N/2) = (1+\alpha)N/2$ and the unique ground state has momentum $p = 0$.
It now remains to calculate $E_0(S_z^{tot} - 1, p)$ and to determine

$$B_{Sat} \;=\; \max_p \frac{1}{2}\left\{E_0(S_z^{tot}) - E_0(S_z^{tot}-1,p)\right\} \equiv \max_p \frac{1}{2}\Delta E_0^{tot}(p)\,. \tag{B.4}$$

For that purpose momentum eigenstates $|p>$ are used that are generated via

$$|p> \;=\; \frac{1}{\sqrt{N}}\sum_{x=0}^{N-1} e^{ipx}T^x|rep> \quad ; \quad < rep|rep >=< p|p >= 1$$

$|rep>$ being a representative "one-magnon" state with $N-1$ up spins on positions $0\ldots N-2$ and one flipped spin at site $N-1$. The translation operator T satisfies

$$T|p> \;=\; e^{-ip}|p>\;.$$

Finally, the unperturbed operator $H_0(\alpha)$ fulfills

$$H_0(\alpha)|p> \;=\; (1+\alpha)\left(\frac{N}{2}-2\right)+2\cos(p)+2\alpha\cos(2p) \tag{B.5}$$

resulting in

$$B_{Sat} \;=\; \max_p < p|1+\alpha-\cos p-\alpha\cos 2p-\hat{D}_j(q)|p> \;. \tag{B.6}$$

In the following the p-value of the maximum will be denoted p_0.

B.2 Frustrated chain

A simple calculation yields:

$$B_{Sat} \;=\; \begin{cases} 2 & \text{for } \alpha \le 1/4 \quad , \quad p_0=\pi \\ 1+2\alpha+\frac{1}{8\alpha} & \text{for } \alpha \ge 1/4 \quad , \quad p_0=\arccos\left(-\frac{1}{4\alpha}\right) \end{cases} \tag{B.7}$$

B.3 Dimerization $D_1(\pi)$, $D_2(\pi)$

Using the relations given in B.1 one obtains

$$N^{1/2}D_j(\pi)|p> \;=\; \begin{cases} i\sin(p+\pi)|p+\pi> & j=1 \\ (1-\cos(p+\pi))|p+\pi> & j=2 \end{cases} \tag{B.8}$$

and, considering states $|p>$, $|p+\pi>$ with $p \in]-\pi/2,\pi/2]$ (a first Brillouin zone for a system with a doubled unit cell in real space), one obtains the eigenvalues

$$\Delta E_0^{tot}(p) \;=\; -2(1+\alpha-\alpha\cos 2p) \pm 2\cdot \begin{cases} \sqrt{\cos^2(p)+\delta^2\sin^2(p)} & , \quad j=1 \\ \sqrt{\cos^2(p)+4\delta^2\sin^4(p)} & , \quad j=2 \end{cases} . \tag{B.9}$$

They obey $\Delta E_0^{tot}(p) = \Delta E_0^{tot}(p+\pi)$ – the expected behaviour of a perturbation with $q=\pi$.
Results of the evaluation of the magnetic saturation fields for the two cases are summarized in figures B.1, B.2.
It should be added that the classification $p_0=\pi/2$ in the figures requires system sizes $N=4n$. Those with $N=4n+2$ would yield a momentum $p_0=\pi/2-\pi/N$ instead.

B.4 Dimerization $D_1^c(\pi/2)$, $D_2^c(\pi/2)$

In the case of $q=\pi/2$ the first Brillouin zone can be chosen to be $]-\pi/4,\pi/4]$ with 4 eigenvalues for each p-value of the intervall.
One first calculates

$$\begin{aligned} N^{1/2}D_1^c(\pi/2)|p> \;=\; & \frac{1+i}{4}(1-\cos(p)+\sin(p))|p+\frac{\pi}{2}> \\ & +\frac{1-i}{4}(1-\cos(p)-\sin(p))|p-\frac{\pi}{2}> \end{aligned} \tag{B.10}$$

$$N^{1/2}D_2^c(\pi/2)|p> \;=\; -\frac{1}{2}\sin(2p)\left(|p+\frac{\pi}{2}> -|p-\frac{\pi}{2}>\right) \tag{B.11}$$

and then – using the states $|p^l> \equiv |p+l\cdot\pi/2>$, $l=0,1,2,3$, ($|p^l>=|p^{l+4}>$) – diagonalizes the resulting 4×4-matrix.
Since analytic expressions for $p_o(\alpha,\delta)$ and $B_{Sat}(\alpha,\delta)$ are not easy to present the figures B.3i, B.4 and B.5, B.6 show numerical results for these quantities obtained for $N=1000$. Again, for system sizes $N=8n+4$ $p_0=\pi/4$ has to be replaced by $p_0=\pi/4-\pi/N$.

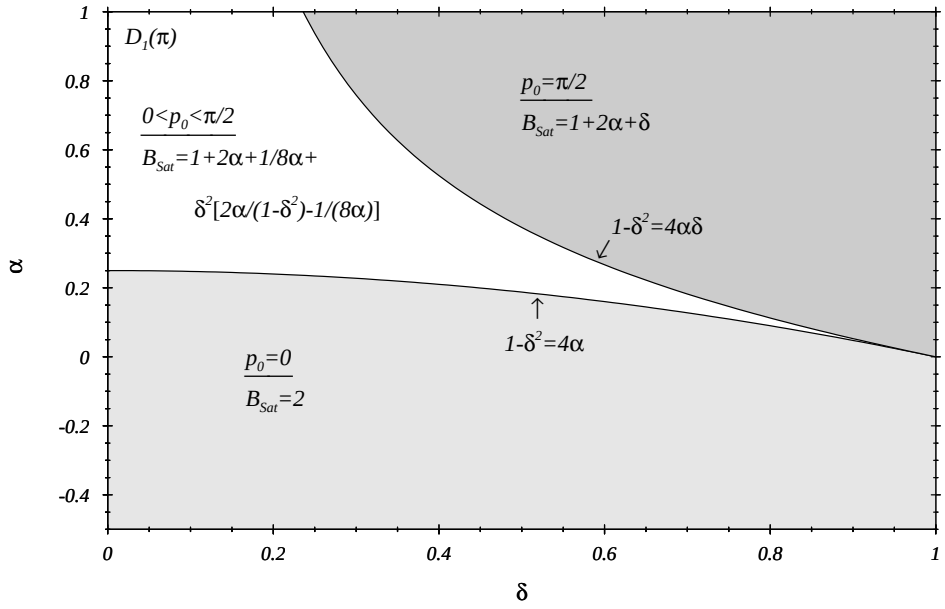

Figure B.1: Minimum position $p = p_0$ of $E_0(\alpha, \delta, S_z = N/2 - 1, p)$ and magnetic saturation field B_{Sat} for $H_{1,\pi}(B, \alpha, \delta)$

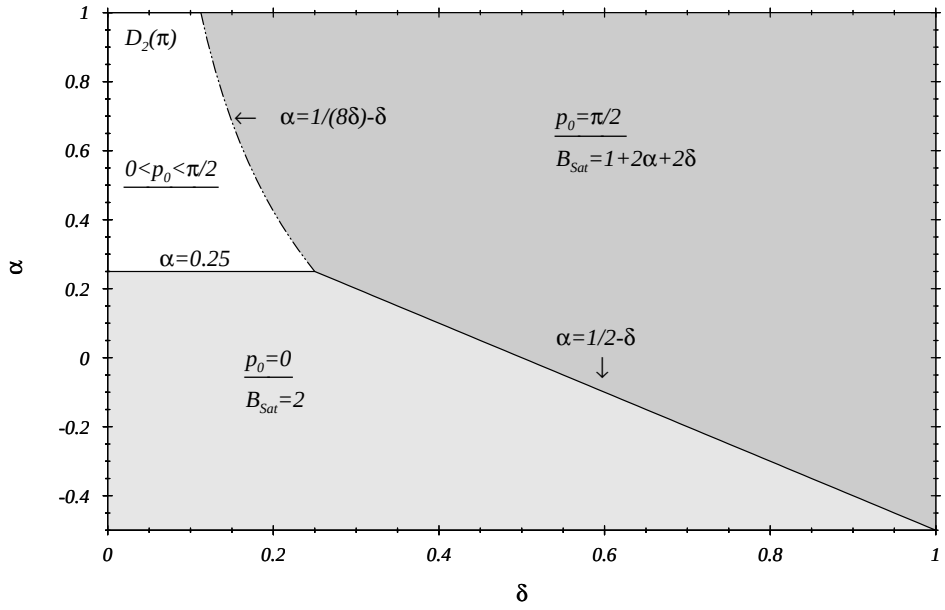

Figure B.2: Minimum position $p = p_0$ of $E_0(\alpha, \delta, S_z = N/2 - 1, p)$ and magnetic saturation field B_{Sat} for $H_{2,\pi}(B, \alpha, \delta)$

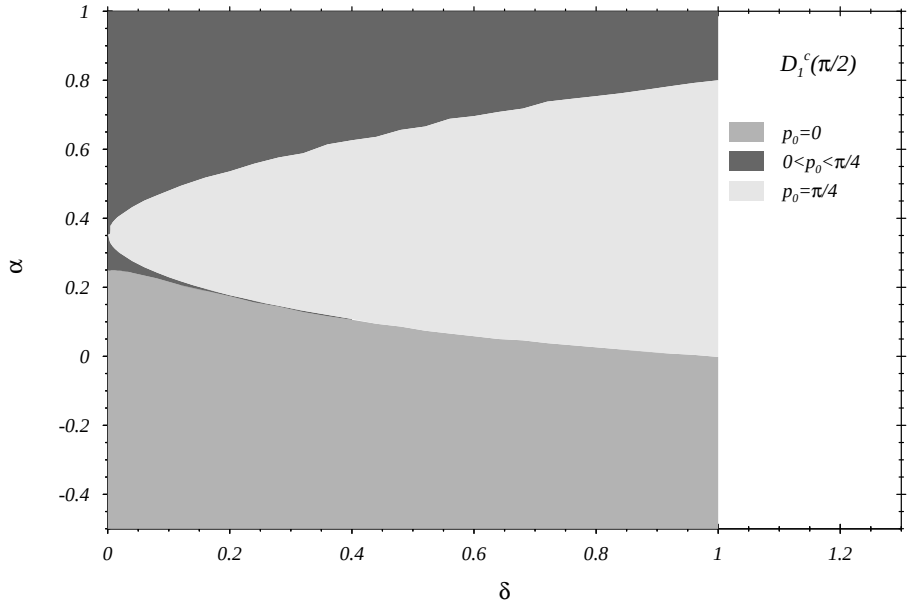

Figure B.3: Minimum position $p = p_0$ of $E_0(S_z = N/2 - 1, p)$ for $H_{1,\pi/2}(B, \alpha, \delta)$

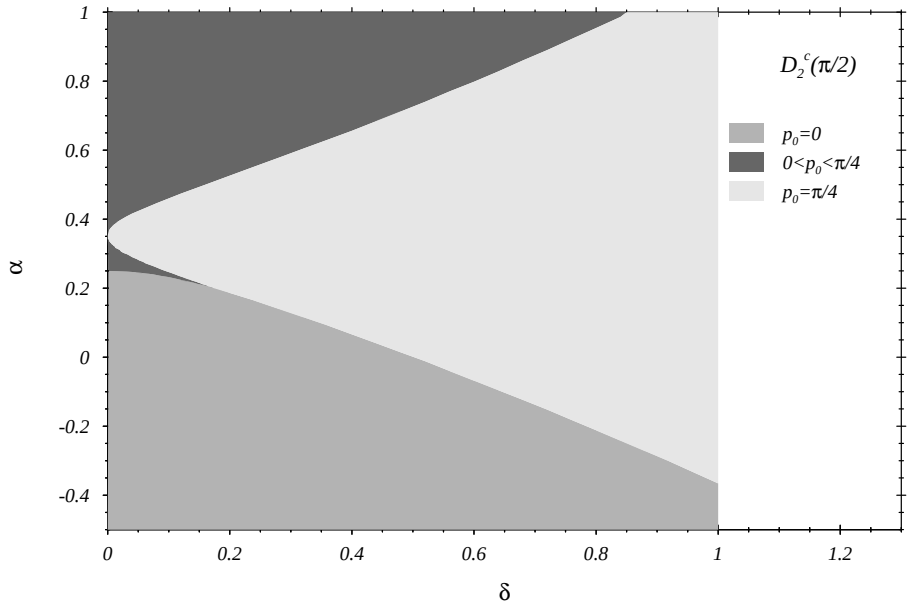

Figure B.4: Minimum position $p = p_0$ of $E_0(S_z = N/2 - 1, p)$ for $H_{2,\pi/2}(B, \alpha, \delta)$

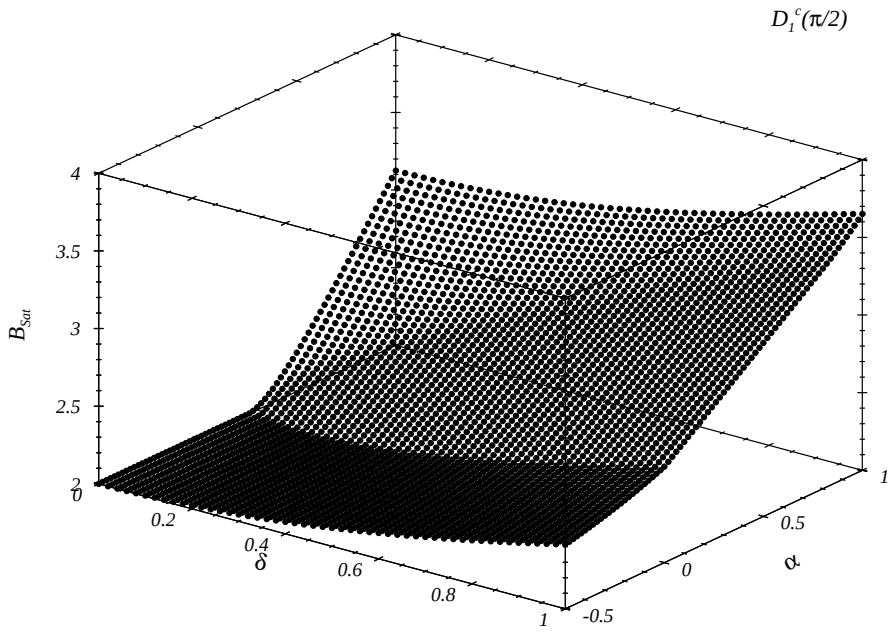

Figure B.5: Magnetic saturation field B_{Sat} for $H_{1,\pi/2}(B, \alpha, \delta)$

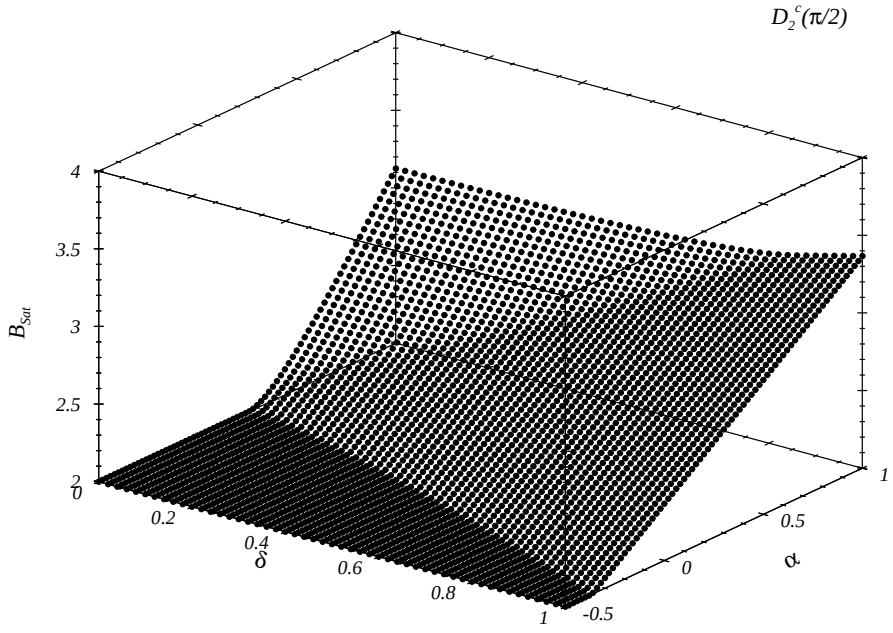

Figure B.6: Magnetic saturation field B_{Sat} for $H_{2,\pi/2}(B, \alpha, \delta)$

Appendix C

Finite-size analysis – the "Bulirsch-Stoer" (BST)-method

In a 1964 publication "*Fehlerabschätzungen und Extrapolation mit rationalen Funktionen bei Verfahren vom Richardson-Typus*" *Bulirsch and Stoer* [36] presented an algorithm that –in later applicationsi [109]– turned out to be very reliable and useful for applications to critical phenomena. The algorithm's applicability was shown to be in most cases equal or superior to other -in particular the *van den Broeck- Schwartz* (VBS) [205]– algorithms.
The BST-algorithm is extensively described and discussed in [109, 110], as well as compared with the VBS-algorithm. Here, we are not going into technical aspects but give two examples for the algorithm's application to a sequence of finite-system data.

C.1 Ground state energy per site for the isotropic Heisenberg chain ($m = 0$)

As a first set of finite-size data we consider the ground state energies per site $E_0(N, S_z = 0)/N$ shown in Fig. C.1 for the isotropic Heisenberg chain described by the Hamiltonian $H = 2\sum_n \mathbf{S}_n\mathbf{S}_{n+1}$.

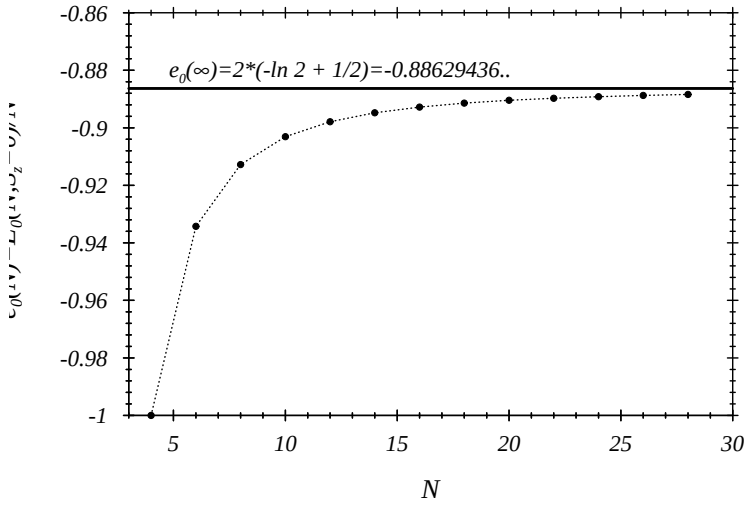

Figure C.1: Ground state energies $E_0(N, S_z = 0)/N$ of the isotropic Heisenberg chain

Together with the energies for systems $N = 4, 6, .., 28$ (calculated with help of the Lanczos algorithm) the figure as well shows the limiting value $\lim_{N\to\infty} E_0(N)/N = e_0(\infty) = 2(-\ln 2 + 1/4)$ [120] (cf. Sec. 2.4).
In the following we will apply the BST-algorithm for 3 different subsets of the given data to show how the algorithm approaches the (in this particular example known) result for the TDL. The data ($e_N \equiv E_0(N)/N$) obviously fulfill a basic prerequisite for the application of the algorithm – a limiting, convergent behaviour of the input data, that is arranged in the consecutive list $f_i = f(h_i)$, $i = 0, 1, .., N_m$. Following [110] (here $h_i = 1/N_i$), the initial sequence of data ($h_i,\ f_i,\ i = 0, .., N_m$) forms $T(0,0), T(0,1), .., T(0,N_m)$ ($T(-1,i) = 0\ \forall\ i$), which is consecutively narrowed to $T_{N_m,0}$:

$$\text{e.g. for } N_m = 2: \qquad \begin{array}{ccc} & T(0,0) & \\ & & T(1,0) \\ T(0,1) & & \\ & & T(1,1) \\ & T(0,2) & \end{array} \qquad T(2,0)\,,$$

Table C.1: Evaluation scheme of the Bulirsch-Stoer(BST) algorrithm

following the rule

$$\begin{aligned} T(m,i) \;=\; & T(m-1,i+1) + (T(m-1,i+1) - T(m-1,i)) \cdot \\ & \left[\left(\frac{h_i}{h_{i+m}}\right)^{\omega}\left(1 - \frac{T(m-1,i+1) - T(m-1,i)}{T(m-1,i+1) - T(m-2,i+1)}\right) - 1\right]^{-1} . \qquad \text{(C.1)} \\ & m = 1, 2, .., N_m \quad , \quad i = 0, 1, .., N_m - m \end{aligned}$$

The exponent ω is a free parameter that is used to minimize e.g. the difference $\Delta T_{N_m-1} \equiv |T(N_m - 1, 0) - T(N_m - 1, 1)|$ of the last occuring $T(N_m - 1, 0),\ T(N_m - 1, 1)$.

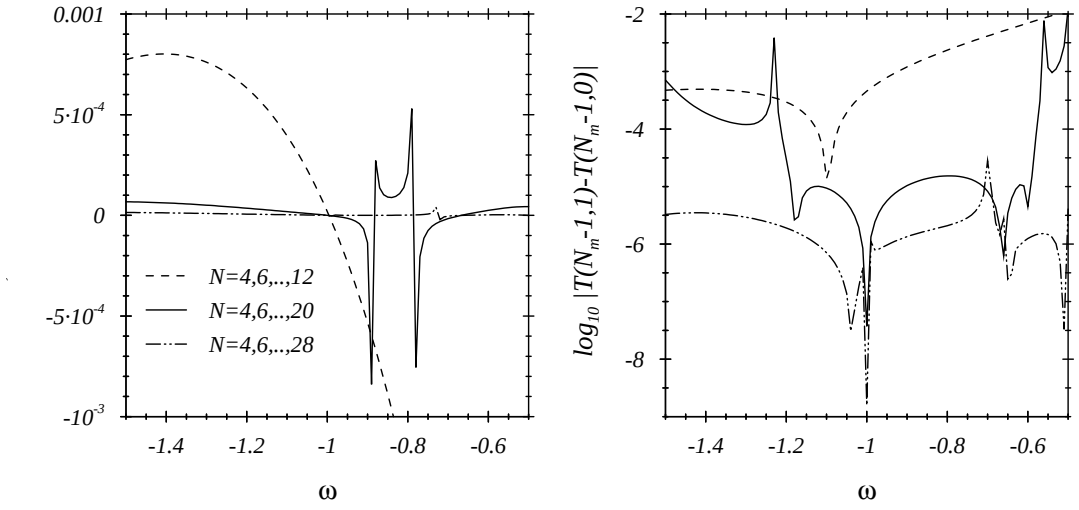

Figure C.2: Performance of the BST-algorithm for 3 sets of data and resolution $d\omega = 0.01$

The latter process is now shown in Fig. C.2 where ω has been varied in steps of 0.01 and 3 subsets $N = 4, 6, .., 12;\ 4, 6, .., 20;\ 4, 6, .., 28$ have been evaluated. The l.h.s. of the figure shows the difference between the obtained extrapolation of $e_{0,BST}(N, \omega)$ and the exact one, while the r.h.s. gives the common logarithm of ΔT_{N_m-1}. The obtained results –even for $N \leq 12$– are already very accurate (leading to $\omega \simeq -1$ see Table C.2), however, especially the inclusion of more and more sites shows the appearance of further relative minima ω^*.

N	ω	$T(N_m, 0)$	$\Delta T_{N_m-1})$	$1 - T(N_m, 0)/e_0(\infty)$
$4, 6, \ldots, 12$	-1.10	-0.8858995685E+00	0.1381766189E-04	0.4454418726E-03
$4, 6, \ldots, 12$	-1.00	-0.8862966031E+00	0.1329150175E-05	-0.2529611163E-05
$4, 6, \ldots, 12$	-1.00	-0.8862943677E+00	0.1590312326E-08	-0.7424293492E-08

Table C.2: BST-results for $d\omega = 0.01$ and comparisons with the known result

$d\omega_{min}$	ω_{min}	ΔT_{N_m-1}	$T(N_m, 0)$	N
.01	-1.10000	0.1381766189E-04	-0.8858995685E+00	
.001	-1.09600	0.8946852482E-06	-0.8859117396E+00	4,6,..,12
.0001	-1.09620	0.1518724292E-06	-0.8859111257E+00	
.01	-1.00000	0.3715772090E-07	-0.8862943797E+00	
.001	-1.00300	0.3134795867E-08	-0.8862937652E+00	4,6,..,20
.0001	-1.00300	0.3134795867E-08	-0.8862937652E+00	
.01	-1.00000	0.1590312326E-08	-0.8862943677E+00	
.001	-1.03700	0.5493834276E-09	-0.8862931590E+00	4,6,..,28
.0001	-1.03710	0.4393009290E-09	-0.8862931563E+00	

Table C.3: Influence of higher resolution (smaller $d\omega$) on BST-results

This might on one hand be due to the additionally occuring logarithmic corrections in the ground state energies, on the other hand, when using a higher resolution for the $d\omega$ (shown in Table C.3) one has in addition to take into account that the used energy values carry subtle uncertainties due to the Lanczos iteration. In any case, the BST algorithm gives excellent numerical approximations to the known ground state energy per site – this even on the basis of very few and small system sizes.

Fig. C.3 shows another important influence of the chosen subsets for the extrapolation – the seperate choice of "even ($N = 4n$) or odd ($N = 4n + 2$)" system sizes ($n \in \mathbb{N}$). The l.h.s. of the figure shows the unambiguous approach of a single ω^*, whereas the r.h.s. shows that the inclusion of the largest system ($N = 28$) –though determined with the same Lanczos termination error– again leads to the appearance of further minima. The choice of the "right" ω^*, however, is profoundly simplified. The obtained accruracies, though, are comparable to those obtained earlier for similar N_{max} ($e_0 = -0.88629 + O(10^{-5})$).

The BST-evaluations of plateau widths and boundaries that are frequently used in the main parts of this work usually reached $\Delta T_{N_m-1} \simeq 10^{-4}...10^{-6}$.

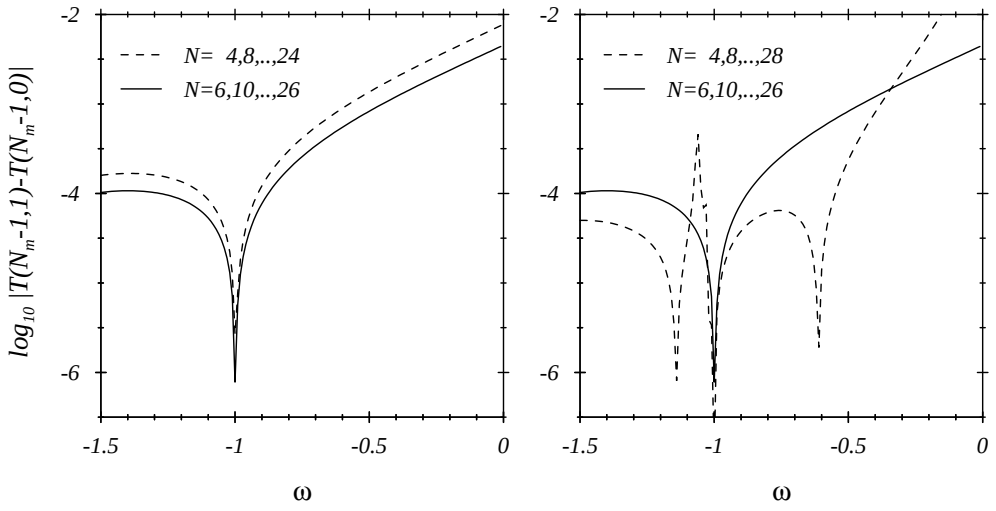

Figure C.3: Different choice of data sets ($N = 4n$, $4n + 2$ for the BST extrapolation

C.2 Evaluation of α_c (fluid-dimer transition) on the basis of $N = 8, 10, 12$ spins and comparison with *Okamoto, Nomura* [166]

In this paragraph we briefly want to comment on the behaviour and quality of small system evaluations of α_c, i.e. the frustration value characterizing the transition from the spin-fluid to the dimerized phase (see Sec. 5.1.2).
Fig. 5.2 already documented the closeness of the finite-system results for the degeneracy of the lowest singlet and triplet excitation. We will now use the three $\alpha_c(N)$ values –given in Table C.4 (simply obtained from the linearized behaviour of the two excitation energies closest to their crossing point; $\Delta\alpha = 0.02$)– and apply the BST-algorithm to determine their approximate $N \to \infty$ limit. In addition, we will use data from *Okamoto, Nomura* [166] ($N = 8, 10, .., 24$) and give results of BST fits.

N	$\alpha_c(N)$	$\alpha_c(N)$ (Okamoto, Nomura '92)
8	0.246315	0.24630338
10	0.244488	0.24449187
12	0.243470	0.24348191
14		0.24286642
16		0.24246468
18		0.24218827
20		0.24199002
22		0.24184301
24		0.24173095

Table C.4: Fluid-dimer transition values for systems $N = 8, 10, 12$ and data from Okamoto, Nomura[166]

Table C.4 first shows that the mentioned linearizations to obtain $\alpha_c(N)$ ($N = 8, 10, 12$) approach the data of Okamoto, Nomura ($\Delta\alpha = 0.01$) very well. Indeed, BST fits of both subsets do almost give the same results (see Table C.5; data of Sec. 5.1.2 shown in seperate line).

Fig. C.4 shows the results of BST fits performed for different subsets of data taken from Okamoto, Nomura. The choice of subsequent system sizes again produces the occurrence of several minima for increasing N_{max} (l.h.s. of the figure), whereas the differentiation of "even ($N = 4n$) and odd ($N = 4n + 2$)" system sizes shown on the r.h.s. results (for $N < 24$) in an unambiguous minimum close to $\omega = -2.0$. As in case of the ground state per site discussed in the previous paragraph the uniqueness of ω^* is lost for increasing N. The hint to $\omega^* \simeq -2.0$, however, is very evident.
The latter exponent agrees very well with

$$\alpha_c(N) \quad = \quad \alpha_c + \frac{const.}{N^2} \tag{C.2}$$

analyzed by [166]. Together with the behaviour shown on the r.h.s. of Fig. C.4 this will be used to consider relative minima ω^* for all sets of data closest to $\omega = -2.0$ (see Table C.5). Table C.5 as well gives the deviation $\Delta_{N_m-1}(\omega^*)$ of the final step of the algorithm (cf. Sec. C.1).
Comparing the BST results, a VBS extrapolation ([205]) and further analyses done in [166] with the to date best known value of α_c (*Eggert* [66]; $\alpha_c = 0.241167 \pm 0.000005$), it turns out that the BST results give slightly more accurate extrapolations than VBS (0.24112218 in [166]), however, the least squares fit to C.2 ($0.241155 \pm 3 \cdot 10^{-6}$ [166]) came even closer to Eggert's value. The shown extrapolations as well as the result of [166] may be summarized as $\alpha_c = 0.2411 + O(10^{-4}$.

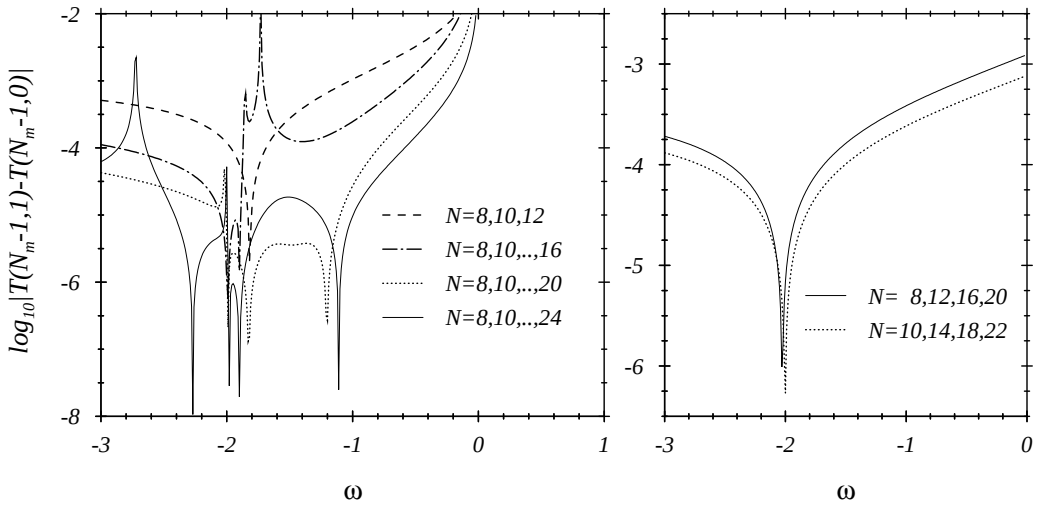

Figure C.4: BST fits for different subsets of data from Table C.4

The numerical data of [166] –$\alpha_c(N)$ given up to 8 digits– result from a linear interpolation (step width $\Delta\alpha = 0.01$) as well and we did not attempt any improvement. Moreover, it does not seem advisable to try the evaluation of $\alpha_c(N)$ for slightly larger spin chains. The latter aspect appears unfavourable considering the N-dependence of $\alpha_c(N)$ given in Table C.5 and might reflect the influence of logarithmic corrections by marginal terms or even higher order contributions from irrelevant terms..
As the authors and others pointed out (see Sec. 5.1.2) the determination of α_c is a highly susceptible problem and its approach to $O(10^{-5}$ with rather small system sizes again underlines the usefulness of small system evaluations.

N	ω^*	$\alpha_c(N)$	$\Delta T_{N_m-1}(\omega^*)$
8,10,12	-1.82	0.2409205	0.27400E-06
8,10,12	-1.82	0.2409507	0.19779E-05
8,10,..,16	-1.99	0.2411384	0.57113E-06
8,10,..,20	-1.99	0.2411384	0.21372E-06
8,10,..,24	-1.98	0.2411357	0.28408E-07
8,12,..,24	-1.98	0.2411349	0.16961E-06
8,12,16,20	-2.03	0.2411499	0.97790E-06
10,14,18,22	-2.00	0.2411399	0.53845E-06

Table C.5: BST results for minima ω^* closest to $\omega = -2.0$ for different sets of data

C.3 Résumé

The performed and shown evaluations are thought to underline the following quite general points:

1. The BST algorithm is known to give reliable results for the TDL of given input data with a generic convergent behaviour. Even a small number of points can therefore be used to obtain insight and information about the respective finite-size behaviour – as will extensively be used in the discussion of magnetization plateaus.

2. Expectations in the accuracy of the obtained BST-results e.g. the value for $e_0(\infty)$ of the first example discussed in this appendix should be oriented at the precision and number of the input data.

3. The obtained exponent ω_0 minimizing ΔT_{N_m-1} cannot automatically be considered the single exponent describing the h-dependence of the data input. In case of the occurrence of several exponents or even subleading logarithmic corrections (not to mention a completely logarithmic behaviour) the obtained ω-value can only be considered a kind of effective exponent for the problem.

4. There is no general argument about the BST algorithm being superior to others. Its increasing use by different scientists, however, may serve as *a priori* argument for its value.

Generally speaking, a reliable interpretation of the obtained BST-results is strongly improved by a frequent application and use of the algorithm and –as far as possible– related to tests of its results on the basis of exactly known results or types of behaviour like the one in this appendix. The exponent $\omega_0 \simeq -1.00$ for the above example is e.g. in good agreement with known conformal theories.

List of Tables

List of Figures

Bibliography

[1] I. Affleck, E. H. Lieb, Lett. Math. Phys. **12**, 57 (1986)

[2] I. Affleck, F. D. M. Haldane, Phys. Rev. B **36**, 5291 (1987)

[3] I. Affleck, D. Gepner, H. Schulz, T. Ziman, J. Phys. A **22**, 511 (1988)

[4] I. Affleck, T. Kennedy, E. H. Lieb, H. Tasaki, Commun. Math. Phys. **115**, 477 (1988)

[5] I. Affleck, J. Phys.: Condens. Matter 1, 3047 (1989)

[6] I. Affleck, J. Bonner, Phys. Rev. B **42**, 954 (1990)

[7] I. Affleck, M. Gelfand, R. Singh, J. Phys. A **27**, 7313 (1994)

[8] I. Affleck, M. Oshikawa, Phys. Rev. B **60**, 1038 (1999)

[9] F. C. Alcaraz, M. N. Barber, M. T. Bachelor, Ann. Phys. **182**, 280 (1988)

[10] P. W. Anderson, Phys. Rev. **86**, 694 (1952)

[11] M. Arai, M. Fujita, M. Motokawa, J. Akimitsu, S. M. Bennington, Phys. Rev. Lett. **77**, 3649 (1996)

[12] N. W. Ashcroft, N. D. Mermin, *Solid State Physics*, Saunders (1976)

[13] J. F. Audet, A. Fledderjohann, C. Gerhardt, M. Karbach, H. Kröger, K.-H. Mütter, M. Schmidt, *Critical properties of 1-D spin 1-2 antiferromagnetic Heisenberg model*, in: J. W. Clark, M. L. Ristig (eds.) *Theory of spin lattices and lattice gauge models*, Lecture notes in physics 494 (1997)

[14] P. Azaria, P. Lecheminant, A. A. Neresyan, Phys. Rev. B **58**, R8881 (1998)

[15] H. M. Babujian, Nucl. Phys. B **215**, 317 (1983)

[16] D. Baeriswyl, ed., *The Hubbard model: its physics and mathematical physics*, New York, Plenum Press (1995)

[17] T. Barnes, E. Dagotto, J. Riera, E. S. Swanson, Phys. Rev. B **47**, 3196 (1993)

[18] R. J. Baxter, Ann. Phys. (N.Y.) **70**, 323 (1972)

[19] R. J. Baxter, Exactly Solved models in Statistical Mechanics, Academic Press (1980)

[20] J. G. Bednorz, K. A. Müller, Z. Phys. B **64**, 188 (1986)

[21] A. A. Belavin, A. M. Polyakov, A. B. Zamolodchikov, Nucl. Phys. B **241**, 333 (1984)

[22] H. A. Bethe, Z. Phys. **71**, 205 (1931)

[23] R. J. Birgeneau, R. Dingle, M. T. Hutchings, G. Shirane, S. L. Holt, Phys. Rev. Lett. **26**, 718 (1971)

[24] R. F. Bishop, J. B. Parkinson, Y. Xiang, Phys. Rev. B **43**, R13782 (1991)

[25] R. F. Bishop, J. B. Parkinson, Y. Xiang, Phys. Rev. B **44**, 9425 (1991)

[26] R. F. Bishop, J. B. Parkinson, Y. Xiang, Phys. Rev. B **46**, 880 (1992)

[27] R. F. Bishop, J. B. Parkinson, Y. Xiang, J. Phys.: Condens. Matter **4**, 5783 (1992)

[28] M. Bocquet, Th. Jolicœur, cond-mat/9904169

[29] N. M. Bogoliubov, A. G. Izergin, V. E. Korepin, Nucl. Phys. B **275**, 687 (1986)

[30] N. M. Bogoliubov, A. G. Izergin, V. E. Korepin, J. Phys. A **20**, 5361 (1987)

[31] A. H. Bougourzi, M. Couture, M. Kacir, Phys. Rev. B **54**, R12669 (1996)

[32] J. C. Bonner, M. E. Fisher, Phys. Rev. **135**, A 640 (1964)

[33] S. G. Brush, Rev. Mod. Phys. **39**, 883 (1967)

[34] B. Buechner, U. Ammerdahl, T. Lorenz, W. Brenig, G. Dhalenne, A. Revcolevschi, Phys. Rev. Lett. **77**, 1624 (1996)

[35] L. N. Bulaevskii, A. I. Buzdin, D. I. Khomskii, Sol. St. Commun. **27**, 5 (1978)

[36] R. Bulirsch, J. Stoer, Num. Math. **6**, 413 (1964)

[37] D. C. Cabra, A. Honecker, P. Pujol, Phys. Rev. Lett. **79**, 5126 (1997)

[38] D. C. Cabra, A. Honecker, P. Pujol, Phys. Rev. B **58**, 6241 (1998)

[39] D. C. Cabra, A. Honecker, P. Pujol, Eur. Phys. J. B **13**, 55 (2000)

[40] D. C. Cabra, M. D. Grynberg, Phys. Rev. B **59**, 119 (1999)

[41] J. L. Cardy, Nucl. Phys. B **270**, 186 (1986)

[42] J. L. Cardy, *Phase Transition and Critical Phenomena 11*, Domb, Lebowitz (eds.), Academic Press, London (1987)

[43] G. Castilla, S. Chakravarty, V. J. Emery, Phys. Rev. Lett. **75**, 1823 (1995)

[44] D. M. Ceperly, in *Recent Progress in Many-Body Theories*, eds. E. Schachinger et al., Plenum (1995)

[45] S. Chakravarty, B. I. Halperin, D. R. Nelson, Phys. Rev. Lett. **60**, 1057 (1988)

[46] S. Chakravarty, B. I. Halperin, D. R. Nelson, Phys. Rev. B **39**, 2344 (1989)

[47] R. Chitra, S. Pati, H. R. Krishnamurthy, D. Sen, S. Ramasesha, Phys. Rev. B **52**, 6581 (1995)

[48] J. des Cloizeaux, J. J. Pearson, Phys. Rev. **128**, 2131 (1962)

[49] J. des Cloizeaux, M. Gaudin, J. Math. Phys. **7**, 1384 (1966)

[50] R. Coldea, D. A. Tennant, R. A. Cowley, D. F. McMorrow, B. Dorner, Z. Tylczynski, J. Phys.: Condens. Matter **8**, 7473 (1996)

[51] M. C. Cross, D. S. Fisher, Phys. Rev. B **19**, 402 (1979)

[52] M. C. Cross, Phys. Rev. B **20**, 4606 (1979)

[53] J. K. Cullum, R. A. Willoughby, *Lanczos Algorithms for Large Symmetric Eigenvalue Computations, Vol. 1 Theory* Birkhäuser (1985)

[54] E. Dagotto, A. Moreo, Phys. Rev. B **38**, R5087 (1988)

[55] E. Dagotto, A. Moreo, Phys. Rev. Lett. **63**, 2148 (1989)

[56] E. Dagotto, J. Riera, D. J. Scalapino, Phys. Rev. B **45**, R5744 (1992)

[57] E. Dagotto, Rev. Mod. Phys. **66**, 763 (1994)

[58] E. Dagotto, T. M. Rice, Sci. **271**, 618 (1996)

[59] E. Dagotto, Rep. Prog. Phys. **62**, 1525 (1999)

[60] R. F. Dashen, Phys. Rev. D **10**, 4130 (1974)

[61] H. L. Davis, Phys. Rev. **120**, 789 (1960)

[62] D. C. Dender, D. Davidović, D. H. Reich, C. Broholm, K. Lefmann, G. Aeppli, Phys. Rev. B **53**, 2583 (1996)

[63] D. C. Dender, P. R. Hammer, D. H. Reich, C. Broholm, G. Aeppli, Phys. Rev. Lett. **79**, 1750 (1997)

[64] P. A. M. Dirac, Proc. Roy. Soc. A **117**, 610 (1928)

[65] S Eggert, I Affleck, M Takahashi, Phys. Rev. Lett. **73**, 332 (1994)

[66] S. Eggert, Phys. Rev. B **54**, R9612 (1996)

[67] Y. Endoh, G. Shirane, R. J. Birgeneau, P. M. Richards, S. L. Holt, Phys. Rev. Lett. **32**, 170 (1974)

[68] K. Fabricius, K.-H- Mütter, H. Grosse, Phys. Rev. B **42**, 4656 (1990)

[69] K. Fabricius, U. Löw, K.-H. Mütter, P. Ueberholz, Phys. Rev. B **44**,7476 (1991)

[70] K. Fabricius, U. Löw, K.-H- Mütter, Phys. Rev. B **44**, 9981 (1991)

[71] K. Fabricius, M. Karbach, U. Löw, K.-H. Mütter, Phys. Rev. B **45**, 5315 (1992)

[72] K. Fabricius, U. Löw and K.-H. Mütter , J. Phys. C **7**, 5629 (1995)

[73] K. Fabricius, U. Löw, K.-H. Mütter, Phys. Rev. B **51**, 8270 (1995)

[74] K. Fabricius, A. Kluemper, U. Löw, B. Buechner, T. Lorenz, G. Dhalenne, A. Revcolevschi, Phys. Rev. B **57**, 1102 (1998)

[75] L. D. Faddeev, L. A. Takhtadzhan, LOMI Proc. **109**, 143 (1989)

[76] P. Fazekas, *Lecture notes on electron correlation and magnetism*, World Scientific (1999)

[77] M. E. Fisher, in *Critical Phenomena*, Proc. 51st Enrico Fermi Summer School, Varena, ed. by M. S. Green, Academic Press (1972)

[78] M. E. Fisher, M. N. Barber, Phys. Rev. Lett. **28**, 1516 (1972)

[79] A. Fledderjohann, M. Karbach, K.-H. Mütter, P. Wielath, J. Phys. C **7**, 8993 (1995)

[80] A. Fledderjohann, M. Karbach, K.-H. Mütter, Phys. Rev. B **53**, 11543 (1996)

[81] A. Fledderjohann, C. Gerhardt, K.-H. Mütter, A. Schmitt, M. Karbach, Phys. Rev. B **54**, 7168 (1996)

[82] A. Fledderjohann, C. Gros, Euro. Phys. Lett. **37**, 189 (1997)

[83] A. Fledderjohann, K.-H. Mütter, M.-S. Yang, M. Karbach, Phys. Rev. B **57**, 956 (1998)

[84] A. Fledderjohann, K.-H. Mütter, M. Karbach, Europ. Phys. J. B **5**, 487 (1998)

[85] A. Fledderjohann, K.-H. Mütter, M. Karbach, Europ. Phys. J. B **7**, 225 (1999)

[86] A. Fledderjohann, C. Gerhardt, M. Karbach, K.-H. Mütter, R. Wießner, Phys. Rev. B **59**, 991 (1999)

[87] H. C. Fogedby, J. Phys. C **11** , 4767 (1978)

[88] P. Di Francesco, P. Mathieu, D. Sénéchal, *Conformal Field Theory*, Springer (1997)

[89] E. R. Gagliano, C. A. Balseiro, Phys. Rev. Lett. **59**, 2999 (1987)

[90] A. W. Garrett, S. E. Nagler, D. A. Tennant, B. C. Sales, T. Barnes, Phys. Rev. Lett. **79**, 745 (1997)

[91] C. Gerhardt, A. Fledderjohann, E. Aysal, K.-H. Mütter, J. F. Audet, H. Kröger, J. Phys.: Condens. Matter **9**, 3435 (1997)

[92] C. Gerhardt, K.-H. Mütter, H. Kröger, Phys. Rev. B **57**, 11504 (1998)

[93] W. Gilbert, *De Magnete*, Dover Publications (1958), republication of the P. Fleury Mottelay translation (1893)

[94] O. Golinelli, T. Jolicœur, R. Lacaze, Phys. Rev. B **50**, 3037 (1994)

[95] M. Greven, R. J. Birgeneau, Y. Endoh, M. A. Kastner, M. Matsuda, G. Shirane, Z. Phys. B **96**, 465 (1995)

[96] R. B. Griffiths, Phys. Rev. **133**, A768 (1964)

[97] C. Gros, W. Wenzel, A. Fledderjohann, P. Lemmens, M. Fischer, G. Güntherodt, M. Weiden, C. Geibel, F. Steglich, Phys. Rev. B **55**, 15048 (1997)

[98] O. Haan, J.-U. Klaetke, K.-H. Mütter, Phys. Rev. B **46**, 5723 (1992)

[99] F. D. M. Haldane, Phys. Rev. B **25**, 4925 (1982) ; Phys. Rev. B**26**, 5257 (1982)

[100] F. D. M. Haldane, Phys. Rev. Lett. **50**, 1153 (1983)

[101] F. D. M. Haldane, Phys. Lett. **93**A, 464 (1983)

[102] F. D. M. Haldane, Phys. Rev. Lett. **50**, 635 (1988)

[103] F. D. M. Haldane, M. R. Zirnbauer, Phys. Rev. Lett. **71**, 4055 (1993)

[104] K. A. Hallberg, P. Horsch, G. Martinez, Phys. Rev. B **52**, R719 (1995)

[105] M. Hase, I. Terasaki, K. Uchinokura, Phys. Rev. Lett. **70**, 3651 (1993)

[106] T. Hauer, A. Rákos, F. Woynarovich, Nucl. Phys. B **562(3)**, 497 (1999)

[107] W. Heisenberg, Z. Phys. **39**, 499 (1926)

[108] W. Heisenberg, Z. Phys. **46**, 619 (1928)

[109] M. Henkel, G. Schütz, J. Phys. A **21**, 2617 (1988)

[110] P. Christe, M. Henkel, Springer (1993); M. Henkel, *Conformal Invariance and Critical Phenomena*, Springer (1999)

[111] K. Hida, J. Phys. Soc. Jpn. **63**, 2359 (1994)

[112] T. Hikihara, M. Kaburagi, H. Kawamura, T. Tonegawa, cond-mat/9910159

[113] S. Hirata, K. Nomura, cond-mat/9910159

[114] K. Hirakawa, Y. Kurogi, Suppl. Prog. Theo. Phys. **46**, 147 (1970)

[115] K. Hirota, D. E. Cox, J. E. Lorenzo, G. Shirane, J. M. Tranquada, M. Hase, K. Uchinokura, H. Kojima,Y. Shibuya, I. Tanaka, Phys. Rev. Lett. **73**, 736 (1994)

[116] P. C. Hohenberg, W. F. Brinkman, Phys. Rev. B **10**, 128 (1974)

[117] A. Honecker, Phys. Rev. B **59**, 6790 (1999)

[118] J. Hubbard, Proc. Roy. Soc. **A** 276, 238 (1963)

[119] J. Hubbard, Proc. Roy. Soc. A **277**, 237 (1964)

[120] L. Hulthén, Arkiv Mat. Astron. Fys. A 11 **26**, 1 (1938)

[121] D. A. Huse, Phys. Rev. B **37**, R2380 (1988)

[122] D. Ihle, C. Schindelin, A. Weiße, H. Fehske. Phys. Rev. B **60**, 9240 (1999)

[123] M. Isobe, Y. Ueda, J. Phys. Soc. Jpn. **65**, 1178 (1996)

[124] E. Ising, Z. Phys. **31**, 253 (1925)

[125] *Conformal Invariance and Applications to Statistical Mechanics*, eds. C. Itzykson, H. Saleur, J.-B. Zuber, World Scientific (1988)

[126] I. S. Jacobs, J. W. Bray, H. R. Hart, Jr., L. V. Interrante, J. S. Kasper, G. D. Watkins, D. E. Prober, J. C. Bonner, Phys. Rev. **14**, 3036 (1976)

[127] M. Karbach, K.-H. Mütter, Z. Phys. B **90**, 83 (1993)

[128] M. Karbach, K.-H. Mütter, M. Schmidt, Phys. Rev. B **50**, 9281 (1994)

[129] M. Karbach, Thesis, Univ. of Wuppertal (1994)

[130] M. Karbach, K.-H. Mütter, J. Phys. A: Math. Gen. **28**, 4469 (1995)

[131] M. Karbach, K.-H. Mütter, M. Schmidt, J. Phys.: Condens. Matter **7**, 2829 (1995)

[132] M. Karbach, G. Müller, A. H. Bougourzi, A. Fledderjohann, K.-H. Mütter, Phys. Rev. B **55** (1997)

[133] M. Karbach, private communications

[134] E. H. Kim, J. Solyom, preprint, cond-mat/9903241

[135] A. Klümper, Eur. Phys. J. B **5**, 677 (1998)

[136] A. K. Kolezhuk, Phys. Rev. B **59**, 4181 (1999)

[137] J. M. Kosterlitz, D. J. Thouless, J. Phys. C **6**, 1181 (1973)

[138] R. Kubo, Phys. Rev. **87**, 568 (1952)

[139] C. Lanczos, J. Res. Nat. Bureau Standards **45**, 255 (1950)

[140] K. J. B. Lee, P. Schlottmann, Phys. Rev. B **36**, 466 (1987)

[141] K. Lefmann, C. Rischel, Phys. Rev. B **54**, 6340 (1996)

[142] W. Lenz, Phys. Z. **21**, 613 (1920)

[143] E. Lieb, T. Schultz, D. Mattis, Annals of Phys. **16**, 407 (1961)

[144] E. Lieb, D. Mattis, J. Math. Phys. **3**, 749 (1962)

[145] H. Q. Lin, Phys. Rev. B **42**, 6561 (1990)

[146] W. S. Lovesey, S. P. Collins, *X-ray scattering and absorption by magnetic materials*, Clarendon Press (1996)

[147] A. Luther, I. Peschel, Phys. Rev. B **12**, 3908 (1975)

[148] C. K. Majumdar, D. K. Gosh, J. Math. Phys. **10**, 1388 (1969)

[149] C. K. Majumdar, D. K. Gosh, J. Math. Phys. **10**, 1399 (1969)

[150] C. K. Majumdar, J. Phys. C **3**, 911 (1970)

[151] W. Marshall, Proc. Roy. Soc. (London) A **232**, 48 (1955)

[152] W. Marshall, W. S. Lovesey, *Theory of neutron scattering: the use of neutrons for the investigation of condensed matter* , Clarendon Press (1971)

[153] D. C. Mattis, *The Theory of Magnetism*, Springer (1981)

[154] D. C. Mattis, ed.,*The Many-Body Problem*, World Scientific (1994)

[155] N. D. Mermin, H. Wagner, Phys. Rev. Lett. **17**, 1133 (1966)

[156] G. Müller, H. Thomas, G. Beck, and J.C. Bonner, Phys. Rev. B **24**, 1429 (1981)

[157] G. Müller, H. Thomas, M.W. Puga. and G. Beck, J.Phys. C: Solid State Phys. C **14**, 3399 (1981).

[158] G. Müller, Phys. Rev. B **26**, 1311 (1982)

[159] K.-H. Mütter, Z. Phys. B **96**, 105 (1994)

[160] K.-H. Mütter et al., in preparation (2000)

[161] S. E. Nagler, D. A. Tennant, R. A. Cowley, T. G. Perring, S. K. Satija, Phys. Rev. B **44**, 12361 (1991)

[162] T. Niemeijer, Physica **36**, 377 (1966)

[163] M. den Nijs, Phys. Rev. B **23**, 6111 (1981)

[164] M. Nishi, O. Fujita, J. Akimitsu, Phys. Rev. B **50**, 6508 (1994)

[165] J. Oitmaa, D. D. Betts, Can. J. Phys. **56**, 897 (1978)

[166] K. Okamoto, K. Nomura, Phys. Lett. A **169**, 433 (1992)

[167] R. Orbach, Phys. Rev. **112**, 309 (1958)

[168] M. Oshikawa, M. Yamanaka, I. Affleck, Phys. Rev. Lett. **78**, 1984 (1997)

[169] M. Oshikawa, I. Affleck, Phys. Rev. Lett. **79**, 2883 (1997)

[170] M. Parrinello, T. Arai, Phys. Rev. B **10**, 265 (1974)

[171] W. Pauli, Z. Phys. **43**, 601 (1927)

[172] A. M. Polyakov, J. E. T. P. Lett. **12**, 381 (1970)

[173] V. Privman, M. Fisher, J. Stat. Phys. **33**, 385 (1983)

[174] V. Privman, M. Fisher, Phys. Rev. B **30**, 32 (1984)

[175] E. Pytte, Phys. Rev. B **10**, 4637 (1974)

[176] J. Riera, A. Dobry, Phys. Rev. B **51**, 16098 (1995)

[177] S. K. Satija, J. D. Axe, G. Shirane, H. Yoshizawa, K. Hirakawa Phys. Rev. B **21**, 2001 (1980)

[178] M. Schmidt, C. Gerhardt, K.-H. Mütter, M. Karbach, J. Phys. C **8**, 553 (1996)

[179] M. Schmidt, Thesis, WUB-DIS 96-9, Univ. of Wuppertal (1996)

[180] A. Schmitt, K.-H. Mütter, M. Karbach, J. Phys. A: Math. Gen. **29**, 3951 (1996)

[181] U. Schollwoeck, Th. Jolicœur, Europhys. Lett. **30**, 493 (1995)

[182] U. Schollwoeck, Th. Jolicœur, T. Garel, Phys. Rev. B **53**, 3304 (1996)

[183] H. J. Schulz, T. A. L. Ziman, Europhys. Lett. **18**, 355 (1992)

[184] H. J. Schulz, T. A. L. Ziman, D. Poilblanc, J. Physique I, **6**, 675 (1996)

[185] B. S. Shastry, B. Sutherland, Phys. Rev. Lett. **17**, 964 (1981)

[186] B. S. Shastry, Phys. Rev. Lett. **60**, 639 (1988)

[187] M. Takahashi, Phys. Rev. B **50**, 3045 (1994)

[188] J. C. Talstra, F. D. M. Haldane, Phys. Rev. B **50**, 6889 (1994)

[189] D. A. Tennant, R. A. Cowley, S. E. Nagler, A. M. Tsvelik, Phys. Rev. B **52**, 13368 (1995)

[190] P. Tomczak, A. R. Ferchmin, J. Richter, Phys. Rev. B **54**, 395 (1996)

[191] Sin-itiro Tomonaga, *The Story of Spin*, The University of Chicago Press (1997)

[192] T. Tonegawa, Solid State Comm. **40**, 983 (1981)

[193] T. Tonegawa, I. Harada, J. Phys. Soc. Jpn. **56**, 2153 (1987)

[194] T. Tonegawa, I. Harada, Physica B **155**, 379 (1989)

[195] T. Tonegawa, I. Harada, J. Phys. Soc. Jpn. **58**, 2902 (1989)

[196] T. Tonegawa, I. Harada, M. Kaburagi, J. Phys. Soc. Jpn. **61**, 4665 (1992)

[197] T. Tonegawa, T. Nishida, M. Kaburagi, Phsica B **246-247**, 368 (1998)

[198] K. Totsuka, M. Suzuki, J. Phys.: Condens matter **7**, 6079 (1995)

[199] K. Totsuka, Phys. Lett. A **228**, 103 (1997)

[200] K. Totsuka, Phys. Rev. B **57**, 3454 (1998)

[201] A. M. Tsvelik, *Quantum Field Theory in Condensed Matter Physics*, Cambridge University Press (1995)

[202] S. Tye, B. I. Halperin, S. Chakravarty, Phys. Rev. Lett. **62**, 835 (1989)

[203] G. S. Uhrig, H. J. Schulz, Phys. Rev. B **54**, R9624 (1996)

[204] G. S. Uhrig, Phys. Rev. Lett. **79**, 163 (1997)

[205] J.-M. van den Broeck, L. W. Schwartz, SIAM J. Math. Anal. **10**, 658 (1979)

[206] V. S. Viswanath, S. Zhang, J. Stolze and G. Müller, Phys. Rev. B **49**, 9702 (1994)

[207] V. S. Viswanath and G. Müller, *The Recursion Method – Application to Many Body Dynamics* Springer Lecture Notes in Physics m 23, Springer Verlag, New York (1994)

[208] C. Waldtmann, U. Schollwöck, K. Maisinger, H. U. Evertz, preprint (1999)

[209] L. R. Walker, Phys. Rev. **116**, 1089 (1959)

[210] R. E. Walstedt, H. W. de Wijn, H. J. Guggenheim, Phys. Rev. Lett. **25**, 1119 (1970)

[211] R. Werner, thesis, Univ. of Dortmund (1999),
http://eldorado.uni-dortmund.de:8080/FB2/ls8/forschung/1999/werner

[212] S. R. White, Phys. Rev. Lett. **69**, 2863 (1992);

[213] S. R. White, D. A. Huse, Phys. Rev. B **48**, 3844 (1993)

[214] S. R. White, Phys. Rev. B **48**, 10345 (1993)

[215] R. M. Wießner, Diploma dissertation, Univ. Wuppertal, WUD 97-21 (1997)

[216] R. M. Wießner, A. Fledderjohann, K.-H. Mütter, M. Karbach,
Phys. Rev. B **60**, 6545 (1999)

[217] R. M. Wießner, A. Fledderjohann, K.-H. Mütter, M. Karbach,
to be published, Eur. Phys. J. B (2000)

[218] R. M. Wießner, thesis, Univ. Wuppertal, WUD 2000-2 (2000)

[219] H. W. de Wijn, R. E. Walstedt, L. R. Walker, H. J. Guggenheim,
Phys. Rev. Lett. **24**, 832 (1970)

[220] C. N. Yang, C. P. Yang, Phys. Rev. **150**, 321/327 (1966), Phys. Rev. **151**, 258 (1966)

[221] M.-S. Yang, K.-H. Mütter, Z. Phys. B **104**, 117 (1997)

Methodische Grundprinzipien:

(1) In einer wissenschaftlichen Untersuchung darf man nur von dem ausgehen, was wahr ist und mit Evidenz gewußt wird. (2) Alle Fragestellungen einer Untersuchung sind derart in kleine Einheiten zu unterteilen, daß man zunächst bei jenen Problemen ansetzen kann, die sich lösen lassen. (3) Zunächst muß man bei den einfachen und leicht zu erkennenden Dingen ansetzen und darf erst danach zu den schwierigeren vordringen. (4) Alle Probleme sind in einer Untersuchung möglichst vollständig aufzuzählen.

René Descartes, Discours de la méthode

(Bd. VI, 18 f. aus Œuvres de Descartes. Publiées par Ch. Adam et P. Tannery. 11 Bde. Paris 1982-91 („Nouvelle présentation"). Übersetzung: Dominik Perler[a].)

[a] L. Kreimendahl (Hrsg.), *Philosophen des 17. Jahrhunderts*, Wissenschaftliche Buchgesellschaft Darmstadt (1999)

Danksagung

Besonderer Dank gilt Herrn Prof. Dr. K.-H. Mütter, der die Anfertigung der vorliegenden Arbeit hilfreich unterstützte und dessen Interesse und stete Diskussionsbereitschaft zu zahllosen Anregungen führten.

Herrn Dr. J. Gruneberg danke ich für zahlreiche klärende Diskussionen sowie die kritische Durchsicht der vorliegenden Arbeit.

Allen ehemaligen und gegenwärtigen Kollegen der Lehrstuhlgruppe Mütter danke ich für ihre stete Bereitschaft zur Diskussion. Besonderer Dank für vielerlei Zusammenarbeit und Diskussion gebührt hierbei den Herrn Dres. M. Karbach, P. Wielath und R. M. Wießner.

Der Deutschen Forschungsgemeinschaft danke ich für das mir gewährte Habilitandenstipendium (Fl 209/2-1), das die Entstehung der Arbeit wesentlich unterstützte.

Weiterhin danke ich all denen, die bei der Planung und Ausführung dieser Arbeit ihren Rat und ihre Hilfe beitrugen sowie denjenigen, die das Begutachten derselben vornehmen werden.

Meinen Eltern gebührt steter Dank.